

Transcriptional Regulation of Autophagy

by

Meiyan Jin

A dissertation submitted in partial fulfillment
of the requirements for the degree of
Doctor of Philosophy
(Molecular, Cellular and Developmental Biology)
in the University of Michigan
2016

Doctoral Committee:

Professor Daniel J. Klionsky, Chair
Associate Professor Ken Inoki
Associate Professor Anuj Kumar
Professor Laura J. Olsen

© Meiyang Jin

All rights reserved

2016

To my parents and grandparents

ACKNOWLEDGEMENTS

I do not have enough words to thank the people who helped me become who I am.

I would like to thank my advisor Daniel Klionsky, for his trust and understanding. He is the best advisor I could ever ask for. Thank you for being the person who is always there to help so I can explore the world of science without fears. Thank you for all the encouragement so I can still believe my dream will come true.

I would like to thank my current and former thesis committee members, Dr. Laura Olsen, Dr. Anuj Kumar, Dr. Ken Inoki, and Dr. John Kim, for all their valuable suggestions and insightful comments. Also thanks to Dr. Laura Olsen for being a great advisor when I was in her lab as an undergraduate exchange student and thanks to her for all the advice and help since then.

I would like to thank all the members of the Klionsky lab. Thank you for your companionship for many years, and sharing your knowledge and happiness with me. I thank Ke Wang, Kai Mao, Midori Umekawa, and Steven Backues for their help when I just joined the lab. Thanks to Amélie Bernard and Xu Liu for being great friends and collaborators. It was enjoyable to work with you. You are like a sister and a brother I never had. Thanks to Damián Gatica for being a great listener. I also would like to thank Ting Han who gave me an opportunity to learn something beyond autophagy and provided insightful advice on my projects.

Last but not least, I would like to thank my family for their endless love and support. Thanks to my parents and grandparents who gave me a dream to become a scientist—thank you for being always proud of me. Thanks to my husband Zepeng Yao for everything he has done for me; I'm the luckiest woman to be with you.

PREFACE

This thesis summarizes the research projects I participated in while working in Dr. Daniel J. Klionsky's laboratory since September 2009. Through these projects we gain a better understanding of how the transcription of autophagy-related (*ATG*) genes are regulated and how the magnitude of the different *ATG* gene products modulates the size and the number of autophagosomes.

Chapters 1 and 6 are parts of a review paper published in *FEBS Letters* (doi:10.1016/j.febslet.2014.06.015) with some modifications. Chapter 2, 3, 4, and 5 were published in *PNAS* (doi: 10.1073/pnas.1200313109), *Current Biology* (doi:10.1016/j.cub.2014.04.048), *Autophagy* (doi: 10.1080/15548627.2015.1099796), and again *Current Biology* (doi:10.1016/j.cub.2014.12.049), respectively.

Chapter 2 describes the identification of Ume6 as a transcriptional repressor of *ATG8*. Clinton R. Bartholomew, Tsukasa Suzuki, Zhou Du, Steven K. Backues, Melinda A. Lynch-Day, Midori Umekawa, Avani Kamath, Mantong Zhao, Zhiping Xie and I performed experiments described in the publication. I designed and performed experiments to study how the activity of Ume6 is regulated through its phosphorylation by the kinase Rim15 upon nitrogen starvation. Dr. Ken Inoki and Dr. Daniel Klionsky helped with analyzing data.

Chapter 3 describes my observation that Pho23, as a negative transcription regulator of autophagy, modulates the frequency of autophagosome formation through its regulation of *ATG9* transcription. I identified the role of Pho23 in autophagy through a genetic screen, and initiated this project. I designed and performed most of the experiments, and Ding He, Steven K. Backues,

and Xu Liu performed the experiments described in Figure 3 and 5 of the paper. Mallory A. Freeberg from Dr. John K. Kim's lab analyzed the RNA-seq data described in Figure 4 A-C of the paper.

Chapter 4 describes a large-scale study of transcriptional regulation of *ATG* genes in cells deficient for different transcription factors. Dr. Amélie Bernard and I contributed equally to the project. We initiated the project and performed all the experiments described in the paper. Ziheng Xu helped with strain construction.

Chapter 5 describes the detailed molecular mechanism of how Rph1 regulates transcription of *ATG* genes. Rph1 was identified in the large-scale study described in Chapter 4, which, as noted above, was conducted by Amélie Bernard and me. Amélie Bernard designed and performed the majority of the follow-up experiments. I performed experiments to study autophagy regulation in the Rph1 overexpression strain, and analyzed Rph1 binding motifs at *ATG* gene promoter regions. Elizabeth Delorme-Axford and Steven K. Backues performed transmission electron microscopy to verify the reduced autophagosome formation in Rph1 overexpressing cells. Patricia González-Rodríguez and Jens Füllgrabe from Dr. Bertrand Joseph's lab (Karolinska Institutet, Sweden) performed experiments to study the mammalian homolog of Rph1, KDM4.

TABLE OF CONTENTS

DEDICATION.....	ii
ACKNOWLEDGEMENTS.....	iii
PREFACE.....	iv
LIST OF TABLES.....	viii
LIST OF FIGURES.....	x
ABSTRACT.....	xiii
CHAPTER 1. Introduction.....	1
1.1 Introduction of autophagy.....	1
1.2 Cytoplasmic regulation of autophagy: Atg proteins.....	3
1.3 Physiology and pathology.....	7
1.4 Nuclear regulation: transcriptional regulation of autophagy.....	8
1.5 References.....	12
CHAPTER 2. The Ume6 Transcription Factor is Part of a Signaling Cascade that Regulates Autophagy.....	18
2.1 Abstract.....	18
2.2 Introduction.....	18
2.3 Results.....	19
2.4 Discussion.....	25
2.5 Materials and Methods.....	27
2.6 Acknowledgments.....	28
2.7 References.....	28
CHAPTER 3. Transcriptional Regulation by Pho23 Modulates the Frequency of Autophagosome Formation.....	41
3.1 Introduction.....	41
3.2 Results.....	43
3.3 Discussion.....	53

3.4 Experimental Procedures.....	56
3.5 Acknowledgments.....	58
3.6 References.....	58
CHAPTER 4. A Large-scale Analysis of Autophagy Related Gene Expression Identifies New	
Regulators of Autophagy.....	75
4.1 Abstract.....	75
4.2 Introduction.....	76
4.3 Results.....	78
4.4 Discussion.....	85
4.5 Materials and Methods.....	88
4.6 Acknowledgments.....	90
4.7 References.....	90
CHAPTER 5. Rph1/KDM4 Mediates Nutrient-limitation Signaling that Leads to the	
Transcriptional Induction of Autophagy.....	120
5.1 Introduction.....	120
5.2 Results.....	122
5.3 Discussion.....	132
5.4 Experimental Procedures.....	136
5.5 Acknowledgments.....	141
5.6 References.....	142
CHAPTER 6. Summary.....	
6.1 Regulation of the size of autophagosomes.....	171
6.2 Regulation of the number of autophagosomes.....	174
6.3 Future directions.....	175
6.4 References.....	177

LIST OF TABLES

Table 2.1 Strains used in this study	31
Table 3.1. Strains used in this study	61
Table 3.2. WT vs. <i>pho23Δ</i> TEM data	63
Table 3.3. De-multiplexing results in 22M-31M reads of RNA-seq samples	64
Table 3.4. Mapping the reads of RNA-seq samples to the yeast transcriptome using Bowtie2...	65
Table 3.5. A9 strains TEM data	66
Table 3.5. GO term analysis for genes upregulated in <i>PHO23</i> deletion cells	67
Table 4.1. DNA binding protein identified as potential regulator of <i>ATG</i> gene expression.....	93
Table 4.S1. mRNA level of the indicated <i>ATG</i> genes in deletion mutants analyzed after nitrogen starvation.....	94
Table 4.S2. mRNA level of the deletion mutants analyzed after glucose starvation.....	98
Table 4.S3. mRNA level of the deletion mutants analyzed in growing conditions.....	102
Table 4.S4. Analysis of the putative DNA binding sites of transcription factors in <i>ATG</i> promoters.	106
Table 4.S5. Strains used in this study.	107
Table 4.S6. Primers used in this study.....	108
Table 5.1. Strains used in this study	146
Table 5.2. RT-qPCR primers used in this study	148
Table 5.3. WT vs. OE Rph1 TEM data.....	149
Table 5.4. Analysis of Rph1 binding motifs in <i>ATG</i> promoters	150

Table 5.5. Rph1 DNA binding motifs..... 151

LIST OF FIGURES

Figure 2.1 The Ume6-Sin3-Rpd3 complex represses Atg8 expression.....	32
Figure 2.2 Ume6 binds the <i>ATG8</i> promoter and negatively regulates <i>ATG8</i> transcription.....	33
Figure 2.3 Rim15 promotes Ume6 phosphorylation and functions as a positive regulator of Atg8 induction.	34
Figure 2.4 Ume6 negatively regulates autophagy.....	35
Figure 2.5 SIN3A and SIN3B play redundant roles in regulating LC3 expression.....	37
Figure 2.S1 Autophagosome volume is increased in <i>ume6Δ</i> cells.	38
Figure 2.S2 SIN3A and SIN3B play redundant roles in regulating LC3 expression.	40
Figure 3.1. Pho23 represses the transcription of several <i>ATG</i> genes when autophagy is suppressed.	68
Figure 3.2. Pho23 negatively regulates autophagy activity.	69
Figure 3.3. <i>pho23Δ</i> cells have an increased frequency of autophagosome formation.....	70
Figure 3.4. <i>pho23Δ</i> cells maintain higher <i>ATG9</i> expression levels relative to the wild type after autophagy is activated.....	72
Figure 3.5. The Atg9 protein level correlates with autophagosome formation frequency and autophagy activity.....	73
Figure 3.S1. Pho23 regulates ATG gene transcription in an Rpd3-dependent manner.....	74
Figure 4.1. A screen for DNA-binding proteins involved in the regulation of ATG gene expression.	109

Figure 4.2. Gln3, Gat1 and Gcn4 are transcriptional modulators of <i>ATG</i> genes upon nitrogen starvation.....	110
Figure 4.3. Gln3, Gat1 and Gcn4 affect autophagy activity.	111
Figure 4.4. Spt10 and Fyv5 are transcriptional repressors of <i>ATG</i> gene expression.	113
Figure 4.5. Sfl1 promotes <i>ATG</i> gene expression and autophagy.	114
Figure 4.S1. mRNA quantification of <i>ATG</i> genes in the mutants identified in the screen as potential autophagy transcriptional regulators.	115
Figure 4.S2. mRNA quantification of <i>ATG</i> genes in newly generated deletion strains.	116
Figure 4.S3. The deletion of <i>FYV5</i> and the overexpression of <i>SFL1</i> affect the level of the Pho8 Δ 60 protein.	117
Figure 4.S4. Evidence for direct DNA-binding of transcription factors on <i>ATG</i> promoters.	118
Figure 5.1. Rph1 represses the expression of nitrogen-sensitive <i>ATG</i> genes in nutrient-replete conditions.....	153
Figure 5.2. Rph1 negatively regulates autophagy.....	155
Figure 5.3. The level of Atg7 regulates autophagy.....	156
Figure 5.4. The overexpression of Rph1 inhibits autophagy and decreases cell survival in nitrogen starvation conditions.....	157
Figure 5.5. Rph1 DNA binding ability but not histone demethylase activity is required for its function in autophagy	159
Figure 5.6. Rim15-dependent phosphorylation of Rph1 upon nitrogen starvation releases its repression on <i>ATG</i> gene expression and autophagy.	161
Figure 5.7. <i>KDM4</i> regulates autophagy in mammalian cells.....	163

Figure 5.S1. Rph1 represses the expression of nitrogen-sensitive <i>ATG</i> genes in nutrient-replete conditions.....	165
Figure 5.S2. The overexpression of Rph1 blocks the biogenesis of autophagic bodies.....	167
Figure 5.S3. Rph1 DNA binding ability but not histone demethylase activity is required for its function in autophagy	168
Figure 5.S4. Rim15-dependent phosphorylation of Rph1 upon nitrogen starvation releases its repression on <i>ATG</i> gene expression and autophagy	169
Figure 6.1. A model of transcriptional regulation of autophagy in yeast.	179

ABSTRACT

Macroautophagy (hereafter autophagy) is a cellular recycling process through which cytoplasmic contents are delivered into the lysosome/vacuole for degradation by double-membrane organelles, autophagosomes. Autophagy is essential for cell survival under stress; however, too much autophagy can also be detrimental. Autophagy activity can be regulated by modulating the size or the number of autophagosomes. Although there are more than 40 autophagy-related (*ATG*) genes that have been identified, it is not fully understood how most of these genes contribute to these aspects of regulation. Autophagy is highly conserved among eukaryotic cells, and its molecular machinery has been best characterized in the budding yeast *Saccharomyces cerevisiae*. In my thesis studies, I use budding yeast as the model organism, taking advantage of its utility in genetic/genomic screening; in addition, high-throughput sequencing and powerful autophagy assays have been developed uniquely in the yeast system, to explore how autophagy is modulated through transcriptional regulation.

When I joined the Klionsky lab, I became involved in the study of a negative transcriptional regulator of autophagy, Ume6. Deletion of the *UME6* gene results in an increase in the size, but not the number, of autophagosomes by increasing the expression of Atg8. From a subsequent genetic screen for autophagy modulators, I identified another transcription repressor of autophagy, Pho23. Intriguingly, Pho23 ended up being characterized as a specific regulator of the number, but not the size, of autophagosomes, or it can be viewed as controlling the rate of autophagosome formation by regulating Atg9 expression. These studies support a model whereby the size and numbers of autophagosomes are independently regulated through precise

transcriptional regulation of different *ATG* genes.

Collaborating with Amélie Bernard, a postdoc in the lab, to further explore the transcriptional regulation network of autophagy, we analyzed 139 yeast strains each deleted for a single gene encoding a transcription factor; we profiled the transcription of several *ATG* genes in each strain. Through this screen we identified Gcn4, Slf1, Gat1 and Gln3 as transcriptional activators, and Spt10, Fyv5, and Rph1 as transcriptional repressors of autophagy. We also further investigated the detailed molecular mechanisms of the regulation of autophagy by Rph1.

CHAPTER 1. Introduction¹

1.1 Introduction of autophagy

Macroautophagy, hereafter referred to as autophagy, is a conserved process among eukaryotic cells, through which cytoplasmic components are delivered to the vacuole (in yeasts or plants) or lysosomes (in mammals) for degradation [1]. The autophagy-lysosome system and the ubiquitin-proteasome system (UPS) are the two major subcellular degradation systems. However, in contrast to the UPS, which is primarily a degradative pathway, autophagy has a much greater range of functions, participating in cellular adaptation and remodeling, the recycling of macromolecular building blocks, and even biosynthetic trafficking [2].

The morphological hallmark of autophagy is a double-membrane vesicle, termed an autophagosome, which is assembled *de novo*. That is, formation of the autophagosome occurs by a process that is distinct from vesicle formation throughout the secretory pathway. In the latter, transient transport vesicles bud off from a pre-existing organelle already containing their cargo [3, 4]. In contrast, the autophagosome is formed in a step-wise manner, providing a tremendous flexibility and capacity with regard to cargo sequestration. In yeast cells, autophagy occurs at a low basal, constitutive level. In response to various types of stress, or changing nutrient conditions, autophagy is upregulated. The induction of autophagy involves the recruitment of

¹ This chapter and Chapter 6 are reprinted from Meiyang Jin and Daniel J. Klionsky, Regulation of autophagy: Modulation of the size and number of autophagosomes, FEBS Letters, 2014;588(15): 2457-63, doi: 10.1016/j.febslet.2014.06.015, with minor modifications, with permission from John Wiley and Sons.

various autophagy-related (Atg) proteins to a peri-vacuolar site, termed the phagophore assembly site (PAS), where they nucleate and assemble into the initial sequestering compartment, a double-membrane structure named the phagophore. The phagophore can surround cytoplasmic materials randomly, or in the case of selective autophagy targeted cargo molecules are sequestered through direct interaction between receptors, scaffold proteins, and protein components in the phagophore membrane. Upon completion of elongation the phagophore seals to generate an intact double-membrane vesicle; at this stage, formation of the autophagosome is completed. Subsequently, the outer membrane of the autophagosome fuses with the vacuole, exposing the inner vesicle to the hydrolytic environment of the vacuole lumen. Breakdown of the vesicle membrane, and degradation of the cargo ensues. The resulting macromolecules are released back into the cytosol through various permeases and recycled [1].

While the UPS is restricted to the degradation of ubiquitinated proteins that must be unfolded to gain access to the associated proteases, autophagy mediates the degradation of a wider range of targets, including soluble proteins, protein aggregates, damaged organelles, or even invasive pathogens. Nonselective autophagy is primarily a starvation response in which cytoplasm, potentially including organelles that are randomly sequestered, is delivered to the vacuole to provide macromolecules for catabolism (to provide energy), or for the synthesis of essential proteins. In contrast, during selective autophagy, the phagophore membrane is in close apposition to the cargo, preventing bulk cytoplasm from being sequestered [5]. Various types of cargo are selectively degraded through autophagy including protein aggregates (aggrephagy), mitochondria (mitophagy), peroxisomes (pexophagy), lipid droplets (lipophagy), and pathogens (xenophagy) [6]. Finally, although most types of autophagy are degradative in nature, selective autophagy can also serve a biosynthetic function. For example, during the cytoplasm-to-vacuole

targeting (Cvt) pathway the precursor form of aminopeptidase I (prApe1) forms into a dodecamer in the cytosol. The dodecamer subsequently assembles into a larger self-interacting complex that is selectively sequestered by a phagophore. Upon completion, the double-membrane compartment is referred to as a Cvt vesicle. This vesicle targets to and fuses with the vacuole, again releasing the inner vesicle into the lumen. In this case, after lysis of the single-membrane vesicle, the contents are not degraded. Instead, a propeptide that keeps prApe1 inactive is proteolytically removed to generate the mature, active form of the hydrolase [7].

1.2 Cytoplasmic regulation of autophagy: Atg proteins

Most of our understanding of the molecular machinery of autophagy has been achieved within the past two decades. In particular, studies relying on genetic analyses in yeast contributed to the identification of the majority of the known protein components that participate in autophagy. At present, more than 30 Atg proteins have been identified in yeast, and orthologs of most of these proteins are present in higher eukaryotes, indicating an evolutionarily conserved molecular machinery. A subset of the Atg proteins that is required for autophagosome formation (or for the generation of selective double-membrane compartments including the Cvt vesicle) is referred to as the molecular core machinery of autophagy. These proteins participate in different steps of autophagy, and, based on their roles in autophagosome formation and interaction with each other, they can be divided into several functional units.

1.2.1 Atg1 kinase complex and induction

The yeast Atg1 kinase complex contains the only kinase of the core machinery, Atg1, and its regulatory subunit, Atg13. The Atg1 complex senses the signals of autophagy induction, delivered from several upstream signaling inputs, such as the target of rapamycin (TOR) [8], protein kinase A (PKA), and Sch9 pathways [9-11]. Atg1 is a serine/threonine protein kinase

[12, 13], and the kinase activity of Atg1 requires its interaction with Atg13 [14]. During starvation-induced autophagy, Atg1 kinase activity is upregulated, which requires association of Atg1-Atg13 with a stable ternary complex composed of Atg17-Atg31-Atg29 [14-16]. Atg17 is proposed to be the first Atg protein that is recruited to the starvation-specific PAS upon autophagy induction (Atg11 serves this role in growing conditions [17]), and its correct localization is essential for the nucleation of other Atg proteins at this site [18]. Atg29 is a phosphoprotein that contains a C-terminal inhibitory domain; phosphorylation of the C terminus is necessary to relieve inhibition, although the mechanism and the relevant kinase are not known [19]. Similarly, the targets of Atg1 kinase that are involved in autophagy have not been well characterized. Atg1 can be autophosphorylated at Thr266 in the activation loop, and this modification is required for Atg1 kinase activity [20]. BECN1, the mammalian homolog of yeast Vps30/Atg6, is phosphorylated by ULK1 (a mammalian Atg1 homolog) [21], and Atg9 has been identified as one of the direct targets of Atg1 in yeast [22].

1.2.2 PtdIns3K complex and nucleation

Vps34 is the only phosphatidylinositol 3-kinase (PtdIns3K) in yeast, and the autophagy-specific PtdIns3K complex I, which is composed of Vps34, Vps15, Vps30, Atg14 and Atg38 is thought to act downstream of the Atg1 kinase complex (complex II, which contains Vps38 instead of Atg14, generates PtdIns3P at the endosome) [23-25]. The main function of the PtdIns3K complex is to generate PtdIns3P at the PAS, and recruit PtdIns3P binding proteins, such as Atg18, to the PAS [26, 27].

1.2.3 Ubl conjugation system and expansion

Atg8 and Atg12 are two ubiquitin-like (Ubl) proteins that belong to two distinct conjugation systems that are part of the core autophagy machinery. These proteins are not

homologs of ubiquitin, but have structural similarity, containing ubiquitin folds. Both of the Ubl systems are essential for the expansion of the phagophore [28,29]. A C-terminal glycine of Atg12 is stoichiometrically conjugated to an internal lysine of Atg5 in a process that is very reminiscent of ubiquitination; the first step involves activation of Atg12 by the E1-like enzyme Atg7 (a homolog of the ubiquitin-activating enzyme), which is followed by conjugation to Atg5 via an E2-like enzyme, Atg10 [29, 30]. An E3 ubiquitin ligase-like enzyme for Atg12–Atg5 conjugation has not been identified. Atg12–Atg5 further forms a complex with Atg16, a small coiled-coil protein [31], and the Atg12–Atg5-Atg16 complex forms larger oligomers via homo-oligomerization mediated by the Atg16 coil-coiled domain [32].

Atg8, the second Ubl protein of autophagy, undergoes a unique type of post-translational modification. Atg8 is initially synthesized with a C-terminal extension (a single arginine residue in yeast) that is proteolytically removed by the Atg4 cysteine protease. The same E1-like enzyme that is used in the Atg12–Atg5 conjugation system, Atg7, activates the modified Atg8; however, conjugation requires a separate E2-like enzyme, Atg3, which attaches the exposed C-terminal glycine to the lipid phosphatidylethanolamine (PE) [28]. The Atg12–Atg5-Atg16 complex may act as the E3 ligase for Atg8–PE conjugation [33], although it is not essential [34]. Besides its putative E3-like activity, Atg12–Atg5-Atg16 is also required for the PAS localization of Atg8 [18]. Unlike the Atg12–Atg5-Atg16 complex that localizes exclusively on the outer membrane of the phagophore [35], Atg8–PE is initially located on both sides of the phagophore during expansion; Atg8 on the outer surface of the completed autophagosome is removed by a second Atg4-dependent cleavage (referred to as deconjugation), whereas some of the Atg8 on the inner surface remains inside the completed autophagosome [36, 37]. The Atg8 that lines the concave surface of the phagophore plays an important role in cargo recognition during selective types of

autophagy [38]. In contrast, the population located on the outer surface is involved in determining the size of the autophagosome and may play a role in the formation of a coat-like structure by interdigitating with the Atg12–Atg5-Atg16 complex [37, 38].

1.2.4 Atg9 and its cycling system

Atg9 is the only transmembrane protein in the core machinery [41]. Atg9 has a unique localization pattern different from the other core machinery proteins. Most Atg proteins are present in two populations, one being diffuse in the cytosol, and the second, that is thought to be the active pool, localized at the PAS; the latter appears as a single punctum in growing conditions that becomes much more intense (based on monitoring of fluorophore-tagged Atg proteins by microscopy) following autophagy induction. Interestingly, Atg9 localizes to multiple punctate structures. One of these punctate structures is the PAS, but the other sites are located proximal to the mitochondria; these latter populations are called Atg9 peripheral sites, Atg9 reservoirs or tubulovesicular clusters (TVCs) [41-43]. Based on studies with a temperature-sensitive Atg1 mutant, Atg9 is proposed to cycle between the peripheral sites/TVCs and the PAS. Anterograde movement to the PAS is dependent on Atg11, Atg23, Atg27 and the Arp2/3 complex, whereas retrograde trafficking depends on the Atg1-Atg13, and Atg2-Atg18 proteins [42, 44, 45]. The PtdIns3K complex is also required for Atg9 trafficking, which may reflect the fact that Atg18 is a PtdIns3P-binding protein. The exact function of Atg9 is not known, but it is proposed to be involved in delivering membrane to the PAS, or in directing this process. Membrane-bound Atg9 moves between the PAS and the peripheral sites/TVCs on single-membrane vesicles [46, 47]. Atg9 PAS localization is dependent on Atg17; the Atg17-Atg31-Atg29 complex forms a crescent-shaped structure that may recruit the Atg9 vesicles to the early phagophore [19, 48].

1.3 Physiology and pathology

Autophagy occurs at a constitutive basal level, but is upregulated when it is induced by different types of stress such as starvation or shifting to an alternative carbon source, hypoxia, or pathogen infection. In a nutrient-rich condition the basal level of autophagy is critical for normal homeostasis, performing housekeeping roles such as the removal of misfolded and damaged proteins, the biosynthetic delivery of vacuole-resident enzymes, or maintaining proper metabolism. Recent studies have mostly focused on stress-induced autophagy; however, basal autophagy plays a very important role as part of the quality control machinery, limiting the accumulation of damaged organelles and misfolded proteins that may contribute to many types of neurodegenerative diseases, such as Huntington, Alzheimer and Parkinson disease [49]. In the heart, basal autophagy is important for maintaining cardiomyocyte size and global cardiac structure and function [50], whereas in the liver it may play a role in preventing misfolding diseases such as α_1 -antitrypsin deficiency [51]. The degradation of depolarized mitochondria by basal mitophagy also prevents spurious inflammation caused by reactive oxygen species and DNA released from damaged mitochondria [52].

When a cell senses stress, autophagy is induced. Under starvation conditions, cells degrade proteins and lipids through autophagy to maintain energy homeostasis. Autophagy-defective cells display a tremendous reduction in viability during starvation, and autophagy-defective mice cannot survive after birth, when the maternal trans-placental nutrient supply is disrupted [53]. In addition autophagy triggered in oocytes by fertilization is essential for preimplantation development in mammals [54]. As mentioned above, autophagy is also induced by pathogen infection, and the selective autophagy of pathogens, xenophagy, can target and kill invasive pathogens, including bacteria and viruses; therefore, this process is essential for maintaining a

healthy innate immune system. Conversely, some microbes have evolved to evade or even subvert autophagy for their own purposes, establishing a replicative niche within autophagosomes, or relying on autophagy to provide nutrients [55]. Besides its functions in preventing infectious diseases, autophagy is involved in immunity by delivering antigens for major histocompatibility (MHC) presentation. The intracellular substrates of autophagy can be loaded on MHC class II, which is usually considered to present extracellular antigens, explaining how the MHC class II pathway contributes to intracellular antigen presentation [56].

Too little autophagy is harmful, but too much autophagy can also be deleterious—uncontrolled autophagy may cause cell death. Autophagy functions as a mechanism of tumor suppression, but cancer cells can also use autophagy to help them to survive in a hypoxic and low-nutrient environment, or to carry out its cytoprotective function following anticancer treatments that may damage organelles. Furthermore, autophagy plays different roles in different tissues. Inhibition of autophagy in liver cells causes accumulation of hepatic lipids, while inhibition of autophagy in adipose tissue causes decreased white adipose mass. Therefore, a tight regulation of autophagy in terms of its magnitude and in a tissue-specific manner will be crucial for the therapy of autophagy-related diseases.

1.4 Nuclear regulation: transcriptional regulation of autophagy

Like many other cellular processes, the induction of autophagy involves not only the post-translational modification and action of the Atg proteins, but also a coordinated transcriptional activation of the *ATG* genes. The abnormal expression of many *ATG* genes has been observed in various human diseases [57-60] suggesting the physiological significance of transcriptional regulation of autophagy. Although the transcriptional induction of *ATG* genes was first reported more than ten years ago, at present our knowledge of the transcription factors that are involved in

autophagy regulation is very limited, even in the yeast system, where the molecular mechanism of autophagy has been most intensively studied. Some progress has been made with regard to transcriptional regulation in the mammalian system in recent years, and I briefly highlight these findings along with data from yeast below.

1.4.1 FOXO transcription factors

The conserved forkhead box-containing protein O subfamily (FOXO) transcription factors regulate autophagy in different cell types and organisms. The FOXO proteins shuttle between the cytoplasm and the nucleus, which is regulated by phosphorylation, and they have both transcription-dependent and -independent roles in autophagy regulation. Here we consider the transcription-dependent roles of FOXO family members. There is only one FOXO protein in worms and flies, whereas there are four members, FOXO1, FOXO3, FOXO4, and FOXO6, in mammals [61]. In general, FOXO transcription factors function as activators of autophagy. Under stress stimuli such as nutrient deprivation, phosphorylation of FOXO proteins by AKT1 is blocked, and FOXO transcription factors translocate into the nucleus. In mouse muscle cells, some of the *Atg* genes including *Lc3b*, and *Gabarapl1* are directly targeted and activated by FOXO3 as indicated by chromatin immunoprecipitation (ChIP) assays [62, 63]. In neurons, transcription of *Atg* genes such as *Atg3*, *Atg5*, and *Atg12* is activated by FOXO1 [64]. Transcriptional regulation of autophagy by FOXO transcription factors has also been reported in various other types of cells, including cardiomyocytes, hepatocytes, and primary renal proximal tubular cells [59]. The positive regulation of autophagy by FOXO transcription factors in muscle is conserved in *Drosophila* [65]. In budding yeast, the role of Fhl1, the homolog of FOXO transcription factors, in transcriptional regulation of autophagy has not been directly tested. However, CHIP-chip data from several independent studies revealed that this protein directly

targets to the promoters of several *ATG* genes including *ATG13*, *ATG27* and *ATG31* [8, 66], indicating that a conserved regulation may exist in the yeast system.

1.4.2 *TFEB* vs *ZKSCAN3*

The autophagosome itself is not a degradative compartment. Accordingly, the autophagosome cooperates in the degradation of its cargos with the lysosome in order to fulfill its roles in the degradation and recycling of cytoplasmic materials. Under starvation conditions, both autophagosome and lysosome biogenesis are upregulated. For the transcriptional regulation, two master switches, transcription factor EB (TFEB) as the activator, and ZKSCAN3 as the repressor, have been reported to regulate both autophagosome and lysosome biogenesis. Overexpression of TFEB induces autophagy, while *TFEB* RNA interference decreases autophagy. Starvation induces TFEB translocation to the nucleus and activates the transcription of several lysosomal and autophagy genes by directly binding to their promoters [67]. This organized pattern of control is referred to as the coordinated lysosomal expression and regulation (CLEAR) network [68]. Conversely, silencing ZKSCAN3, a zinc family DNA-binding repressor protein, upregulates the mRNA level of several autophagy and lysosomal genes, and ChIP experiments suggest that ZKSCAN3 represses transcription of these target genes by direct binding at the respective promoters [69]. Interestingly, in contrast to TFEB, ZKSCAN3 accumulates in the cytosol during starvation.

1.4.3 *E2F1* vs *NFKB*

BNIP3 is as an activator for hypoxia-induced autophagy [70], and its transcription is regulated in an opposite manner by two transcription factors, E2F1 and NFKB. *Bnip3* is a direct target of E2F1, which functions as a transcription activator. NFKB competes with E2F1 for binding at the *Bnip3* promoter, and therefore represses its expression [71]. Besides BNIP3, E2F1

also activates other *ATG* genes including *LC3*, *ULK1*, and *ATG5*, and induces autophagy activity [72]. NFκB represses *BNIP3*, however, NFκB activates other *ATG* genes such as *BECN1* [73].

1.4.4 GATA family factors

GATA family zinc finger transcription factors regulate nitrogen catabolite repression (NCR)-sensitive genes, which produce enzymes and permeases required for using an alternative (nonpreferred) nitrogen source. Gln3, a yeast GATA family transcription activator, is regulated by Tor, and Gln3 is reported to positively regulate *ATG14* transcription [74]. This regulatory event is one of the first examples of transcriptional control of autophagy, and this regulation is conserved in *Drosophila* [75]. In yeast, GATA family factors include the relatively well-studied activators Gat1 and Gln3, and the repressors Gzf3 and Dal80. In addition to these factors, there are other DNA-binding proteins containing the conserved GATA-type zinc finger in yeast, such as Gat2, Gat3 and Gat4, whose functions are not clear. Whether other GATA family factors besides Gln3, have roles in the regulation of autophagy is not yet known.

In mammals, GATA1 activates the transcription of *ATG4*, *ATG12*, *BNIP3*, and mammalian homologs of *ATG8* (*MAP1LC3B*, *GABARAP*, *GABARAPL1*, and *GABARAPL2/GATE-16*). GATA1 directly binds at the promoters of *BNIP3*, *MAP1LC3B*, *GABARAP*, and *GABARAPL2* [76]. Interestingly, GATA1 activates the transcription of *FOXO3*, and transcriptional regulation of *MAP1LC3B* requires *FOXO3*. In contrast, knockdown of *TFEB* does not affect GATA1-mediated autophagy gene induction [76]. Another GATA transcription factor, GATA4, inhibits autophagy by inducing the transcription of *BCL2*, and repressing the transcription of *ATG5*, *ATG7*, *ATG12*, and *BECN1* [77], which is surprising because GATA4 is generally known as a transcriptional activator. Whether GATA4 represses transcription of *ATG* genes through direct binding at their promoters is unclear at this time.

1.4.5 Other transcription factors

Other transcription factors such as TP53/p53 and STAT are involved in autophagy regulation, and their roles have been reviewed recently [78, 79]. The function of the yeast transcriptional repressor Ume6, and Pho23 in autophagy regulation will be discussed in detail in Chapters 2 and 3, respectively. Collaborating with Amélie Bernard, a postdoc from the lab, to further explore the transcriptional regulation network of autophagy, we analyzed the transcriptional change of seven *ATG* genes before and after autophagy induction by real-time reverse transcription-PCR (qRT-PCR) in ~150 yeast mutant strains. We newly identified several autophagy transcription regulators from this large-scale study, and the detailed results are discussed in Chapter 4. One of these newly identified autophagy regulators, Rph1, was further studied with regard to the detailed mechanism of its regulation of autophagy, and the results are discussed in Chapter 5.

1.5 References

- [1] Xie, Z. and Klionsky, D.J. (2007) Autophagosome formation: core machinery and adaptations. *Nat Cell Biol.* 9, 1102-9.
- [2] Reggiori, F. and Klionsky, D.J. (2013) Autophagic processes in yeast: mechanism, machinery and regulation. *Genetics.* 194, 341-61.
- [3] Noda, T., Suzuki, K. and Ohsumi, Y. (2002) Yeast autophagosomes: de novo formation of a membrane structure. *Trends Cell Biol.* 12, 231-5.
- [4] Kovacs, A.L., Palfia, Z., Rez, G., Vellai, T. and Kovacs, J. (2007) Sequestration revisited: integrating traditional electron microscopy, de novo assembly and new results. *Autophagy.* 3, 655-62.
- [5] Sawa-Makarska, J., Abert, C., Romanov, J., Zens, B., Ibiricu, I. and Martens, S. (2014) Cargo binding to Atg19 unmasks additional Atg8 binding sites to mediate membrane-cargo apposition during selective autophagy. *Nat. Cell Biol.* 16, 425–433.
- [6] Mijaljica, D., Nazarko, T.Y., Brumell, J.H., Huang, W.P., Komatsu, M., Prescott, M., Simonsen, A., Yamamoto, A., Zhang, H., Klionsky, D.J. and Devenish, R.J. (2012) Receptor protein complexes are in control of autophagy. *Autophagy.* 8, 1701-5.
- [7] Lynch-Day, M.A. and Klionsky, D.J. (2010) The Cvt pathway as a model for selective autophagy. *FEBS Lett.* 584, 1359-66.

- [8] MacIsaac, K.D., Wang, T., Gordon, D.B., Gifford, D.K., Stormo, G.D. and Fraenkel, E. (2006) An improved map of conserved regulatory sites for *Saccharomyces cerevisiae*. BMC Bioinformatics. 7, 113.
- [9] Mizushima, N. (2010) The role of the Atg1/ULK1 complex in autophagy regulation. Curr Opin Cell Biol. 22, 132-9.
- [10] Yang, Z. and Klionsky, D.J. (2010) Mammalian autophagy: core molecular machinery and signaling regulation. Curr Opin Cell Biol. 22, 124-31.
- [11] Yorimitsu, T., Zaman, S., Broach, J.R. and Klionsky, D.J. (2007) Protein kinase A and Sch9 cooperatively regulate induction of autophagy in *Saccharomyces cerevisiae*. Mol Biol Cell. 18, 4180-9.
- [12] Matsuura, A., Tsukada, M., Wada, Y. and Ohsumi, Y. (1997) Apg1p, a novel protein kinase required for the autophagic process in *Saccharomyces cerevisiae*. Gene. 192, 245-50.
- [13] Straub, M., Bredschneider, M. and Thumm, M. (1997) AUT3, a serine/threonine kinase gene, is essential for autophagocytosis in *Saccharomyces cerevisiae*. J Bacteriol. 179, 3875-83.
- [14] Kamada, Y., Funakoshi, T., Shintani, T., Nagano, K., Ohsumi, M. and Ohsumi, Y. (2000) Tor-mediated induction of autophagy via an Apg1 protein kinase complex. J Cell Biol. 150, 1507-13.
- [15] Kabeya, Y., Kamada, Y., Baba, M., Takikawa, H., Sasaki, M. and Ohsumi, Y. (2005) Atg17 functions in cooperation with Atg1 and Atg13 in yeast autophagy. Mol Biol Cell. 16, 2544-53.
- [16] Cao, Y., Nair, U., Yasumura-Yorimitsu, K. and Klionsky, D.J. (2009) A multiple ATG gene knockout strain for yeast two-hybrid analysis. Autophagy. 5, 699-705.
- [17] Cheong, H., Nair, U., Geng, J. and Klionsky, D.J. (2008) The Atg1 kinase complex is involved in the regulation of protein recruitment to initiate sequestering vesicle formation for nonspecific autophagy in *Saccharomyces cerevisiae*. Mol Biol Cell. 19, 668-81.
- [18] Suzuki, K., Kubota, Y., Sekito, T. and Ohsumi, Y. (2007) Hierarchy of Atg proteins in pre-autophagosomal structure organization. Genes Cells. 12, 209-18.
- [19] Mao, K., Chew, L.H., Inoue-Aono, Y., Cheong, H., Nair, U., Popelka, H., Yip, C.K. and Klionsky, D.J. (2013) Atg29 phosphorylation regulates coordination of the Atg17-Atg31-Atg29 complex with the Atg11 scaffold during autophagy initiation. Proc Natl Acad Sci U S A. 110, E2875-84.
- [20] Yeh, Y.Y., Wrasman, K. and Herman, P.K. (2010) Autophosphorylation within the Atg1 activation loop is required for both kinase activity and the induction of autophagy in *Saccharomyces cerevisiae*. Genetics. 185, 871-82.
- [21] Russell, R.C., Tian, Y., Yuan, H., Park, H.W., Chang, Y.Y., Kim, J., Kim, H., Neufeld, T.P., Dillin, A. and Guan, K.L. (2013) ULK1 induces autophagy by phosphorylating Beclin-1 and activating VPS34 lipid kinase. Nat Cell Biol. 15, 741-50.
- [22] Papinski, D., Schuschnig, M., Reiter, W., Wilhelm, L., Barnes, C.A., Maiolica, A., Hansmann, I., Pfaffenwimmer, T., Kijanska, M., Stoffel, I., Lee, S.S., Brezovich, A., Lou, J.H., Turk, B.E., Aebersold, R., Ammerer, G., Peter, M. and Kraft, C. (2014) Early steps in autophagy depend on direct phosphorylation of Atg9 by the Atg1 kinase. Mol Cell. 53, 471-83.
- [23] Araki, Y., Ku, W.C., Akioka, M., May, A.I., Hayashi, Y., Arisaka, F., Ishihama, Y. and Ohsumi, Y. (2013) Atg38 is required for autophagy-specific phosphatidylinositol 3-kinase complex integrity. J Cell Biol. 203, 299-313.
- [24] Jao, C.C., Ragusa, M.J., Stanley, R.E. and Hurley, J.H. (2013) A HORMA domain in

- Atg13 mediates PI 3-kinase recruitment in autophagy. *Proc. Natl. Acad. Sci. U.S.A.* 110, 5486–5491.
- [25] Kihara, A., Noda, T., Ishihara, N. and Ohsumi, Y. (2001) Two distinct Vps34 phosphatidylinositol 3-kinase complexes function in autophagy and carboxypeptidase Y sorting in *Saccharomyces cerevisiae*. *J. Cell Biol.* 152, 519–530. [
- [26] Juhasz, G., Hill, J.H., Yan, Y., Sass, M., Baehrecke, E.H., Backer, J.M. and Neufeld, T.P. (2008) The class III PI(3)K Vps34 promotes autophagy and endocytosis but not TOR signaling in *Drosophila*. *J Cell Biol.* 181, 655-66.
- [27] Stromhaug, P.E., Reggiori, F., Guan, J., Wang, C.W. and Klionsky, D.J. (2004) Atg21 is a phosphoinositide binding protein required for efficient lipidation and localization of Atg8 during uptake of aminopeptidase I by selective autophagy. *Mol Biol Cell.* 15, 3553-66.
- [28] Ichimura, Y., Kirisako, T., Takao, T., Satomi, Y., Shimonishi, Y., Ishihara, N., Mizushima, N., Tanida, I., Kominami, E., Ohsumi, M., Noda, T. and Ohsumi, Y. (2000) A ubiquitin-like system mediates protein lipidation. *Nature.* 408, 488-92.
- [29] Mizushima, N., Noda, T., Yoshimori, T., Tanaka, Y., Ishii, T., George, M.D., Klionsky, D.J., Ohsumi, M. and Ohsumi, Y. (1998) A protein conjugation system essential for autophagy. *Nature.* 395, 395-8.
- [30] Shintani, T., Mizushima, N., Ogawa, Y., Matsuura, A., Noda, T. and Ohsumi, Y. (1999) Apg10p, a novel protein-conjugating enzyme essential for autophagy in yeast. *Embo J.* 18, 5234-41.
- [31] Mizushima, N., Noda, T. and Ohsumi, Y. (1999) Apg16p is required for the function of the Apg12p-Apg5p conjugate in the yeast autophagy pathway. *Embo J.* 18, 3888-96.
- [32] Kuma, A., Mizushima, N., Ishihara, N. and Ohsumi, Y. (2002) Formation of the approximately 350-kDa Apg12-Apg5-Apg16 multimeric complex, mediated by Apg16 oligomerization, is essential for autophagy in yeast. *J Biol Chem.* 277, 18619-25.
- [33] Hanada, T., Noda, N.N., Satomi, Y., Ichimura, Y., Fujioka, Y., Takao, T., Inagaki, F. and Ohsumi, Y. (2007) The Atg12-Atg5 conjugate has a novel E3-like activity for protein lipidation in autophagy. *J Biol Chem.* 282, 37298-302.
- [34] Cao, Y., Cheong, H., Song, H. and Klionsky, D.J. (2008) In vivo reconstitution of autophagy in *Saccharomyces cerevisiae*. *J Cell Biol.* 182, 703-13.
- [35] Mizushima, N., Yamamoto, A., Hatano, M., Kobayashi, Y., Kabeya, Y., Suzuki, K., Tokuhiya, T., Ohsumi, Y. and Yoshimori, T. (2001) Dissection of autophagosome formation using Apg5-deficient mouse embryonic stem cells. *J Cell Biol.* 152, 657-68.
- [36] Huang, W.-P., Scott, S.V., Kim, J. and Klionsky, D.J. (2000) The itinerary of a vesicle component, Aut7p/Cvt5p, terminates in the yeast vacuole via the autophagy/Cvt pathways. *J Biol Chem.* 275, 5845-51.
- [37] Kirisako, T., Ichimura, Y., Okada, H., Kabeya, Y., Mizushima, N., Yoshimori, T., Ohsumi, M., Takao, T., Noda, T. and Ohsumi, Y. (2000) The reversible modification regulates the membrane-binding state of Apg8/Aut7 essential for autophagy and the cytoplasm to vacuole targeting pathway. *J Cell Biol.* 151, 263-76.
- [38] Shintani, T., Huang, W.P., Stromhaug, P.E. and Klionsky, D.J. (2002) Mechanism of cargo selection in the cytoplasm to vacuole targeting pathway. *Dev Cell.* 3, 825-37.
- [39] Xie, Z., Nair, U. and Klionsky, D.J. (2008) Atg8 controls phagophore expansion during autophagosome formation. *Mol Biol Cell.* 19, 3290-8.
- [40] Kaufmann, A., Beier, V., Franquelim, H.G. and Wollert, T. (2014) Molecular mechanism of autophagic membrane-scaffold assembly and disassembly. *Cell.* 156, 469-81.

- [41] Noda, T., Kim, J., Huang, W.-P., Baba, M., Tokunaga, C., Ohsumi, Y. and Klionsky, D.J. (2000) Apg9p/Cvt7p is an integral membrane protein required for transport vesicle formation in the Cvt and autophagy pathways. *J Cell Biol.* 148, 465-80.
- [42] Reggiori, F., Tucker, K.A., Stromhaug, P.E. and Klionsky, D.J. (2004) The Atg1-Atg13 complex regulates Atg9 and Atg23 retrieval transport from the pre-autophagosomal structure. *Dev Cell.* 6, 79-90.
- [43] Mari, M., Griffith, J., Rieter, E., Krishnappa, L., Klionsky, D.J. and Reggiori, F. (2010) An Atg9-containing compartment that functions in the early steps of autophagosome biogenesis. *J Cell Biol.* 190, 1005-22.
- [44] Sekito, T., Kawamata, T., Ichikawa, R., Suzuki, K. and Ohsumi, Y. (2009) Atg17 recruits Atg9 to organize the pre-autophagosomal structure. *Genes Cells.* 14, 525-38.
- [45] Yen, W.L., Legakis, J.E., Nair, U. and Klionsky, D.J. (2007) Atg27 is required for autophagy-dependent cycling of Atg9. *Mol Biol Cell.* 18, 581-93.
- [46] Reggiori, F., Shintani, T., Nair, U. and Klionsky, D.J. (2005) Atg9 cycles between mitochondria and the pre-autophagosomal structure in yeasts. *Autophagy.* 1, 101-9.
- [47] Yamamoto, H., Kakuta, S., Watanabe, T.M., Kitamura, A., Sekito, T., Kondo-Kakuta, C., Ichikawa, R., Kinjo, M. and Ohsumi, Y. (2012) Atg9 vesicles are an important membrane source during early steps of autophagosome formation. *J Cell Biol.* 198, 219-33.
- [48] Ragusa, M.J., Stanley, R.E. and Hurley, J.H. (2012) Architecture of the Atg17 complex as a scaffold for autophagosome biogenesis. *Cell.* 151, 1501-12.
- [49] Nixon, R.A. (2013) The role of autophagy in neurodegenerative disease. *Nat Med.* 19, 983-97.
- [50] Nakai, A., Yamaguchi, O., Takeda, T., Higuchi, Y., Hikoso, S., Taniike, M., Omiya, S., Mizote, I., Matsumura, Y., Asahi, M., Nishida, K., Hori, M., Mizushima, N. and Otsu, K. (2007) The role of autophagy in cardiomyocytes in the basal state and in response to hemodynamic stress. *Nat Med.* 13, 619-24.
- [51] Perlmutter, D.H. (2009) Autophagic disposal of the aggregation-prone protein that causes liver inflammation and carcinogenesis in alpha-1-antitrypsin deficiency. *Cell Death Differ.* 16, 39-45.
- [52] Deretic, V. (2012) Autophagy as an innate immunity paradigm: expanding the scope and repertoire of pattern recognition receptors. *Curr Opin Immunol.* 24, 21-31.
- [53] Kuma, A., Hatano, M., Matsui, M., Yamamoto, A., Nakaya, H., Yoshimori, T., Ohsumi, Y., Tokuhiya, T. and Mizushima, N. (2004) The role of autophagy during the early neonatal starvation period. *Nature.* 432, 1032-6.
- [54] Tsukamoto, S., Kuma, A., Murakami, M., Kishi, C., Yamamoto, A. and Mizushima, N. (2008) Autophagy is essential for preimplantation development of mouse embryos. *Science.* 321, 117-20.
- [55] Ravikumar, B., Sarkar, S., Davies, J.E., Futter, M., Garcia-Arencibia, M., Green-Thompson, Z.W., Jimenez-Sanchez, M., Korolchuk, V.I., Lichtenberg, M., Luo, S., Massey, D.C., Menzies, F.M., Moreau, K., Narayanan, U., Renna, M., Siddiqi, F.H., Underwood, B.R., Winslow, A.R. and Rubinsztein, D.C. (2010) Regulation of mammalian autophagy in physiology and pathophysiology. *Physiol Rev.* 90, 1383-435.
- [56] Nedjic, J., Aichinger, M., Mizushima, N. and Klein, L. (2009) Macroautophagy, endogenous MHC II loading and T cell selection: the benefits of breaking the rules. *Curr Opin Immunol.* 21, 92-7.

- [57] Chen, D., Pang, S., Feng, X., Huang, W., Hawley, R.G. and Yan, B. (2013) Genetic analysis of the ATG7 gene promoter in sporadic Parkinson's disease. *Neurosci Lett.* 534, 193-8.
- [58] Liu, H., He, Z., von Rutte, T., Yousefi, S., Hunger, R.E. and Simon, H.U. (2013) Down-regulation of autophagy-related protein 5 (ATG5) contributes to the pathogenesis of early-stage cutaneous melanoma. *Sci Transl Med.* 5, 202ra123.
- [59] Wang, J., Pan, X.L., Ding, L.J., Liu, D.Y., Da-Peng, L. and Jin, T. (2013) Aberrant expression of Beclin-1 and LC3 correlates with poor prognosis of human hypopharyngeal squamous cell carcinoma. *PLoS One.* 8, e69038.
- [60] Jo, Y.K., Kim, S.C., Park, I.J., Park, S.J., Jin, D.H., Hong, S.W., Cho, D.H. and Kim, J.C. (2012) Increased expression of ATG10 in colorectal cancer is associated with lymphovascular invasion and lymph node metastasis. *PLoS One.* 7, e52705.
- [61] Webb, A.E. and Brunet, A. (2014) FOXO transcription factors: key regulators of cellular quality control. *Trends Biochem Sci.* 39, 159-169.
- [62] Mammucari, C., Milan, G., Romanello, V., Masiero, E., Rudolf, R., Del Piccolo, P., Burden, S.J., Di Lisi, R., Sandri, C., Zhao, J., Goldberg, A.L., Schiaffino, S. and Sandri, M. (2007) FoxO3 controls autophagy in skeletal muscle in vivo. *Cell Metab.* 6, 458-71.
- [63] Zhao, J., Brault, J.J., Schild, A., Cao, P., Sandri, M., Schiaffino, S., Lecker, S.H. and Goldberg, A.L. (2007) FoxO3 coordinately activates protein degradation by the autophagic/lysosomal and proteasomal pathways in atrophying muscle cells. *Cell Metab.* 6, 472-83.
- [64] Xu, P., Das, M., Reilly, J. and Davis, R.J. (2011) JNK regulates FoxO-dependent autophagy in neurons. *Genes Dev.* 25, 310-22.
- [65] Demontis, F. and Perrimon, N. (2010) FOXO/4E-BP signaling in *Drosophila* muscles regulates organism-wide proteostasis during aging. *Cell.* 143, 813-25.
- [66] Venters, B.J., Wachi, S., Mavrich, T.N., Andersen, B.E., Jena, P., Sinnamon, A.J., Jain, P., Roller, N.S., Jiang, C., Hemeryck-Walsh, C. and Pugh, B.F. (2011) A comprehensive genomic binding map of gene and chromatin regulatory proteins in *Saccharomyces*. *Mol Cell.* 41, 480-92.
- [67] Settembre, C., Di Malta, C., Polito, V.A., Garcia Arencibia, M., Vetrini, F., Erdin, S., Erdin, S.U., Huynh, T., Medina, D., Colella, P., Sardiello, M., Rubinsztein, D.C. and Ballabio, A. (2011) TFEB links autophagy to lysosomal biogenesis. *Science.* 332, 1429-33.
- [68] Palmieri, M., Impey, S., Kang, H., di Ronza, A., Pelz, C., Sardiello, M. and Ballabio, A. (2011) Characterization of the CLEAR network reveals an integrated control of cellular clearance pathways. *Hum Mol Genet.* 20, 3852-66.
- [69] Chauhan, S., Goodwin, J.G., Manyam, G., Wang, J., Kamat, A.M. and Boyd, D.D. (2013) ZKSCAN3 is a master transcriptional repressor of autophagy. *Mol Cell.* 50, 16-28.
- [70] Bellot, G., Garcia-Medina, R., Gounon, P., Chiche, J., Roux, D., Pouyssegur, J. and Mazure, N.M. (2009) Hypoxia-induced autophagy is mediated through hypoxia-inducible factor induction of BNIP3 and BNIP3L via their BH3 domains. *Mol Cell Biol.* 29, 2570-81.
- [71] Shaw, J., Yurkova, N., Zhang, T., Gang, H., Aguilar, F., Weidman, D., Scramstad, C., Weisman, H. and Kirshenbaum, L.A. (2008) Antagonism of E2F-1 regulated Bnip3 transcription by NF-kappaB is essential for basal cell survival. *Proc Natl Acad Sci U S A.* 105, 20734-9.
- [72] Polager, S., Ofir, M. and Ginsberg, D. (2008) E2F1 regulates autophagy and the transcription of autophagy genes. *Oncogene.* 27, 4860-4.
- [73] Copetti, T., Bertoli, C., Dalla, E., Demarchi, F. and Schneider, C. (2009) p65/RelA modulates BECN1 transcription and autophagy. *Mol Cell Biol.* 29, 2594-608.

- [74] Chan, T.F., Bertram, P.G., Ai, W. and Zheng, X.F. (2001) Regulation of APG14 expression by the GATA-type transcription factor Gln3p. *J Biol Chem.* 276, 6463-7.
- [75] Banreti, A., Lukacsovich, T., Csikos, G., Erdelyi, M. and Sass, M. (2012) PP2A regulates autophagy in two alternative ways in *Drosophila*. *Autophagy.* 8, 623-36.
- [76] Kang, Y.A., Sanalkumar, R., O'Geen, H., Linnemann, A.K., Chang, C.J., Bouhassira, E.E., Farnham, P.J., Keles, S. and Bresnick, E.H. (2012) Autophagy driven by a master regulator of hematopoiesis. *Mol Cell Biol.* 32, 226-39.
- [77] Kobayashi, S., Volden, P., Timm, D., Mao, K., Xu, X. and Liang, Q. (2010) Transcription factor GATA4 inhibits doxorubicin-induced autophagy and cardiomyocyte death. *J Biol Chem.* 285, 793-804.
- [78] Pietrocola, F., Izzo, V., Niso-Santano, M., Vacchelli, E., Galluzzi, L., Maiuri, M.C. and Kroemer, G. (2013) Regulation of autophagy by stress-responsive transcription factors. *Semin Cancer Biol.* 23, 310-22.
- [79] Fullgrabe, J., Klionsky, D.J. and Joseph, B. (2014) The return of the nucleus: transcriptional and epigenetic control of autophagy. *Nat Rev Mol Cell Biol.* 15, 65-74.

CHAPTER 2. The Ume6 Transcription Factor is Part of a Signaling Cascade that Regulates Autophagy²

2.1 Abstract

Autophagy has been implicated in a number of physiological processes important for human health and disease. Autophagy involves the formation of a double-membrane cytosolic vesicle, an autophagosome. Central to the formation of the autophagosome is the ubiquitin-like protein Atg8 (LC3 in mammalian cells). Following autophagy induction, Atg8 shows the greatest change in expression of any of the proteins required for autophagy. The magnitude of autophagy is in part controlled by the amount of Atg8; thus, controlling Atg8 protein levels is one potential mechanism for modulating autophagy activity. We have identified a negative regulator of *ATG8* transcription, Ume6, which acts along with a histone deacetylase complex including Sin3 and Rpd3 to negatively regulate Atg8 levels; deletion of any of these components leads to an increase in Atg8 and a concomitant increase in autophagic activity. A similar regulatory mechanism is present in mammalian cells, indicating that this process is highly conserved.

2.2 Introduction

Macroautophagy, hereafter referred to as autophagy, is an evolutionarily conserved process employed by eukaryotic cells for the bulk degradation of intracellular proteins and organelles (1). Autophagy is not only vital for cell survival in nutrient-poor conditions (2), but is also linked to

² This chapter is reprinted from Clinton R. Bartholomew, Tsukasa Suzuki, Zhou Du, Steven K. Backues, Meiyang Jin, Melinda A. Lynch-Day, Midori Umekawa, Avani Kamath, Mantong Zhao, Zhiping Xie, Ken Inoki, and Daniel J. Klionsky. Ume6 transcription factor is part of a signaling cascade that regulates autophagy. PNAS 2012; 109 (28) 11206-10; doi:10.1073/pnas.1200313109, with minor modifications.

various physiological processes including immune defense, tumor suppression, and prevention of neurodegeneration (3). Whereas autophagy plays a primary protective role, it can also contribute to cell death; thus, the magnitude of autophagy must be carefully regulated.

Central to autophagy is the formation of autophagosomes (4), double-membrane-bound structures that engulf and deliver cytoplasmic materials to the vacuole/lysosome for degradation. During autophagosome formation, the autophagy-related ubiquitin-like protein, Atg8/LC3, covalently modifies phosphatidylethanolamine (PE). Almost one-fourth of the characterized autophagy-related (Atg) proteins in yeast are involved in the formation or stability of Atg8–PE, which plays a critical role in controlling expansion of the phagophore (the initial sequestering membrane), and in determining autophagosome size, thereby regulating autophagy activity (5, 6). Upon starvation, the level of *ATG8* mRNA sharply increases leading to a subsequent induction of the Atg8 protein level (7, 8). The increase in the amount of Atg8 during autophagy is critical for supplying a sufficient amount of this protein to maintain normal levels of autophagy; yeast strains deficient in Atg8 induction generate abnormally small autophagosomes (5). Thus, characterization of how Atg8 protein levels are modulated is of tremendous importance in both understanding the regulation of autophagy and for the elucidation of potential therapeutic targets. However, little is known about the mechanisms regulating Atg8 transcription.

2.3 Results

2.3.1 The Ume6-Sin3-Rpd3 complex represses Atg8 expression.

To identify candidate transcriptional regulators of *ATG8*, we analyzed the promoter region and identified an upstream regulatory sequence, URS1, which is a consensus binding site for the transcription factor Ume6 (Figure 2.1A), which was previously identified during a whole-genome microarray analysis (9-11). The URS1 consensus site consists of two invariant GGC

repeats, which tend to be immediately preceded by a C and several T nucleotides, and followed by a T and two A nucleotides, although some variability exists in these positions (9). We examined the promoter regions of other ATG genes and note that the gene encoding Atg23 also contains a potential URS1 site. Ume6 is a zinc cluster protein that both represses and activates transcription of a diverse set of genes involved in meiosis and metabolism in response to nutritional cues such as glucose, nitrogen and inositol (9, 12-14). If Ume6 regulates Atg8 then a *ume6Δ* strain should have altered Atg8 protein levels. We examined the protein level of Atg8 in a *ume6Δ* strain in vegetative (growing) conditions and found that it was substantially induced relative to the wild type (Figure 2.1B).

Ume6 exerts control of transcription by forming a complex with the co-repressor Sin3 and the histone deacetylase Rpd3 (15). Accordingly, we extended our analysis by examining the level of Atg8 in *rpd3Δ* and *sin3Δ* strains. Similar to the result with the *ume6Δ* strain, both the *sin3Δ* and *rpd3Δ* strains displayed a substantial induction of Atg8 expression in nutrient-rich conditions (Figure 2.1B). Together, our data suggest that the Ume6-Sin3-Rpd3 complex negatively regulates Atg8 expression, and consequently the amount of Atg8, available during autophagy.

2.3.2 *Ume6 binds the ATG8 promoter and negatively regulates ATG8 transcription.*

To determine whether Ume6 regulates *ATG8* at a transcriptional level, we examined β -galactosidase activity in wild-type and *ume6Δ* strains expressing LacZ under the control of the *ATG8* promoter in nutrient-rich and nitrogen starvation conditions. The β -galactosidase activity in the *ume6Δ* strain was substantially higher than that seen in the wild-type strain under growing conditions (Figure 2.2A), suggesting that Ume6 negatively regulates *ATG8* transcription, rather than exerting its effect directly on the Atg8 protein. The β -galactosidase activity in the *ume6Δ*

strain increased only slightly under starvation conditions, suggesting that the transcription of *ATG8* in growing conditions was close to the maximal level seen when fully induced (Figure 2.2A). To further test if Ume6 binds the *ATG8* promoter, we conducted a chromatin immunoprecipitation (ChIP) analysis in a strain expressing Ume6 tagged with protein A (Ume6-PA). We examined the binding of Ume6-PA to the *ATG8* URS1 region and a sequence 3 kb upstream of the *ATG8* start codon (-3K) region which served as a negative control; binding at the promoter of *INO1* was examined as a positive control (16). The quantitative-PCR results showed that Ume6-PA binding to the URS1 region was approximately 19 times higher than that seen in the -3K control and was at a level similar to that detected for the *INO1* promoter (Figure 2.2B), suggesting that Ume6 actually bound to the *URS1* element of the *ATG8* promoter.

2.3.3 Rim15 promotes Ume6 phosphorylation and functions as a positive regulator of Atg8 induction.

During meiosis, removal of Sin3 and Rpd3 from the Ume6 complex is regulated by the protein kinase Rim15 in response to nitrogen and glucose limitation. For example, when cells are grown on acetate as the sole carbon source in conditions of nitrogen limitation, Rim15 promotes Ume6 phosphorylation and disrupts the association of Sin3 and Rpd3 with the complex, thus relieving transcriptional repression of the target genes (12). In addition, we have shown that Rim15 is a positive regulator of autophagy (17, 18), although its relevant target(s) had not been identified. Therefore, we decided to investigate a potential role for Rim15 in Ume6-regulated Atg8 induction. Accordingly, we first tested whether Rim15 promotes Ume6 phosphorylation during autophagy. In wild-type cells upon nitrogen starvation, Ume6 exhibited a slower migration, which is consistent with the previous finding (12) that Ume6 is subject to phosphorylation (Figure 2.3A). However, *RIM15* deletion caused a block in Ume6

phosphorylation in starvation conditions, suggesting that Rim15 promotes Ume6 phosphorylation during autophagy (Figure 2.3A).

To further investigate the role of Rim15 in regulating Atg8 induction, we decided to examine Atg8 levels in the presence and absence of this kinase. Accurate measurement of Atg8 levels is complicated by the continuous degradation of Atg8-PE in the vacuole during autophagy (Atg8 is one of the few Atg proteins that remains associated with the completed autophagosome, and a portion of the protein is delivered into the vacuole lumen where it is degraded). Thus, we utilized a *pep4Δ* background strain. The hydrolase activity of Pep4, a vacuolar aspartyl protease, is required for the breakdown of autophagic bodies (the single-membrane intraluminal vesicles that result from fusion of autophagosomes with the vacuole), and the subsequent degradation of Atg8-PE. Therefore, we examined Atg8 levels in wild-type, *rim15Δ* and *rim15Δ ume6Δ* strains in which the *PEP4* locus was deleted to prevent the turnover of Atg8-PE. Prior to nitrogen starvation, wild-type cells displayed a basal level of Atg8, and even after a short 15-min period of nitrogen starvation, an increase in Atg8-PE could be detected (Figure 2.3B). In *rim15Δ* cells, the basal level of Atg8 was clearly lower, and there was a lag in the generation of Atg8-PE, indicating that Rim15 functions as a positive regulator of Atg8 induction. Deletion of *UME6* in the *rim15Δ* strain rescued the induction defect in response to nitrogen starvation, suggesting that Rim15 acts upstream of Ume6 to regulate Atg8 synthesis during autophagy.

2.3.4 *Ume6 negatively regulates autophagy activity.*

To determine if modulation of Atg8 levels by Ume6 has a physiological effect on autophagy we measured autophagy activity using the Pho8Δ60 assay (19). This assay measures the autophagy-dependent alkaline phosphatase activity of Pho8Δ60, a modified vacuolar alkaline phosphatase precursor that remains in the cytosol; Pho8Δ60 can only be delivered to the vacuole

via autophagy, in which case a C-terminal propeptide is subsequently removed, resulting in enzymatic activation. Therefore, the alkaline phosphatase activity of Pho8 Δ 60 reflects the magnitude of nonselective autophagic cargo delivery.

In growing conditions, the wild-type strain displayed a basal level of Pho8 Δ 60-dependent alkaline phosphatase activity, whereas the *ume6* Δ strain displayed an increase in the basal level of autophagy consistent with a role for Ume6 in negatively regulating autophagy by limiting the amount of Atg8 (Figure 2.4A, 0 h SD-N). Upon nitrogen starvation, Pho8 Δ 60 activity increased in the wild-type cells, but remained at the background level in an *atg1* Δ mutant, which is defective for autophagy. In *ume6* Δ cells, autophagy was induced more rapidly and to a higher level as indicated by Pho8 Δ 60 activity compared to that seen in the wild type (Figure 2.4A). Thus, Ume6 acts as a negative regulator of autophagy activity.

We further sought to determine how deletion of *UME6* caused an upregulation of autophagy. An increase in the magnitude of autophagic cargo delivery suggested the possibility that more autophagosomes were being formed and/or the size of the autophagosomes were increased in the *ume6* Δ strain as compared to the wild-type cells. After nitrogen starvation for either 1 or 2 h, the number and size of autophagic bodies per cell was examined by transmission electron microscopy (TEM) analysis after 1 and 2 h starvation. The mean number of autophagic bodies per cell section was slightly higher in the *ume6* Δ cells than wild-type at the 1 h (3.1 ± 0.4 and 2.3 ± 0.3 , respectively) and 2 h (4.7 ± 0.4 and 4.0 ± 0.4 , respectively) time points, but this difference was not statistically significant [$p = 0.25$ (1 h) and $p = 0.19$ (2 h)]. A highly significant difference ($p < 5 \times 10^{-8}$), however, was observed in the size of the autophagic bodies. The autophagic bodies of *ume6* Δ cells had an average cross-sectional radius that was 22% and 17% larger than that found in the wild-type cells at the 1 and 2 h time points, respectively (Figure

2.4B,C and Figure 2.S1). Notably, this translates into a substantial difference in average volume. To estimate the actual volume of the autophagic bodies from the observed cross-sectional radii, we used a statistical method previously developed for this purpose (20). The calculations indicated that the *ume6Δ* cells had autophagosomes that were 68% and 112% larger by volume than wild-type autophagosomes at the 1- and 2-h time points, respectively. This approximately 2.1-fold increase in autophagosome volume at the 2-h time point is quite similar to the 1.8-fold increase in Pho8Δ60 activity at the same time point (Figure 2.4A,B); thus, a small increase in the diameter of autophagosomes has robust effects on the magnitude of bulk autophagy. We also noted that the average cross-sectional area of the wild-type and *ume6Δ* cells was 7.3 μm² and 11.6 μm², respectively, based on the measurements of over 300 cells each; however, no data suggest that autophagosome or autophagic body size is affected by cell size.

2.3.5 *SIN3A* and *SIN3B* play redundant roles in regulating *LC3* expression.

We next explored the possibility that the mechanism of Atg8/LC3 regulation that we discovered here was conserved in higher eukaryotes. The transcription factor Ume6 has no clear homolog in mammalian cells, but two homologs of SIN3 (*SIN3A* and *SIN3B*) and eleven homologs of RPD3 exist in vertebrates. Accordingly, SIN3 was chosen for further study. *SIN3A* and *SIN3B* were knocked down by treating HeLa cells with three individual shRNA targeted to *SIN3A* and two individual shRNA targeted to *SIN3B* alone and in combination, with nearly identical results in terms of the degree of knockdown; *SIN3A* and *SIN3B* mRNA levels were reduced to approximately 9 to 30% and 15 to 36% of the scrambled control, respectively (Figure 2.5B). Knockdown of *SIN3A* and *SIN3B* individually had little or no effect on LC3 levels compared to the scrambled control (Figure 2.S2A). In contrast, when *SIN3A* and *SIN3B* were simultaneously knocked down, a robust increase in LC3 levels was readily apparent in various

shRNA combinations under nutrient-rich conditions in HeLa cells (Figure 2.5A,B). The same results were also found for HEK293T and human fibroblast cell lines (Figure 2.5A). The increase in LC3 protein levels was not attributable to indirect effects through protein level or activity of the MTOR complex, as the amount of MTOR and its associated protein RPTOR were unchanged (Figure 2.5A), nor was there an effect on the activity of MTORC1 or MTORC2 as determined by the phosphorylation state of their targets RPS6KB1/S6K and EIF4EBP1/4EBP1, or AKT1, respectively (Figure 2.5A, 2.S2B). Furthermore, we examined autophagic flux by exposing the cells to NH₄Cl, which raises the lysosomal pH and prevents the turnover of LC3 (similar in effect to deleting the *PEP4* gene in yeast). The presence of NH₄Cl resulted in elevated levels of LC3-II, indicating that the knockdown of SIN3A/B caused an increase in basal autophagy, and not just an increase in the level of LC3. Note that in human fibroblasts, the lack of a clear difference in LC3 levels in the absence, but not the presence, of NH₄Cl indicates a rapid rate of lysosomal turnover of this protein (21).

2.4 Discussion

Our findings suggest that in response to nitrogen starvation the kinase Rim15 phosphorylates Ume6. During meiosis this phosphorylation causes the dissociation of Ume6 from Sin3-Rpd3 leading to transcriptional activation (12, 14). Rim15 plays an important role in integrating many nutrient regulatory signals and therefore plays a central role in regulating autophagy (17, 22). Rim15 is negatively regulated through direct phosphorylation by cAMP-dependent protein kinase A (PKA) and Sch9 in the presence of glucose and nitrogen (23, 24), and is involved in the autophagy induction that occurs upon PKA-Sch9 inactivation (18). PKA and Sch9 are upstream sensors that act to negatively regulate autophagy; however, the downstream components in this signaling pathway are unknown, and how PKA and Sch9

signaling affects the autophagy machinery to regulate autophagosome formation has not been previously elucidated. Yeast Sch9 is homologous to mammalian RPS6KB2/p70S6 kinase or AKT1 (18). In mammalian cells, AKT1 phosphorylates and inactivates the FOXO family of transcription factors (25). During muscle atrophy FOXO3 induces the expression of multiple autophagy genes including *Lc3*, *Gabrapl1* (an *Lc3* homolog), *Ulk1*, *Atg4*, *Atg12*, *Pik3c3/Vps34* and *Becn1* (26, 27); and in hepatic tissue, FOXO1 regulates the autophagy genes *Gabarapl1*, *Pik3c2* and *Atg12* (28). Although Ume6 is not conserved in mammalian cells, the regulation of the FOXO family by Sch9 and AKT1 suggests that the pathway regulating Atg8/LC3 may be conserved from yeast to human. Just as the knockdown of SIN3A and SIN3B promotes an increase in cellular LC3 levels, inhibition of RPD3 promotes a similar increase (29-31), although the detailed mechanism has not been determined.

One frequently overlooked method of regulating the magnitude of autophagy is the regulation of the size of the autophagosome. Research in yeast has shown that the average size of the autophagosome is modulated by the amount of available Atg8 (5). Our results provide strong evidence that transcriptional repression plays a major role in regulating Atg8/LC3 levels, and this upregulation results in an increase in the size of the autophagosome. Basal autophagy is especially important in the liver and other cells such as neurons and myocytes, which, after differentiation, cease dividing. Modulation of LC3 levels through inhibition of histone deacetylation at the *LC3* locus may be a viable option to increase basal autophagy in non-dividing terminally differentiated cells.

2.5 Materials and Methods

2.5.1 Yeast.

Gene disruptions and PA tag integrations were performed using a standard method (32). Yeast cells were grown in rich medium (YPD; 1% yeast extract, 2% peptone and 2% glucose) or synthetic minimal medium (SMD; 0.67% yeast nitrogen base, 2% glucose, supplemented with the appropriate amino acids and vitamins). Autophagy was induced in starvation medium (SD-N; 0.17% yeast nitrogen base without amino acids, containing 2% glucose). The yeast strains used in this study are listed in Table 2.1. Protein extraction, immunoblot, GFP-Atg8 processing and alkaline phosphatase (Pho8 Δ 60) assays were performed as previously described (18, 19, 33). Yeast strains containing the β -galactosidase reporter plasmid ATG8p-LacZ(416) were grown in SMD or shifted to SD-N to induce autophagy, and then examined with a β -galactosidase assay as described previously (34). Chromatin immunoprecipitation was performed as previously described (35).

Samples for TEM were prepared as described previously (5). Sections (85 nm) were cut using a Leica Ultracut-E microtome at the University of Michigan Microscopy and Image Analysis Laboratory. Images were acquired on a Philips CM100 BioTwin electron microscope at the University of Michigan MCDB departmental TEM facility. The observed radii of the autophagic body cross-sections were determined and used to estimate the actual radii as described (20), which were converted to volume. Statistical significance was determined using the Mann-Whitney U test.

2.5.2 Cell Culture.

Knockdown of *SIN3* homologs was performed by cloning *SIN3A*- and *SIN3B*-targeted shRNA into the pLKO1 lentiviral expression vector, and these plasmids were co-transfected

together with psPAX2 and pMP2 plasmids into actively growing cells. HeLa, HEK293T, and human fibroblast cells were infected with isolated viruses, selected for puromycin resistance and analyzed on the 7th day after infection with scrambled DNA as a control. Cell lysates were suspended in NP-40 buffer and subjected to SDS-PAGE and western blot analysis.

2.6 Acknowledgments

D.J.K., C.R.B, M.J., M.Z., M.A.L.-D., Z.D., M.U. and Z.X. were supported by NIH grant GM53396. M.U. was also supported in part by the Japan Society for the Promotion of Science. K.I., T.S. and A.K. were supported by NIH grant DK083491.

2.7 References

1. Xie Z & Klionsky DJ (2007) Autophagosome formation: core machinery and adaptations. *Nat Cell Biol* 9:1102-1109.
2. Yorimitsu T & Klionsky DJ (2005) Autophagy: molecular machinery for self-eating. *Cell Death Differ* 12:1542-1552.
3. Mizushima N, Levine B, Cuervo AM, & Klionsky DJ (2008) Autophagy fights disease through cellular self-digestion. *Nature* 451:1069-1075.
4. Klionsky DJ, *et al.* (2011) A comprehensive glossary of autophagy-related molecules and processes (2nd edition). *Autophagy* 7:1273-1294.
5. Xie Z, Nair U, & Klionsky DJ (2008) Atg8 controls phagophore expansion during autophagosome formation. *Mol Biol Cell* 19:3290-3298.
6. Weidberg H, *et al.* (LC3 and GATE-16/GABARAP subfamilies are both essential yet act differently in autophagosome biogenesis. *EMBO J* 29:1792-1802.
7. Huang W-P, Scott SV, Kim J, & Klionsky DJ (2000) The itinerary of a vesicle component, Aut7p/Cvt5p, terminates in the yeast vacuole via the autophagy/Cvt pathways. *J Biol Chem* 275:5845-5851.
8. Kirisako T, *et al.* (1999) Formation process of autophagosome is traced with Apg8/Aut7p in yeast. *J Cell Biol* 147:435-446.
9. Williams RM, *et al.* (2002) The Ume6 regulon coordinates metabolic and meiotic gene expression in yeast. *Proc Natl Acad Sci USA* 99:13431-13436.
10. Park HD, Luche RM, & Cooper TG (1992) The yeast *UME6* gene product is required for transcriptional repression mediated by the *CARI URS1* repressor binding site. *Nucleic Acids Res* 20:1909-1915.
11. Strich R, *et al.* (1994) *UME6* is a key regulator of nitrogen repression and meiotic development. *Genes Dev* 8:796-810.
12. Pnueli L, Edry I, Cohen M, & Kassir Y (2004) Glucose and nitrogen regulate the switch from histone deacetylation to acetylation for expression of early meiosis-specific genes in budding yeast. *Mol Cell Biol* 24:5197-5208.

13. Washburn BK & Esposito RE (2001) Identification of the Sin3-binding site in Ume6 defines a two-step process for conversion of Ume6 from a transcriptional repressor to an activator in yeast. *Mol Cell Biol* 21:2057-2069.
14. Xiao Y & Mitchell AP (2000) Shared roles of yeast glycogen synthase kinase 3 family members in nitrogen-responsive phosphorylation of meiotic regulator Ume6p. *Mol Cell Biol* 20:5447-5453.
15. Kadosh D & Struhl K (1997) Repression by Ume6 involves recruitment of a complex containing Sin3 corepressor and Rpd3 histone deacetylase to target promoters. *Cell* 89:365-371.
16. Jackson JC & Lopes JM (1996) The yeast *UME6* gene is required for both negative and positive transcriptional regulation of phospholipid biosynthetic gene expression. *Nucleic Acids Res* 24:1322-1329.
17. Yang Z, Geng J, Yen W-L, Wang K, & Klionsky DJ (2010) Positive or negative roles of different cyclin-dependent kinase Pho85-cyclin complexes orchestrate induction of autophagy in *Saccharomyces cerevisiae*. *Mol Cell* 38:250-264.
18. Yorimitsu T, Zaman S, Broach JR, & Klionsky DJ (2007) Protein kinase A and Sch9 cooperatively regulate induction of autophagy in *Saccharomyces cerevisiae*. *Mol Biol Cell* 18:4180-4189.
19. Noda T, Matsuura A, Wada Y, & Ohsumi Y (1995) Novel system for monitoring autophagy in the yeast *Saccharomyces cerevisiae*. *Biochem Biophys Res Commun* 210:126-132.
20. Xie Z, *et al.* (2009) Indirect estimation of the area density of Atg8 on the phagophore. *Autophagy* 5:217-220.
21. Klionsky DJ, *et al.* (2012) Guidelines for the use and interpretation of assays for monitoring autophagy. *Autophagy* 8:in press.
22. Swinnen E, *et al.* (2006) Rim15 and the crossroads of nutrient signalling pathways in *Saccharomyces cerevisiae*. *Cell Div* 1:3.
23. Pedruzzi I, *et al.* (2003) TOR and PKA signaling pathways converge on the protein kinase Rim15 to control entry into G₀. *Mol Cell* 12:1607-1613.
24. Reinders A, Bürckert N, Boller T, Wiemken A, & De Virgilio C (1998) *Saccharomyces cerevisiae* cAMP-dependent protein kinase controls entry into stationary phase through the Rim15p protein kinase. *Genes Dev* 12:2943-2955.
25. Salih DA & Brunet A (2008) FoxO transcription factors in the maintenance of cellular homeostasis during aging. *Curr Opin Cell Biol* 20:126-136.
26. Mammucari C, *et al.* (2007) FoxO3 controls autophagy in skeletal muscle in vivo. *Cell Metab* 6:458-471.
27. Zhao J, *et al.* (2007) FoxO3 coordinately activates protein degradation by the autophagic/lysosomal and proteasomal pathways in atrophying muscle cells. *Cell Metab* 6:472-483.
28. Liu HY, *et al.* (2009) Hepatic autophagy is suppressed in the presence of insulin resistance and hyperinsulinemia: inhibition of FoxO1-dependent expression of key autophagy genes by insulin. *J Biol Chem* 284:31484-31492.
29. Park JH, *et al.* (2011) A new synthetic HDAC inhibitor, MHY218, induces apoptosis or autophagy-related cell death in tamoxifen-resistant MCF-7 breast cancer cells. *Invest New Drugs* in press.
30. Ahn MY, Ahn SG, & Yoon JH (2011) Apicidin, a histone deacetylase inhibitor, induces both apoptosis and autophagy in human oral squamous carcinoma cells. *Oral Oncol* 47:1032-1038.

31. Chen MY, *et al.* (2011) Decitabine and suberoylanilide hydroxamic acid (SAHA) inhibit growth of ovarian cancer cell lines and xenografts while inducing expression of imprinted tumor suppressor genes, apoptosis, G2/M arrest, and autophagy. *Cancer* 117:4424-4438.
32. Longtine MS, *et al.* (1998) Additional modules for versatile and economical PCR-based gene deletion and modification in *Saccharomyces cerevisiae*. *Yeast* 14:953-961.
33. Shintani T & Klionsky DJ (2004) Cargo proteins facilitate the formation of transport vesicles in the cytoplasm to vacuole targeting pathway. *J Biol Chem* 279:29889-29894.
34. Rose M & Botstein D (1983) Construction and use of gene fusions to *lacZ* (β -galactosidase) that are expressed in yeast. *Meth Enzymol* 101:167-180.
35. Aparicio O, *et al.* (2005) Chromatin immunoprecipitation for determining the association of proteins with specific genomic sequences in vivo. *Curr Protoc Mol Biol* Chapter 21:Unit 21 23.

Table 2.1 Strains used in this study

Strain	Genotype	Reference
BY4742	MAT α <i>his3Δ1 leu2Δ0 ura3Δ0</i>	Invitrogen
FRY143	SEY6210 <i>pep4Δ::LEU2 vps4Δ::TRP1</i>	(1)
<i>rim15Δ</i>	BY4742 <i>rim15Δ::KanMX6</i>	Invitrogen
<i>rpd3Δ</i>	BY4742 <i>rpd3Δ::KanMX6</i>	Invitrogen
SEY6210	MAT α <i>his3Δ200 leu2-3,112 lys2-801 suc2-Δ9 trp1Δ901 ura3-52</i>	(2)
<i>sin3Δ</i>	BY4742 <i>sin3Δ::KanMX6</i>	Invitrogen
<i>ume6Δ</i>	BY4742 <i>ume6Δ::KanMX6</i>	Invitrogen
W303-1B	MAT α <i>ade2-1 his3-11,15 leu2,3,112 trp1-1 ura3-1 can1-100</i>	(3)
YCB193	SEY6210 <i>pho8::pho8Δ60 pho13Δ</i>	This Study
YCB194	SEY6210 <i>atg1Δ::HIS3 pho8::pho8Δ60 pho13Δ</i>	This Study
YCB197	SEY6210 <i>ume6Δ::HIS3 pho8::pho8Δ60 pho13Δ</i>	This Study
YCB234	SEY6210 <i>pep4Δ::LEU2 vps4Δ::TRP1 ume6Δ::KanMX6</i>	This Study
YZD005	W303-1B <i>pep4Δ::URA3 pho13Δ pho8Δ60</i>	This Study
YZD006	W303-1B <i>pep4Δ::URA3 pho13Δ pho8Δ60 rim15Δ::BLE</i>	This Study
YZD007	W303-1B <i>pep4Δ::URA3 pho13Δ pho8Δ60 rim15Δ::BLE <i>ume6Δ::HIS3</i></i>	This Study

Table references:

(1) Cheong H, *et al.* (2005) Atg17 regulates the magnitude of the autophagic response. *Mol Biol Cell* 16:3438-3453.

(2) Robinson JS, Klionsky DJ, Banta LM, & Emr SD (1988) Protein sorting in *Saccharomyces cerevisiae*: isolation of mutants defective in the delivery and processing of multiple vacuolar hydrolases. *Mol Cell Biol* 8:4936-4948.

(3) Thomas BJ & Rothstein R (1989) Elevated recombination rates in transcriptionally active DNA. *Cell* 56:619-630.

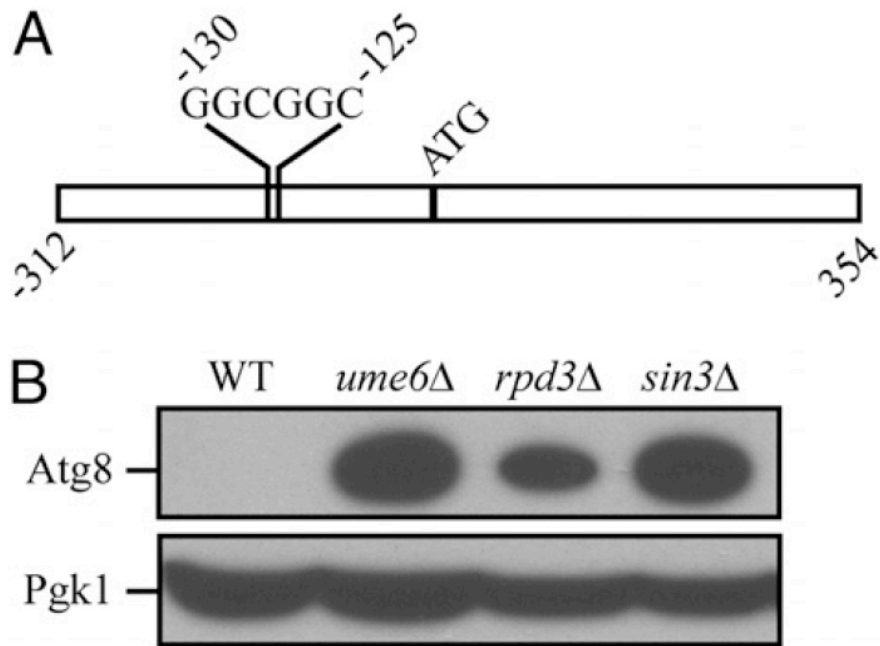


Figure 2.1 The Ume6-Sin3-Rpd3 complex represses *Atg8* expression.

(A) Diagram depicting the URS1 site in the *ATG8* promoter. (B) The Ume6-Sin3-Rpd3 complex represses *Atg8* expression. Wild-type (BY4742), *ume6* Δ , *sin3* Δ and *rpd3* Δ yeast cells were grown in rich medium to mid-log phase. Protein extracts from cells were prepared and subjected to immunoblotting with anti-*Atg8* and anti-*Pgk1* antiserum (the latter as a loading control).

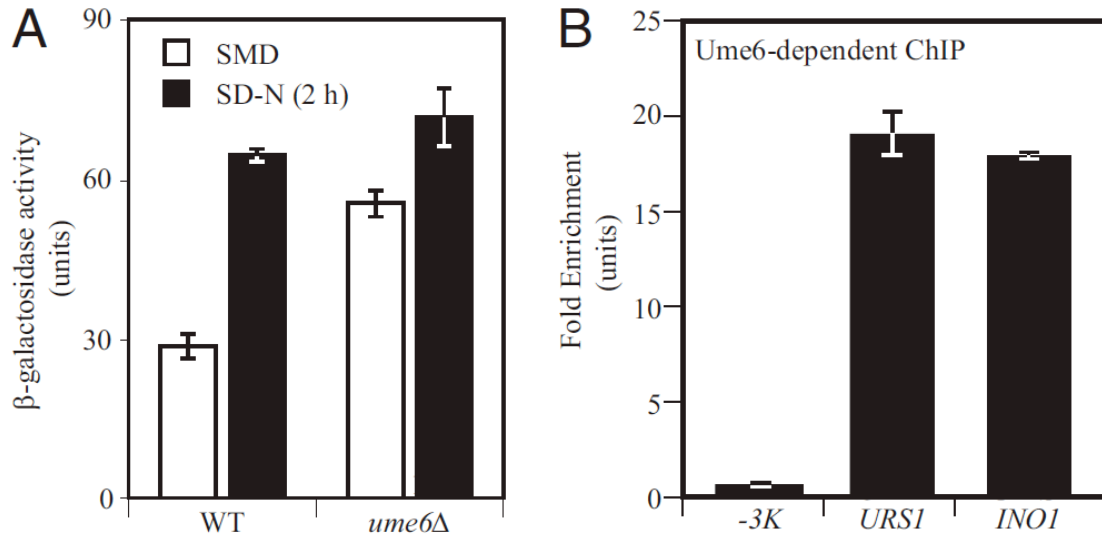


Figure 2.2 Ume6 binds the *ATG8* promoter and negatively regulates *ATG8* transcription. (A) Expression of Atg8-LacZ in a *UME6* deletion strain. Wild-type and *ume6Δ* cells containing LacZ driven by the *ATG8* promoter were grown to mid-log phase and switched to nitrogen starvation medium (SD-N) for 2 h. β -galactosidase activity was measured from protein extracts. (B) Protein A-tagged Ume6 binds the *ATG8* promoter. ChIP analysis was conducted on two regions of the *ATG8* promoter: the URS1 region and a region -3 kb upstream of the *ATG8* start codon (-3K), which was used as a negative control. The URS1 region in the *INO1* promoter served as a positive control. The ChIP results were normalized to the input DNA and calibrated to the -3K PCR product, which was set to 1.0. Error bars represent the standard deviation of at least three independent experiments.

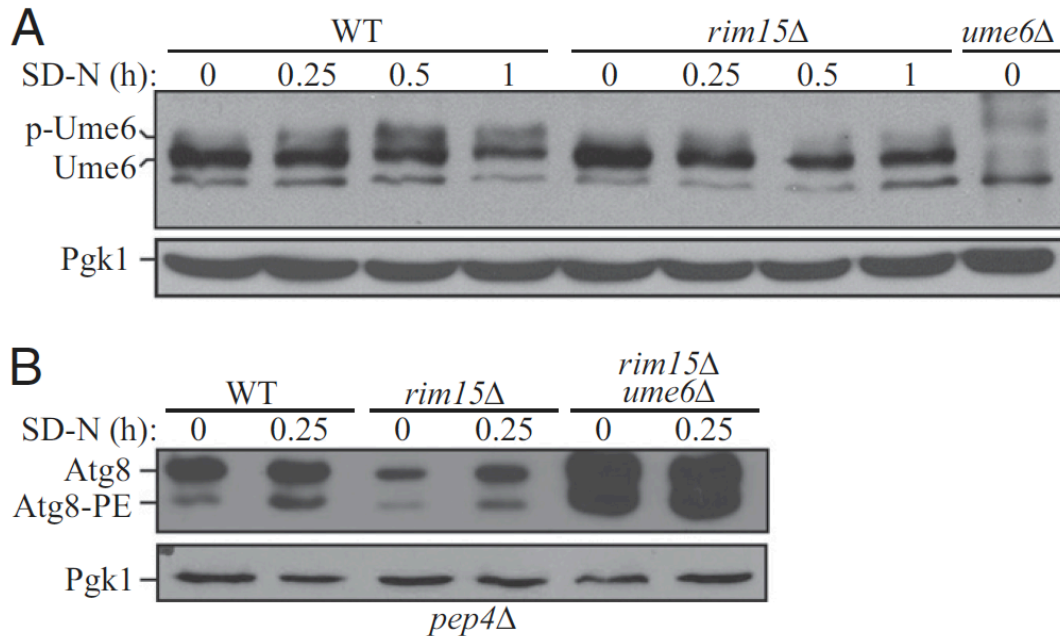


Figure 2.3 Rim15 promotes Ume6 phosphorylation and functions as a positive regulator of Atg8 induction.

(A) Rim15 is required for Ume6 phosphorylation in starvation conditions. Wild-type (WT, BY4742) and *rim15Δ* cells were grown in rich medium and starved in SD-N for up to 1 h. Cells were collected and protein extracts were analyzed with anti-Ume6 and anti-Pgk1 (loading control) antisera. (B) Wild-type (WT, YZD005), *rim15Δ* (YZD006), and *rim15Δ ume6Δ* (YZD007) cells in a *pep4Δ* background were grown in rich medium and shifted to SD-N for starvation. Cells were collected at the indicated time points and subjected to immunoblotting with anti-Atg8 and anti-Pgk1 antisera.

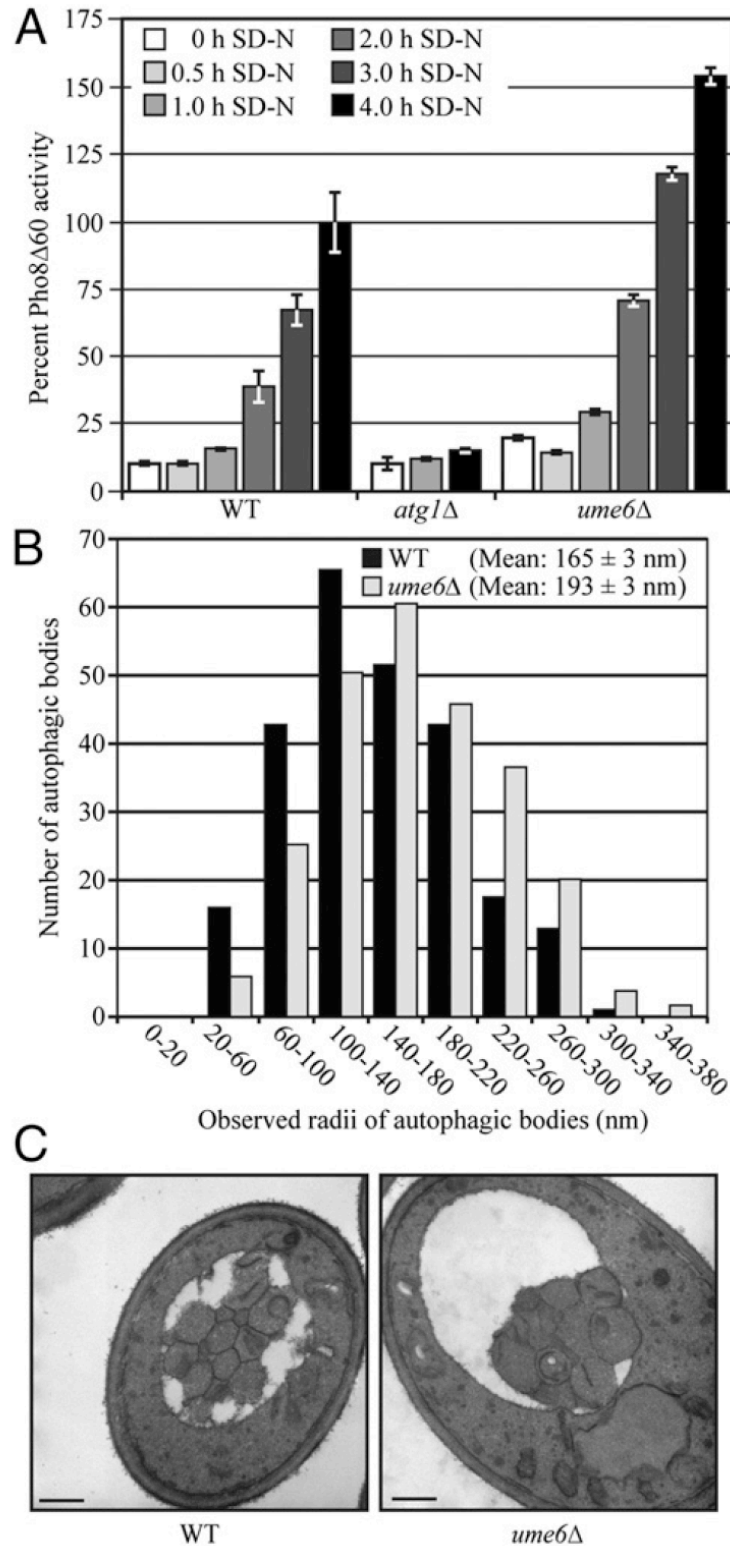


Figure 2.4 Ume6 negatively regulates autophagy.

(A) Autophagy as measured by the Pho8Δ60 assay is increased in *ume6Δ* cells. Wild-type (YCB193, SEY6210), *atg1Δ* (YCB194) and *ume6Δ* (YCB197) cells were grown in SMD medium, then starved for 0, 0.5, 1, 2, 3 and 4 h. The Pho8Δ60 activity was measured as

described in *Materials and Methods* and normalized to the activity of the wild-type cells, which was set to 100%. Error bars indicate the SEM of three independent experiments. (B) Autophagosome size is increased in *ume6Δ* cells. Wild-type (FRY143, SEY6210) and *ume6Δ* (YCB234) strains with deletions of *VPS4* and *PEP4* to eliminate vesicles generated from the multivesicular body pathway and the breakdown of autophagic bodies, respectively, were grown in rich medium and starved in SD-N for 2 h. Samples were collected, prepared and examined by TEM as described in *Materials and Methods*. The radius of each autophagosome was determined as described in *Materials and Methods*. The error represents the SEM for > 400 autophagic bodies. (C) Representative TEM images of the cells in (B). Scale bars are 500 nm.

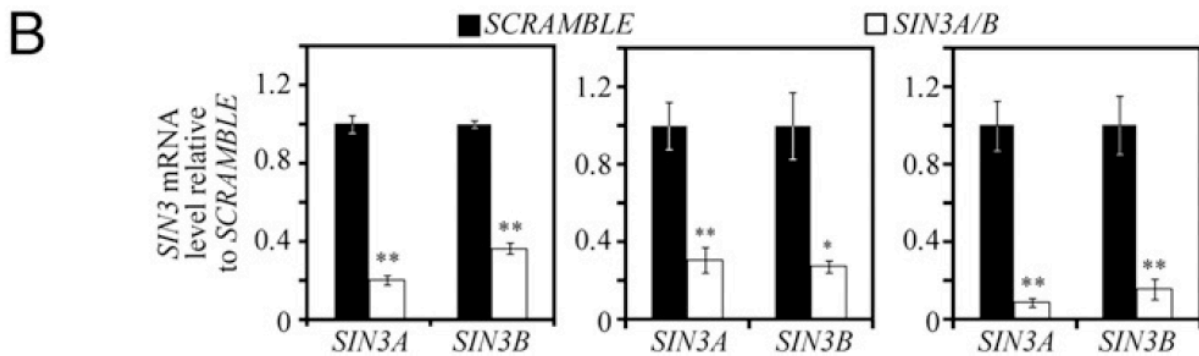
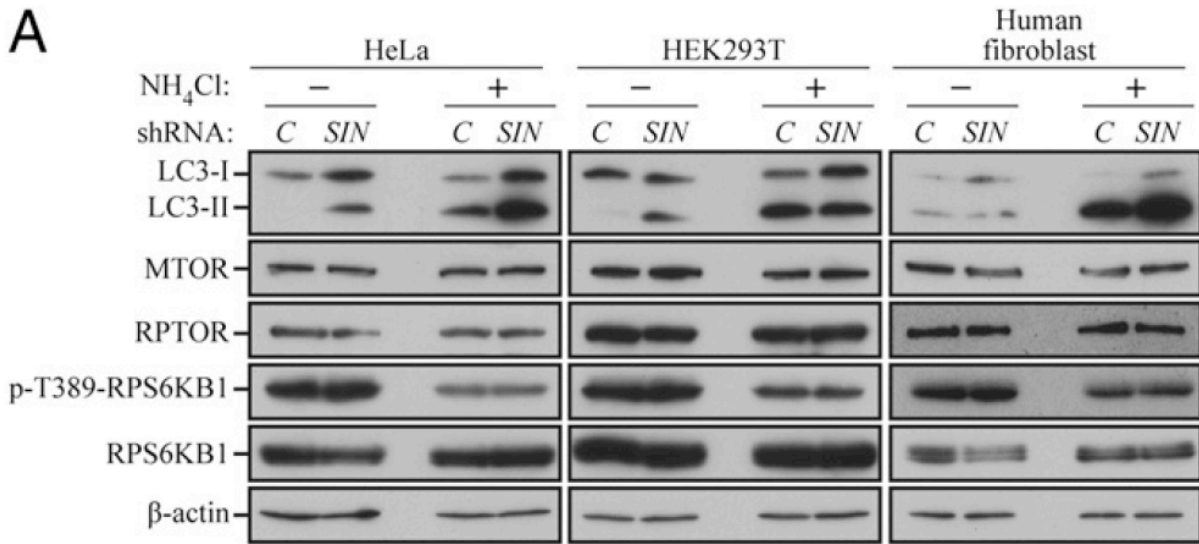


Figure 2.5 SIN3A and SIN3B play redundant roles in regulating LC3 expression.

(A) *SIN3A*- and *SIN3B*-targeted shRNA was prepared and used to generate viruses as described in *Materials and Methods*. The shRNA-expressing viruses were infected in combination into HeLa, HEK293T, and human fibroblast cells using scrambled DNA as a control (C). Cell lysates were analyzed by immunoblotting with the indicated antibodies. (B) *SIN3A* and *SIN3B* mRNA levels were monitored by qPCR in shRNA-treated cells. The values for scrambled DNA were set to 1.0 and the other values were normalized. * and ** represent $p < 0.05$ and $p < 0.01$ respectively. Error bars represent the standard deviation.

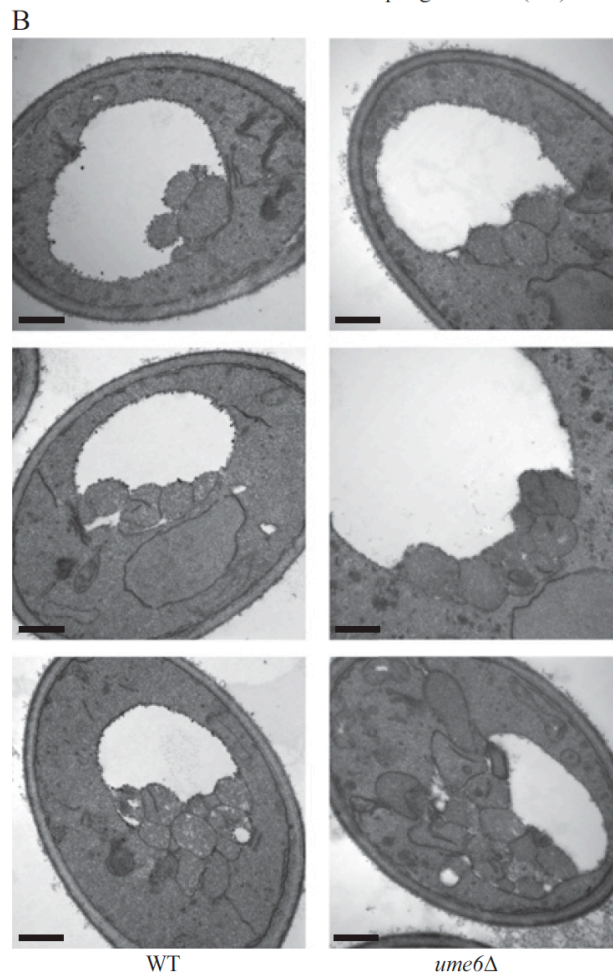
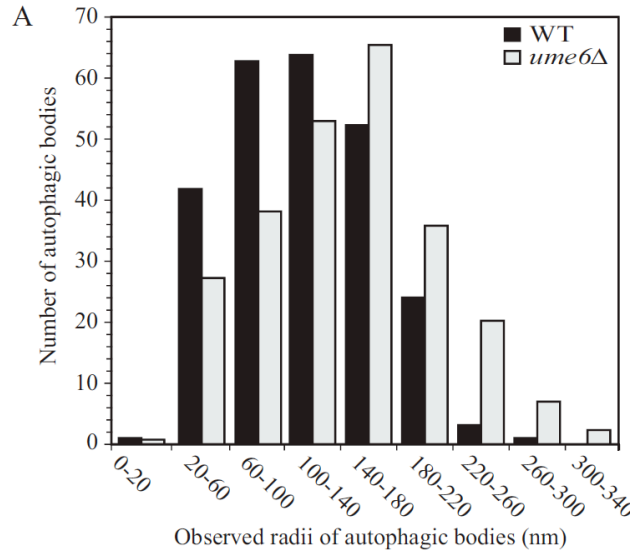


Figure 2.S1 Autophagosome volume is increased in *ume6Δ* cells.

(A) Wild-type (FRY143, SEY6210) and *ume6Δ* (YCB234) strains with *vps4Δ* and *pep4Δ* deletions to eliminate vesicles generated from the multivesicular body pathway and the breakdown of autophagic bodies, respectively, were grown in rich medium and starved in SD-N

for 1 h. Samples were collected, prepared and examined by TEM as described in *Materials and Methods*. The radius of each autophagosome was determined as described in *Materials and Methods*. The error represents the SEM for >225 autophagic bodies. (B) Supplemental images for Figure 2.4C. Wild-type (FRY143, SEY6210) and *ume6* Δ (YCB234) strains were grown as above and starved in SD-N for 2 h. Samples were collected, prepared and examined by TEM as described in *Materials and Methods*. Scale bars are 500 nm.

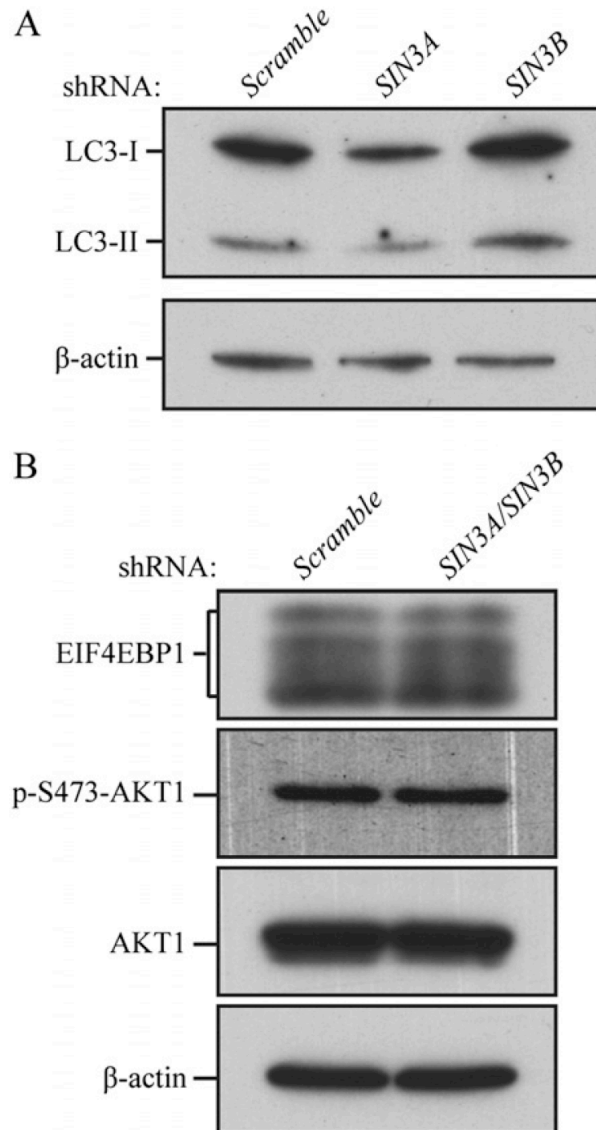


Figure 2.S2 SIN3A and SIN3B play redundant roles in regulating LC3 expression.

(A) *SIN3A*- and *SIN3B*-targeted shRNA was prepared and used to generate viruses as described in *Materials and Methods*. The shRNA-expressing viruses were singly infected into HeLa cells using scrambled DNA as a control. Cell lysates were analyzed by immunoblotting with anti-LC3 and anti-actin antiserum (the latter as a loading control). (B) *SIN3A* and *SIN3B* were knocked down in combination, and cell lysates were analyzed with the indicated antibodies.

CHAPTER 3. Transcriptional Regulation by Pho23 Modulates the Frequency of Autophagosome Formation³

3.1 Introduction

Macroautophagy, hereafter referred to as autophagy, is a highly conserved, intracellular degradation and recycling process that is tightly regulated by nutrient depletion and many other kinds of stress. In yeast, autophagy is essential for survival in nutrient-poor conditions and for adaptive responses to other changing environmental conditions through cellular remodeling [1]. In higher eukaryotes, autophagy is required for normal development and physiology, whereas autophagic dysfunction is associated with many types of human disease, including cancer, neurodegeneration, and metabolic disorders [2, 3]. Under stress conditions, portions of the cytoplasm are sequestered within a transient double-membrane structure, termed the phagophore. The phagophore is initiated and expanded from the phagophore assembly site [4], a peri-vacuolar punctum nucleated by most of the essential molecular machinery of autophagy. After elongation and completion, the phagophore forms a double-membrane vesicle, called the autophagosome. The autophagosome is then delivered to the vacuole (functionally analogous to mammalian lysosomes) and its outer membrane fuses with the vacuole limiting membrane, releasing its inner vesicle together with the enclosed cargo into the vacuole lumen. The cargo, including cytosolic proteins and even entire organelles, is broken down into macromolecular constituents such as

³ This chapter is reprinted from Meiyang Jin, Ding He, Steven K. Backues, Mallory A. Freeberg, Xu Liu, John K. Kim, Daniel J. Klionsky, Transcriptional Regulation by Pho23 Modulates the Frequency of Autophagosome Formation, *Current Biology*, 2014; 24(12):1314-22, <http://dx.doi.org/10.1016/j.cub.2014.04.048>, with minor modifications, with permission from Elsevier.

amino acids by vacuolar hydrolases, and recycled into the cytosol, to allow cells to survive during stress conditions [5].

Our understanding of the molecular mechanism of autophagy has been greatly advanced by yeast genetic studies in the past two decades, and more than 30 autophagy-related (*ATG*) genes have been identified as important players that are needed to initiate, complete, and regulate this complex process [1, 6-8]. Although an early study examining genome-wide changes in gene expression under different environmental conditions provided the first indication that many *ATG* genes were transcriptionally regulated upon autophagy induction [9], little is known about the specific transcriptional regulators of autophagy. Furthermore, how differential induction of *ATG* gene expression leads to different levels of Atg proteins and contributes to each step of the autophagy pathway is not well understood.

Altered expression of many *ATG* genes has been observed in various human diseases [10-13], suggesting a connection between autophagy regulation and disease progression. At present, *ATG8* is one of the best-characterized genes encoding a component of the core autophagy machinery, and it represents the only example in which studies have shown how protein level directly contributes to function in autophagosome formation: expression of *ATG8* is negatively regulated by the transcription factor Ume6, and the Atg8 protein controls phagophore expansion during autophagosome formation; the amount of Atg8 correlates with autophagosome size [14, 15]. However, how the induction of expression of other *ATG* genes contributes to autophagy is still unknown, and which transcriptional regulators participate in this event remains to be determined.

Here, we identified Pho23 as a transcriptional repressor for autophagy, which negatively controls the mRNA levels, and subsequent protein levels, of many components of the autophagy

core machinery, including *ATG1*, *ATG7*, *ATG8*, *ATG9*, and *ATG14*. We also detected elevated autophagy activity and increased frequency of autophagosome formation in *pho23Δ* cells. We subsequently focused on the regulation of *ATG9*, the gene for which transcription was most strongly affected by Pho23. Atg9 is the only transmembrane protein required for autophagosome formation, and it displays a relatively unique subcellular distribution and trafficking pattern [16-18]. Therefore, we wanted to determine how the amount of Atg9 affects autophagosome function and morphology separate from other Atg proteins such as Atg8, which mainly regulates the size of autophagosomes [15]. We found that Atg9 has a role in regulating the frequency of autophagosome formation, and Atg9 protein levels correlate with the number of autophagosomes. These findings advance our understanding of the molecular events occurring during autophagy induction, of how gene expression is regulated, and how this regulation modulates different aspects of autophagosome formation.

3.2 Results

3.2.1 Pho23 Represses the Transcription of ATG Genes.

ATG8 is an essential component of the autophagy machinery, and both its mRNA and protein levels are significantly elevated after a short time of autophagy induction [19]. Furthermore, among the *ATG* genes, *ATG8* is the most well-studied example of how altered expression levels affect the autophagy outcome; reduced *ATG8* expression results in a decrease in the average size of autophagosomes, and a corresponding reduction in autophagy activity [15]. These features make the Atg8 protein level a good indicator for transcriptional induction of autophagy. Accordingly, we screened more than 200 yeast null mutant strains in the BY4742 background focusing on transcriptional regulators that could potentially control *ATG* gene expression, using the Atg8 protein level as detected by western blot for the initial readout. From

the screen, a consistently increased Atg8 protein level in growing conditions (SD-N, t = 0), but not after nitrogen starvation, was detected in a *PHO23* deletion mutant strain relative to the wild-type control, and this phenotype was further confirmed in two additional yeast backgrounds (Figure 3.1A, Table 3.1).

To determine whether Pho23 also regulates the expression of other *ATG* genes, we also examined the mRNA levels of several genes encoding the core-machinery of autophagy, including *ATG1*, *ATG7*, *ATG8*, *ATG9*, *ATG12*, *ATG14*, and *ATG29*, in both wild-type and *pho23Δ* cells, by RT-qPCR (Figure 3.1B). For most of these genes the mRNA levels during vegetative growth clearly increased in *pho23Δ* cells compared to the wild type, with the exception being *ATG12*, which showed less than a 10% increase. We further tested whether the transcriptional increase in these genes seen in the *pho23Δ* cells resulted in a correlative change in protein levels, similar to the result with Atg8 (Figure 3.1A). Protein extracts were prepared from cells in growing conditions (i.e., when Pho23 is predicted to act as a negative regulator) and analyzed by western blot. We found elevated levels of Atg1, Atg7, Atg9, and Atg14, and to a lesser extent Atg29, in the *pho23Δ* strain relative to the wild type (Figure 3.1C). In contrast, there was no clear change in the level of Atg12. Together, these results identified Pho23 as a potential transcriptional repressor of autophagy.

3.2.2 Cells Lacking Pho23 Have Increased Autophagy Activity and Generate More Autophagosomes

To determine whether Pho23 can regulate autophagy activity through its transcriptional regulation of *ATG* genes, different well-established assays were performed to measure autophagy activity in *pho23Δ* versus wild-type cells. A plasmid that expresses GFP-Atg8 driven by the *CUPI* promoter was transformed into both wild-type and *PHO23* deletion strains to examine

GFP-Atg8 processing; we used the *CUP1* promoter to eliminate Pho23-dependent effects on GFP-Atg8 expression. The GFP-Atg8 processing assay is based on the fact that a population of GFP-Atg8 is attached on the inner membrane of the autophagosome and released into the vacuole upon autophagy; this chimera is processed through the action of vacuolar hydrolases to generate free GFP in the vacuole lumen. Thus, the conversion of GFP-Atg8 into GFP is used as a read-out for nonselective autophagic degradation [20]. An increasing amount of GFP-Atg8 processing was observed in the wild-type and *pho23Δ* strains following autophagy induction (Figure 3.2A). A reduced amount of the full-length chimera was seen in *pho23Δ* cells compared with the wild type after 1 h starvation, and this difference became more significant following 2 h of nitrogen starvation, suggesting increased autophagy flux in *pho23Δ* cells.

To extend our analysis we took advantage of the quantitative Pho8Δ60 assay. The Pho8Δ60 protein is an altered form of the vacuolar alkaline phosphatase that cannot be delivered to the vacuole via the secretory pathway; the cytosolic zymogen can be sequestered within an autophagosome, and activated within the vacuole lumen [21]. Measuring the Pho8Δ60-dependent alkaline phosphatase activity can therefore be used to monitor nonselective autophagy. The Pho8Δ60 activity was measured for samples prepared from wild-type and *pho23Δ* cells after 0, 1, 2 and 3 h of nitrogen starvation. In agreement with the GFP-Atg8 processing assay, *pho23Δ* cells showed increased autophagy activity compared with the wild-type cells after 2 and 3 h of nitrogen starvation (Figure 3.2B).

We further tested whether Pho23 may affect selective autophagy by looking at the maturation of the precursor form of aminopeptidase I (prApe1). The mature form of this enzyme (Ape1) is a vacuole-resident hydrolase, and prApe1 is constitutively delivered to this organelle through the cytoplasm-to-vacuole targeting (Cvt) pathway. Following delivery, prApe1 is

processed to a mature, active form that migrates as a lower molecular weight form during SDS-PAGE; vacuolar delivery can thus be monitored by western blot. The Cvt pathway is considered to be a selective type of autophagy, which is dependent on Atg19, the receptor for prApe1 [22]. When we compared prApe1 maturation between wild-type and *pho23Δ* cells, the majority of the protein was present as the mature form even in growing conditions, although *pho23Δ* cells appeared to have even less of the precursor form remaining; however, under these conditions it was difficult to determine whether there was a significant difference in prApe1 processing between the two strains (Figure 3.2C). To solve this technical problem, we took advantage of the phenotype of the *vac8Δ* mutant; in these cells prApe1 processing is essentially blocked in growing conditions, but is restored by nitrogen starvation [23]. Importantly, vacuolar delivery of prApe1 in these cells requires the specificity components Atg19 and Atg11, indicating that the import is still a selective process. In the *vac8Δ pho23Δ* strain, we observed a low level of prApe1 processing even in growing conditions, and an increased level of processing relative to the control *vac8Δ* (WT) strain after a short time of nitrogen starvation (Figure 3.2D), indicating increased vacuolar delivery of prApe1 by selective autophagy in the absence of Pho23.

The elevated autophagy activity seen in the *pho23Δ* cells could be accounted for by an increased size or number of autophagosomes. Accordingly, we used transmission electron microscopy (TEM) to examine autophagic bodies, the single-membrane vesicles that result from the fusion of autophagosomes with the vacuole. We generated strains deleted for the *PEP4* gene, which codes for a key hydrolase that is needed to break down autophagic bodies, and the *VPS4* gene, which is necessary for the multivesicular body pathway. The wild-type (*pep4Δ vsp4Δ*) and *pep4Δ pho23Δ vsp4Δ* strains were grown to mid-log phase and switched to starvation conditions. Samples were prepared and analyzed by TEM (Figure 3.3A). Quantification of the TEM images

indicated that the average sizes of autophagosome in the *pho23Δ* and wild-type strains were similar (Table 3.2); in contrast, the number of autophagic bodies per cell was nearly doubled in the *pho23Δ* cells relative to the wild type after 3 h of starvation (Figure 3.3B). These results further support the hypothesis that Pho23 negatively regulates autophagy, and that this regulation may operate by controlling the frequency of autophagosome formation rather than the extent of autophagosome expansion (i.e., regulating the number rather than the size of autophagosomes).

The increased number of autophagosomes generated in the *pho23Δ* cells indicated an increased frequency of autophagosome formation. To test whether this difference in frequency of formation was due to the increased rate of generating single autophagosomes, or to shortened gaps between the formation of two autophagosomes, we used fluorescence live imaging of cells expressing GFP-Atg8, which labels the forming autophagosome. The lifetime of each individual GFP-Atg8 punctum reflects the time needed to complete the formation of the represented autophagosome [24]. The average lifetime of the GFP-Atg8 puncta was 6.1 min in *pho23Δ*, cells versus 9.6 min in the wild type (Figure 3.3C, D), indicating that in the Pho23-depleted cells each single autophagosome could be generated in a shorter time than in the wild-type cells. Overall, our results suggest an accelerated process of autophagosome formation when *PHO23* is deleted; therefore, more autophagosomes can be generated in a given time of autophagy induction in the mutant cells.

3.2.3 *Pho23 Regulates Autophagy in an Rpd3-Dependent Manner*

To further understand the mechanism of how Pho23 regulates the transcription of *ATG* genes, we looked at Rpd3, a histone deacetylase (HDAC), which is associated with Pho23 and is required for the function of the Rpd3 large (Rpd3L) complex in gene repression [25]. Rpd3 occupies the promoter of many genes, and it is brought to different clusters of gene promoters by

alternative recruiters [26]. Although Pho23 is not required for the enzyme activity of the Rpd3L complex, it functions as one of the recruiters essential for the specific localization of the Rpd3L complex to its target promoters [27, 28].

To understand whether the Pho23-dependent repression of *ATG* genes is related to Rpd3, we analyzed available data from a previous genomic study in which the transcriptome of 165 histone-modifying genes, including *PHO23* and *RPD3*, was established by two-channel microarray [4]. We compared the genes that showed more than a 1.5-fold increase in the *pho23Δ* and *rpd3Δ* strains from their microarray study, and found that Rpd3 regulates most of the genes targeted by Pho23 (122 of 143), including *ATG1*, *ATG7*, and *ATG9*, indicating that Pho23 may suppress transcription in an Rpd3-dependent manner (Figure 3.S1A). To test this hypothesis we compared the mRNA level of these *ATG* genes in wild-type, *pho23Δ*, *rpd3Δ*, and *pho23Δ rpd3Δ* deletion strains (Figure 3.S1B). All of the single- and double-deletion mutants showed increased mRNA levels of *ATG1*, *ATG7*, *ATG8*, *ATG9*, and *ATG14* compared with the wild-type strain. Furthermore, an additive increase of *ATG1*, *ATG7*, *ATG9*, and *ATG14* mRNA levels was not detected in the *pho23Δ rpd3Δ* double-deletion strain relative to the *rpd3Δ* mutant, suggesting that in *rpd3Δ* cells Pho23 no longer represses the transcription of these *ATG* genes.

Of the *ATG* genes we tested, *ATG8* was an exception in that the *pho23Δ rpd3Δ* double mutant displayed a higher level of expression relative to either single mutant (Figure 3.S1B). Previously, we showed that Ume6, a DNA-binding protein that belongs to the Rpd3L complex, suppresses autophagy (at least in part) through its direct repression of *ATG8* transcription [14]. We further tested the possibility that Pho23 regulates *ATG* gene transcription through Ume6, by monitoring the *ATG* gene mRNA levels in a *ume6Δ* strain compared to the *pho23Δ ume6Δ* double-deletion mutant (Figure 3.S1B). Whereas deletion of *PHO23* in the *ume6Δ* background

did not result in an additional increase of *ATG8* mRNA, other *ATG* genes, including *ATG1*, *ATG7*, *ATG9* and *ATG14* showed a higher mRNA level in the double-deletion mutant. These data suggest that the role of Pho23 in the repression of *ATG8* transcription is regulated less by Rpd3, and rather is Ume6 dependent, whereas for the other *ATG* genes tested, the deletion of *UME6* does not release the Pho23-dependent transcriptional repression.

Finally, we examined the protein level of Atg1, Atg8 and Atg9 by western blot in cells lacking *RPD3*, *UME6* and/or *PHO23* (Figure 3.S1C) and found that the results were consistent with the respective mRNA patterns. That is, in the *rpd3Δ* background, deletion of *PHO23* did not further increase the Atg protein levels, whereas in the *ume6Δ* background Atg1 and Atg9, but not Atg8, were more highly expressed when *PHO23* was also deleted. These results support the model that there are different forms of Rpd3L that target various groups of genes through different subunits of the complex; Pho23 and Ume6 belong to different, but partly overlapping, Rpd3 complexes, which have different effects on autophagy gene expression. This model may explain why in *pho23Δ* cells we observed more, but not enlarged, autophagosomes (Figure 3.3A, B), which is different from the phenotype of larger autophagosomes in *ume6Δ* cells observed in the previous study [14].

3.2.4 *Pho23 Is Required for Extended Repression of ATG9 Transcription*

The Atg proteins participate in different steps of autophagy; therefore, the change of expression of different *ATG* genes may cause different effects on autophagy. At present, Atg8 is the only protein reported to affect the size of autophagosomes [15]; however, there are no clear data as to whether any of the Atg proteins play a role in regulating the frequency of autophagosome formation.

To better understand how Pho23 regulates the autophagosome number per cell, we next examined the Pho23-dependent regulation of the known *ATG* genes relative to the entire genome. Polyadenylated RNA was isolated from wild-type and *pho23Δ* yeast cells in growing and starvation conditions, and analyzed by RNA-seq using the Illumina platform. In growing conditions, 12 out of 28 (41%) of the *ATG* genes showed a more than 2-fold increase in mRNA levels in *pho23Δ* cells compared to the wild type, while only 322 out of all 6,650 (5%) genes from the whole genome showed a similar increase (Figure 3.4A, Table 3.3 and 3.4). We performed a gene ontology (GO) enrichment analysis for these 322 transcripts, and identified the autophagy pathway as one of the top hits (Table 3.5). After 2 h of nitrogen starvation, none of the *ATG* genes showed a more than 2-fold increase in transcript levels in *pho23Δ* cells relative to the wild type (Figure 3.4B). These results suggest that Pho23 acts as a potential autophagy-specific transcriptional repressor, which keeps autophagic transcription at a basal level when the process is suppressed, and its negative effect on most target genes is released by the starvation-dependent induction of autophagy.

From the RNA-seq data, we further compared mRNA levels of the *ATG* genes that showed the greatest increase in the absence of Pho23 (Figure 3.4C). After nitrogen starvation, when the role of Pho23 in repressing the transcription of most of its *ATG* targets is largely diminished, we still observed a moderate repression of Pho23 on a limited numbers of its genes including *ATG8* and *ATG9*. Because *Atg8* regulates autophagosome size rather than number [15], *ATG9* seemed a likely candidate to be a key target gene whose regulation by Pho23 controls the frequency of autophagosome formation.

To determine whether the extended repression of *ATG9* mRNA transcription by Pho23 correlated with an altered level of protein synthesis, we examined the protein levels of *Atg9* at

various time points (0, 0.5, 1, and 2 h) after autophagy induction by nitrogen starvation. To prevent the potential degradation of Atg proteins by autophagy, we again utilized the *pep4Δ* mutation. The expression pattern of the Atg9 protein was consistent with that of the mRNA; the *pho23Δ* strain displayed a higher level of Atg9 relative to the wild type at time zero, and this was maintained throughout the time course (Figure 3.4D). In contrast, the Atg1 protein level, which we used as a control because *ATG1* expression was not dependent on Pho23 after starvation (Figure 3.4C), showed a clear difference between the wild-type and *pho23Δ* strains only at the early time points, and this difference essentially disappeared by 1 h of starvation.

These results highlighted *ATG9* as the *ATG* gene that is most strongly affected by Pho23 repression; Pho23 regulates *ATG9* transcription even after starvation, when the transcriptional repression by Pho23 on most of the other *ATG* genes is released.

3.2.5 The Level of *ATG9* Expression Regulates the Frequency of Autophagosome Formation

Atg9 is the only characterized transmembrane protein among the autophagy core machinery, and it displays a dynamic trafficking pattern between the PAS and the tubulo-vesicular clusters that are proposed to represent membrane reservoirs for phagophore expansion [17, 18, 29, 30]. These characteristics support a model wherein Atg9 functions in directing membrane to the phagophore from other organelles, and the movement of Atg9 is required for autophagosome formation. Single-membrane vesicles containing Atg9 are proposed to fuse to initiate phagophore formation, indicating that Atg9 may also have roles in early steps of autophagosome biogenesis [31]. The apparent extended repression of *ATG9* transcription by Pho23, and the increase in autophagic bodies/autophagosomes seen in the *pho23Δ* strain led us to hypothesize that the Atg9 protein level correlates with the frequency of autophagosome formation, and thus determines in part the number of autophagosomes per cell.

To test this hypothesis, we generated four strains that express different levels of *ATG9*. HDY001 (referred to here as A9 Δ) is the *atg9* Δ negative control; HDY003 (A9Lo) expresses *ATG9-GFP* under the control of the *ATG23* promoter and thus synthesizes a level of Atg9 lower than that of the wild type; HDY002 (A9WT) expresses *ATG9-GFP* driven by the endogenous *ATG9* promoter; and HDY007 (A9OE) expresses *ATG9-GFP* driven by the *ATG8* promoter integrated into a wild-type strain in addition to the endogenous *ATG9* gene and expresses a higher level of Atg9 than the wild-type. The Atg9 or Atg9-GFP protein levels in these strains were confirmed by western blotting using anti-Atg9 antiserum (Figure 3.5A). Next, we quantified the autophagy activity of these strains using the Pho8 Δ 60 assay. All four strains showed similar levels of basal Pho8 Δ 60 activity in growing conditions, but the Pho8 Δ 60 activities after 3 h of nitrogen starvation varied (Figure 3.5B). As expected, the A9WT strain showed a clear induction of Pho8 Δ 60 activity after starvation (this value was set to 100% and used for the normalization of the other activities), while the activity of the A9 Δ strain remained at the background level. The A9Lo strain showed approximately 60% of the Pho8 Δ 60 activity of A9WT, and the A9OE strain displayed approximately 130% of the activity of A9WT, being significantly higher than the wild-type level. These results indicated that the Atg9 protein level correlates with/regulates autophagy activity.

Finally, as with the *pho23* Δ strain, the changes in autophagy activity could be due to differences in autophagosome size and/or number. Therefore, we deleted *PEP4* in each of these strains and measured the size and counted the number of autophagic bodies after 3 h of nitrogen starvation using TEM. As expected, no autophagic bodies were observed in the A9 Δ strain. For the other strains, the estimated average number of autophagic bodies per cell was increased in the order of increased *ATG9* expression (Figure 3.5C and 3.5D), which again strongly supports our

hypothesis that the Atg9 protein level regulates the frequency of autophagosome formation and thus controls the autophagic body number in each cell. At higher levels of Atg9 expression, the highest correlation was seen between autophagic body number and Pho8 Δ 60 activity, whereas Atg9 protein expression appeared to be saturating near that of the wild type (Figure 3.5E). These results also provide a partial explanation for the increased autophagic body numbers we observed in the *pho23 Δ* cells (Figure 3.3A and 3.3B), since *ATG9* expression was significantly increased in these cells before, and continued after, autophagy induction.

3.3 Discussion

Here, we identified Pho23 as a transcriptional repressor, the absence of which causes increased transcription of several autophagy genes, increased frequency of autophagosome formation, and elevated autophagy activity. Pho23, together with Yng1 and Yng2, compose the inhibitor of growing (ING) family in yeast [32]. The ING family proteins share a significant sequence identity on their conserved C terminal plant homeodomain (PHD) finger, and each of them has been identified as a subunit of distinct chromatin modification complexes [28]. Pho23 has two human homologs, ING1 and ING2, which associate with a HDAC complex, and are candidate tumor suppressors [33]. In yeast, Pho23 is associated with Rpd3, a HDAC, and is required for the gene repressive function of the Rpd3L complex [25]. Although Pho23 is not required for the HDAC activity of Rpd3, it is essential for the specific recruitment of Rpd3 to the promoters of its target genes [27, 28]. In this study, we found that Pho23 represses the transcription of certain *ATG* genes in an Rpd3-dependent manner, which raises the possibility that Rpd3 controls *ATG* gene transcription specifically through Pho23. However, there is no evidence that Pho23 can directly bind to DNA, and therefore the recruitment of the Pho23-Rpd3 complex may further depend on additional DNA binding molecules. One of the DNA-binding

components of the Rpd3L complex, Ume6, represses the transcription of *ATG8* and autophagy activity [27, 28], but our data suggest that Pho23-dependent transcriptional repression of *ATG* genes other than *ATG8* is independent of Ume6. Thus, the DNA-binding partner of Pho23 that may target the Pho23-Rpd3 complex to the promoters of *ATG* genes remains to be identified.

Recently, HDACs have become potential targets for various disease therapies, including cancer and metabolic disorders [34]. Our findings reveal a possible mechanism for how HDACs may play a role in these diseases through the regulation of autophagy. HDAC inhibitors have been studied as candidate drugs for various diseases including cancer, and our finding that Pho23 may target autophagy genes in a more specific manner than Rpd3 suggests a potential therapeutic strategy; targeting the ING proteins rather than the histone deacetylase itself may increase the efficiency, while decreasing the side effects, of particular drugs.

In cells lacking *PHO23*, several *ATG* genes displayed an increase in expression. Thus, it was not immediately clear which gene product(s) accounted for the observed increase in autophagosome number. In order to specifically examine the role of Atg9, we constructed strains in which only the expression of the *ATG9* gene was altered. In this report, we show, by comparing Pho8 Δ 60 activity and autophagic body numbers, that the amount of Atg9 regulates autophagy activity by modulating the number of autophagosomes (Figure 3.5). Generally, higher levels of Atg9 result in more autophagic bodies, and higher autophagy activity; however, with a more careful comparison, we found that the Atg9 level is not correlated in an absolutely linear manner with autophagic body number or autophagy activity (Figure 3.5E). The A9Lo cells, which express only 21% of the Atg9 of the A9WT cells and form only one third the number of autophagosomes, showed as high as 48% of the induction of the autophagy activity relative to the A9WT cells. This observation can be explained by the increased average size of the

autophagic bodies observed in the A9Lo cells (Table 3.6). We do not know the reason for this increase in size; however, we suggest that this may be due to the delay of autophagosome formation caused by the reduced amount of Atg9, which could provide additional time for the phagophore to expand. Overall, the reduced number of autophagosomes seen with lower levels of Atg9 reflects a role for this protein in the rate of autophagosome expansion or closure, but further studies will be needed to make this determination. Conversely, the A9OE cells, whose Atg9 expression level is almost twice that of the A9WT cells, showed only a moderate increase (~ 25%) of autophagic bodies and autophagy activity. Most likely, only increasing the Atg9 level beyond that of the wild type is not sufficient to dramatically increase autophagosome formation, as other Atg proteins may become limiting.

In cells lacking *PHO23*, a significantly increased number of autophagic bodies/cell was detected (Figure 3.3B), even higher than in the A9OE cells. This increase is likely primarily due to the elevated Atg9 protein levels in the *pho23Δ* cells, but its magnitude suggests that the increased expression level of other Atg proteins such as Atg7, Atg14, and Atg29 whose expression is also increased in *pho23Δ* mutants may be involved as well. Carefully designed experiments will be needed to separate the functions of these other proteins from Atg9 in order to test their roles in regulating autophagosome number, because some of them affect the trafficking of this protein.

In summary, our results suggest a relatively direct connection between Atg9 level and autophagosome formation frequency. Additionally, the data show that Pho23 represses *ATG* gene expression levels, especially in growing conditions, and that this repression—in particular, the repression of *ATG9*—decreases the frequency of autophagosome formation and limits autophagic activity.

3.4 Experimental Procedures

3.4.1 Yeast strains, Media and Culture

Yeast strains used are listed in Table 3.1. Gene deletions or integrations were performed using a standard method [35]. Samples for growing conditions are collected from mid-log phase yeast cells grown in rich medium [YPD: 1% (w/v) yeast extract, 2% (w/v) peptone, and 2% (w/v) glucose; or SMD: 0.67% yeast nitrogen base, 2% glucose, and auxotrophic amino acids and vitamins as needed]. Autophagy was induced through nitrogen starvation by shifting cells in mid-log phase from YPD to SD-N [0.17% yeast nitrogen base without ammonium sulfate or amino acids, and 2% (w/v) glucose] for the indicated times.

3.4.2 Plasmids

Plasmid *pRS406-P_{ATG9}-ATG9-GFP* contains 1000 base pairs of *ATG9* 5' sequence in front of the *ATG9-GFP* open reading frame; plasmid *pRS406-P_{ATG23}-ATG9-GFP* contains 750 base pairs of the *ATG23* 5' sequence instead of the *ATG9* promoter; plasmid *pRS406-P_{ATG8}-ATG9-GFP* replaces the *ATG9* promoter with 1000 base pairs of the *ATG8* 5' sequence. These *ATG9-GFP*-expressing plasmids or the corresponding empty vector (*pRS406*) were linearized and integrated into the wild-type or *atg9* Δ strain to generate the A9 strains indicated in Table 3.1.

3.4.3 RNA-seq

Yeast cells were grown in YPD to mid-log phase, and then shifted to SD-N. Total RNAs were extracted using the Master-Pure yeast RNA purification Kit (Epicentre Biotechnologies). cDNA library preparation and Illumina high-throughput sequencing was performed by the DNA sequencing core at the University of Michigan. Reads from multiplexed libraries were scanned for a perfect match to each unique 6 nt barcode. If more than one barcode was matched perfectly,

the 3'-most barcode was chosen. Remaining reads were scanned for 1 mismatch to each 6 nt barcode. If more than one barcode was matched with 1 mismatch, the 3'-most barcode was chosen. The mean sequencing error rate for each library was estimated from the mean quality score. Reads were mapped using Bowtie2 [36] (parameters: -f -v 3 -k 500 --best --strata) to the yeast transcriptome derived from yeast genome version S228C. Alignments with quality score less than 88 were discarded. A majority of mapped reads mapped to a unique locus in the transcriptome; these reads were used to calculate reads per kilobase per million mapped reads (RPKM) for each yeast gene (for details see Tables 3.3, 3.4). The *pho23* sequencing data have been accepted and published as a GEO dataset with accession number GSE57031.

3.4.4 RT-qPCR

Yeast cells were grown in YPD to mid-log phase, and then shifted to SD-N. Total RNAs were extracted using the RNeasy Mini kit (Qiagen), and reverse transcription was performed using the High Capacity cDNA Reverse Transcription Kit (Applied Biosystems). Realtime PCR was performed using the Power SYBR Green PCR Master Mix (Applied Biosystems).

3.4.5 GFP-Atg8 Live Imaging

Cells were immobilized for live imaging as described previously [15]. Images were collected on a Deltavision Elite deconvolution microscope (GE Healthcare/Applied Precision) with a 100x objective and a CCD camera (CoolSnap HQ, Photometrics). 12-image stacks (0.4- μ m spacing, to cover the entire cell) were taken each minute for 45 min, deconvolved, projected, and manually analyzed to determine GFP-Atg8 puncta lifetime.

3.4.6 Other Methods

Western blot, the GFP-Atg8 processing and Pho8 Δ 60 assays, and TEM were performed as described previously [20, 37, 38]. Antisera to Atg8 [39], Atg1 [40], Atg9 [16], Ape1 [41], Pgk1 (a generous gift from Dr. Jeremy Thorner, University of California, Berkeley), and a commercial antibody that reacts with PA (no longer available) were used as described previously.

3.4.7 Statistical Analysis

Two-tailed Student's *t*-test and two-tailed paired Student's *t*-test was used to determine statistical significance.

3.5 Acknowledgments

This work was supported by NIH grants GM053396 to DJK, and GM088565 to JKK, and by the National Science Foundation Open Data IGERT Grant 0903629 to MAF, and was funded in part through the Protein Folding Diseases FastForward Initiative, University of Michigan.

3.6 References

1. Tsukada, M., and Ohsumi, Y. (1993). Isolation and characterization of autophagy-defective mutants of *Saccharomyces cerevisiae*. *FEBS Lett* 333, 169-174.
2. Huang, J., and Klionsky, D.J. (2007). Autophagy and human disease. *Cell Cycle* 6, 1837-1849.
3. Mizushima, N., Levine, B., Cuervo, A.M., and Klionsky, D.J. (2008). Autophagy fights disease through cellular self-digestion. *Nature* 451, 1069-1075.
4. Lenstra, T.L., Benschop, J.J., Kim, T., Schulze, J.M., Brabers, N.A., Margaritis, T., van de Pasch, L.A., van Heesch, S.A., Brok, M.O., Groot Koerkamp, M.J., et al. (2011). The specificity and topology of chromatin interaction pathways in yeast. *Mol Cell* 42, 536-549.
5. Xie, Z., and Klionsky, D.J. (2007). Autophagosome formation: core machinery and adaptations. *Nat Cell Biol* 9, 1102-1109.
6. Harding, T.M., Morano, K.A., Scott, S.V., and Klionsky, D.J. (1995). Isolation and characterization of yeast mutants in the cytoplasm to vacuole protein targeting pathway. *J Cell Biol* 131, 591-602.
7. Klionsky, D.J., Cregg, J.M., Dunn, W.A., Jr., Emr, S.D., Sakai, Y., Sandoval, I.V., Sibirny, A., Subramani, S., Thumm, M., Veenhuis, M., et al. (2003). A unified nomenclature for yeast autophagy-related genes. *Dev Cell* 5, 539-545.

8. Thumm, M., Egner, R., Koch, B., Schlumpberger, M., Straub, M., Veenhuis, M., and Wolf, D.H. (1994). Isolation of autophagocytosis mutants of *Saccharomyces cerevisiae*. *FEBS Lett* 349, 275-280.
9. Gasch, A.P., Spellman, P.T., Kao, C.M., Carmel-Harel, O., Eisen, M.B., Storz, G., Botstein, D., and Brown, P.O. (2000). Genomic expression programs in the response of yeast cells to environmental changes. *Mol Biol Cell* 11, 4241-4257.
10. Chen, D., Pang, S., Feng, X., Huang, W., Hawley, R.G., and Yan, B. (2013). Genetic analysis of the ATG7 gene promoter in sporadic Parkinson's disease. *Neurosci Lett* 534, 193-198.
11. Liu, H., He, Z., von Rutte, T., Yousefi, S., Hunger, R.E., and Simon, H.U. (2013). Down-regulation of autophagy-related protein 5 (ATG5) contributes to the pathogenesis of early-stage cutaneous melanoma. *Sci Transl Med* 5, 202ra123.
12. Jo, Y.K., Kim, S.C., Park, I.J., Park, S.J., Jin, D.H., Hong, S.W., Cho, D.H., and Kim, J.C. (2012). Increased expression of ATG10 in colorectal cancer is associated with lymphovascular invasion and lymph node metastasis. *PLoS One* 7, e52705.
13. Wang, J., Pan, X.L., Ding, L.J., Liu, D.Y., Da-Peng, L., and Jin, T. (2013). Aberrant expression of Beclin-1 and LC3 correlates with poor prognosis of human hypopharyngeal squamous cell carcinoma. *PLoS One* 8, e69038.
14. Bartholomew, C.R., Suzuki, T., Du, Z., Backues, S.K., Jin, M., Lynch-Day, M.A., Umekawa, M., Kamath, A., Zhao, M., Xie, Z., et al. (2012). Ume6 transcription factor is part of a signaling cascade that regulates autophagy. *Proc Natl Acad Sci U S A* 109, 11206-11210.
15. Xie, Z., Nair, U., and Klionsky, D.J. (2008). Atg8 controls phagophore expansion during autophagosome formation. *Mol Biol Cell* 19, 3290-3298.
16. Noda, T., Kim, J., Huang, W.-P., Baba, M., Tokunaga, C., Ohsumi, Y., and Klionsky, D.J. (2000). Apg9p/Cvt7p is an integral membrane protein required for transport vesicle formation in the Cvt and autophagy pathways. *J Cell Biol* 148, 465-480.
17. Reggiori, F., Tucker, K.A., Stromhaug, P.E., and Klionsky, D.J. (2004). The Atg1-Atg13 complex regulates Atg9 and Atg23 retrieval transport from the pre-autophagosomal structure. *Dev Cell* 6, 79-90.
18. Reggiori, F., Shintani, T., Nair, U., and Klionsky, D.J. (2005). Atg9 cycles between mitochondria and the pre-autophagosomal structure in yeasts. *Autophagy* 1, 101-109.
19. Kirisako, T., Baba, M., Ishihara, N., Miyazawa, K., Ohsumi, M., Yoshimori, T., Noda, T., and Ohsumi, Y. (1999). Formation process of autophagosome is traced with Apg8/Aut7p in yeast. *J Cell Biol* 147, 435-446.
20. Shintani, T., and Klionsky, D.J. (2004). Cargo proteins facilitate the formation of transport vesicles in the cytoplasm to vacuole targeting pathway. *J Biol Chem* 279, 29889-29894.
21. Noda, T., and Klionsky, D.J. (2008). The quantitative Pho8 Δ 60 assay of nonspecific autophagy. *Methods Enzymol* 451, 33-42.
22. Lynch-Day, M.A., and Klionsky, D.J. (2010). The Cvt pathway as a model for selective autophagy. *FEBS Lett* 584, 1359-1366.
23. Scott, S.V., Nice, D.C., 3rd, Nau, J.J., Weisman, L.S., Kamada, Y., Keizer-Gunnink, I., Funakoshi, T., Veenhuis, M., Ohsumi, Y., and Klionsky, D.J. (2000). Apg13p and Vac8p are part of a complex of phosphoproteins that are required for cytoplasm to vacuole targeting. *J Biol Chem* 275, 25840-25849.
24. Geng, J., Baba, M., Nair, U., and Klionsky, D.J. (2008). Quantitative analysis of autophagy-related protein stoichiometry by fluorescence microscopy. *J Cell Biol* 182, 129-140.

25. Loewith, R., Smith, J.S., Meijer, M., Williams, T.J., Bachman, N., Boeke, J.D., and Young, D. (2001). Pho23 is associated with the Rpd3 histone deacetylase and is required for its normal function in regulation of gene expression and silencing in *Saccharomyces cerevisiae*. *J Biol Chem* *276*, 24068-24074.
26. Kurdistani, S.K., Robyr, D., Tavazoie, S., and Grunstein, M. (2002). Genome-wide binding map of the histone deacetylase Rpd3 in yeast. *Nat Genet* *31*, 248-254.
27. Wang, S.S., Zhou, B.O., and Zhou, J.Q. (2011). Histone H3 lysine 4 hypermethylation prevents aberrant nucleosome remodeling at the PHO5 promoter. *Mol Cell Biol* *31*, 3171-3181.
28. Avvakumov, N., and Cote, J. (2007). The MYST family of histone acetyltransferases and their intimate links to cancer. *Oncogene* *26*, 5395-5407.
29. Yen, W.-L., Legakis, J.E., Nair, U., and Klionsky, D.J. (2007). Atg27 is required for autophagy-dependent cycling of Atg9. *Mol Biol Cell* *18*, 581-593.
30. Mari, M., Griffith, J., Rieter, E., Krishnappa, L., Klionsky, D.J., and Reggiori, F. (2010). An Atg9-containing compartment that functions in the early steps of autophagosome biogenesis. *J Cell Biol* *190*, 1005-1022.
31. Yamamoto, H., Kakuta, S., Watanabe, T.M., Kitamura, A., Sekito, T., Kondo-Kakuta, C., Ichikawa, R., Kinjo, M., and Ohsumi, Y. (2012). Atg9 vesicles are an important membrane source during early steps of autophagosome formation. *J Cell Biol* *198*, 219-233.
32. Loewith, R., Meijer, M., Lees-Miller, S.P., Riabowol, K., and Young, D. (2000). Three yeast proteins related to the human candidate tumor suppressor p33(ING1) are associated with histone acetyltransferase activities. *Mol Cell Biol* *20*, 3807-3816.
33. Guerillon, C., Larrieu, D., and Pedoux, R. (2013). ING1 and ING2: multifaceted tumor suppressor genes. *Cell Mol Life Sci* *70*, 3753-3772.
34. Tang, J., Yan, H., and Zhuang, S. (2013). Histone deacetylases as targets for treatment of multiple diseases. *Clin Sci (Lond)* *124*, 651-662.
35. Longtine, M.S., McKenzie, A., III, Demarini, D.J., Shah, N.G., Wach, A., Brachat, A., Philippsen, P., and Pringle, J.R. (1998). Additional modules for versatile and economical PCR-based gene deletion and modification in *Saccharomyces cerevisiae*. *Yeast* *14*, 953-961.
36. Langmead, B., and Salzberg, S.L. (2012). Fast gapped-read alignment with Bowtie 2. *Nat Methods* *9*, 357-359.
37. Noda, T., Matsuura, A., Wada, Y., and Ohsumi, Y. (1995). Novel system for monitoring autophagy in the yeast *Saccharomyces cerevisiae*. *Biochem Biophys Res Commun* *210*, 126-132.
38. Backues, S.K., Chen, D., Ruan, J., Xie, Z., and Klionsky, D.J. (2014). Estimating the size and number of autophagic bodies by electron microscopy. *Autophagy*.
39. Huang, W.-P., Scott, S.V., Kim, J., and Klionsky, D.J. (2000). The itinerary of a vesicle component, Aut7p/Cvt5p, terminates in the yeast vacuole via the autophagy/Cvt pathways. *J Biol Chem* *275*, 5845-5851.
40. Abeliovich, H., Zhang, C., Dunn, W.A., Jr., Shokat, K.M., and Klionsky, D.J. (2003). Chemical genetic analysis of Apg1 reveals a non-kinase role in the induction of autophagy. *Mol Biol Cell* *14*, 477-490.
41. Klionsky, D.J., Cueva, R., and Yaver, D.S. (1992). Aminopeptidase I of *Saccharomyces cerevisiae* is localized to the vacuole independent of the secretory pathway. *J Cell Biol* *119*, 287-299.

Table 3.1. Strains used in this study

Name	Genotype	Ref
BY4742	MAT α <i>his3Δ1 leu2Δ0 ura3Δ0</i>	Invitrogen
CWY230	SEY6210 <i>vac8Δ::KAN</i>	(1)
FRY143	SEY6210 <i>vps4Δ::TRP1 pep4Δ::LEU2</i>	(2)
HDY001 (A9 Δ)	WLY176 <i>ATG9Δ::LEU2 pRS406::URA3</i>	This study
HDY002 (A9WT)	WLY176 <i>ATG9Δ::LEU2 pRS406-P_{ATG9}-ATG9-GFP::URA3</i>	This study
HDY003 (A9Lo)	WLY176 <i>ATG9Δ::LEU2 pRS406-P_{ATG23}-ATG9-GFP::URA3</i>	This study
HDY007 (A9OE)	WLY176 <i>pRS406-P_{ATG8}-ATG9-GFP::URA3</i>	This study
JMY015	ZFY202 <i>pho23Δ::KAN</i>	This study
JMY018	BY4742 <i>pho23Δ::HIS5</i>	This study
JMY020	TVY1 <i>pho23Δ::HIS5</i>	This study
JMY047	SEY6210 <i>pho23Δ::HIS5</i>	This study
JMY048	WLY176 <i>pho23Δ::HIS5</i>	This study
JMY050	FRY143 <i>pho23Δ::KAN</i>	This study
JMY093	WLY176 <i>rpd3Δ::HIS5</i>	This study
JMY094	WLY176 <i>pho23Δ::KAN rpd3Δ::HIS5</i>	This study
JMY097	WLY176 <i>ume6Δ::HIS5</i>	This study
JMY098	WLY176 <i>ume6Δ::HIS5 pho23Δ::KAN</i>	This study
JMY099	WLY176 <i>ATG12-PA::HIS5</i>	This study
JMY100	WLY176 <i>pho23Δ::KAN ATG12-PA::HIS5</i>	This study
JMY102	YZX94 <i>pho23Δ::KAN</i>	This study
JMY103	HCY129 <i>pho23Δ::KAN</i>	This study
JMY104	WLY176 <i>ATG7-PA::HIS5</i>	This study
JMY105	WLY176 <i>ATG7-PA::HIS5 pho23Δ::KAN</i>	This study
JMY146	CWY230 <i>pho23Δ::HIS5</i>	This study
HCY129	SEY6210 <i>ATG29-PA::TRP1</i>	(3)
MZY089	SEY6210 <i>atg8Δ::HIS5 P_{ATG8}-GFP-Atg8::LEU2</i>	(4)
SEY6210	MAT α <i>leu2-3,112 ura3-52 his3-Δ200 trp1-Δ901 suc2-Δ9 lys2-801 GAL</i>	(5)
SKB233	SEY6210 <i>atg8Δ::HIS5 P_{ATG8}-GFP-Atg8::LEU2 pho23Δ::KAN</i>	This study
TVY1	SEY6210 <i>pep4Δ::LEU2</i>	(6)
W303-1B	MAT α <i>leu2-3,112 ura3-1 his3-11,15 trp1-1 ade2-1 can1-100</i>	(7)
WLY176	SEY6210 <i>pho13Δ pho8Δ60</i>	(8)
XLY054	WLY176; <i>ATG9Δ::LEU2 pRS406::URA3 pep4Δ::KAN</i>	This study
XLY055	WLY176; <i>ATG9Δ::LEU2 pRS406-P_{ATG23}-ATG9-GFP::URA3 pep4Δ::KAN</i>	This study
XLY056	WLY176; <i>ATG9Δ::LEU2 pRS406-P_{ATG9}-ATG9-GFP::URA3 pep4Δ::KAN</i>	This study
XLY057	WLY176; <i>pRS406-P_{ATG8}-ATG9-GFP::URA3 pep4Δ::KAN</i>	This study
YZX94	BY4742; <i>ATG14-PA::HIS5</i>	This study
ZFY202	W303-1B; <i>pho13Δ pho8Δ60</i>	(9)

Table references:

- (1) Umekawa, M., and Klionsky, D.J. (2012). Ksp1 kinase regulates autophagy via the target of rapamycin complex 1 (TORC1) pathway. *J Biol Chem* 287, 16300-16310.
- (2) Cheong, H., Yorimitsu, T., Reggiori, F., Legakis, J.E., Wang, C.-W., and Klionsky, D.J. (2005). Atg17 regulates the magnitude of the autophagic response. *Mol Biol Cell* 16, 3438-3453.
- (3) Mao, K., Chew, L.H., Inoue-Aono, Y., Cheong, H., Nair, U., Popelka, H., Yip, C.K., and Klionsky, D.J. (2013). Atg29 phosphorylation regulates coordination of the Atg17-Atg31-Atg29 complex with the Atg11 scaffold during autophagy initiation. *Proc Natl Acad Sci U S A* 110, E2875-2884.
- (4) Cebollero, E., van der Vaart, A., Zhao, M., Rieter, E., Klionsky, D.J., Helms, J.B., and Reggiori, F. (2012). Phosphatidylinositol-3-phosphate clearance plays a key role in autophagosome completion. *Curr Biol* 22, 1545-1553.
- (5) Robinson, J.S., Klionsky, D.J., Banta, L.M., and Emr, S.D. (1988). Protein sorting in *Saccharomyces cerevisiae*: isolation of mutants defective in the delivery and processing of multiple vacuolar hydrolases. *Mol Cell Biol* 8, 4936-4948.
- (6) Gerhardt, B., Kordas, T.J., Thompson, C.M., Patel, P., and Vida, T. (1998). The vesicle transport protein Vps33p is an ATP-binding protein that localizes to the cytosol in an energy-dependent manner. *J Biol Chem* 273, 15818-15829.
- (7) Thomas, B.J., and Rothstein, R. (1989). Elevated recombination rates in transcriptionally active DNA. *Cell* 56, 619-630.
- (8) Kanki, T., Wang, K., Baba, M., Bartholomew, C.R., Lynch-Day, M.A., Du, Z., Geng, J., Mao, K., Yang, Z., Yen, W.-L., et al. (2009). A genomic screen for yeast mutants defective in selective mitochondria autophagy. *Mol Biol Cell* 20, 4730-4738.
- (9) Yang, Z., Geng, J., Yen, W.-L., Wang, K., and Klionsky, D.J. (2010). Positive or negative roles of different cyclin-dependent kinase Pho85-cyclin complexes orchestrate induction of autophagy in *Saccharomyces cerevisiae*. *Mol Cell* 38, 250-264.

Table 3.2. WT vs. *pho23Δ* TEM data

	Autophagic body size				
	Measured cross-sectional		Estimated original		
	Mean rad	SD rad	Mean rad	SD rad	Volume
WT sample set 1	154.134	61.579	164.174	57.207	2.61E+07
WT sample set 2	145.456	61.472	150.492	57.964	2.16E+07
WT average			157.333	57.586	2.39E+07
<i>pho23Δ</i> sample set 1	140.472	47.293	153.910	42.607	1.91E+07
<i>pho23Δ</i> sample set 2	133.372	49.776	142.444	46.510	1.64E+07
<i>pho23Δ</i> average			148.177	44.558	1.77E+07
	Vacuole size				
	Measured cross-sectional		Estimated original		
	Mean rad	SD rad	Mean rad	SD rad	
WT sample set 1	996.298	276.647	1132.894	237.068	
WT sample set 2	989.502	265.114	1132.552	218.821	
<i>pho23Δ</i> sample set 1	1015.804	293.056	1148.214	257.471	
<i>pho23Δ</i> sample set 2	978.013	269.367	1107.574	232.527	
	Autophagic body number			Total flux	
	Measured cross-sections/cell	Estimated bodies/cell			
WT sample set 1	5.982	32.714		8.55E+08	
WT sample set 2	7.463	43.532		9.41E+08	
WT average		38.123		8.98E+08	
<i>pho23Δ</i> sample set 1	13.725	80.583		1.54E+09	
<i>pho23Δ</i> sample set 2	15.000	90.619		1.49E+09	
<i>pho23Δ</i> average		85.601		1.51E+09	

Table 3.3. De-multiplexing results in 22M-31M reads of RNA-seq samples

Sample Description	Barcode (5'->3')	Raw reads	% of raw reads		% bases \geq Q30	Mean quality score	Mean error rate
			0 mismatch barcode	1 mismatch barcode			
WT growing	CGATGT	25,263,020	98.4%	1.6%	96.3%	37.88	1.6/10,000
<i>pho23Δ</i> growing	TGACCA	30,612,154	97.8%	2.3%	96.2%	37.86	1.6/10,000
WT starved	GCCAAT	21,992,351	97.8%	2.2%	96.2%	37.85	1.6/10,000
<i>pho23Δ</i> starved	CAGATC	24,344,369	97.9%	2.1%	96.2%	37.87	1.6/10,000
No barcode	NA	3,124,074	NA	NA	93.8%	37.03	2.0/10,000
	<i>Total:</i>	105,335,968					

Table 3.4. Mapping the reads of RNA-seq samples to the yeast transcriptome using Bowtie2

Sample description		WT growing	<i>pho23Δ</i> growing	WT starved	<i>pho23Δ</i> starved
Raw reads		25,263,020	30,612,154	21,992,351	24,344,369
Mapped reads		23,690,179	28,348,799	20,296,160	22,545,466
% of raw		93.8%	92.6%	92.3%	92.6%
Mapped, score ≥88		22,965,459	27,483,468	19,636,451	21,846,077
% of raw		90.9%	89.8%	89.3%	89.7%
Uniquely mapped, score ≥88		17,685,706	21,475,572	17,049,729	18,481,608
% of raw		70.0%	70.2%	77.5%	75.9%
Multi mapped, score ≥88		5,279,753	6,007,896	2,586,722	3,364,469
% of raw		20.9%	19.6%	11.8%	13.8%

Table 3.5. A9 strains TEM data

		Autophagic body size				
		Measured cross-sectional		Estimated original		
		Mean rad	SD rad	Mean rad	SD rad	Volume
Sample 1	A9Lo	151.214	44.113	169.029	36.365	2.32E+07
	A9WT	133.150	35.521	146.124	31.534	1.50E+07
	A9OE	130.633	33.522	143.491	29.268	1.40E+07
Sample 2	A9Lo	150.904	49.666	163.046	46.375	2.29E+07
	A9WT	126.450	33.223	137.063	30.134	1.24E+07
	A9OE	128.857	35.898	138.916	33.148	1.33E+07
		Vacuole size				
		Measured cross-sectional		Estimated original		
		Mean rad	SD rad	Mean rad	SD rad	
Sample 1	A9Lo	839.859	216.434	939.549	194.337	
	A9WT	835.052	219.762	929.285	201.215	
	A9OE	893.063	257.700	989.008	241.469	
Sample 2	A9Lo	885.798	251.927	982.226	234.885	
	A9WT	914.461	255.760	1026.609	233.004	
	A9OE	906.265	255.857	1012.629	235.507	
		Autophagic body number			Total flux	% flux
		Measured cross-sections/cell	Estimated bodies/cell			
Sample 1	A9Lo	2.856	12.686	2.94E+08	50.7%	
	A9WT	8.232	41.660	6.24E+08	107.6%	
	A9OE	10.000	55.496	7.76E+08	133.8%	
Sample 2	A9Lo	3.088	14.314	3.28E+08	56.6%	
	A9WT	7.309	43.105	5.36E+08	92.4%	
	A9OE	9.155	54.567	7.23E+08	124.8%	

Table 3.5. GO term analysis for genes upregulated in *PHO23* deletion cells

GO ID	Term	Number of genes			Fisher test p-value
		In genome	Actual in test set	Expected in test set	
GO:0000422	mitochondrion degradation	29	9	1.39	5.00E-06
GO:0010677	negative regulation of cellular carbohydrate metabolic process	15	6	0.72	3.90E-05
GO:0045912	negative regulation of carbohydrate metabolic process	15	6	0.72	3.90E-05
GO:0005975	carbohydrate metabolic process	336	33	16.07	5.10E-05
GO:0000407	phagophore assembly site	30	8	1.44	5.90E-05
GO:0010906	regulation of glucose metabolic process	32	8	1.53	9.50E-05
GO:0034727	piecemeal microautophagy of nucleus	33	8	1.58	1.20E-04
GO:0034045	phagophore assembly site membrane	7	4	0.34	1.60E-04
GO:0044262	cellular carbohydrate metabolic process	159	19	7.6	1.80E-04
GO:0016236	macroautophagy	45	9	2.15	2.20E-04
GO:0010675	regulation of cellular carbohydrate metabolic process	36	8	1.72	2.30E-04
GO:0005773	vacuole	250	25	11.98	3.40E-04
GO:0006109	regulation of carbohydrate metabolic process	38	8	1.82	3.50E-04
GO:0032258	Cvt pathway	38	8	1.82	3.50E-04
GO:0005952	cAMP-dependent protein kinase complex	4	3	0.19	4.20E-04

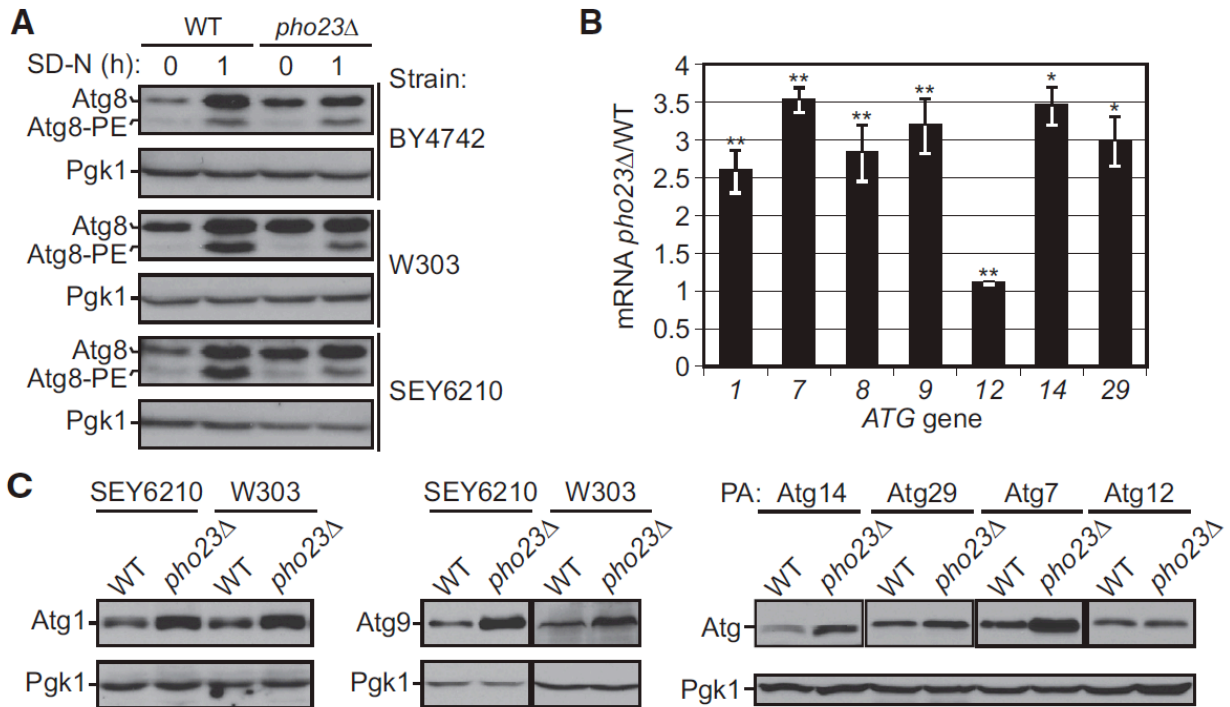


Figure 3.1. Pho23 represses the transcription of several *ATG* genes when autophagy is suppressed.

(A) Protein extracts were generated from wild-type and *pho23Δ* strains in the indicated backgrounds after growth in YPD to mid-log phase (growing conditions), and then shifted to SD-N medium (nitrogen starvation). Proteins were resolved by SDS-PAGE, then detected by western blot with anti-Atg8 and anti-Pgk1 (loading control) antisera. The Atg8 protein level was increased in growing conditions in *pho23Δ* cells relative to the wild type in all three strain backgrounds. (B) The ratio of *pho23Δ* to wild-type mRNA levels of the indicated *ATG* genes was measured by RT-qPCR. RNA extracts were prepared from wild-type (SEY6210) and *pho23Δ* (JMY047) cells after growth in YPD to mid-log phase. The error bars represent the standard error of the mean (SEM) of at least three independent experiments. Two-tailed *t*-test was used for statistical significance; * $p < 0.05$, ** $p < 0.01$. (C) Protein extracts were prepared as in (A) from wild-type and *pho23Δ* strains in growing conditions. The indicated proteins were detected by western blot using antisera to the endogenous proteins or an antibody that detects the protein A (PA) tag. Pgk1 was used as a loading control.

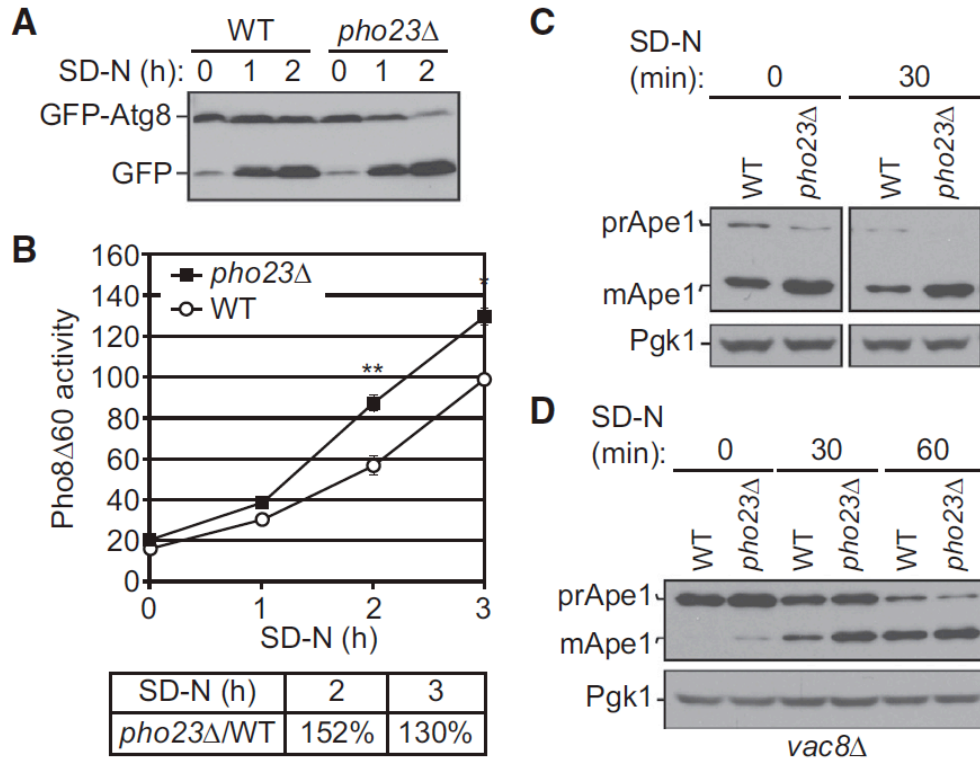


Figure 3.2. Pho23 negatively regulates autophagy activity.

(A) Wild-type (BY4742) and *pho23Δ* (JMY018) cells with a centromeric plasmid expressing *CUPI* promoter-driven *GFP-ATG8* were grown to mid-log phase in SMD-Ura and shifted to SD-N for the indicated times. Autophagy activity was measured by the GFP-Atg8 processing assay. (B) Wild-type (WLY176) and *pho23Δ* (JMY048) cells were grown to mid-log phase in YPD and shifted to SD-N for the indicated times of nitrogen starvation, and autophagy activity was monitored by the Pho8Δ60 assay. Pho8Δ60 activity was normalized to the wild-type strain (set to 100%) after 3 h of nitrogen starvation. The graph shows the average activity from three different experiments. Error bars represent the SEM. Two-tailed paired *t*-test was used for statistical significance; **p*<0.05, ***p*<0.01. (C) Wild-type (SEY6210) and *pho23Δ* (JMY047) cells were grown overnight, diluted to 0.1 OD₆₀₀, grown to mid-log phase (0.6 OD₆₀₀) in YPD, and shifted to SD-N for 30 min of nitrogen starvation. The precursor (pr) and mature (m) forms of Ape1 were separated by SDS-PAGE and detected with anti-Ape1 antiserum by western blotting. Pgk1 was detected with anti-Pgk1 antiserum as a loading control. (D) Precursor Ape1 processing in wild-type (*vac8Δ*; CWY230) and *pho23Δ* (*pho23Δ vac8Δ*; JMY146) cells at 0, 30, and 60 min after nitrogen starvation was detected by western blotting as in (C).

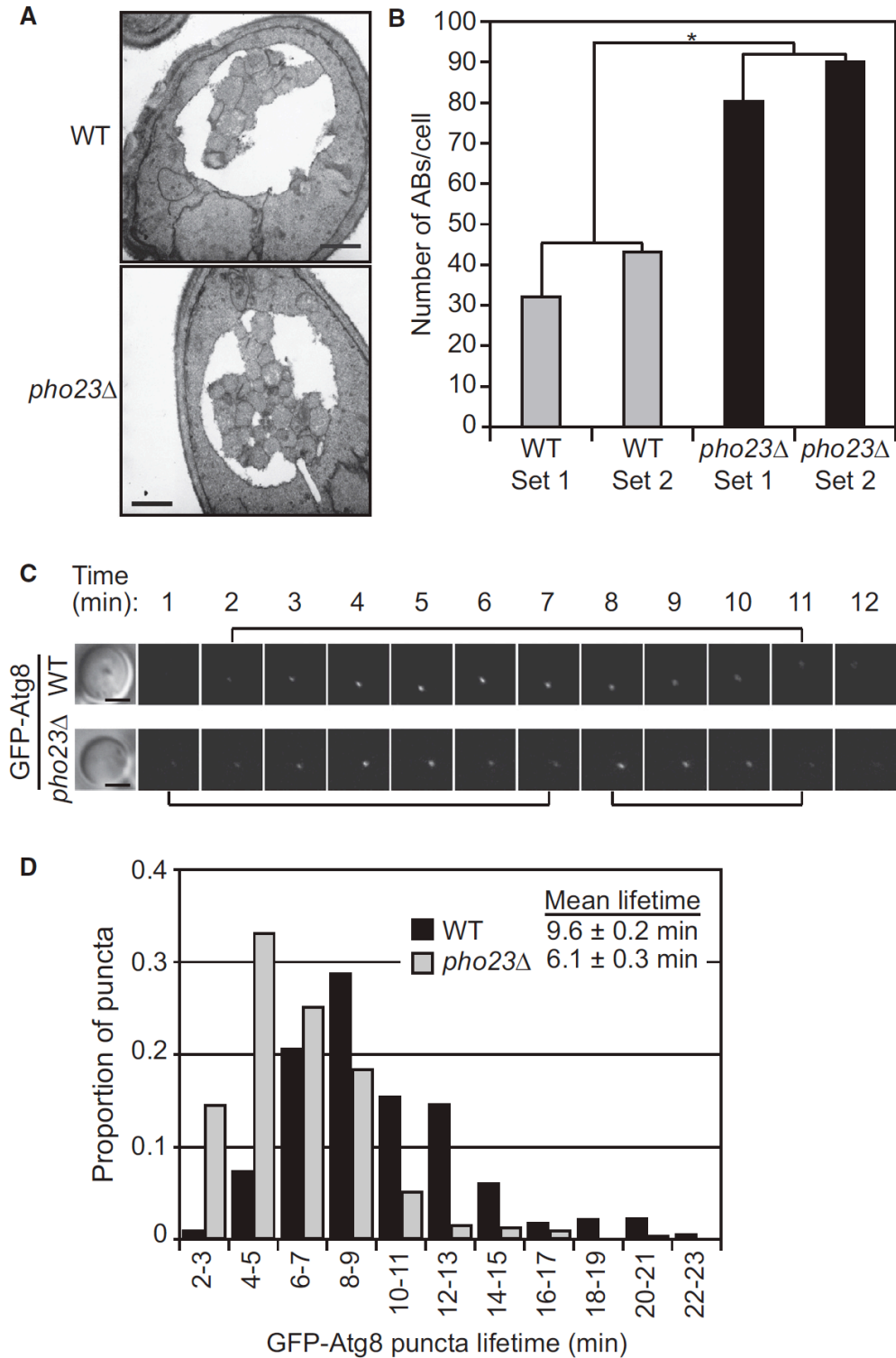


Figure 3.3. *pho23Δ* cells have an increased frequency of autophagosome formation
 (A) Representative TEM images of wild-type (*pep4Δ vps4Δ*; FRY143) and *pho23Δ* (*pep4Δ pho23Δ vps4Δ*; JMY050) cells, after 3 h of nitrogen starvation. More autophagic bodies accumulated in the vacuole of *pho23Δ* cells. Scale bar, 500 nm. (B) Estimated average number of

autophagic body numbers per cell in wild-type and *pho23Δ* strains after 3 h of nitrogen starvation. Estimation was based on the number of autophagic body cross sections observed by TEM in two independent experimental sets of more than 100 cells each for each strain. Two-tailed *t*-test was used for statistical significance; **p*<0.05. (See also Table 3.2.) (C) Representative images of GFP-Atg8 in wild-type (MZY089) and *pho23Δ* (SKB233) cells. Brackets indicate the lifetime of each punctum. Scale bar, 2 μm. (D) Distribution of GFP-Atg8 puncta lifetimes. Cells were imaged for 45 min beginning 40 min after a shift to nitrogen starvation. The lifetime of each individual punctum was determined as the time from when the punctum first appeared and began brightening to the time when it either disappeared or began a second round of brightening (indicating a second round of autophagosome formation from the same PAS). N>300 puncta from >65 cells per condition.

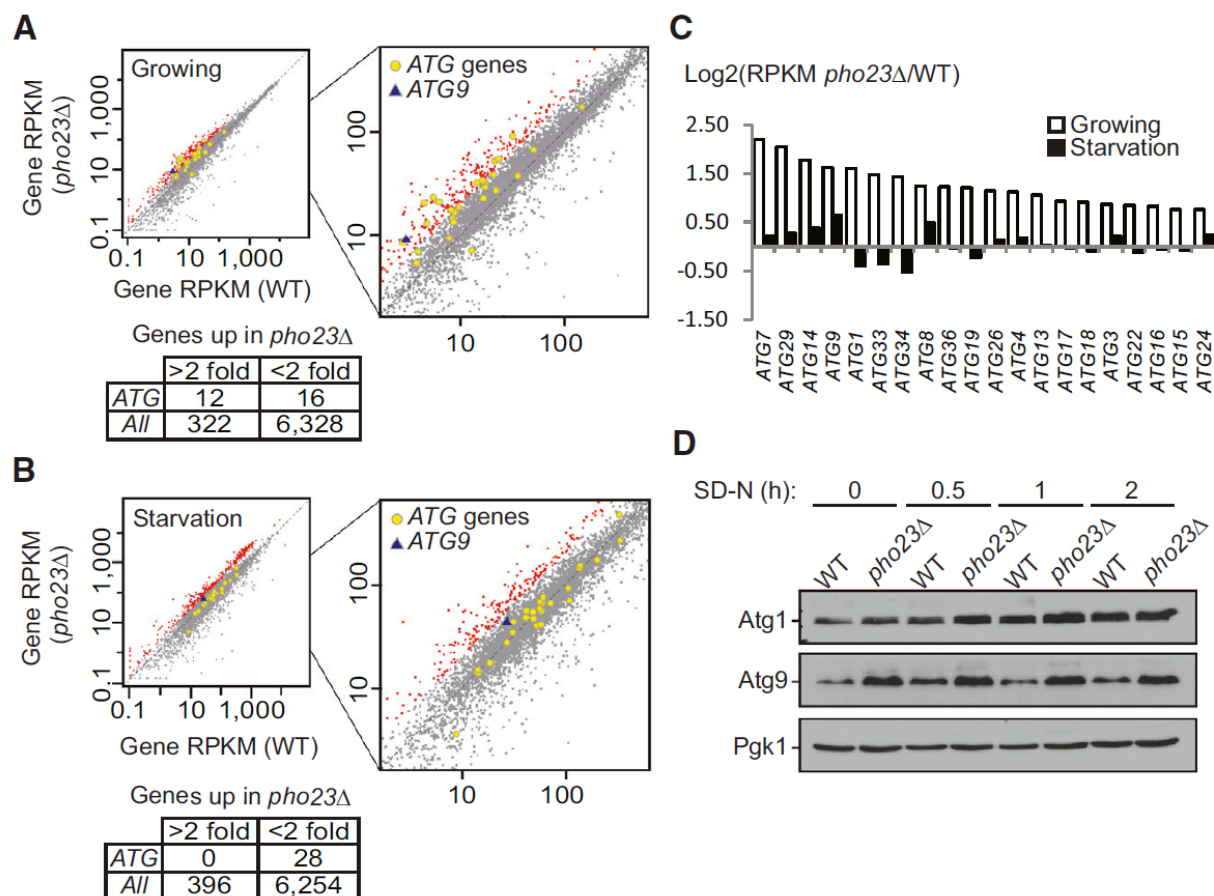


Figure 3.4. *pho23Δ* cells maintain higher *ATG9* expression levels relative to the wild type after autophagy is activated

(A, B) Gene RPKM (reads per kilobase per million mapped reads) values under growing (A) or 2 h nitrogen starvation (B) conditions are shown for the wild-type (SEY6210) versus the *pho23Δ* (JMY047) strains. Genes with expression changes more than 2-fold in *pho23Δ* cells are highlighted in red, while *ATG* genes are indicated by gray-outlined yellow circles, and *ATG9* is indicated by a blue triangle. (C) The ratio of the gene RPKM of the *pho23Δ* strain to the wild type is calculated for the top hits among the *ATG* genes. (D) Atg1, and Atg9 protein levels in wild-type (TVY1) and *pho23Δ* (JMY020) cells in the *pep4Δ* background after 0, 0.5, 1, and 2 h nitrogen starvation were analyzed by western blot. Pgk1 was used as a loading control.

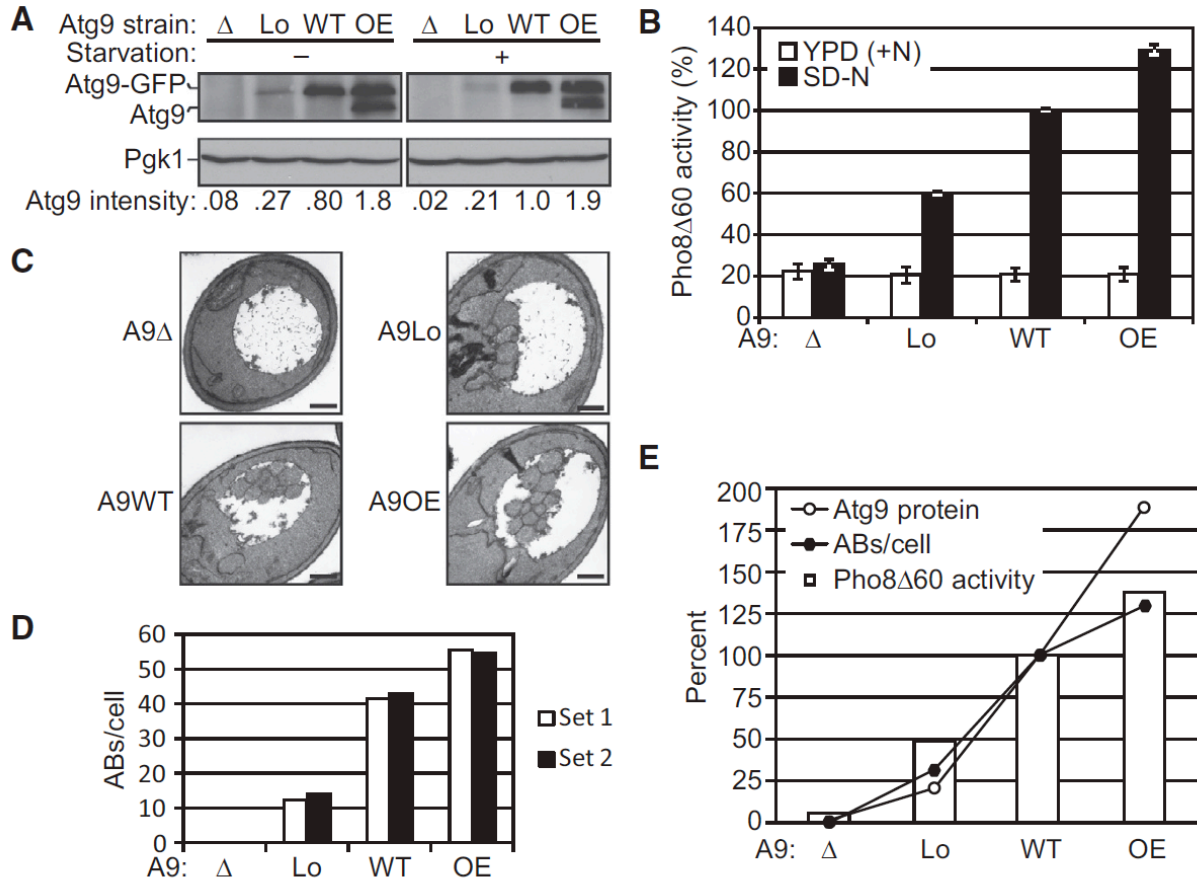


Figure 3.5. The Atg9 protein level correlates with autophagosome formation frequency and autophagy activity

(A) Four strains expressing different levels of Atg9-GFP (A9 Δ , the null control strain; A9Lo, expression controlled by the *ATG23* promoter, and thus lower than WT; A9WT, controlled by the endogenous promoter; and A9OE, expression controlled by the *ATG8* promoter in addition to the endogenous copy of *ATG9*, and thus higher than WT) were grown in YPD to mid-log phase and shifted to SD-N for 3 h. Proteins were resolved by SDS-PAGE, and detected by western blot with anti-Atg9 and anti-Pgk1 (loading control) antisera. Atg9 intensity was measured in ImageJ and represents an average of three independent experiments. (B) Cell lysates were generated as in (A) and autophagy activity was monitored by the Pho8 Δ 60 assay. Pho8 Δ 60 activity was normalized to the A9WT strain (set to 100%) after 3 h starvation. The graph shows the average activity from at least four different experiments. Error bars represent the SEM. (C) Representative TEM images of the four A9 strains, after 3 h starvation. Scale bar, 500 nm. (D) Estimated average number of autophagic bodies per cell in the four A9 strains after 3 h of nitrogen starvation. Estimation was based on the number of autophagic body cross sections observed by TEM in two independent experimental sets of more than 190 cells each for each strain. (E) Atg9 protein level detected by western blot, average autophagic body number/cell estimated by TEM, and starvation-induced Pho8 Δ 60 activity (the average Pho8 Δ 60 activity in growing condition was subtracted) of the four different A9 strains after 3 h starvation were plotted on one graph for comparison.

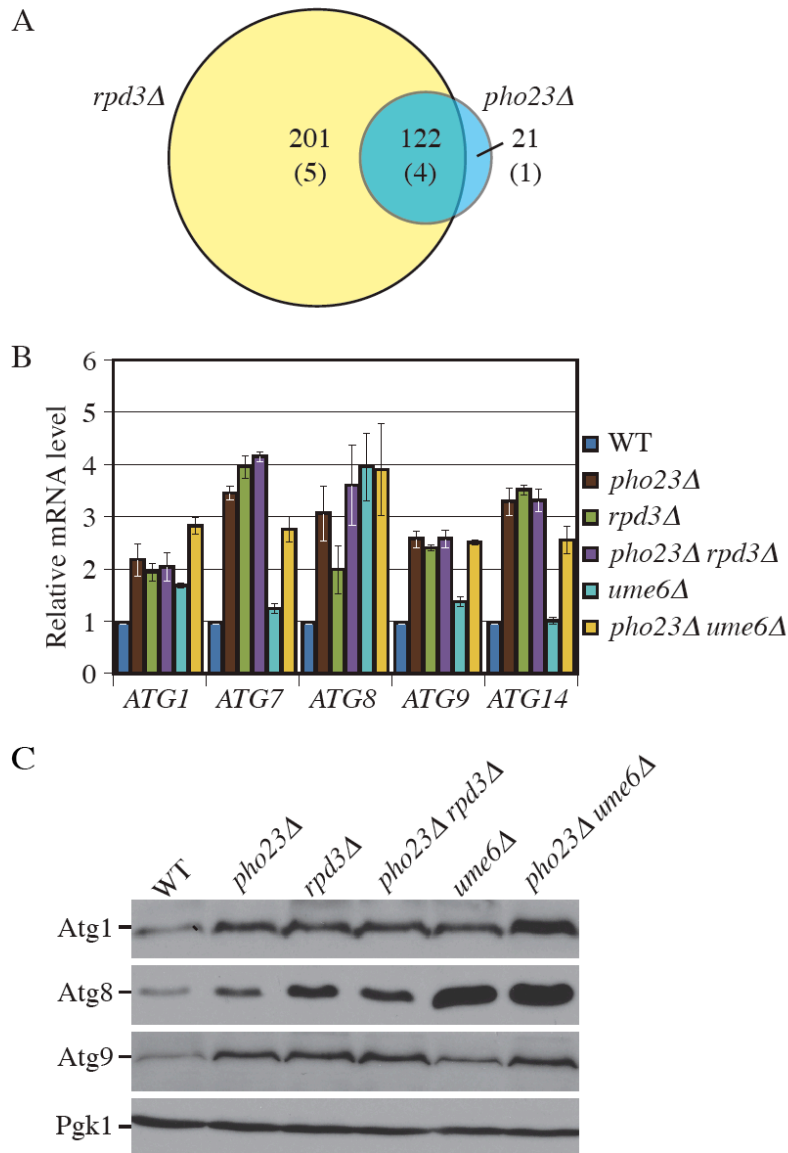


Figure 3.S1. Pho23 regulates ATG gene transcription in an Rpd3-dependent manner

(A) Number of genes that have more than a 1.5-fold change in expression level in *pho23Δ* and *rpd3Δ* strains relative to the wild-type strain are shown. Numbers in parentheses indicate the number of the *ATG* genes upregulated in the mutant strains. (B) Cells were grown in YPD to mid-log phase and RNA extracted as described in Materials and Methods. The relative mRNA levels of different *ATG* genes were measured in wild-type and mutant strains. The mRNA level of each gene in wild-type cells was set to 1, and other values were normalized. The error bars represent the SEM of three independent experiments. (C) Protein levels of Atg1, Atg8, and Atg9 were analyzed from protein extracts generated from mid-log phase wild-type (WLY176), *pho23Δ* (JMY048), *rpd3Δ* (JMY093), *pho23Δ rpd3Δ* (JMY094), *ume6Δ* (JMY097), and *pho23Δ ume6Δ* (JMY098) strains. Endogenous Atg proteins were detected by the indicated antisera, and Pgk1 was used as a loading control.

CHAPTER 4. A Large-scale Analysis of Autophagy Related Gene Expression Identifies New Regulators of Autophagy⁴

4.1 Abstract

Autophagy is a pathway mediating vacuolar degradation and recycling of proteins and organelles, which plays crucial roles in cellular physiology. To ensure its proper cytoprotective function, the induction and amplitude of autophagy are tightly regulated, and defects in its regulation are associated with various diseases. Transcriptional control of autophagy is a critical aspect of autophagy regulation, which remains largely unexplored. In particular, very few transcription factors involved in the activation or repression of autophagy-related gene expression have been characterized. To identify such regulators, we analyzed the expression of representative *ATG* genes in a large collection of DNA-binding mutant deletion strains in growing conditions as well as after nitrogen or glucose starvation. This analysis identified several proteins involved in the transcriptional control of *ATG* genes. Further analyses showed a correlation between variations in expression and autophagy magnitude, thus identifying new positive and negative regulators of the autophagy pathway. By providing a detailed analysis of the regulatory network of the *ATG* genes our study paves the way for future research on autophagy regulation and signaling.

⁴ This chapter is reprinted from Amélie Bernard*, Meiyang Jin*, Ziheng Xu, Daniel J Klionsky. A large-scale analysis of autophagy-related gene expression identifies new regulators of autophagy. *Autophagy*. 2015; 11(11): 2114-22. DOI: 10.1080/15548627.2015.1099796, with minor modifications, with permission from Taylor & Francis. *denotes equal contribution.

4.2 Introduction

Macroautophagy (hereafter referred to as autophagy) is a conserved pathway during which portions of the cytoplasm, organelles, or pathogens are engulfed by a double-membrane structure called the phagophore, which, after completion, forms into an autophagosome that fuses with the vacuole. Upon vacuolar fusion, the autophagy cargo as well as the inner membrane of the autophagosome is degraded. Molecules resulting from autophagy degradation are then recycled back to the cytosol and reused by the cell to maintain homeostasis in unfavorable conditions.¹

Autophagy is highly upregulated upon nutrient limitation as well as multiple stress conditions where it serves cytoprotective functions and promotes cell survival.² As a consequence, the autophagy pathway plays critical roles in mammalian development, cellular physiology and the immune response,³⁻⁵ and defects in autophagy are associated with severe pathologies such as cancer or metabolic diseases.⁶⁻⁷ A basal level of autophagy is also maintained in physiological conditions. For example, in mammals basal autophagy is involved in the degradation of damaged organelles and protein aggregates, which can otherwise lead to various neurodegenerative disorders such as Huntington, Alzheimer and Parkinson diseases.⁹ In yeast, along with a low level of constitutive autophagy the cytoplasm-to-vacuole targeting (Cvt) pathway, a biosynthetic type of selective autophagy, delivers resident enzymes to the vacuole during growth.⁸

High, uncontrolled, autophagy activity can also be detrimental for cells as it can lead to cell death or promote the replication/spread of microbes or cancer cells that, in some instances, can use autophagy as a source of nutrients or to survive in unfavorable conditions.¹⁰⁻¹³ Therefore, to support proper cellular functions, the magnitude of autophagy has to be finely controlled, notably by regulating the autophagy-related (Atg) proteins, the core components of the autophagy machinery. Numerous studies have provided significant advances on the

understanding of the posttranslational modifications of several Atg proteins, which affects their localization and activity, as well as protein-protein interactions; key players of these regulatory networks have been characterized (for review see ref. 14 and 15). The mechanisms involved in transcriptional regulation of *ATG* genes remains, however, largely unknown. Upon stress conditions, the expression of most of the *ATG* genes is upregulated and this correlates with an increase in autophagy activity. Recent studies showed that the transcriptional regulation of *ATG* genes is critical for autophagy: the level of Atg8, for example, correlates with autophagosome size,¹⁶ that of Atg9 correlates with their number,¹⁷ and the amount of Atg7 modulates autophagy amplitude.¹⁸ In higher eukaryotes the family of FOXO transcription factors, GATA1 as well as the master regulator TFEB, activates autophagy,¹⁹⁻²¹ while ZKSCAN3 and GATA4 are involved in the repression of mammalian autophagy related genes.²²⁻²³ In yeast, recent studies characterized Ume6 and Pho23 as transcriptional repressors of *ATG* genes and negative regulators of autophagy.^{24,17} Nevertheless, very few transcription factors involved in the regulation of the expression of *ATG* genes in either yeast or mammals are known. To identify such regulators we conducted a screen in which DNA-binding protein deletion strains were tested for the expression of *ATG* genes. This revealed Rph1 as a master transcriptional repressor of autophagy.¹⁸ Here we report on the overall results of the screen, which identify new autophagy regulators, either activators or repressors of *ATG* gene expression. Candidates showing the highest variations of expression were further characterized to assay their impact on autophagy activity and the Cvt pathway. Together, our results constitute a valuable resource in the understanding of the transcription of autophagy-related genes as well as overall autophagy regulation and provide new directions in autophagy research.

4.3 Results

4.3.1 A screen for DNA-binding proteins regulating the expression of *ATG* genes.

In order to identify new transcriptional regulators of autophagy the expression of a subset of *ATG* genes was analyzed in comparison between wild-type cells and a collection of DNA-binding mutants (Figure 4.1A). To select the target *ATG* genes used in this study we integrated multiple criteria: (i) Most, but not all, *ATG* genes are upregulated after nutrient starvation;¹⁷ targets should show a strong induction of expression, indicating that they are under transcriptional regulation in these conditions. (ii) Variation in the expression of the selected genes should translate into a detectable effect with regard to autophagy; i.e., the amount of the corresponding protein modulates the level of autophagy activity. (iii) Target genes should be representative of different steps of the autophagy pathway and notably of selective autophagy.

Based on these points, we selected *ATG1*, *ATG7*, *ATG8*, *ATG9*, *ATG14*, *ATG29* and *ATG32*: *ATG1* and *ATG29* as markers of autophagy induction, *ATG9* for the supply of lipids to the expanding phagophore, *ATG14* for vesicle nucleation, *ATG7*, *ATG8* and *ATG9* for vesicle expansion and completion, and *ATG32* as a marker of mitophagy, the selective autophagic degradation of mitochondria.²⁵ Furthermore, previous work from our lab showed that the level of Atg7, Atg8 and Atg9 correlates with autophagy activity,¹⁶⁻¹⁸ indicating that modulation in the expression of the corresponding genes should affect the magnitude of autophagic degradation.

An increase in mRNA level upon autophagy activation could result either from the release of a repressive factor or the recruitment of an activator. Therefore gene expression was analyzed by RT-qPCR in nutrient-replete conditions (growing conditions), where the deletion of a repressor should lead to mRNA enrichment, as well as after nitrogen starvation and glucose

starvation where the deletion of a positive factor would result in a reduction in the mRNA level compared to the wild type.

Among the 139 strains analyzed, 61 strains showed a reduction of 1.5X of the induction of at least one *ATG* gene compared to the induction in wild-type cells after nitrogen starvation, and among these, 5 strains showed a more than 2-fold reduction (Figure 4.1B, Table 4.S1). Upon glucose starvation, 37 strains showed a reduction of 1.5X of the induction of at least one *ATG* gene compared to the induction seen in wild-type cells, and among these 1 strain showed a more than 2-fold reduction (Figure 4.1B, Table 4.S2). Finally, 13 strains showed an induction of 1.5 fold or more in the expression of at least one *ATG* gene and 6 showed an increase of more than 2 fold in growing conditions compared to the wild type (Figure 4.1B, Table 4.S3). Note that among the hits, the *ume6* Δ and *rph1* Δ cells showed enriched mRNA levels of *ATG* genes consistent with previous publications (Table 4.S3, Figure 4.S1).^{24,18} The results for all 139 strains in the different conditions are listed in Tables 4.S1 to S3.

As a proof of concept and to assay the level of confidence of the results obtained in the screen, we repeated the analysis with the candidate strains that showed the highest variation compared to wild type, that is, an increase in expression of more than 2X in growing conditions (potential repressors) or a reduction of more than 2X after starvation (potential activators). The deletion of *SPT10*, *FYV5*, *SFL1*, *ZAPI* and *YRMI* led to a significant increase in the expression of at least one *ATG* gene; *sko1* Δ cells showed a similar pattern although the differences were not quite statistically significant (Figure 4.S1A). The deletion of *MBPI* resulted in a large reduction in the induction of expression of most of the analyzed target genes after glucose starvation (Figure 4.S1B), whereas the deletion of *GCN4*, *GLN3*, *GATI* and *SWI5* decreased the induction of the expression of at least one *ATG* gene after nitrogen starvation (Figure 4.S1C). Together

these results confirmed the validity of the results obtained during our screen and identified Spt10, Fyv5, Sfl1, Sko1, Zap1 and Yrm1 as potential transcriptional repressors of autophagy, and Mbp1, Gcn4, Gln3, Gat1 and Swi5 as potential transcriptional activators of autophagy (Table 4.1).

4.3.2 Analysis of transcriptional activators of autophagy

To further characterize the proteins identified during the screen and to verify the screen results we decided to delete our candidate genes in another yeast strain background to eliminate potential strain-dependent phenotypes and also to confirm that the expression defects were due to the correct gene deletion. For all but the *MBP1* deletion, we used the SEY6210 background expressing the modified Pho8 Δ 60 protein that forms the basis of an assay to monitor autophagy activity.²⁶ The deletion of *MBP1* was made in the W303 background, which shows a better response to glucose starvation-induced autophagy (our unpublished observation). Among the potential transcriptional activators, 2 mutants, *swi5* Δ and *mbp1* Δ , now showed comparable *ATG* expression with the wild type after nitrogen and glucose starvation, respectively, indicating that the corresponding gene was unlikely to be involved in autophagy regulation or that the phenotype was strain specific (Figure 4.S2A and 4.B). In contrast, the deletion of *GCN4*, *GLN3*, and *GATI* recapitulated the results observed during the initial screen. In *gcn4* Δ cells, we observed a reduction in the induction of *ATG1* expression as well as Atg1 protein level compared to wild-type cells after nitrogen starvation (Figure 4.2A and 4.B, compare lane 2 to 5 and lane 3 to 6). Under these conditions the expression of *ATG7*, *ATG8*, *ATG9*, *ATG29* and *ATG32* was induced to a lesser extent in *gln3* Δ and *gat1* Δ cells compared to the wild type (Figure 4.2C, lower panel) suggesting that the corresponding proteins are transcriptional activators of *ATG* genes. In addition, the deletion of *GLN3* resulted in an accumulation of *ATG8* and *ATG29*

mRNAs in growing conditions (Figure 4.2C, upper panel) indicating that Gln3 is directly or indirectly involved in the repression of these genes when autophagy is kept at a basal level. Gln3 and Gat1 are both part of the GATA family of transcription factors and bind to similar DNA motifs.²⁷⁻³⁰ The double deletion *gat1Δ gln3Δ* did not have an additive effect on *ATG* expression after nitrogen starvation compared to the single *gln3Δ* or *gat1Δ* strain (Figure 4.2C) suggesting that the 2 proteins may recognize the same consensus sites on *ATG* promoters and work together to induce their transcription.

To determine the effect of such transcriptional variation on protein level we focused on Atg8, as the corresponding gene was one of the most significantly affected in the mutants and because the level of this protein modulates autophagy activity.¹⁶ Consistent with the mRNA data, the level of Atg8 was higher in *gln3Δ* and *gat1Δ gln3Δ* cells compared to the wild type in growing conditions (Figure 4.2D, compare lane 1 to lanes 3 and 7). Shortly after starvation we did not observe a major difference in the overall amount of Atg8 although there was a relative enrichment of the pool of Atg8 conjugated to phosphatidylethanolamine (PE), Atg8-PE, in *gln3Δ* and *gat1Δ gln3Δ* cells (Figure 4.2D, compare lane 2 to lanes 4 and 8). This suggests a more rapid autophagy induction in these cells due to the increased expression of the *ATG* genes in growing conditions. Together these results reveal the role of Gln3 in the repression of some *ATG* genes in growing conditions and show that Gat1, Gcn4 and Gln3 are activators required for the induction of *ATG* gene expression after nitrogen starvation.

To determine how these transcriptional defects affect autophagy flux, we monitored autophagy activity using the Pho8Δ60 assay. In this assay, we use a modified phosphatase precursor, Pho8Δ60, which can only be delivered from the cytoplasm to the vacuole by the autophagy pathway. Inside the vacuole, Pho8Δ60 is activated; therefore, levels of phosphatase

activity of Pho8Δ60 reflect the rate of nonselective autophagy.²⁶ Consistent with a reduction of *ATG* gene expression after nitrogen starvation, the *GATI* deletion strain showed a 20% decrease, whereas the *GCN4* deletion resulted in a 50% reduction in Pho8Δ60-dependent phosphatase activity compared to wild-type cells (Figure 4.3A); *atg1Δ* cells were used as a negative control and showed no induction of autophagy. In contrast, and despite the defects in *ATG* expression after starvation, the deletion of *GLN3* and the double *GATI GLN3* deletion did not show any defects in autophagy activity upon nitrogen starvation (Figure 4.3A). We hypothesized that this could result from the increased expression, notably of *ATG8*, observed in growing conditions in these strains. This may cause an increase in autophagy activity shortly after induction and would therefore counteract the potential repressive effect of the mutations over the time course of this assay. Such a phenotype is seen, for example, in the *ume6Δ* strain, where higher basal Atg8 levels result in a more rapid increase in autophagy activity in starvation conditions.²⁴

To extend our analysis we used the GFP-Atg8 processing assay. During autophagy, Atg8 is lipidated by conjugation with PE and recruited to the phagophore, the precursor to the autophagosome. After the fusion of the autophagosome with the vacuole, the GFP-Atg8 chimera is hydrolyzed: Atg8 is rapidly degraded while the more stable GFP moiety will accumulate. Therefore, the accumulation of free GFP reflects the magnitude of autophagy cargo delivery.³¹ After 3 h of nitrogen starvation the mutants displayed a similar autophagy phenotype compared to that obtained from the Pho8Δ60 assay (Figure 4.3B). The ratio of free GFP:total GFP was decreased compared to that of the wild-type cells in the *gat1Δ* and *gcn4Δ* strains, respectively. The deletion of *GLN3* and the double *GATI GLN3* deletion did not display a major difference compared to wild-type cells after 3 h, but showed higher GFP-Atg8 processing after 1 h of

nitrogen starvation, supporting the hypothesis that higher expression of at least *ATG8* in growing conditions in these strains increased autophagy activity in the short term after its induction.

We also analyzed the effects of transcriptional variation of *ATG* genes on the Cvt pathway, a selective type of autophagy used for the delivery of the resident hydrolase aminopeptidase I (Ape1) to the vacuole,³² by monitoring the processing of precursor (pr)Ape1. Higher expression of *ATG8* and *ATG29* in *gln3Δ* and *gat1Δ gln3Δ* cells led to an increase in the Cvt pathway as shown by the accumulation of mature Ape1 compared to wild-type cells (Figure 4.3C). The *GATI* deletion was similar to wild type, whereas the *GCN4* deletion resulted in a reduction of about 50% in the Cvt pathway. This latter result was unexpected given that *gcn4Δ* cells did not show any mRNA phenotype in growing conditions. We thus propose that this transcription factor might affect the expression of other genes (potentially other *ATG* genes) in these conditions that would account for the defects in prApe1 processing.

4.3.3 Analysis of transcriptional repressors of autophagy

Similar to the transcriptional activators, the phenotype of our potential repressors was tested by generating strains in a new background. Among them, 4 mutants, *sfl1Δ*, *sko1Δ*, *yrmlΔ* and *zap1Δ* now showed comparable *ATG* expression with the wild type in growing conditions indicating that the corresponding protein was unlikely to be a transcriptional repressor of autophagy or that its effect was strain dependent (Figure 4.S2C). In contrast, the deletion of *FYV5* led to a significant upregulation of *ATG1*, *ATG8*, *ATG9* and *ATG14*, whereas the deletion of *SPT10* significantly increased the expression of *ATG1*, *ATG8*, *ATG9*, *ATG29* and *ATG32* in growing conditions (Figure 4.4A). To test whether the effect on gene expression was reflected at the protein level we analyzed the amount of Atg8 and Atg9 protein, which showed major differences in expression in these 2 strains compared to the wild type. Consistent with the mRNA

results, the level of Atg8 and Atg9 was largely increased in *spt10Δ* cells (Figure 4.4B); in contrast the deletion of *FYV5* did not significantly affect the level of these 2 proteins. To explain these discrepancies we propose that Fyv5 may affect a multitude of cellular pathways including protein translation, which, if slowed down, may not reflect mRNA enrichment.

We next tested autophagy activity in these strains using the Pho8Δ60 assay. The deletion of *SPT10* resulted in higher phosphatase activity in growing conditions as well as after starvation (Figure 4.4C). Consistent with this result, autophagy measured by the GFP-Atg8 processing assay was induced to a higher extent in *spt10Δ* cells compared to the wild type (Figure 4.4D). The deletion of *FYV5* has a strong effect on the level of the Pho8Δ60 protein (Figure 4.S3A), which prevented the use of the corresponding assay. However, using the GFP-Atg8 processing assay we did not observe a major effect on autophagy activity in *fyv5Δ* cells (Figure 4.4D). Finally, the analysis of prApe1 showed an increase of the Cvt pathway in *spt10Δ* and *fyv5Δ* cells compared to the wild type (Figure 4.4E).

4.3.4 Characterization of *Sfl1*

We initially selected *Sfl1* as a candidate as the deletion of the *SFL1* gene showed higher *ATG* expression in the screen (Figure 4.S1A), although the generation of a new deletion strain showed that this was likely a false positive result (Figure 4.S2C). Nevertheless, analysis of a strain overexpressing the protein caught our attention: it showed higher expression of several *ATG* genes in growing conditions, and the expression of *ATG8* was especially massively induced (Figure 4.5A). In accordance with an increased level of mRNAs, the overexpression of *Sfl1* resulted in an accumulation of Atg proteins as illustrated by the analysis of Atg1, Atg8 and Atg9 (Figure 4.5B). As the steady state level of the Pho8Δ60 protein was severely reduced in cells overexpressing *Sfl1* results using the Pho8Δ60 assay could be misleading (Figure 4.S3B). Instead

autophagy activity was assayed using the GFP-Atg8 processing assay. The overexpression of Sfl1 led to a large increase in autophagy in growing conditions as well as shortly after starvation, but not after prolonged incubation (Figure 4.5C). The observation that the autophagy activity of wild-type cells reaches that of the mutants with longer times of starvation is consistent with the fact that overexpressing Sfl1 increases the transcription of *ATG* genes only in nutrient-rich conditions; an overaccumulation of Atg proteins can therefore support a jump-start in autophagy activity upon its induction by nitrogen starvation. After longer times of starvation, *ATG* levels in wild-type cells will reach that of the mutant strain, abolishing the difference in autophagy activity relative to the Sfl1 overexpressor.

Because overexpression of Sfl1 resulted in higher expression of *ATG* genes in growing conditions we hypothesized that the Cvt pathway might also be affected in these cells. Indeed, analysis of prApe1 indicated that overexpressing Sfl1 resulted in an overaccumulation of the mature form of Ape1 suggesting that the Cvt pathway was increased (Figure 4.5D). Together our results suggest that Sfl1 acts as a transcriptional activator of autophagy and the Cvt pathway.

4.4 Discussion

In this study, a screen for DNA-binding proteins that modulate *ATG* gene expression identified several transcriptional regulators of autophagy. As a proof of concept of the screen we initially focused on the characterization of proteins for which deletion of the corresponding gene showed the highest variation of *ATG* gene expression. This criterion identified Gcn4, Sfl1, Gat1 and Gln3 as potential transcriptional activators of autophagy, and Spt10 and Fyv5 as putative repressors of *ATG* gene expression. It is worth noting that the transcriptional modulations we observed in the deletion strains might not result from a direct effect of the corresponding protein: the deletion of key regulators may indeed cause cellular stresses or modulate the level of an

intermediate protein which would in turn affect the expression of *ATG* genes. Nonetheless, an analysis of the promoter regions of *ATG* genes identified one or multiple consensus DNA-binding sites in at least one of the *ATG* genes analyzed for Gat1, Gcn4, Gln3 and Sfl1 (Table 4.S4) thus supporting a direct regulation by, at least, these transcriptional regulators. Furthermore, chromatin immunoprecipitation experiments revealed the direct binding of Gcn4 on the promoter of *ATG1* (Figure 4.S4A and B).

Gcn4 was previously shown to modulate autophagy activity upon amino acid and nitrogen starvation conditions,³³⁻³⁴ although the mechanism by which this regulation is achieved was not clearly identified. Our results reveal here that Gcn4 is required for the full induction of *ATG1* expression upon nitrogen starvation. In addition, in cells where the *ATG1* promoter was changed for the Gcn4-insensitive *PMP3* promoter, the deletion of *GCN4* caused less of a reduction of autophagy activity than in wild-type cells (35% instead of 50%; Figure 4.S4C and D). Together these data provide new insights into the function of Gcn4 showing that it regulates autophagy partly through its promotion of *ATG1* expression after starvation, but also indicate that other *GCN4*-sensitive genes, not identified at this time, are also involved. Gat1 and Gln3 are part of the GATA family of transcription factors, which are well-described activators of gene expression upon nutrient starvation conditions. Gln3 was previously suggested to affect the expression of *ATG14*,³⁵ in our study we showed that this protein is required for the induction of several *ATG* genes upon nitrogen starvation, although we did not observe a significant effect on *ATG14*. We also report that the deletion of Gln3 increases the expression of *ATG8* and *ATG29* in growing conditions suggesting that the protein is directly or indirectly involved in the repression of some *ATG* genes. Previous studies showed that the mammalian GATA1 and GATA4 transcription factors are involved in the expression of several autophagy-related genes,^{20,23} suggesting that

the function of the GATA family members in regulating autophagy is conserved from yeast to mammals.

Sfl1 is characterized as a dual transcriptional activator and repressor notably involved in the regulation of flocculation-related genes.³⁶ In mammalian cells, HSF2, a Sfl1 homolog, was suggested to induce autophagy upon heat shock although the molecular mechanism underlying its regulation was not characterized.³⁷ We show here that the overexpression of the Sfl1 protein greatly increases the expression of several *ATG* genes in yeast, especially *ATG8*, as well as autophagy activity in growing conditions. These results suggest that Sfl1 functions as a transcriptional activator of the autophagy pathway.

Our results also show that Spt10 and Fyv5 repress the expression of *ATG* genes in growing conditions and that Spt10 negatively regulates autophagy activity. Based on this finding we propose that Spt10 functions in the maintenance of autophagy at a basal level when environmental conditions are optimal, possibly through its putative histone acetylase activity.

To maintain cell homeostasis and prevent disease, rates of autophagy have to be finely tuned in response to multiple environmental conditions. Several signaling pathways regulating autophagy have been characterized and the activity of Atg proteins is controlled by multiple posttranslational modifications. In the last 10 years, an increasing number of proteins acting in the regulation of autophagy have been identified showing the high complexity of this signaling network. Previous work from our lab revealed the critical importance of transcriptional control of *ATG* genes for autophagy regulation adding yet another layer of complexity to the overall regulation of the pathway.^{17-18,24} Results presented here provide new directions in the understanding of the transcriptional control of autophagy. It is worth noting that all of the autophagy transcriptional regulators analyzed in the present study, or that were previously

characterized, affect the expression of *ATG8*. The level of Atg8 correlates with the size of autophagosomes and the rate of autophagic degradation;¹⁶ regulating the expression of *ATG8* might therefore be pivotal for the modulation of autophagy activity. An *in silico* analysis of the consensus binding sites of *ATG8* regulators indicates putative binding at multiple locations scattered throughout the *ATG8* promoter, suggesting a high activity and complexity at this locus under stress conditions (Figure 4.S4E).

Besides the DNA-binding proteins analyzed in detail in this study, we report here on several proteins for which deletion of the corresponding gene affects *ATG* expression to a lesser extent. Although mild, these effects may be responsible for subtle modification of autophagy rates, which, combined with other signaling pathways, may account for large variations in autophagy activity. Furthermore, the multitude of transcriptional regulators of *ATG* expression certainly reflects the variety of environmental conditions upon which autophagy has to be modulated. Our study should therefore help in unraveling the multiple actors involved in autophagy regulation by identifying downstream effectors of signaling pathways. Finally, as most regulatory pathways are conserved from yeast to mammals, our study of the transcription of yeast autophagy genes may contribute valuable information that can be used for the therapeutic treatment of autophagy-related diseases.

4.5 Materials and Methods

4.5.1 Yeast strains, media and cell culture

Gene disruptions were performed using a standard method.³⁸ Yeast cells were grown in YPD (1% yeast extract, 2% peptone, and 2% glucose [all wt/vol]) or synthetic minimal medium (SMD; 0.67% yeast nitrogen base [ForMedium, CYN0410], 2% glucose, supplemented with the appropriate amino acids and vitamins). Autophagy was induced in nitrogen starvation medium

(SD-N; 0.17% yeast nitrogen base without amino acids [ForMedium, CYN0501], containing 2% glucose) or glucose starvation medium (0.67% yeast nitrogen base, 3% glycerol, supplemented with amino acids and vitamins). The yeast DNA-binding protein mutants analyzed during the screen came from a collection in the BY4742 background except as otherwise indicated. Other strains used in this study are listed in Table 4.S5.

4.5.2 RNA and RT-qPCR

Total RNA was extracted using the NucleoSpin RNA kit (Clontech, 740955). DNase treatment was performed according to the kit instruction to eliminate genomic DNA contamination. RT-qPCR reactions were performed as previously described,¹⁸ using gene-specific primers listed in Table 4.S6. The transcript abundance in samples was determined using a comparative threshold cycle method. The relative abundance of the reference mRNAs of *TAF10*, *TFC1*, *UBC6* or *SLD3* in each sample was determined and used to normalize for differences of total RNA amount according to the method described by Vandesompele et al.³⁹

4.5.3 Statistical analyses

Statistical differences were assayed using one-sample *t* test and student *t* test; *, $p < 0.05$; **, $p < 0.01$; ***, $p < 0.001$.

4.5.4 Other Methods

Protein extraction, immunoblot, GFP-Atg8 processing, and Pho8 Δ 60-dependent phosphatase assays were performed as previously described.^{40-41,31} Antisera to Atg1,⁴² Atg9,⁴³ Atg8,⁴⁴ Pgc1 (a generous gift from Dr. Jeremy Thorner, University of California, Berkeley), Ape1,⁴⁵ monoclonal Dpm1 (Life Technologies, 5C5A7) and monoclonal YFP (Clontech, JL-8) were used as previously described or according to the manufacturer's instructions.

4.6 Acknowledgments

This work was supported by NIH grant GM053396 to DJK and a Rackham predoctoral fellowship to M.J.

4.7 References

1. Xie Z, Klionsky DJ. Autophagosome formation: core machinery and adaptations. *Nat Cell Biol* 2007; 9: 1102-1109.
2. Tsukada M, Ohsumi Y. Isolation and characterization of autophagy-defective mutants of *Saccharomyces cerevisiae*. *FEBS Lett* 1993; 333: 169-174.
3. Levine B, Klionsky DJ. Development by self-digestion: molecular mechanisms and biological functions of autophagy. *Dev Cell* 2004; 6: 463-477.
4. Deretic V, Levine B. Autophagy, immunity, and microbial adaptations. *Cell Host Microbe* 2009; 5: 527-549.
5. Shi CS, Shenderov K, Huang NN, Kabat J, Abu-Asab M, Fitzgerald KA, Sher A, Kehrl JH. Activation of autophagy by inflammatory signals limits IL-1beta production by targeting ubiquitinated inflammasomes for destruction. *Nat Immunol* 2012; 13: 255-263.
6. Huang J, Klionsky DJ. Autophagy and human disease. *Cell Cycle* 2007; 6: 1837-1849.
7. Mizushima N, Levine B, Cuervo AM, Klionsky DJ. Autophagy fights disease through cellular self-digestion. *Nature* 2008; 451: 1069-1075.
8. Lynch-Day MA, Klionsky DJ. The Cvt pathway as a model for selective autophagy. *FEBS Lett* 2010; 584: 1359-1366.
9. Nixon, RA. The role of autophagy in neurodegenerative disease. *Nat Med* 2013; 19: 983-997.
10. Chen Y, Azad MB, Gibson SB. Superoxide is the major reactive oxygen species regulating autophagy. *Cell Death Differ* 2009; 16: 1040-1052.
11. Levine B, Yuan J. Autophagy in cell death: an innocent convict? *J Clin Invest* 2005; 115: 2679-2688.
12. Ravikumar B, Sarkar S, Davies JE, Futter M, Garcia-Arencibia M, Green-Thompson ZW, Jimenez-Sanchez M, Korolchuk VI, Lichtenberg M, Luo S, Massey DC, Menzies FM, Moreau K, Narayanan U, Renna M, Siddiqi FH, Underwood BR, Winslow AR, Rubinsztein DC. Regulation of mammalian autophagy in physiology and pathophysiology. *Physiol Rev* 2010; 90: 1383-1435.
13. Jin M, Klionsky DJ. Regulation of autophagy: Modulation of the size and number of autophagosomes. *FEBS Lett* 2014; 588: 2457-2463.
14. Feng Y, Yao Z, Klionsky DJ. How to control self-digestion: transcriptional, post-transcriptional, and post-translational regulation of autophagy. *Trends Cell Biol* 2015; 25: 354-363.
15. Xie Y, Kang R, Sun X, Zhong M, Huang J, Klionsky DJ, Tang D. Posttranslational modification of autophagy-related proteins in macroautophagy. *Autophagy* 2015; 11: 28-45.
16. Xie Z, Nair U, Klionsky DJ. Atg8 controls phagophore expansion during autophagosome formation. *Mol Biol Cell* 2008; 19: 3290-3298.
17. Jin M, He D, Backues SK, Freeberg MA, Liu X, Kim JK, Klionsky DJ. Transcriptional regulation by pho23 modulates the frequency of autophagosome formation. *Curr Biol* 2014; 24: 1314-1322.

18. Bernard A, Jin M, González-Rodríguez P, Füllgrabe J, Delorme-Axford E, Backues SK, Joseph B, Klionsky DJ. Rph1/KDM4 mediates nutrient-limitation signaling that leads to the transcriptional induction of autophagy. *Curr Biol* 2015; 25: 546-55.
19. Webb AE, Brunet A. FOXO transcription factors: key regulators of cellular quality control. *Trends Biochem Sci.* 2015; 39: 159-169.
20. Kang Y-A, Sanalkumar R, O'Geen H, Linnemann AK, Chang C-J, Bouhassira EE, Farnham PJ, Keles S, Bresnick EH. Autophagy driven by a master regulator of hematopoiesis. *Mol Cell Biol* 2012; 32: 226-239.
21. Settembre C, Di Malta C, Polito VA, Garcia Arencibia M, Vetrini F, Erdin S, Erdin SU, Huynh T, Medina D, Colella P, Sardiello M, Rubinsztein DC, Ballabio A. TFEB links autophagy to lysosomal biogenesis. *Science* 2011; 332: 1429–1433.
22. Chauhan S, Goodwin JG, Manyam G, Wang J, Kamat AM, Boyd DD. ZKSCAN3 is a master transcriptional repressor of autophagy. *Mol Cell* 2013; 50: 16–28.
23. Kobayashi S, Volden P, Timm D, Mao K, Xu X, Liang Q. Transcription factor GATA4 inhibits doxorubicin-induced autophagy and cardiomyocyte death. *J Biol Chem* 2009; 285: 793-804.
24. Bartholomew CR, Suzuki T, Du Z, Backues SK, Jin M, Lynch-Day MA, Umekawa M, Kamath A, Zhao M, Xie Z, Inoki K, Klionsky DJ. Ume6 transcription factor is part of a signaling cascade that regulates autophagy. *Proc Natl Acad Sci U S A* 2012; 109: 11206-11210.
25. Kanki T, Wang K, Cao Y, Baba M, Klionsky DJ. Atg32 is a mitochondrial protein that confers selectivity during mitophagy. *Dev Cell* 2009; 17: 98-109.
26. Noda T, Klionsky DJ. The quantitative Pho8Delta60 assay of nonspecific autophagy. *Methods Enzymol* 2008; 451: 33-42.
27. Hofman-Bang J. Nitrogen catabolite repression in *Saccharomyces cerevisiae*. *Mol Biotechnol* 1999; 12:35-73.
28. Magasanik B, Kaiser CA. Nitrogen regulation in *Saccharomyces cerevisiae*. *Gene* 2002; 290: 1-18.
29. Broach JR. Nutritional control of growth and development in yeast. *Genetics* 2012; 192: 73-105.
30. Conrad M, Schothorst J, Kankipati HN, Van Zeebroeck G, Rubio-Texeira M, Thevelein JM. Nutrient sensing and signaling in the yeast *Saccharomyces cerevisiae*. *FEMS Microbiol Rev* 2014; 38: 254-299.
31. Shintani T, Klionsky DJ. Cargo proteins facilitate the formation of transport vesicles in the cytoplasm to vacuole targeting pathway. *J Biol Chem* 2004; 279: 29889-29894.
32. Klionsky DJ, Emr SD. Autophagy as a regulated pathway of cellular degradation. *Science* 2000; 290: 1717-21.
33. Ecker N, Mor A, Journo D, Abeliovich H. Induction of autophagy flux by amino acid deprivation is distinct from nitrogen starvation-induced macroautophagy. *Autophagy* 2010; 6: 879-890.
34. Yang Z, Geng J, Yen WL, Wang K, Klionsky DJ. Positive or negative roles of different cyclin-dependent kinase Pho85-cyclin complexes orchestrate induction of autophagy in *Saccharomyces cerevisiae*. *Mol Cell* 2010; 23: 250-264.
35. Chan TF, Bertram PG, Ai W, Zheng XF. Regulation of APG14 expression by the GATA-type transcription factor Gln3p. *J Biol Chem* 2001; 276: 6463-7.
36. Robertson LS, Fink GR. The three yeast A kinases have specific signaling functions in pseudohyphal growth. *Proc Natl Acad Sci U S A* 1998; 95: 13783-7.

37. Prasad KV, Taiyab A, Jyothi D, Srinivas UK, Sreedhar AS. Heat shock transcription factors regulate heat induced cell death in a rat histiocyoma. *J Biosci* 2007; 32: 585-593
38. Longtine MS, McKenzie A 3rd, Demarini DJ, Shah NG, Wach A, Brachat A, Philippsen P, Pringle JR. Additional modules for versatile and economical PCR-based gene deletion and modification in *Saccharomyces cerevisiae*. *Yeast* 1998; 14: 953–961
39. Vandesompele J, De Preter K, Pattyn F, Poppe B, Van Roy N, De Paepe A, Speleman F. Accurate normalization of real-time quantitative RT-PCR data by geometric averaging of multiple internal control genes. *Genome Biol* 2002; 3: H0034.
40. Yorimitsu T, Zaman S, Broach JR, Klionsky DJ. Protein kinase A and Sch9 cooperatively regulate induction of autophagy in *Saccharomyces cerevisiae*. *Mol Biol Cell* 2007; 18: 4180–4189.
41. Noda T, Matsuura A, Wada Y, Ohsumi Y. Novel system for monitoring autophagy in the yeast *Saccharomyces cerevisiae*. *Biochem Biophys Res Commun* 1995; 210: 126–132.
42. Abeliovich H, Zhang C, Dunn WA Jr, Shokat KM, Klionsky DJ. Chemical genetic analysis of Apg1 reveals a non-kinase role in the induction of autophagy. *Mol Biol Cell* 2003; 14: 477-490.
43. Noda T, Kim J, Huang W-P, Baba M, Tokunaga C, Ohsumi Y, Klionsky DJ. Apg9p/Cvt7p is an integral membrane protein required for transport vesicle formation in the Cvt and autophagy pathways. *J Cell Biol* 2000; 148: 465-480.
44. Huang WP, Scott SV, Kim J, Klionsky DJ. The itinerary of a vesicle component, Aut7p/Cvt5p, terminates in the yeast vacuole via the autophagy/Cvt pathways. *J Biol Chem* 2000; 275: 5845-5851.
45. Klionsky DJ, Cueva R, Yaver DS. Aminopeptidase I of *Saccharomyces cerevisiae* is localized to the vacuole independent of the secretory pathway. *J Cell Biol* 1992; 119: 287–299.

Table 4.1. DNA binding protein identified as potential regulator of *ATG* gene expression

Gene ID		Deletion phenotype	Description
<i>SPT10</i>	YJL127C	Increased expression in growing condition	Putative histone acetylase
<i>FYV5</i>	YCL058C		Protein involved in the regulation of the mating pathway
<i>SFL1</i>	YOR140W		Transcriptional repressor and activator
<i>SKO1</i>	YNL167C		Basic leucine zipper transcription factor of the ATF/CREB family
<i>ZAP1</i>	YJL056C		Zinc-regulated transcription factor
<i>YRM1</i>	YOR172W		Zinc finger transcription factor
<i>MBP1</i>	YDL056W	Decreased induction upon glucose starvation	Transcription factor
<i>GCN4</i>	YEL009C	Decreased induction upon nitrogen starvation	bZIP transcriptional activator
<i>GLN3</i>	YER040W		Transcriptional activator
<i>GAT1</i>	YFL021W		Transcriptional activator, GATA-1 type zinc finger domain
<i>SWI5</i>	YDR146C		Transcription factor
Gene descriptions are from the Saccharomyces Genome Database, available at http://www.yeastgenome.org			

Table 4.S1. mRNA level of the indicated *ATG* genes in deletion mutants analyzed after nitrogen starvation.

Gene deleted		<i>ATG1^a</i>	<i>ATG7</i>	<i>ATG8</i>	<i>ATG9</i>	<i>ATG14</i>	<i>ATG29</i>	<i>ATG32</i>
<i>GIS1</i>	YDR096W	1.0	1.5	1.2	1.2	1.2	0.9	1.2
<i>YAP6</i>	YDR259C	1.0	1.4	1.1	1.4	1.2	1.0	0.9
<i>HAC1</i>	YFL031W	1.1	0.8	0.9	0.8	0.7	0.9	1.0
<i>SKN7</i>	YHR206W	0.8	1.0	0.7	0.8	0.8	0.7	1.0
<i>MSN2</i>	YMR037C	0.5	0.8	0.8	0.7	0.7	1.1	1.0
<i>MSN4</i>	YKL062W	0.6	0.8	0.7	0.8	0.7	1.3	0.9
<i>RLM1</i>	YPL089C	1.3	1.2	1.0	1.2	0.9	0.9	1.0
<i>URC2</i>	YDR520C	1.3	1.3	1.1	1.2	1.6	1.2	1.3
<i>PHO4</i>	YFR034C	1.2	1.4	1.5	1.0	1.1	1.0	1.3
<i>GCN4</i>	YEL009C	0.2	1.1	0.7	0.5	0.7	1.3	0.3
	YER184C	0.9	1.1	1.2	1.2	1.2	0.9	1.0
<i>GAT4</i>	YIR013C	0.8	0.7	0.8	0.9	0.7	0.8	0.6
<i>RIM101</i>	YHL027W	1.5	1.7	2.0	1.4	1.5	1.3	1.7
<i>YAP1</i>	YML007W	1.0	1.1	0.8	0.9	0.7	0.9	0.9
<i>USV1</i>	YPL230W	1.0	1.2	1.4	1.1	1.0	1.3	0.5
<i>RME1</i>	YGR044C	0.7	0.9	1.0	0.7	0.7	0.7	0.7
<i>RPH1</i>	YER169W	1.1	1.2	1.1	1.2	1.0	0.9	1.1
<i>SKO1</i>	YNL167C	1.7	1.4	2.3	1.7	1.9	1.0	1.4
<i>RGMI</i>	YMR182C	1.0	0.6	1.0	0.7	1.0	1.2	1.1
<i>CRZ1</i>	YNL027W	0.7	0.9	1.0	0.7	0.7	0.6	0.7
<i>FKH2</i>	YNL068C	0.8	1.3	1.6	1.2	1.4	1.0	1.0
<i>ZAP1</i>	YJL056C	0.8	1.0	0.9	0.9	0.9	1.3	1.2
<i>CIN5</i>	YOR028C	1.2	1.6	2.0	1.4	1.7	1.1	0.7
<i>SIP4^b</i>	YJL089W	0.8	0.8	0.8	1.1	0.8	1.1	0.7
<i>OAF1</i>	YAL051W	0.9	0.9	1.9	1.0	1.5	1.2	0.7
<i>ADRI^b</i>	YDR216W	1.1	1.0	0.8	1.2	0.9	1.3	1.0
	YLR278C	0.7	0.7	0.9	0.8	0.9	1.1	1.4
<i>GAL4</i>	YPL248C	0.8	1.0	1.8	1.2	1.4	0.9	0.8
<i>RTG3</i>	YBL103C	1.1	0.8	0.5	0.5	0.6	1.0	0.7
<i>PHO2</i>	YDL106C	0.8	0.8	0.7	0.8	0.8	0.6	1.0
<i>CAD1</i>	YDR423C	1.2	1.1	0.9	1.1	0.9	0.9	1.1
	YKL222C	1.0	0.9	0.9	1.0	1.1	1.1	1.2
<i>TOD6</i>	YBL054W	1.0	1.3	1.9	1.3	1.5	1.1	1.0
<i>STP2</i>	YHR006W	1.4	1.4	1.5	1.4	1.5	0.8	1.4

<i>CBF1</i>	YJR060W	1.7	0.9	0.9	1.4	1.1	0.9	1.4
<i>TEC1</i>	YBR083W	1.2	1.3	2.0	1.2	1.1	1.2	1.0
<i>MSN1</i>	YOL116W	1.0	1.0	0.8	0.7	0.7	1.0	0.9
<i>COM2</i>	YER130C	1.5	1.5	1.3	1.5	1.2	1.0	1.5
<i>ASH1</i>	YKL185W	0.9	0.7	1.0	0.8	0.6	0.8	0.6
<i>XBP1</i>	YIL101C	1.1	1.0	1.0	1.1	1.1	1.4	1.0
<i>NRG1</i>	YDR043C	0.7	0.8	0.9	0.8	1.0	1.0	0.7
<i>SW14</i>	YER111C	0.7	0.7	0.6	0.7	0.5	0.6	0.9
<i>MIG1^b</i>	YGL035C	1.0	0.6	0.6	0.9	0.7	0.9	0.8
<i>SOK2</i>	YMR016C	0.8	0.9	1.0	0.9	0.7	0.8	0.6
<i>CUP9</i>	YPL177C	1.4	1.1	1.0	1.1	1.3	1.1	1.4
<i>PPR1</i>	YLR014C	0.8	0.9	0.7	0.7	0.6	0.9	0.8
<i>RDR1</i>	YOR380W	1.2	1.2	1.3	1.3	1.2	1.1	1.2
<i>LEU3</i>	YLR451W	1.1	1.1	1.1	1.1	1.1	0.9	1.5
<i>RDS1</i>	YCR106W	1.2	1.0	0.9	0.9	1.0	1.1	1.2
<i>DAL80</i>	YKR034W	0.8	0.7	0.8	0.7	0.6	0.7	1.0
<i>SPT10</i>	YJL127C	1.5	1.1	0.9	1.0	1.4	1.2	2.8
<i>YOX1</i>	YML027W	1.2	0.9	1.1	1.1	1.1	1.1	1.3
<i>YHP1</i>	YDR451C	1.1	0.8	0.9	0.9	1.0	1.2	1.1
<i>STB3</i>	YDR169C	1.2	1.0	1.3	1.0	0.9	1.1	1.1
<i>UME6</i>	YDR207C	0.9	0.4	1.0	0.7	0.3	1.0	1.8
<i>PDR3</i>	YBL005W	0.7	1.1	1.1	1.1	1.3	0.7	1.0
<i>EDS1</i>	YBR033W	0.8	0.6	0.6	0.6	0.6	0.8	0.5
<i>NRG2</i>	YBR066C	0.7	0.7	0.9	0.9	0.5	0.8	0.6
<i>TBS1</i>	YBR150C	0.8	0.7	0.7	0.7	0.9	0.7	0.5
<i>SMP1</i>	YBR182C	1.1	1.4	1.2	1.2	1.6	0.9	1.4
<i>ERT1</i>	YBR239C	0.9	0.8	0.9	1.1	1.4	0.8	0.8
<i>REI1</i>	YBR267W	0.8	0.5	0.5	0.7	0.7	0.7	0.8
<i>FYV5</i>	YCL058C	2.9	1.8	1.4	1.6	1.5	2.5	3.3
<i>HCM1</i>	YCR065W	0.9	0.7	0.6	0.8	1.1	0.5	1.2
<i>NHP10</i>	YDL002C	0.8	1.2	1.1	1.3	1.6	0.9	1.3
<i>RPN4</i>	YDL020C	0.9	1.2	1.5	1.3	1.2	1.1	1.0
<i>STP4</i>	YDL048C	1.0	1.0	1.0	0.8	1.1	1.2	0.9
<i>MBP1</i>	YDL056W	0.9	0.8	1.5	1.2	1.1	0.9	0.7
<i>UGA3</i>	YDL170W	1.3	0.8	0.8	1.1	1.6	0.9	1.0
<i>LYS14</i>	YDR034C	0.8	0.7	0.9	0.9	0.9	1.0	nd
<i>SWI5</i>	YDR146C	0.4	1.1	1.5	1.4	1.1	1.0	1.0

<i>UPC2</i>	YDR213W	1.4	1.3	1.4	1.3	1.6	1.5	1.3
<i>MET32</i>	YDR253C	0.9	0.8	0.9	0.7	0.7	1.0	1.0
<i>SUM1</i>	YDR310C	1.4	1.1	1.1	1.0	1.0	1.4	1.2
<i>ARO80</i>	YDR421W	1.1	1.3	1.1	1.2	1.3	1.2	nd
<i>STP1</i>	YDR463W	0.9	0.8	2.0	1.5	1.0	0.9	0.9
<i>MIG3</i>	YER028C	1.0	1.0	1.0	1.0	0.9	1.1	1.1
<i>GLN3</i>	YER040W	0.4	0.8	0.7	0.6	0.6	0.6	0.6
	YER064C	1.1	1.1	1.4	1.2	1.6	1.4	1.3
<i>ARG5,6</i>	YER069W	1.2	1.1	1.2	1.2	1.2	1.2	1.2
<i>DOT6</i>	YER088C	0.7	0.6	0.5	0.6	0.5	0.8	0.6
<i>GAT1</i>	YFL021W	0.6	0.4	0.6	0.7	0.6	0.5	0.2
<i>PDR1</i>	YGL013C	0.9	0.5	0.8	0.6	0.6	0.9	0.7
<i>TOS8</i>	YGL096W	0.8	0.6	0.6	0.8	1.1	0.6	0.7
<i>SUT1</i>	YGL162W	1.1	1.1	0.9	1.0	0.9	0.6	0.9
<i>CUP2</i>	YGL166W	1.3	1.3	1.2	1.4	1.6	0.9	1.3
<i>MIG2</i>	YGL209W	1.4	1.4	1.4	1.4	1.3	1.2	1.2
<i>FZF1</i>	YGL254W	1.1	1.2	1.1	1.0	0.9	1.0	1.1
	YGR067C	1.2	1.1	1.2	1.2	1.5	1.5	1.2
<i>MGA1</i>	YGR249W	1.1	1.3	0.9	1.0	1.1	0.7	1.0
<i>YAP3</i>	YHL009C	0.7	0.7	0.5	0.7	0.6	0.7	0.6
<i>NDT80</i>	YHR124W	1.2	1.0	0.8	0.8	0.9	0.8	0.9
<i>STB5</i>	YHR178W	0.7	0.8	0.9	0.9	0.8	0.6	0.8
<i>CST6</i>	YIL036W	1.2	1.0	1.1	1.1	1.1	1.0	1.0
<i>VHR1</i>	YIL056W	1.5	1.3	0.7	0.8	0.6	1.1	0.9
<i>ASG1</i>	YIL130W	1.2	1.4	1.5	1.6	2.2	1.4	1.7
<i>FKH1</i>	YIL131C	0.7	0.7	0.7	0.7	0.6	0.7	0.9
<i>GSM1</i>	YJL103C	1.2	1.1	1.3	1.1	0.9	1.5	1.4
<i>GZF3</i>	YJL110C	0.9	0.7	0.9	0.8	0.7	0.9	0.9
<i>RSF2</i>	YJR127C	1.6	1.5	1.2	1.8	1.7	1.5	1.6
<i>PUT3</i>	YKL015W	1.0	1.0	1.3	0.8	0.8	1.1	1.2
<i>RGT1</i>	YKL038W	0.7	0.7	0.8	0.7	0.7	0.9	0.7
<i>PHD1</i>	YKL043W	1.0	1.0	0.8	1.0	0.7	0.8	1.1
<i>BAS1</i>	YKR099W	1.2	1.0	1.2	0.8	0.9	0.7	2.0
	YLL054C	0.8	0.7	1.0	0.9	1.3	0.9	0.7
<i>GAT3</i>	YLR013W	0.8	0.9	1.2	1.1	0.8	0.9	0.8
<i>CHA4</i>	YLR098C	0.9	1.0	0.9	1.2	1.1	0.7	1.3
<i>ACE2</i>	YLR131C	1.1	1.5	1.1	1.2	1.2	1.0	1.3

<i>RFX1</i>	YLR176C	nd	1.0	0.8	1.2	1.2	1.6	1.3
<i>ECM22</i>	YLR228C	1.0	1.1	0.9	1.2	1.0	0.7	0.9
<i>PDR8</i>	YLR266C	1.1	1.3	1.0	1.3	1.2	1.1	nd
<i>STP3</i>	YLR375W	1.1	1.0	1.0	0.9	0.9	1.1	1.0
<i>WAR1</i>	YML076C	0.9	0.8	0.9	0.8	0.7	1.0	0.7
	YML081W	0.8	0.8	1.2	0.8	1.3	0.7	0.8
<i>DAT1</i>	YML113W	1.5	1.9	2.1	2.3	2.4	1.6	1.9
<i>STB4</i>	YMR019W	1.0	0.8	1.0	1.1	1.2	0.8	1.0
<i>CAT8^b</i>	YMR280C	1.2	1.0	0.9	1.4	1.0	1.5	1.0
<i>DAL82</i>	YNL314W	0.9	0.9	0.7	0.8	0.9	0.9	0.9
	YNR063W	1.4	1.1	1.2	1.0	1.0	1.2	1.2
<i>YAP7</i>	YOL028C	0.7	1.5	1.4	1.3	1.2	1.0	1.1
<i>HAL9</i>	YOL089C	1.2	1.2	1.8	1.6	0.7	1.1	1.1
<i>AZF1</i>	YOR113W	0.7	0.8	0.8	0.9	0.6	1.7	1.1
<i>SFL1</i>	YOR140W	1.2	1.0	1.0	1.3	1.6	1.3	1.1
<i>YRR1</i>	YOR162C	1.2	0.9	0.9	0.9	1.0	1.0	1.4
<i>YRM1</i>	YOR172W	0.6	1.0	2.3	0.8	1.3	1.0	1.0
<i>TEA1</i>	YOR337W	1.1	1.3	1.1	1.3	0.9	0.9	1.0
<i>TYE7</i>	YOR344C	1.1	0.8	0.7	0.8	0.8	1.0	0.9
<i>ECM23</i>	YPL021W	0.9	0.8	0.9	0.7	0.9	1.3	1.1
<i>MET31</i>	YPL038W	0.9	1.2	1.4	1.2	1.7	1.4	2.0
<i>RDS2^c</i>	YPL133C	0.9	1.2	1.4	1.2	1.7	1.4	2.0
<i>AFT2</i>	YPL202C	1.0	1.2	1.4	1.1	1.0	1.2	0.7
<i>HAA1</i>	YPR008W	1.3	1.4	1.5	1.2	0.9	1.0	1.6
<i>SUT2</i>	YPR009W	0.9	0.8	0.8	0.9	1.0	0.8	1.2
<i>CMR3</i>	YPR013C	1.3	1.2	1.4	1.5	1.6	1.3	1.2
	YPR015C	0.9	1.0	1.1	1.2	1.3	0.7	0.7
	YPR022C	1.1	1.0	1.3	1.2	1.3	1.5	1.2
<i>NHP6A</i>	YPR052C	0.7	0.7	0.7	0.8	1.1	0.8	0.7
<i>ROX1</i>	YPR065W	1.4	1.2	1.0	1.3	1.5	0.9	1.6
	YPR196W	1.3	1.1	1.2	1.1	1.2	1.4	1.0

^a Values are relative to the level in wild-type cells, which was set to 1.

^b The deletions of these genes were made in the W303-1B background and analyzed in comparison with the corresponding wild-type cells.

^c The deletion strain of *RDS2* was in the BY4741 background and was analyzed with the corresponding wild-type cells.

nd, No data.

Table 4.S2. mRNA level of the deletion mutants analyzed after glucose starvation.

Gene deleted		<i>ATG1^a</i>	<i>ATG7</i>	<i>ATG8</i>	<i>ATG9</i>	<i>ATG14</i>	<i>ATG29</i>	<i>ATG32</i>
<i>GIS1</i>	YDR096W	1.2	1.2	1.0	1.3	0.8	0.8	0.9
<i>YAP6</i>	YDR259C	0.9	1.2	1.2	1.0	0.8	0.8	0.9
<i>HAC1</i>	YFL031W	1.3	1.1	1.0	0.9	1.1	1.6	1.1
<i>SKN7</i>	YHR206W	0.7	1.3	1.3	0.9	1.3	1.4	1.4
<i>MSN2</i>	YMR037C	1.0	1.3	1.1	1.2	1.0	1.0	0.7
<i>MSN4</i>	YKL062W	1.1	1.3	1.4	1.2	0.9	1.2	1.6
<i>RLM1</i>	YPL089C	0.9	1.2	1.2	0.5	1.1	1.4	1.0
<i>URC2</i>	YDR520C	1.0	0.8	0.8	0.5	0.8	1.3	1.1
<i>PHO4</i>	YFR034C	1.6	1.7	1.2	1.5	1.2	1.0	2.1
<i>GCN4</i>	YEL009C	0.8	1.1	1.0	1.0	1.1	1.1	0.9
	YER184C	1.0	1.2	1.3	1.4	1.3	1.4	0.8
<i>GAT4</i>	YIR013C	0.6	1.0	1.6	1.2	1.2	1.7	1.2
<i>RIM101</i>	YHL027W	1.7	1.9	0.8	1.7	1.2	0.9	2.1
<i>YAP1</i>	YML007W	0.8	1.4	1.5	1.1	1.2	1.6	1.0
<i>USV1</i>	YPL230W	1.4	2.7	2.8	2.0	2.1	2.6	nd
<i>RME1</i>	YGR044C	1.0	1.9	2.2	1.7	1.0	1.6	nd
<i>RPH1</i>	YER169W	0.9	0.9	0.8	0.7	0.9	1.0	0.9
<i>SKO1</i>	YNL167C	1.9	1.5	1.1	1.9	2.0	1.7	3.9
<i>RGM1</i>	YMR182C	0.8	0.9	1.0	0.8	0.7	0.8	1.4
<i>CRZ1</i>	YNL027W	1.0	1.2	0.8	0.9	0.8	0.9	1.0
<i>FKH2</i>	YNL068C	0.9	2.6	nd	1.8	1.8	2.9	2.8
<i>ZAP1</i>	YJL056C	1.6	1.1	1.1	1.5	1.1	1.0	1.3
<i>CIN5</i>	YOR028C	0.8	0.8	0.7	0.9	0.9	0.9	1.2
<i>SIP4^b</i>	YJL089W	0.9	1.0	0.8	1.1	0.8	0.7	1.4
<i>OAF1</i>	YAL051W	0.9	1.1	1.0	1.0	0.9	1.1	1.2
<i>ADRI^b</i>	YDR216W	0.9	1.5	1.4	1.6	1.3	1.3	nd
	YLR278C	0.6	0.9	1.1	0.9	1.2	1.5	1.9
<i>GAL4</i>	YPL248C	0.8	0.9	0.8	0.9	1.3	1.0	1.5
<i>RTG3</i>	YBL103C	nd	nd	nd	nd	nd	nd	nd
<i>PHO2</i>	YDL106C	1.9	1.1	0.9	2.7	2.0	1.1	1.8
<i>CAD1</i>	YDR423C	0.9	0.9	0.9	1.0	0.9	1.0	1.0
	YKL222C	0.8	0.8	0.9	1.0	1.0	1.1	1.0
<i>TOD6</i>	YBL054W	1.0	1.3	1.2	1.0	1.0	1.4	1.6
<i>STP2</i>	YHR006W	5.0	2.1	0.7	2.3	1.2	1.3	3.7
<i>CBF1</i>	YJR060W	1.3	0.8	0.6	1.3	0.9	1.0	1.0

<i>TEC1</i>	YBR083W	1.2	1.6	1.5	1.3	1.1	1.3	1.1
<i>MSN1</i>	YOL116W	1.5	1.3	1.4	1.3	1.1	1.8	1.4
<i>COM2</i>	YER130C	1.1	0.9	1.0	0.8	0.9	0.9	1.0
<i>ASH1</i>	YKL185W	0.8	0.8	1.2	1.2	1.0	1.2	0.9
<i>XBP1</i>	YIL101C	0.7	1.0	1.1	0.9	1.3	1.2	0.8
<i>NRG1</i>	YDR043C	1.0	0.9	0.9	1.3	1.0	1.1	1.0
<i>SWI4</i>	YER111C	0.6	1.0	0.8	0.7	1.0	1.2	2.8
<i>MIG1^b</i>	YGL035C	1.2	0.8	0.9	1.2	0.9	0.8	1.3
<i>SOK2</i>	YMR016C	1.8	1.0	1.2	2.2	1.2	1.1	1.1
<i>CUP9</i>	YPL177C	1.1	1.2	1.1	1.5	1.0	1.5	1.1
<i>PPR1</i>	YLR014C	0.9	1.3	0.8	1.0	1.1	1.3	1.3
<i>RDR1</i>	YOR380W	1.1	1.0	1.5	1.1	1.2	1.4	1.3
<i>LEU3</i>	YLR451W	1.7	1.9	1.2	2.3	1.5	1.5	2.5
<i>RDS1</i>	YCR106W	1.2	1.3	1.0	1.6	1.1	1.2	2.0
<i>DAL80</i>	YKR034W	0.6	0.5	1.0	0.7	0.9	1.0	0.9
<i>SPT10</i>	YJL127C	4.3	0.8	0.5	1.8	0.8	0.6	4.9
<i>YOX1</i>	YML027W	1.0	0.9	1.0	1.2	1.2	1.2	0.9
<i>YHP1</i>	YDR451C	0.8	1.0	1.1	1.0	1.3	1.2	0.7
<i>STB3</i>	YDR169C	0.9	1.3	1.5	1.4	1.5	1.7	1.6
<i>UME6</i>	YDR207C	2.8	1.2	1.6	1.9	1.3	0.9	2.9
<i>PDR3</i>	YBL005W	0.8	1.3	1.0	1.2	1.0	1.2	1.0
<i>EDS1</i>	YBR033W	1.2	0.8	0.9	1.1	0.9	0.9	1.1
<i>NRG2</i>	YBR066C	1.3	0.9	0.9	1.4	1.0	1.0	1.1
<i>TBS1</i>	YBR150C	1.7	0.8	1.2	1.6	1.2	1.1	1.2
<i>SMPI</i>	YBR182C	0.9	1.0	1.1	0.9	1.0	1.2	1.2
<i>ERT1</i>	YBR239C	0.8	0.5	0.6	0.8	1.0	0.7	1.0
<i>REI1</i>	YBR267W	0.9	1.0	1.4	1.0	2.4	1.7	1.9
<i>FYV5</i>	YCL058C	2.5	1.4	1.4	2.4	2.0	3.2	2.3
<i>HCM1</i>	YCR065W	1.3	1.2	0.7	1.0	1.3	0.9	1.6
<i>NHP10</i>	YDL002C	0.9	1.0	1.1	0.9	1.3	1.5	1.0
<i>RPN4</i>	YDL020C	2.0	1.8	2.1	2.6	3.0	2.1	1.8
<i>STP4</i>	YDL048C	1.2	1.1	0.9	1.5	1.2	1.2	0.9
<i>MBP1</i>	YDL056W	0.4	0.5	0.3	0.5	1.0	0.4	0.4
<i>UGA3</i>	YDL170W	1.1	0.9	0.8	0.9	1.1	1.0	1.4
<i>LYS14</i>	YDR034C	1.3	1.3	0.9	1.4	1.5	1.3	nd
<i>SWI5</i>	YDR146C	0.7	0.7	0.7	0.7	0.7	0.7	1.0
<i>UPC2</i>	YDR213W	2.3	1.1	0.9	1.7	1.3	0.8	1.0

<i>MET32</i>	YDR253C	0.8	0.7	0.9	0.9	0.8	1.0	1.1
<i>SUM1</i>	YDR310C	2.0	0.8	0.7	1.6	0.6	0.8	1.3
<i>ARO80</i>	YDR421W	1.2	1.5	1.4	1.9	1.5	1.2	nd
<i>STP1</i>	YDR463W	1.5	2.5	2.0	2.1	1.4	2.5	nd
<i>MIG3</i>	YER028C	1.6	1.1	1.2	1.3	1.2	0.9	1.2
<i>GLN3</i>	YER040W	1.4	1.1	1.1	2.2	2.0	1.4	2.6
	YER064C	0.8	0.8	1.2	0.9	0.9	1.0	1.0
<i>ARG5,6</i>	YER069W	1.9	1.6	1.5	1.7	1.2	1.4	1.5
<i>DOT6</i>	YER088C	1.4	0.9	0.7	1.0	0.9	1.2	1.4
<i>GAT1</i>	YFL021W	0.6	1.0	1.5	1.1	1.3	1.9	1.5
<i>PDR1</i>	YGL013C	0.9	1.0	0.8	0.5	1.0	1.0	1.0
<i>TOS8</i>	YGL096W	1.0	1.1	0.9	0.8	1.1	1.0	1.2
<i>SUT1</i>	YGL162W	1.1	1.1	0.8	1.2	0.9	0.8	1.2
<i>CUP2</i>	YGL166W	1.9	1.1	1.0	1.7	1.1	0.9	1.1
<i>MIG2</i>	YGL209W	1.5	1.6	1.2	2.0	1.2	1.5	1.4
<i>FZF1</i>	YGL254W	0.8	0.9	0.7	0.9	0.6	0.8	0.8
	YGR067C	1.8	1.1	1.1	1.5	1.0	0.9	0.9
<i>MGA1</i>	YGR249W	1.0	1.2	1.0	1.6	1.0	1.0	1.0
<i>YAP3</i>	YHL009C	1.1	0.8	0.9	1.0	0.9	0.9	1.0
<i>NDT80</i>	YHR124W	0.9	0.8	0.8	1.0	0.9	1.0	1.0
<i>STB5</i>	YHR178W	1.0	1.0	1.0	0.9	1.2	0.9	1.1
<i>CST6</i>	YIL036W	1.0	1.3	1.5	1.1	1.1	1.1	0.8
<i>VHR1</i>	YIL056W	1.2	1.5	1.6	1.1	1.1	1.4	1.0
<i>ASG1</i>	YIL130W	1.0	0.9	1.0	1.1	0.8	1.1	1.1
<i>FKH1</i>	YIL131C	0.6	0.5	0.6	0.6	0.5	0.7	0.7
<i>GSM1</i>	YJL103C	0.9	1.0	1.6	0.9	1.0	1.8	1.1
<i>GZF3</i>	YJL110C	0.6	1.0	2.1	1.1	1.0	1.6	1.5
<i>RSF2</i>	YJR127C	1.6	1.7	1.3	1.6	1.1	0.9	1.1
<i>PUT3</i>	YKL015W	0.7	0.9	0.8	0.6	1.1	0.7	0.8
<i>RGT1</i>	YKL038W	0.7	0.7	0.7	0.6	0.6	0.8	0.7
<i>PHD1</i>	YKL043W	1.3	1.0	0.8	1.6	0.8	1.0	1.3
<i>BAS1</i>	YKR099W	1.0	0.6	0.6	0.6	0.9	0.6	1.5
	YLL054C	1.2	0.7	0.7	1.3	1.1	0.8	1.0
<i>GAT3</i>	YLR013W	0.6	0.9	1.6	0.9	1.2	1.8	1.2
<i>CHA4</i>	YLR098C	0.8	0.7	0.9	0.6	0.5	1.3	1.0
<i>ACE2</i>	YLR131C	1.4	1.3	1.3	1.2	1.3	1.6	1.2
<i>RFX1</i>	YLR176C	1.0	1.0	1.1	1.0	1.1	1.1	0.7

<i>ECM22</i>	YLR228C	0.9	1.1	0.9	0.9	0.8	1.0	0.9
<i>PDR8</i>	YLR266C	0.9	0.9	0.8	0.9	0.8	1.5	1.5
<i>STP3</i>	YLR375W	1.0	1.2	1.5	1.2	1.3	1.4	1.1
<i>WAR1</i>	YML076C	0.8	0.8	1.0	0.8	0.8	1.1	0.9
	YML081W	1.2	0.8	1.1	1.1	1.3	1.1	1.4
<i>DAT1</i>	YML113W	1.0	0.8	0.9	0.8	0.9	0.7	0.8
<i>STB4</i>	YMR019W	1.3	0.8	0.9	1.3	1.0	0.9	1.7
<i>CAT8^b</i>	YMR280C	1.1	1.0	1.1	1.0	1.2	1.1	1.3
<i>DAL82</i>	YNL314W	1.0	1.0	0.9	1.1	0.8	0.8	1.1
	YNR063W	1.0	1.1	1.0	1.0	1.4	1.3	1.2
<i>YAP7</i>	YOL028C	0.9	0.9	0.9	0.9	0.8	1.0	1.1
<i>HAL9</i>	YOL089C	1.4	1.2	1.0	1.1	1.6	0.9	1.4
<i>AZF1</i>	YOR113W	1.3	1.2	0.9	1.0	0.9	0.9	1.5
<i>SFL1</i>	YOR140W	1.4	0.7	0.6	1.4	0.8	0.6	0.8
<i>YRR1</i>	YOR162C	0.9	0.8	0.9	0.8	1.3	1.1	1.3
<i>YRM1</i>	YOR172W	2.2	1.8	2.6	2.0	3.2	2.1	1.8
<i>TEA1</i>	YOR337W	1.3	0.9	0.9	1.3	0.6	0.9	1.1
<i>TYE7</i>	YOR344C	1.1	0.8	0.7	0.8	0.7	1.2	0.9
<i>ECM23</i>	YPL021W	1.0	0.9	1.1	1.2	1.0	1.2	1.2
<i>MET31</i>	YPL038W	0.8	0.8	1.1	0.9	0.8	1.0	1.2
<i>RDS2^c</i>	YPL133C	0.7	1.0	1.5	0.9	1.0	1.1	0.9
<i>AFT2</i>	YPL202C	1.1	0.8	1.0	1.0	1.2	1.5	2.0
<i>HAA1</i>	YPR008W	1.5	1.0	1.1	0.8	0.6	1.7	1.7
<i>SUT2</i>	YPR009W	1.1	1.0	0.9	0.8	1.2	1.1	1.2
<i>CMR3</i>	YPR013C	1.0	0.9	1.2	1.1	1.1	1.2	1.2
	YPR015C	1.3	0.8	0.8	1.2	1.1	1.0	1.1
	YPR022C	1.0	0.9	1.1	1.2	1.0	1.1	1.0
<i>NHP6A</i>	YPR052C	1.0	0.6	0.5	0.9	0.8	0.7	0.9
<i>ROX1</i>	YPR065W	1.6	1.4	1.8	1.8	2.2	1.2	1.1
	YPR196W	1.3	1.1	0.9	1.3	1.0	0.8	0.8

a Values are relative to the level in wild-type cells, which was set to 1.

b The deletions of these genes were made in the W303-1B background and analyzed in comparison with the corresponding wild-type cells.

c The deletion strain of *RDS2* was in the BY4741 background and was analyzed with the corresponding wild-type cells.

nd, No data.

Table 4.S3. mRNA level of the deletion mutants analyzed in growing conditions.

Gene deleted		<i>ATG1^a</i>	<i>ATG7</i>	<i>ATG8</i>	<i>ATG9</i>	<i>ATG14</i>	<i>ATG29</i>	<i>ATG32</i>
<i>GIS1</i>	YDR096W	1.3	1.2	0.9	1.1	0.8	0.8	1.0
<i>YAP6</i>	YDR259C	1.0	0.7	0.9	0.9	0.5	0.8	0.1
<i>HAC1</i>	YFL031W	1.0	0.8	0.3	0.8	0.6	0.6	0.7
<i>SKN7</i>	YHR206W	0.6	0.4	0.7	0.2	0.6	0.9	0.8
<i>MSN2</i>	YMR037C	0.6	0.5	0.7	0.4	0.5	0.8	0.4
<i>MSN4</i>	YKL062W	0.8	0.9	0.7	0.8	0.4	0.6	0.1
<i>RLM1</i>	YPL089C	0.8	0.6	0.7	0.3	0.7	0.9	0.7
<i>URC2</i>	YDR520C	0.9	0.8	0.9	0.7	0.7	0.8	0.6
<i>PHO4</i>	YFR034C	0.9	0.9	0.8	0.8	0.9	0.8	1.3
<i>GCN4</i>	YEL009C	1.0	1.1	1.7	0.6	1.1	1.2	0.9
	YER184C	0.9	0.9	0.8	1.1	1.0	1.1	1.1
<i>GAT4</i>	YIR013C	1.3	1.0	1.3	1.0	1.0	1.4	1.2
<i>RIM101</i>	YHL027W	0.9	0.7	0.7	0.8	0.6	0.6	0.1
<i>YAP1</i>	YML007W	0.9	0.7	0.9	0.5	0.8	0.9	0.7
<i>USV1</i>	YPL230W	0.8	0.7	0.7	0.8	0.6	0.7	0.9
<i>RME1</i>	YGR044C	0.7	1.0	0.7	0.8	0.5	0.8	0.1
<i>RPH1</i>	YER169W	1.8	2.7	1.4	2.4	2.1	1.9	2.0
<i>SKO1</i>	YNL167C	1.5	1.5	1.5	1.0	0.8	1.4	2.1
<i>RGM1</i>	YMR182C	0.7	0.7	0.8	0.7	0.7	0.8	0.6
<i>CRZ1</i>	YNL027W	0.7	0.8	0.5	0.7	0.4	0.5	0.2
<i>FKH2</i>	YNL068C	0.6	0.6	0.6	0.6	0.7	0.5	1.1
<i>ZAP1</i>	YJL056C	3.0	2.1	2.7	2.6	2.3	1.6	2.0
<i>CIN5</i>	YOR028C	0.8	0.7	0.7	0.6	0.7	0.7	1.0
<i>SIP4^b</i>	YJL089W	1.4	1.1	1.6	1.0	0.6	1.1	0.9
<i>OAF1</i>	YAL051W	0.9	0.8	0.7	0.6	0.7	0.7	1.0
<i>ADRI^b</i>	YDR216W	1.1	0.9	1.2	1.4	nd	1.3	0.9
	YLR278C	0.8	0.9	0.7	1.0	1.1	1.1	1.6
<i>GAL4</i>	YPL248C	0.9	0.9	0.7	0.8	0.9	0.7	1.0
<i>RTG3</i>	YBL103C	0.7	0.8	0.6	0.6	0.4	0.4	0.1
<i>PHO2</i>	YDL106C	0.9	0.7	0.7	0.9	0.8	1.0	1.1
<i>CAD1</i>	YDR423C	0.7	0.8	0.8	0.8	0.8	0.8	1.0
	YKL222C	0.9	0.7	0.7	0.9	1.0	1.0	1.1
<i>TOD6</i>	YBL054W	0.7	0.7	0.6	0.6	0.6	0.7	1.0
<i>STP2</i>	YHR006W	0.9	0.9	0.7	0.7	0.4	0.5	0.1
<i>CBF1</i>	YJR060W	0.8	0.9	0.6	0.9	0.9	1.1	1.0

<i>TEC1</i>	YBR083W	0.8	0.8	0.7	0.6	0.7	0.7	0.7
<i>MSN1</i>	YOL116W	1.3	0.9	0.8	1.0	0.8	0.9	1.2
<i>COM2</i>	YER130C	0.9	1.0	0.9	0.9	1.0	0.8	1.0
<i>ASH1</i>	YKL185W	1.2	1.1	1.5	1.2	1.3	1.2	0.9
<i>XBP1</i>	YIL101C	1.0	1.0	0.8	1.1	1.1	1.2	1.0
<i>NRG1</i>	YDR043C	0.8	0.8	0.8	0.9	0.9	1.0	0.9
<i>SWI4</i>	YER111C	0.5	0.6	0.6	0.2	0.6	0.7	1.3
<i>MIG1^b</i>	YGL035C	1.1	1.0	1.1	1.1	0.8	0.8	0.8
<i>SOK2</i>	YMR016C	0.8	0.6	1.1	0.3	0.9	1.1	0.8
<i>CUP9</i>	YPL177C	1.0	1.1	1.1	1.2	1.0	1.2	1.2
<i>PPR1</i>	YLR014C	1.0	1.1	1.1	1.0	1.0	1.1	0.9
<i>RDR1</i>	YOR380W	1.1	1.1	1.3	1.0	1.2	1.2	1.1
<i>LEU3</i>	YLR451W	0.9	0.7	0.8	0.8	0.8	0.8	1.0
<i>RDS1</i>	YCR106W	1.0	1.1	1.1	1.3	1.0	0.9	1.3
<i>DAL80</i>	YKR034W	1.1	1.2	1.0	1.1	1.2	1.5	0.9
<i>SPT10</i>	YJL127C	2.2	1.5	1.2	1.9	1.9	1.2	3.5
<i>YOX1</i>	YML027W	0.9	0.8	0.7	0.9	0.8	1.0	1.3
<i>YHP1</i>	YDR451C	1.1	1.2	1.0	1.3	1.4	1.3	1.2
<i>STB3</i>	YDR169C	0.9	1.2	1.1	1.0	1.1	1.0	1.1
<i>UME6</i>	YDR207C	3.1	1.2	3.8	2.0	1.1	1.1	3.5
<i>PDR3</i>	YBL005W	0.7	0.7	1.0	0.6	0.8	1.3	0.6
<i>EDS1</i>	YBR033W	1.0	0.9	0.8	0.9	0.8	0.7	0.9
<i>NRG2</i>	YBR066C	0.7	0.8	0.9	0.9	0.8	0.8	0.8
<i>TBS1</i>	YBR150C	0.9	0.9	0.8	1.1	1.0	0.9	0.9
<i>SMP1</i>	YBR182C	0.9	1.0	1.0	0.4	0.9	0.9	0.9
<i>ERT1</i>	YBR239C	0.9	0.9	1.0	1.1	1.2	1.1	1.2
<i>REI1</i>	YBR267W	1.1	0.6	0.7	1.4	1.2	0.7	1.6
<i>FYV5</i>	YCL058C	1.3	1.3	1.8	1.7	3.3	2.6	1.5
<i>HCM1</i>	YCR065W	0.9	0.6	0.6	0.6	0.7	0.7	0.9
<i>NHP10</i>	YDL002C	1.1	0.7	0.8	0.5	0.7	0.9	0.9
<i>RPN4</i>	YDL020C	1.2	0.9	1.2	0.5	1.1	1.5	0.9
<i>STP4</i>	YDL048C	0.9	1.0	0.7	0.8	1.1	1.2	1.0
<i>MBP1</i>	YDL056W	1.2	1.2	1.0	0.9	1.2	1.1	nd
<i>UGA3</i>	YDL170W	1.3	1.2	1.0	1.1	1.1	1.1	1.8
<i>LYS14</i>	YDR034C	1.2	1.1	1.1	1.1	1.2	1.3	nd
<i>SWI5</i>	YDR146C	0.8	0.4	0.6	0.6	0.5	0.7	nd
<i>UPC2</i>	YDR213W	1.3	0.9	1.2	1.0	1.4	1.1	1.0

<i>MET32</i>	YDR253C	1.0	0.7	0.9	0.9	0.8	0.9	1.3
<i>SUM1</i>	YDR310C	1.1	0.7	1.1	0.8	0.8	0.9	0.9
<i>ARO80</i>	YDR421W	1.2	1.2	1.0	1.4	1.4	1.3	nd
<i>STP1</i>	YDR463W	0.8	0.8	0.8	0.7	0.8	1.1	nd
<i>MIG3</i>	YER028C	0.8	0.8	1.1	0.8	0.8	0.8	0.8
<i>GLN3</i>	YER040W	1.2	0.9	0.8	0.9	0.8	1.0	1.6
	YER064C	1.1	1.1	0.8	0.9	0.8	1.0	0.9
<i>ARG5,6</i>	YER069W	1.0	1.1	1.4	1.1	1.1	1.1	1.1
<i>DOT6</i>	YER088C	1.3	0.7	0.6	0.9	0.8	0.7	1.0
<i>GAT1</i>	YFL021W	1.3	1.2	1.5	1.1	1.4	1.3	0.9
<i>PDR1</i>	YGL013C	0.8	0.9	0.9	0.8	0.9	0.8	0.7
<i>TOS8</i>	YGL096W	1.1	0.9	0.8	0.9	0.8	0.8	0.9
<i>SUT1</i>	YGL162W	0.9	1.1	1.0	1.0	0.9	0.8	1.3
<i>CUP2</i>	YGL166W	0.9	0.9	1.0	0.9	0.8	0.8	0.8
<i>MIG2</i>	YGL209W	1.2	1.2	1.1	1.3	1.1	1.2	1.4
<i>FZF1</i>	YGL254W	1.0	1.1	1.1	1.2	1.0	1.0	1.2
	YGR067C	1.1	0.9	1.1	1.0	0.8	0.9	0.9
<i>MGA1</i>	YGR249W	1.2	1.1	1.1	1.3	1.1	1.0	1.3
<i>YAP3</i>	YHL009C	0.8	0.8	0.8	0.9	0.9	0.7	0.9
<i>NDT80</i>	YHR124W	0.7	0.9	0.8	0.9	0.9	0.8	0.7
<i>STB5</i>	YHR178W	1.3	1.1	1.0	1.1	1.1	0.9	1.3
<i>CST6</i>	YIL036W	1.0	0.8	0.6	0.9	0.8	0.7	1.2
<i>VHR1</i>	YIL056W	0.9	0.8	0.7	0.9	0.8	0.7	1.1
<i>ASG1</i>	YIL130W	1.2	0.9	0.6	0.9	0.8	0.8	1.0
<i>FKH1</i>	YIL131C	0.5	0.5	0.5	0.5	0.6	0.6	0.7
<i>GSM1</i>	YJL103C	0.8	0.7	0.9	0.8	0.9	0.8	1.4
<i>GZF3</i>	YJL110C	1.1	1.1	1.2	1.3	1.3	1.2	0.8
<i>RSF2</i>	YJR127C	0.9	1.0	1.2	1.1	1.0	0.9	0.9
<i>PUT3</i>	YKL015W	1.4	1.2	1.3	1.2	1.0	1.0	1.1
<i>RGT1</i>	YKL038W	0.9	0.8	0.9	0.9	0.9	0.9	1.0
<i>PHD1</i>	YKL043W	0.9	0.9	0.8	0.9	0.8	0.7	1.2
<i>BAS1</i>	YKR099W	0.8	0.7	1.4	0.7	0.5	0.9	0.9
	YLL054C	0.8	0.9	0.9	1.2	1.0	1.0	1.0
<i>GAT3</i>	YLR013W	1.5	1.1	1.2	1.3	1.5	1.3	1.3
<i>CHA4</i>	YLR098C	1.2	1.2	1.1	1.1	1.0	1.0	1.2
<i>ACE2</i>	YLR131C	0.9	1.1	0.9	0.8	0.7	1.0	0.9
<i>RFX1</i>	YLR176C	0.9	0.8	0.9	0.8	1.0	0.8	0.6

<i>ECM22</i>	YLR228C	0.8	0.7	1.0	0.7	0.7	0.8	0.6
<i>PDR8</i>	YLR266C	0.7	0.8	0.7	0.8	0.9	1.0	nd
<i>STP3</i>	YLR375W	0.9	1.2	0.8	1.0	1.0	1.1	1.2
<i>WAR1</i>	YML076C	0.7	0.7	0.8	0.8	0.7	0.9	0.7
	YML081W	1.0	1.0	1.0	1.2	1.3	1.0	1.1
<i>DAT1</i>	YML113W	1.0	0.9	1.0	1.1	0.9	0.8	0.9
<i>STB4</i>	YMR019W	0.8	0.8	0.7	0.9	0.9	0.8	0.9
<i>CAT8^b</i>	YMR280C	0.9	0.8	0.8	1.0	0.9	1.0	1.3
<i>DAL82</i>	YNL314W	0.9	0.9	1.0	0.9	0.9	0.9	0.8
	YNR063W	0.9	0.9	1.0	0.8	1.1	1.0	1.0
<i>YAP7</i>	YOL028C	1.2	1.6	1.1	1.3	1.2	1.0	1.1
<i>HAL9</i>	YOL089C	1.2	1.0	1.0	1.1	1.2	1.0	1.4
<i>AZF1</i>	YOR113W	1.1	1.1	0.9	0.9	0.9	0.9	0.9
<i>SFL1</i>	YOR140W	1.7	1.5	1.9	1.8	1.4	1.5	2.1
<i>YRR1</i>	YOR162C	1.1	1.1	1.3	1.2	1.2	1.1	1.7
<i>YRM1</i>	YOR172W	1.0	0.8	1.8	0.6	1.3	0.9	0.9
<i>TEA1</i>	YOR337W	1.0	1.1	1.0	1.2	1.1	0.8	0.9
<i>TYE7</i>	YOR344C	0.8	0.9	0.8	0.8	0.7	0.7	0.7
<i>ECM23</i>	YPL021W	1.3	1.3	1.1	0.9	0.9	1.3	1.0
<i>MET31</i>	YPL038W	1.6	1.2	1.0	1.1	1.1	1.5	1.5
<i>RDS2^c</i>	YPL133C	1.1	0.6	1.0	0.7	1.2	0.7	1.1
<i>AFT2</i>	YPL202C	1.0	0.8	0.8	0.7	0.7	0.9	1.4
<i>HAA1</i>	YPR008W	1.3	0.9	1.0	1.0	1.1	0.8	1.8
<i>SUT2</i>	YPR009W	0.9	0.8	0.8	1.0	0.9	0.8	0.8
<i>CMR3</i>	YPR013C	1.0	1.1	1.2	1.0	1.1	1.1	0.9
	YPR015C	0.8	0.9	0.8	1.1	0.9	0.8	0.8
	YPR022C	1.4	1.4	1.1	1.1	0.9	1.2	1.1
<i>NHP6A</i>	YPR052C	0.9	1.0	1.0	1.1	1.0	1.0	0.9
<i>ROX1</i>	YPR065W	0.8	0.6	0.6	0.6	0.5	0.7	1.1
	YPR196W	1.1	1.0	1.2	1.1	1.1	1.0	1.0

a Values are relative to the level in wild-type cells, which was set to 1.

b The deletions of these genes were made in the W303-1B background and analyzed in comparison with the corresponding wild-type cells.

c The deletion strain of *RDS2* was in the BY4741 background and was analyzed with the corresponding wild-type cells.

nd, No data.

Table 4.S4. Analysis of the putative DNA binding sites of transcription factors in *ATG* promoters.

	<i>ATG1</i>	<i>ATG7</i>	<i>ATG8</i>	<i>ATG9</i>	<i>ATG14</i>	<i>ATG29</i>	<i>ATG32</i>
Fyv5							
Gat1	+	+	+	+	+	+	+
Gcn4	+	+	+	+	+	+	+
Gln3	+	+	+	+	+	+	+
Sfl1	+	+	+	+			
Spt10							

Promoter regions of *ATG* genes (1000 base pairs upstream of the start codon) were analyzed using the online software YetFasCo (<http://yetfasco.cabr.utoronto.ca>). '+' indicates the presence of at least one consensus binding site in the promoter of the gene.

Table 4.S5. Strains used in this study.

Name	Genotype	Reference
SEY6210	<i>MATα his3Δ200 leu2-3,112 lys2-801 suc2-Δ9 trp1Δ901 ura3-52</i>	(1)
W303-1B	<i>MATα ade2-1 can1-100 his3-11,15 leu2-3,112 trp1-1 ura3-1</i>	(2)
WLY176	SEY6210 <i>pho13Δ pho8Δ60</i>	(3)
WLY192	WLY176, <i>atg1Δ::HIS5</i>	(4)
ZFY202	W303-1B, <i>pho13Δ pho8Δ60::HIS3</i>	(5)
YAB122	ZFY202, <i>cat8Δ::HIS3</i>	This study
YAB123	ZFY202, <i>sip4Δ::HIS3</i>	This study
YAB124	ZFY202, <i>mig1Δ::HIS3</i>	This study
YAB125	ZFY202, <i>adr1Δ::HIS3</i>	This study
YAB377	WLY176, <i>ZEO1p-SFL1::KanMX6</i>	This study
YAB384	WLY176, <i>gat1Δ::KanMX6</i>	This study
YAB385	WLY176, <i>gln3Δ::HIS3</i>	This study
YAB386	YAB383, <i>gat1Δ gln3Δ::HIS3</i>	This study
YAB387	WLY176, <i>gcn4Δ::HIS3</i>	This study
YAB388	ZFY202, <i>mbp1Δ::URA3</i>	This study
YAB410	WLY176, <i>sfl1Δ::URA3</i>	This study
YAB411	WLY176, <i>sko1Δ::URA3</i>	This study
YAB412	WLY176, <i>yrm1Δ::URA3</i>	This study
YAB413	WLY176, <i>zap1Δ::URA3</i>	This study
YAB414	WLY176, <i>fyv5Δ::URA3</i>	This study
YAB415	WLY176, <i>spt10Δ::URA3</i>	This study
YAB416	WLY176, <i>swi5Δ::URA3</i>	This study
ZYY124	WLY176, <i>GCN4-PA::LEU2</i>	This study
JMY236	WLY176, <i>PMP3p-ATG1::KanMX6</i>	This study
JMY237	WLY176, <i>gcn4Δ::HIS3 PMP3p-ATG1::KanMX6</i>	This study

Table references:

1. Robinson JS, Klionsky DJ, Banta LM, Emr SD. Protein sorting in *Saccharomyces cerevisiae*: isolation of mutants defective in the delivery and processing of multiple vacuolar hydrolases. *Mol Cell Biol* 1988; 8:4936-48.
2. Wallis JW, Chretien G, Brodsky G, Rolfe M, Rothstein R. A hyper-recombination mutation in *S. cerevisiae* identifies a novel eukaryotic topoisomerase. *Cell* 1989; 58:409-19.
3. Mao K, Chew LH, Inoue-Aono Y, Cheong H, Nair U, Popelka H, Yip CK, Klionsky DJ. Atg29 phosphorylation regulates coordination of the Atg17-Atg31-Atg29 complex with the Atg11 scaffold during autophagy initiation. *Proc Natl Acad Sci USA* 2013; 110:E2875-84.
4. Kanki T, Wang K, Baba M, Bartholomew CR, Lynch-Day MA, Du Z, Geng J, Mao K, Yang Z, Yen W-L, Klionsky DJ. A genomic screen for yeast mutants defective in selective mitochondria autophagy. *Mol Biol Cell* 2009; 20:4730-8.
5. Yang Z, Geng J, Yen W-L, Wang K, Klionsky DJ. Positive or negative roles of different cyclin-dependent kinase Pho85-cyclin complexes orchestrate induction of autophagy in *Saccharomyces cerevisiae*. *Mol Cell* 2000; 38:250-64.

Table 4.S6. Primers used in this study.

Gene name	Sequence (5' 3')	Use
<i>ATG1 F</i>	ATCTAAGATGGCCGCACATATG	qPCR
<i>ATG1 R</i>	AGGGTAGTCACCATAGGCATTC	qPCR
<i>ATG1 -900 F</i>	CCGCTGCTCCGCATTACATATC	ChIP
<i>ATG1 -900 R</i>	GTAATGCGGCTGTGTAGGGTG	ChIP
<i>ATG1 -800 F</i>	GAAAGATATCTGTAAACAACGAC	ChIP
<i>ATG1 -800 R</i>	CAGTGGTATTAGTCATTGATGTG	ChIP
<i>ATG1 -700 F</i>	TTTACGCTGCACATCAATGACT	ChIP
<i>ATG1 -700 R</i>	TCCTTACATTACCGCCCAATCC	ChIP
<i>ATG1 -150 F</i>	TCTGGGGAAACAGAGAACAGTAC	ChIP
<i>ATG1 -150 R</i>	TTCTCCTATCTCCTTTGCCTTATG	ChIP
<i>ATG7 F</i>	ATGAGCATTGTCCAGCATGTAG	qPCR
<i>ATG7 R</i>	GACCTCCTGCTTTATGACTGAC	qPCR
<i>ATG8 F</i>	GAAGGCCATCTTCATTTTTGTC	qPCR
<i>ATG8 R</i>	TTCTCCTGAGTAAGTGACATAC	qPCR
<i>ATG9 F</i>	CGTACTAACAGAGTCTTTCCTTG	qPCR
<i>ATG9 R</i>	CTAAGACACCACCTTATTGAG	qPCR
<i>ATG14 F</i>	TACTGGACCAGTACGATGTG	qPCR
<i>ATG14 R</i>	TGCAGGATGTCCTCTTTGTG	qPCR
<i>ATG29 F</i>	ATGAGGCGTTACAACATTTGC	qPCR
<i>ATG29 R</i>	TCGTCATCTGAACTACCGCAC	qPCR
<i>ATG32 F</i>	GGGCAAATGAATACTTTTGTCTTGCATGC	qPCR
<i>ATG32 R</i>	CCCAGTGCCAAAATCCGATTAGATTCATC	qPCR
<i>ChrVI260K F</i>	ATTCCAAACGGTGTTCTTTAC	ChIP
<i>ChrVI260K R</i>	AAAGTAAACGGTGGTCTCTGTG	ChIP
<i>HIS5 F</i>	TGGTATAGTGACGTAGTTAGTGC	ChIP
<i>HIS5 R</i>	GAACAGAACTGTGTGCATCC	ChIP
<i>TAF10 F</i>	ATATTCCAGGATCAGGTCTTCCGTAGC	qPCR
<i>TAR10 R</i>	GTAGTCTTCTCATTCTGTTGATGTTGTTGTTG	qPCR
<i>TFC1 F</i>	GCTGGCACTCATATCTTATCGTTTCACAATGG	qPCR
<i>TFC1 R</i>	GAACCTGCTGTCAATACCGCCTGGAG	qPCR
<i>SLD3 F</i>	CGCAACTTCAAAGCATCATTGAATCGC	qPCR
<i>SLD3 R</i>	GGGGCTTATTAGTGGGAGTAGAGG	qPCR
<i>UBC6 F</i>	GATACTTGGAATCCTGGCTGGTCTGTCTC	qPCR
<i>UBC6 R</i>	AAAGGGTCTTCTGTTTCATCACCTGTATTTGC	qPCR

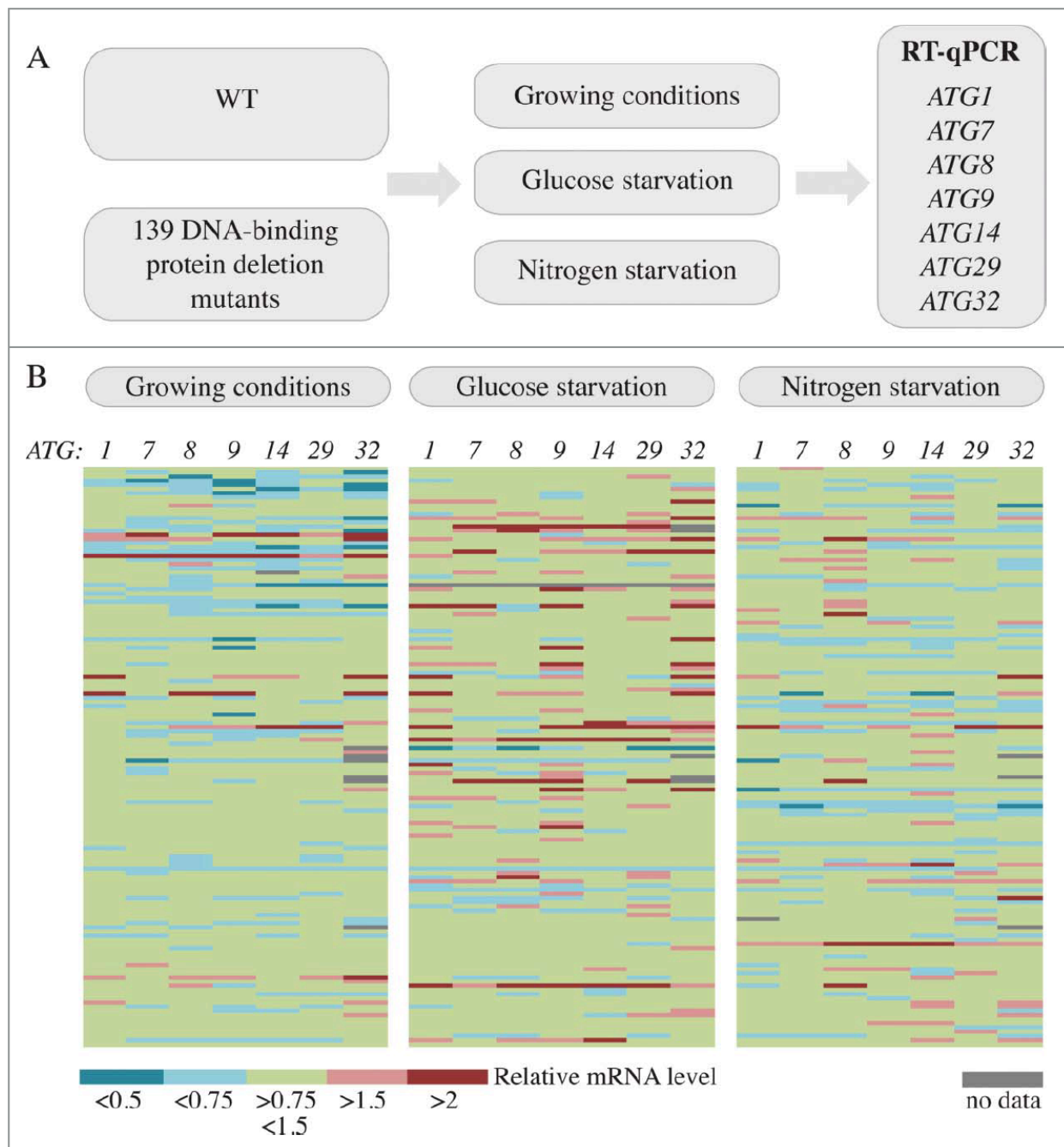


Figure 4.1. A screen for DNA-binding proteins involved in the regulation of *ATG* gene expression.

(A) Schematic of the screen. (B) Color graph illustrating the results of the screen. Each line represents the mRNA level of an independent mutant relative to the wild type in the same condition, which was set to 1.

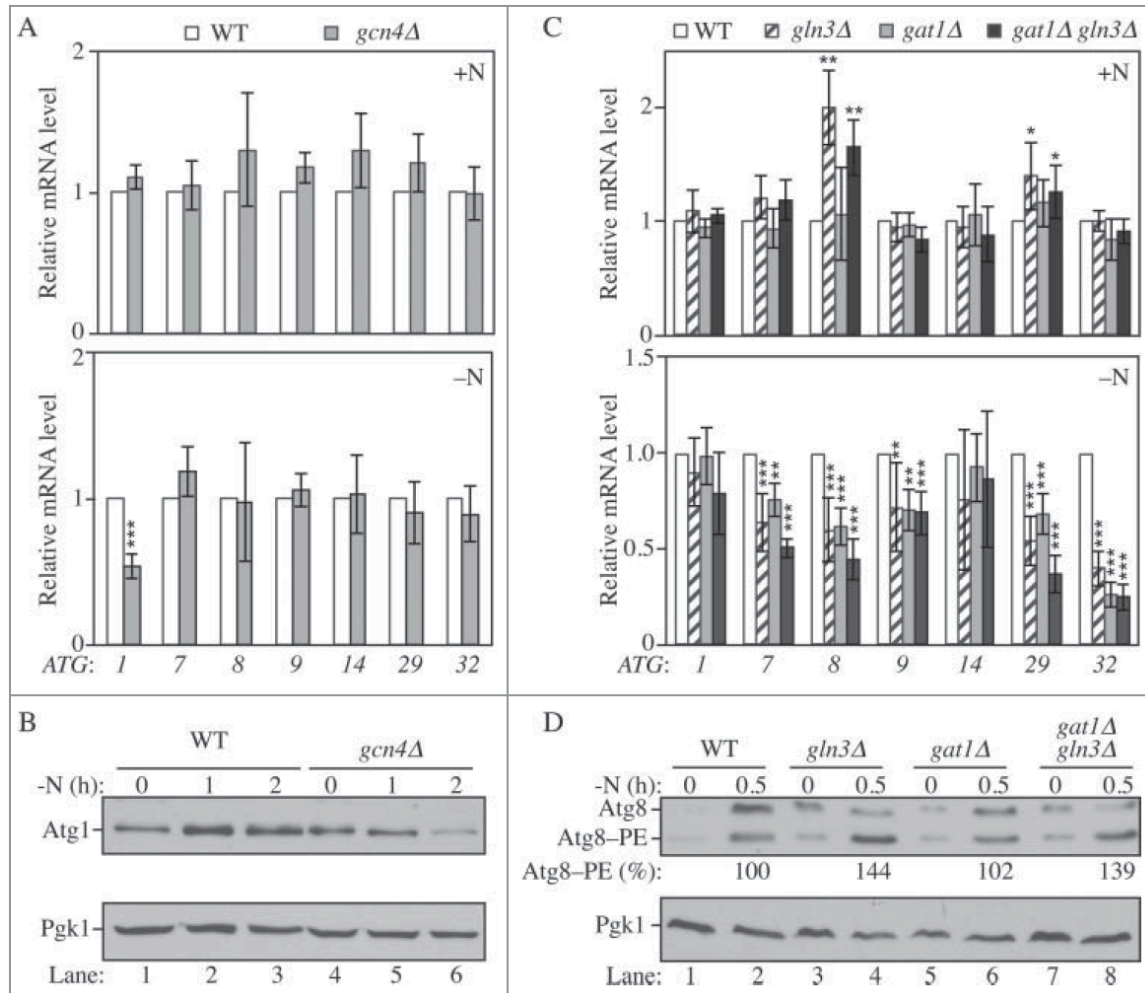


Figure 4.2. Gln3, Gat1 and Gcn4 are transcriptional modulators of *ATG* genes upon nitrogen starvation.

(A-B) Gcn4 is required for the proper induction of *ATG1* upon nitrogen starvation. (A) Wild-type (WLY176; SEY6210) and *gcn4Δ* (YAB387) cells were grown in YPD (+N) until mid-log phase (upper panel) and then starved for nitrogen (-N) for 1 h (lower panel). mRNA levels were quantified by RT-qPCR. The mRNA level of individual *ATG* genes was normalized to the mRNA level of the corresponding gene in wild-type cells, which was set to 1. The data represent the average of at least 3 independent experiments. (B) Wild-type and *gcn4Δ* cells were grown in YPD until mid-log phase and then starved for nitrogen (-N) for the indicated times. Protein extracts were analyzed by western blot with anti-Atg1 and anti-Pgk1 (loading control) antisera. (C-D) Gln3 and Gat1 are required for the proper induction of *ATG7*, *ATG8*, *ATG9*, *ATG29* and *ATG32* after nitrogen starvation; the deletion of *GLN3* increases the expression of *ATG8* and *ATG29* in growing conditions. (C) Wild-type (WLY176), *gln3Δ* (YAB385), *gat1Δ* (YAB384) and *gat1Δ gln3Δ* (YAB386) cells were grown and mRNA analyzed as in (A). The data represent the average of at least 3 independent experiments. (D) For the analysis of Atg8 protein level, wild-type (WLY176; SEY6210), *gln3Δ* (YAB385), *gat1Δ* (YAB384) and *gat1Δ gln3Δ* (YAB386) cells were grown as in (B). Protein extracts were analyzed by western blot with anti-Atg8 and anti-Pgk1 (loading control) antisera. The percent Atg8-PE of total Atg8 is indicated.

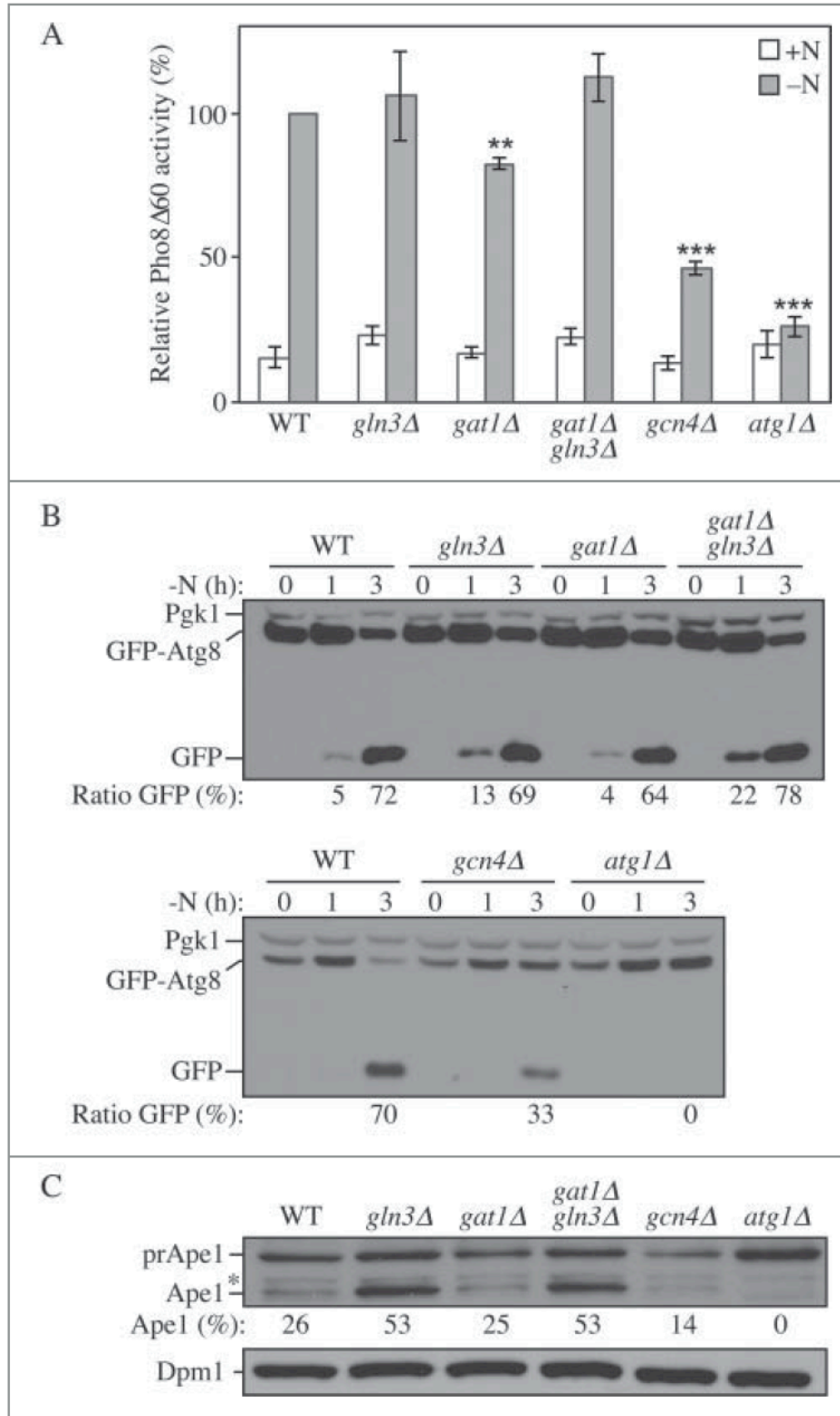


Figure 4.3. Gln3, Gat1 and Gcn4 affect autophagy activity.

Wild-type (WLY176), *gln3Δ* (YAB385), *gat1Δ* (YAB384), *gat1Δ gln3Δ* (YAB386), *gcn4Δ* (YAB387) and *atg1Δ* (WLY192) cells were grown in YPD (+N) and then starved for nitrogen for the indicated times. (A) Autophagy activity as measured by the Pho8Δ60 assay is decreased

in *gat1Δ* and *gcn4Δ* cells. Cells were starved for nitrogen for 3 h (-N). The Pho8Δ60 activity was measured and normalized to the activity of the wild-type cells after starvation, which was set to 100%. n=3 independent experiments. (B) Autophagy as measured by the GFP-Atg8 processing assay is increased shortly after starvation in *gln3Δ* and *gat1Δ gln3Δ* cells, but decreased in *gat1Δ* and *gcn4Δ* cells. Cells were transformed with an integrating plasmid carrying a GFP-Atg8 construct under the control of the *CUP1* promoter. Cells were collected and protein extracts analyzed by western blot with anti-YFP antibody and anti-Pgk1 (loading control) antiserum. The percentage of free GFP:total GFP is indicated. (C) The Cvt pathway as measured by the maturation of prApe1 is increased in *gln3Δ* and *gat1Δ gln3Δ* cells but decreased in *gcn4Δ* cells. Cells were grown in nutrient-rich medium until mid-log phase and then collected. Protein extracts were analyzed by western blot with anti-Ape1 antiserum and anti-Dpm1 (loading control) antibody. prApe1, precursor form; Ape1, mature form. The percentage of Ape1:total Ape1 is indicated. *, Nonspecific band.

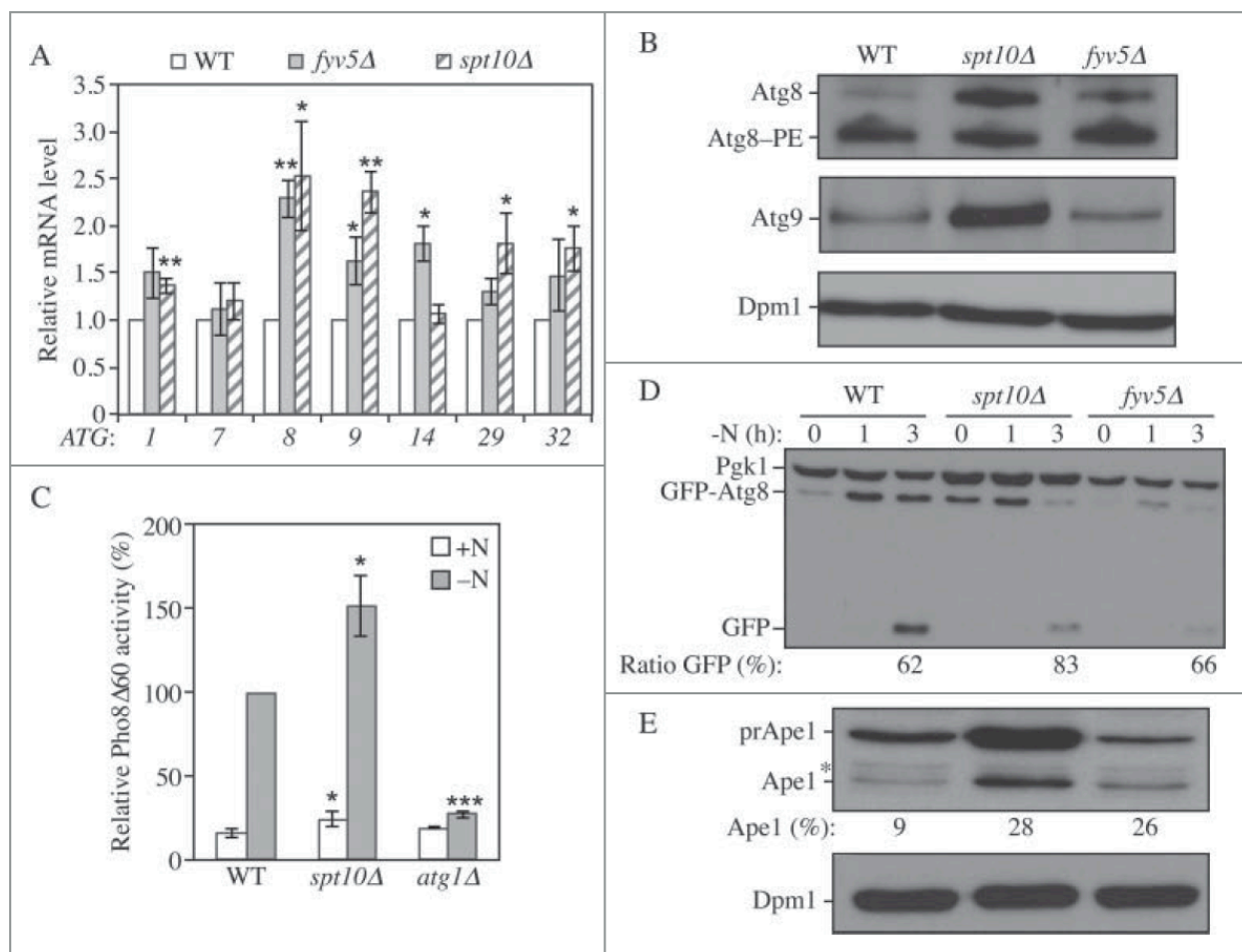


Figure 4.4. Spt10 and Fyv5 are transcriptional repressors of ATG gene expression.

Wild type (WLY176), *spt10Δ* (YAB415), *fyv5Δ* (YAB414) and *atg1Δ* (WLY192) cells were grown in YPD (+N) until mid-log phase. (A) Spt10 and Fyv5 repress the expression of ATG genes in growing conditions. mRNA was extracted and quantified by RT-qPCR as in Figure 4.2. Data represent the average of at least 3 independent experiments. (B) Protein extracts were analyzed by western blot with anti-Atg8, anti-Atg9 and anti-Dpm1 (loading control) antisera and antibodies. (C-D) Autophagy is increased in *spt10Δ* cells. Cells were grown in YPD until mid-log phase (+N) and then starved for nitrogen (-N) for the indicated times. (C) The Pho8Δ60 activity was measured and normalized as in Figure 4.2 for cells that were starved for 3 h. Data represent the average of at least 3 independent experiments. (D) Cells were transformed with an integrating plasmid carrying a GFP-Atg8 construct under the control of the endogenous ATG8 promoter. Protein extracts were analyzed by western blot with anti-YFP antibody and anti-Pgc1 (loading control) antisera. The percentage of free GFP:total GFP is indicated. (E) The Cvt pathway as measured by the maturation of prApe1 is increased in *spt10Δ* and *fyv5Δ* cells. Proteins were extracted from cells grown in nutrient-rich conditions, and the extracts were analyzed by western blot with anti-Ape1 antiserum and anti-Dpm1 (loading control) antibody. prApe1, precursor form; Ape1, mature form. The percentage of Ape1:total Ape1 is indicated. *, Nonspecific band.

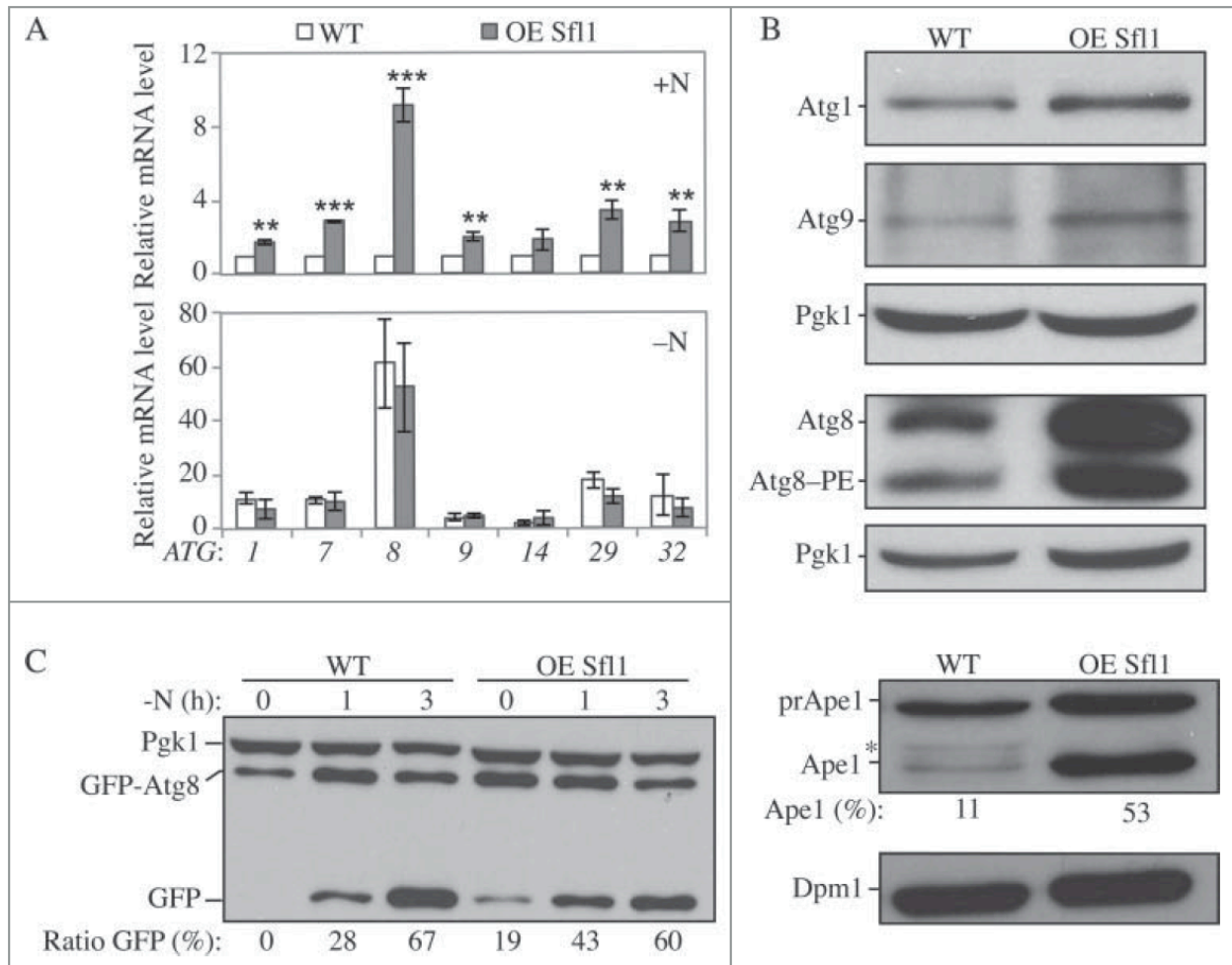


Figure 4.5. Sfl1 promotes *ATG* gene expression and autophagy.

(A-B) The overexpression of Sfl1 induces the expression of *ATG* genes and proteins. Wild-type cells (WLY176, SEY6210) and cells with overexpressed (OE) Sfl1 (YAB377) were grown in YPD (+N) until mid-log phase. (A) Cells in growing conditions (+N, upper panel) and after 1 h of nitrogen starvation (-N, lower panel) were collected. mRNA levels were analyzed and quantified as in Figure 4.2. Data represent the average of at least 3 independent experiments. (B) Protein extracts were analyzed by western blot with anti-Atg1, anti-Atg9, anti-Atg8 and anti-Pgk1 (loading control) antisera. (C) The overexpression of Sfl1 promotes autophagy activity in growing conditions. Cells were transformed with an integrating plasmid carrying a GFP-Atg8 construct under the endogenous *ATG8* promoter. Protein extracts were analyzed by western blot with anti-YFP antibody and anti-Pgk1 (loading control) antisera. The percentage of free GFP:total GFP is indicated. (D) The Cvt pathway as measured by the maturation of prApe1 is increased in cells overexpressing Sfl1. Proteins were extracted from cells grown in nutrient-rich conditions. Extracts were analyzed by western blot with anti-Ape1 antiserum and anti-Dpm1 (loading control) antibody. prApe1, precursor form; Ape1, mature form. The percentage of Ape1:total Ape1 is indicated. *, Nonspecific band.

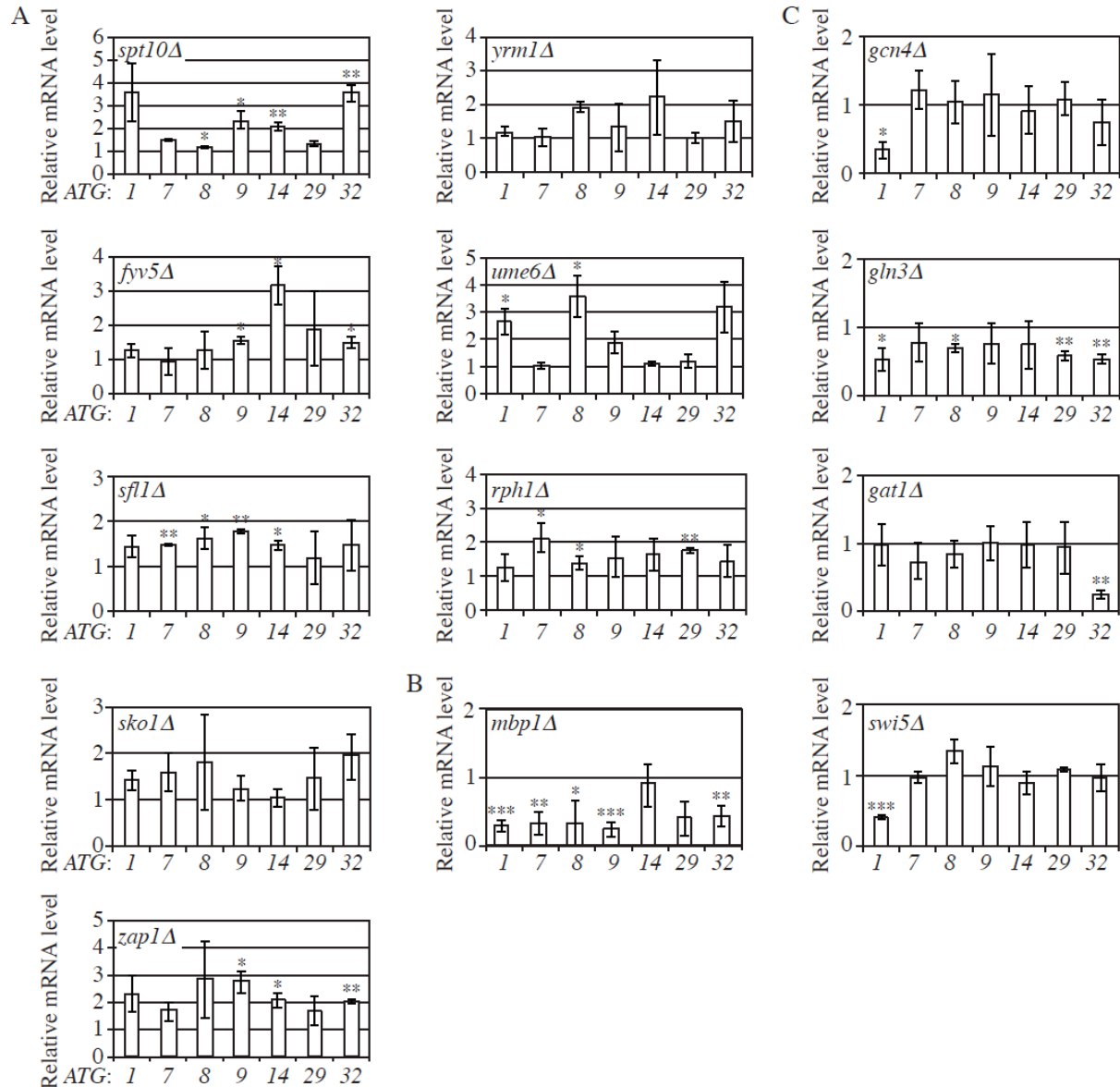


Figure 4.S1. mRNA quantification of *ATG* genes in the mutants identified in the screen as potential autophagy transcriptional regulators.

Deletion strains from a BY4742 collection were grown alongside the corresponding wild-type strain in YPD medium until mid-log phase. mRNA levels were quantified by RT-qPCR. The mRNA level of individual *ATG* genes was normalized to the mRNA level of the corresponding gene in wild-type cells, which was set to 1. The data represent the average of at least 3 independent experiments. (A) mRNA levels were quantified from cells in growing conditions. (B) mRNA levels were quantified after 2 h of glucose starvation. (C) mRNA levels were quantified after 1 h of nitrogen starvation.

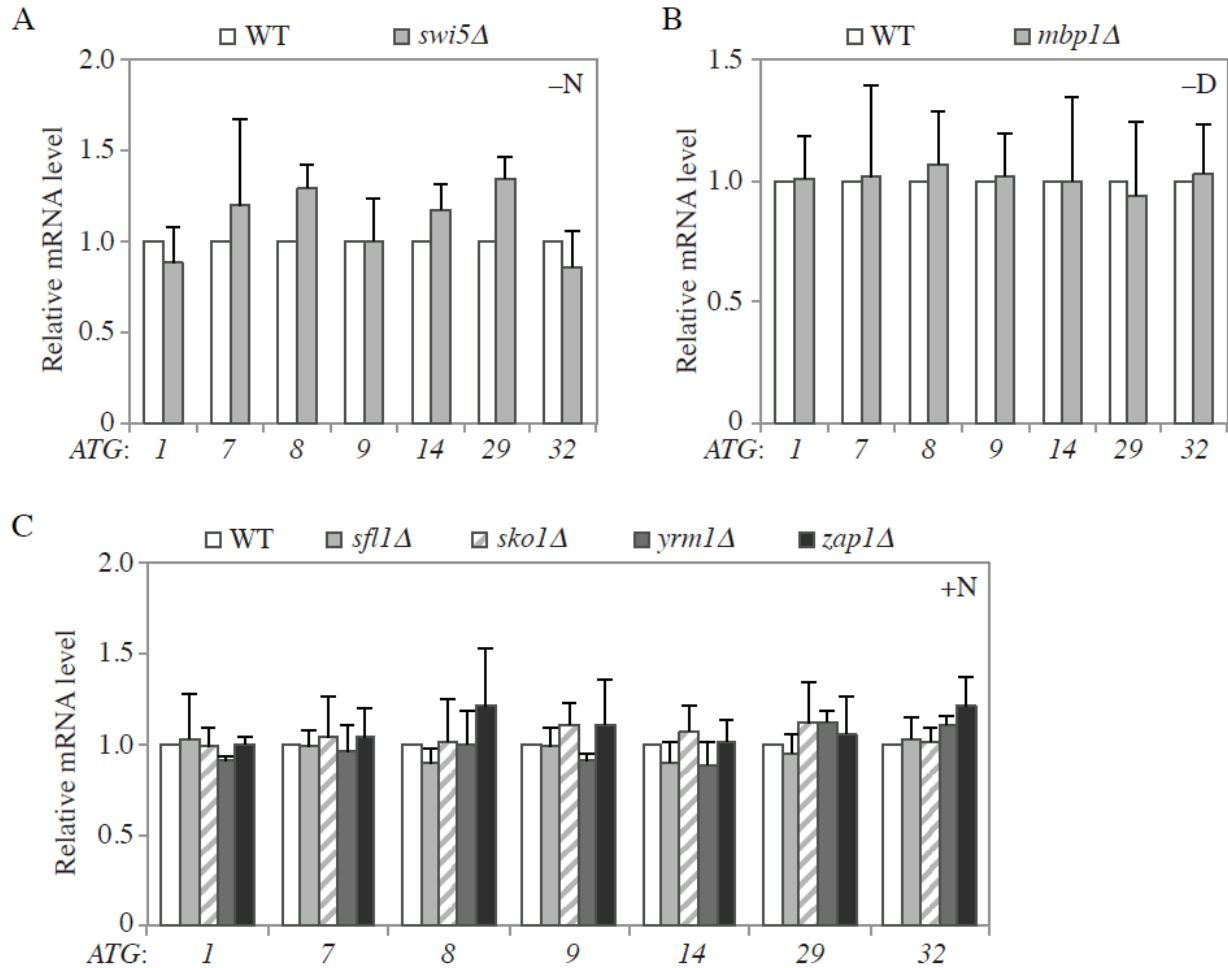


Figure 4.S2. mRNA quantification of *ATG* genes in newly generated deletion strains.

Cells were grown alongside the corresponding wild-type strain in YPD medium until mid-log phase. mRNA levels were quantified by RT-qPCR. The mRNA level of individual *ATG* genes was normalized to the mRNA level of the corresponding gene in wild-type cells, which was set to 1. The data represent the average of at least 3 independent experiments. (A) mRNA of wild type (WLY176, SEY6210) and *swi5Δ* (YAB416) cells were analyzed after 1 h of nitrogen starvation (-N). (B) mRNA of wild-type (ZFY202, W303-1B) and *mbp1Δ* (YAB388) cells were analyzed after 2 h of glucose starvation (-D). (C) mRNA of wild-type (WLY176, SEY6210), *sfl1Δ* (YAB410), *sko1Δ* (YAB411), *yrm1Δ* (YAB412) and *zap1Δ* (YAB413) cells were analyzed in rich conditions (+N).

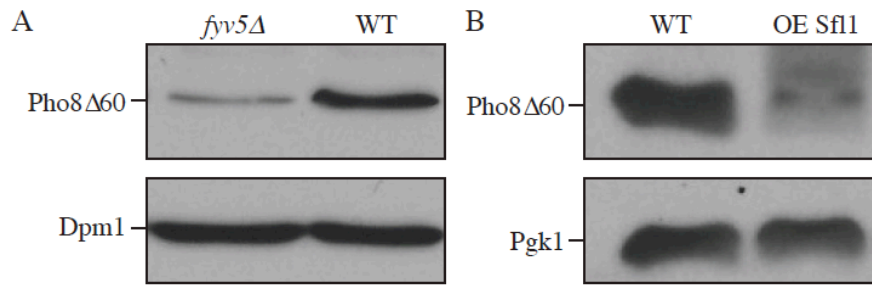


Figure 4.S3. The deletion of *FYV5* and the overexpression of *SFL1* affect the level of the Pho8Δ60 protein.

Wild-type (WLY176, SEY6210), *fyv5Δ* (YAB414) and overexpressed (OE) Sfl1 (YAB377) cells were grown in YPD medium until mid-log phase. (A) Protein extracts were analyzed by western blot with anti-Pho8 antiserum and anti-Dpm1 (loading control) antibody. (B) Protein extracts were analyzed by western blot with anti-Pho8 and anti-Pgk1 (loading control) antisera.

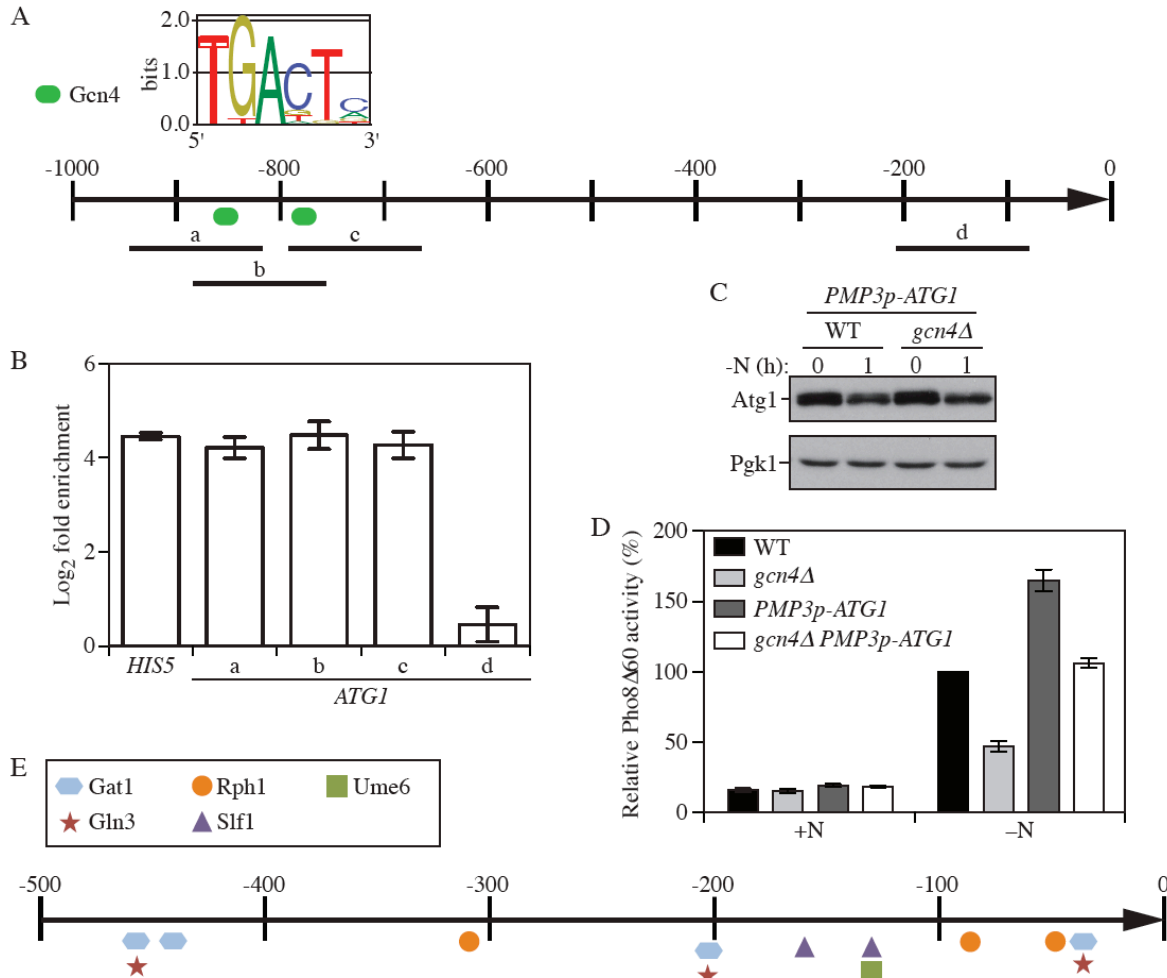


Figure 4.S4. Evidence for direct DNA-binding of transcription factors on *ATG* promoters.

(A) Schematic of the *ATG1* promoter (1000 base pairs upstream of the coding sequence) positioning the 2 consensus binding sites for Gcn4 (in green) and its sequence. Black bars indicate the fragments amplified by chromatin immunoprecipitation (ChIP) in (B). (B) Gcn4 binds the *ATG1* promoter. The ChIP results represent the fold-enrichment of Gcn4-PA cells (ZYY124, WLY176) compared to non-tagged wild-type cells (WLY176). ChIP was conducted on the *HIS5* promoter as a positive control, 3 different locations around the Gcn4 consensus sites on the *ATG1* promoter (a, b, c as marked in [A]), an *ATG1* promoter location which does not overlap with the Gcn4 consensus site (d as marked in [A]) and a large noncoding region located at 260 kb on chromosome VI which was used for normalization. (C-D) Changing the promoter of *ATG1* for the promoter of *PMP3* prevents the Gcn4-driven defects in *ATG1* expression. The promoter of *ATG1* was replaced with the promoter of *PMP3* on the genome (*PMP3p-ATG1*, JMY236), and *GCN4* was deleted (JMY237). Cells were grown in YPD (+N) until mid-log phase and then starved for nitrogen (-N). (C) Protein extracts from cells starved for 1 h were analyzed by western blot with anti-Atg1 and anti-Pgk1 (loading control) antisera. (D) The Pho8Δ60 activity was measured and normalized as in Figure 4.2 for cells starved for 3 h. Data represent the average of 3 independent experiments. (E) *In silico* analysis of the *ATG8* promoter positioning the consensus sites for known or newly identified DNA-binding proteins regulating

the expression of *ATG8*. The schematic represents 500 base pairs upstream of the *ATG8* coding sequence, which starts at 0.

CHAPTER 5. Rph1/KDM4 Mediates Nutrient-limitation Signaling that Leads to the Transcriptional Induction of Autophagy⁵

5.1 Introduction

Macroautophagy (hereafter referred to as autophagy) is a highly conserved pathway during which portions of the cytoplasm, superfluous or damaged organelles, or invasive pathogens are delivered to the vacuole (in yeast and plants) or the lysosome (in mammals) for degradation and subsequent recycling. Morphologically, autophagy starts with the nucleation of the phagophore, the initial membrane structure, at a peri-vacuolar site called the phagophore assembly site, or PAS (Figure 5.S1A, [1]). Through the acquisition of lipids, the phagophore then expands, surrounding its cargo, and ultimately seals to generate a double-membrane vesicle called the autophagosome. After autophagosome fusion with the vacuole, the inner membrane of the vesicle as well as its cargo are degraded and recycled into the cytosol. The macromolecules resulting from this pathway are then used by the cell to maintain cellular homeostasis during deleterious conditions [2].

Autophagy is highly upregulated upon multiple stress conditions and notably nutrient limitation where it plays critical roles in cell adaptation and survival [3]. The autophagy pathway plays a role in cellular physiology, and mammalian development as well as the immune response [4-6], and autophagy impairments are associated with various human pathologies such as cancer

⁵ This chapter is reprinted from Amélie Bernard, Meiyang Jin, Patricia González-Rodríguez, Jens Füllgrabe, Elizabeth Delorme-Axford, Steven K. Backues, Bertrand Joseph, Daniel J. Klionsky, Rph1/KDM4 Mediates Nutrient-Limitation Signaling that Leads to the Transcriptional Induction of Autophagy, *Current Biology*, 2015; 25 (5): 546-555, <http://dx.doi.org/10.1016/j.cub.2014.12.049>, with minor modifications, with permission from Elsevier.

or metabolic diseases [7-8]. Autophagy also occurs at a constitutive basal level in physiological conditions. In yeast, the cytoplasm-to-vacuole targeting (Cvt) pathway is essential for the biosynthetic delivery of vacuolar enzymes during growth [9]. In mammals, basal autophagy functions in the quality control machinery involved in the degradation of damaged organelles and protein aggregates which, when accumulated, lead to various neurodegenerative disorders such as Huntington, Alzheimer and Parkinson diseases [10].

If a sub-optimal autophagy activity can be detrimental, a supra-optimal level can also be deleterious for the cells; uncontrolled autophagy leads to cell death [11-12], certain microbes rely on autophagy to provide nutrients [13], and cancer cells can also use autophagy to help survive in an unfavorable environment [14]. Therefore, to support proper cellular functions, rates of autophagy have to be finely regulated. Over the past 20 years, extensive molecular studies of autophagy have led to the identification of the core components of the autophagy machinery, encoded by the autophagy-related (*ATG*) genes (for review see ref. [15]); yet the regulatory pathways governing their functions remain largely unknown. In particular the transcriptional regulation of the *ATG* genes is still mostly unexplored (for review see ref. [14]).

The expression of most of the *ATG* genes, and their corresponding proteins, highly increases upon autophagy induction after nitrogen starvation [16]. Given the energy cost for such an induction, it has been suggested that this upregulation is critical for the normal modulation of autophagy and for the pathway to reach full amplitude when most needed. Furthermore, the reported abnormal expression of several *ATG* genes in various human diseases supports the proposed physiological importance of their transcriptional regulation [17-20]. Recent studies in yeast identified Ume6 as a transcriptional repressor of *ATG8* [21] and showed that the level of Atg8 controls the size of the autophagosome [22]. Conversely, the level of Atg9, regulated by

Pho23, controls the frequency of formation (hence the number) of autophagosomes [16].

Nevertheless, very few transcription factors have been identified as regulating the expression of *ATG* genes in either yeast or mammals and the contribution of the induction of specific *ATG* genes in autophagy activity is still poorly understood.

At the starting point of this study a search for new transcriptional regulators of autophagy was initiated by the screen of a collection of over 150 mutants lacking a single transcription factor or DNA-binding protein. Analysis of the expression of a set of *ATG* genes in this library led to the identification of Rph1 as a master transcriptional repressor of autophagy.

5.2 Results

5.2.1 *Rph1* Is a Transcriptional Repressor of *ATG* Genes

In order to identify transcriptional regulators of autophagy we compared the expression of a subset of *ATG* genes in wild-type cells to that in a library of DNA binding protein deletion mutants. *ATG1*, *ATG7*, *ATG8*, *ATG9*, *ATG14* and *ATG29* were selected as target genes because they encode proteins involved in different steps of the autophagy pathway (Figure 5.S1A) and because they show a strong induction after nitrogen starvation, indicating that they are under transcriptional control in these conditions (Figure 5.1A,B; [16]). The DNA binding protein mutants displayed a range of phenotypes (data not shown), and *rph1Δ* in particular showed a significant upregulation of *ATG7*, *ATG8*, *ATG9*, *ATG14* and *ATG29* accompanied with a modest induction of *ATG1* in growing conditions (Figure 5.1A, Table 5.S1, Table 5.S2). Similarly, the deletion of *RPH1* resulted in an increased expression of *ATG32* (Figure 5.1A), a marker of mitophagy (the selective autophagic degradation of mitochondria). In contrast, deleting *RPH1* had essentially no effect on the transcription of *ATG10*, an autophagy-related gene that displays no change in expression in response to nitrogen deprivation (Figure 5.1A,B). Additionally, there

was no significant difference in the mRNA levels of *ATG* genes between the *rph1Δ* strain and wild-type cells after starvation (Figure 5.1B). This difference between growing and starvation conditions suggests that Rph1 represses the expression of nitrogen-sensitive *ATG* genes specifically in nutrient-replete conditions.

Rph1 is a DNA-binding protein, which contains two C₂H₂ zinc-finger motifs as well as a Jumonji C histone demethylase catalytic domain. Rph1 has a paralog, Gis1, and previous studies report that Rph1 and Gis1 have distinct as well as overlapping targets [23-26]. Whereas the deletion of *GIS1* had a very minor effect on the expression of some of the *ATG* genes that we examined, the *gis1Δ rph1Δ* double mutant showed an enhanced induction of the mRNA level of these genes compared to the single *RPH1* deletion in growing conditions (Figure 5.1A,B). This finding indicates that Rph1 plays a predominant role in the regulation of *ATG* genes, but that its absence can be partially compensated by Gis1.

Consistent with the changes observed at the mRNA levels, *rph1Δ* cells showed a strong enrichment of the proteins Atg7, Atg8, Atg9, Atg14 and Atg29 and a modest increase in Atg1 compared to the wild type; in contrast the level of Atg10 was unaffected (Figure 5.1C-E, Figure 5.S1B,C). This phenotype was exacerbated in *gis1Δ rph1Δ* cells as suggested by the analysis of Atg7 and Atg8 (Figure 5.1C,D). It is worth noting that although the abundance of Atg1, Atg8, Atg9 and Atg14 was higher in *rph1Δ* cells in rich conditions compared to the wild type (Figure 5.1C, compare lanes 3 and 5, Figure 5.S1B,C), the protein levels were still lower than those seen after starvation (Figure 5.1C, compare lanes 5 and 6, Figure 5.S1B,C), indicating that other pathways are contributing to the regulation of the corresponding genes. In contrast, deleting *RPH1* alone was sufficient to increase the Atg7 protein abundance to a higher level than that seen after 3 h of nitrogen starvation in the wild-type cells (Figure 5.1D, compare lanes 6 and 7,

Figure 5.S1B,C), suggesting that Rph1 has a preponderant role in regulating the expression of Atg7. Together these results show that Rph1 is a transcriptional repressor of *ATG* genes.

5.2.2 *Rph1 Is a Negative Regulator of Autophagy*

Finding that Rph1 represses the expression of *ATG* genes in growing conditions suggests that it might be a negative regulator of autophagy. To test this hypothesis autophagy activity was measured using a Pho8 Δ 60 assay in which alkaline phosphatase activity reflects autophagy amplitude [27]. After 1 h of nitrogen starvation, the wild-type cells displayed a substantial induction of alkaline phosphatase activity (50% of the activity seen at 3 h; note that the wild-type activity is set to 100% at each time point in Figure 5.2A), which was blocked by the deletion of *ATG7* (Figure 5.2A). Compared to the wild type, autophagy was induced to a higher level in the *rph1* Δ cells and *gis1* Δ *rph1* Δ cells; in contrast the deletion of *GIS1* alone had no significant effect. We extended this analysis by using a GFP-Atg8 processing assay [28]. After one hour of starvation, autophagy was induced more rapidly and to a higher extent in the *rph1* Δ and *gis1* Δ *rph1* Δ cells, as indicated by the level of free GFP compared to the wild-type (Figure 5.2B,C). Note that the enhanced autophagy activity in *rph1* Δ cells upon short-term nitrogen starvation was attenuated after a prolonged time of induction. This observation is consistent with the fact that deleting *RPH1* increases the transcription of *ATG* genes only in nutrient-rich conditions; a higher abundance of Atg proteins can therefore support a jump-start in autophagy activity upon its induction by nitrogen starvation. After prolonged starvation, Atg protein levels in wild-type cells reach that of the mutant strains, abolishing the difference in autophagy activity relative to the *rph1* Δ and *gis1* Δ *rph1* Δ mutants.

Our results indicated that Rph1 has a major role in the transcriptional regulation of *ATG7* (Figure 5.1, Figure 5.S1B,C). Atg7 is an E1 activating enzyme, which notably mediates the

conjugation of Atg8 to PE and is critical for autophagy (Figure 5.2A). Nevertheless, very little is known concerning the effect of *ATG7* transcriptional regulation on autophagy. To address this, an *atg7* Δ strain was transformed with plasmids in which protein A (PA)-tagged Atg7 was placed under the control of promoters (*FLO5*, *GAL3*, *ATG7* and *SEF1* in increasing order of strength) with different transcriptional activities (Figure 5.3A). Note that in these conditions we did not observe a strong increase in the abundance of Atg7-PA in wild-type cells after starvation (compared to Figure 5.1D and Figure 5.S1B,C), which may reflect expression from a plasmid as opposed to the complete *ATG7* promoter. Lowering Atg7 abundance correlated with a reduction of Atg8–PE conjugates (Figure 5.3A) as well as a reduction in autophagy activity (Figure 5.3B). The finding that Atg7 protein amount directly affects autophagy activity supports a model in which Rph1 regulates autophagy in part by controlling the expression of Atg7. Nevertheless, an increase in Atg7 protein alone was not sufficient to induce autophagy (Figure 5.3B, +N) suggesting that the *rph1* Δ phenotype results from the combined upregulation of multiple *ATG* genes.

5.2.3 The overexpression of Rph1 inhibits autophagy and decreases cell survival in nitrogen starvation conditions

To further test the role of Rph1 in autophagy, *RPH1* was overexpressed under the control of the *ZEO1* promoter (Figure 5.4A). Overexpression of Rph1 caused a severe block in the induction of several *ATG* genes after starvation (Figure 5.4B) but had no effect on the expression of *ATG1*. Furthermore, the reduction in *ATG* transcripts correlated with a decrease in autophagy activity (Figure 5.4C). A decrease in autophagy flux could either result from a reduction in the number of autophagosomes or a reduction in their size. To distinguish between the two hypotheses, cells overexpressing Rph1 were further analyzed using transmission electron

microscopy (TEM). After 2 h of nitrogen starvation, cells overexpressing Rph1 displayed a strong reduction in the average number of autophagic bodies accumulated in the vacuole compared to wild-type cells (Figure 5.4D,E, Figure 5.S2, Table 5.S3); in contrast there was no significant effect on the size of the autophagic bodies (Figure 5.4D,F, Figure 5.S2, Table 5.S3).

Next, the physiological importance of the Rph1-dependent regulation of autophagy was tested by monitoring the survival phenotype of cells overexpressing Rph1 after nitrogen starvation. Wild-type yeast cells showed no significant cell death during the time course of the experiment, whereas a complete block of autophagy in *atg1Δ* cells resulted in a complete loss of viability (Figure 5.4G). In comparison, cells overexpressing Rph1 exhibited a slight growth defect in nitrogen-replete conditions (Figure 5.4G, left panel) and showed a reduced survival rate after prolonged starvation (Figure 5.4G, right panel). Together these results suggest that overexpressed-Rph1 promotes cell death by repressing autophagosome biogenesis and thereby inhibiting autophagy.

5.2.4 Rph1 DNA Binding Ability but Not Histone Demethylase Activity Is Required for its Function in Autophagy

Rph1 is a Jumonji C (JmjC)-containing histone demethylase protein, which is the only demethylase targeting H3K36 tri-methylation in *Saccharomyces cerevisiae* [29]. Previous studies showed that the transcriptional repression of some Rph1 targets is dependent on its histone demethylase activity [30]. We therefore proposed that Rph1 may repress *ATG* genes transcription, and thereby autophagy, in a similar manner. This idea was first tested using a *set2Δ* deletion strain; Set2 is the histone methyltransferase mediating H3K36 methylation in yeast cells [31] and, in this regard, has an opposite function to that of Rph1. Nitrogen starvation did not significantly affect H3K36 tri-methylation (H3K36me3) and *rph1Δ* cells did not show any

difference in the H3K36me3 status compared to wild-type cells (Figure 5.5A). In contrast, the deletion of *SET2* led to a complete block in H3K36me3 marks. Nevertheless, we did not observe an autophagy defect in *set2Δ* cells compared to the wild type (Figure 5.5B), which indicates that the level of H3K36me3 does not regulate autophagy.

Next, we analyzed the previously described Rph1^{H235A} mutant in which the replacement of histidine 235 with alanine inhibits the protein's histone demethylase activity (Figure 5.S3A,B; [30]). Protein analysis verified the stability of Rph1^{H235A} compared to wild-type Rph1 (Figure 5.5C). The *rph1Δ* phenotype was restored to the same extent by either wild-type Rph1 or Rph1^{H235A} (Figure 5.5D, Figure 5.S3C). In addition, cells overexpressing Rph1 or the Rph1^{H235A} mutant showed a similar reduction in autophagy activity compared to wild-type cells (Figure 5.5E,F). Together these results show that the function of Rph1 in autophagy is, at least mostly, independent of its histone demethylase activity.

Previous results from a large-scale ChIP-chip (chromatin immunoprecipitation-on-chip) analysis identified several *ATG* genes as potential direct targets of Rph1 [32]. Consistent with this idea, a DNA motifs search in the promoter region of *ATG* genes identified one or multiple Rph1-binding consensus sites in 23 out of 32 *ATG* genes (Table 5.S4, Table 5.S5). In particular, our analysis revealed the presence of the environmentally regulated Rph1 binding site (TWAGGG; [26]) in the promoter of highly regulated genes such as *ATG7*, *ATG9* and *ATG14* and of a related site (AGGGG) in *ATG8* and *ATG29* but not in those of a modestly affected gene, *ATG1*, or a non-affected gene, *ATG10*. Therefore we tested the importance of the DNA-binding domain of the protein by constructing an Rph1^{ΔZ} mutant, in which the deletion of both zinc-finger motifs at the C-terminal part of the protein prevents DNA binding ([31]; Figure 5.S3A). A ChIP approach showed a 2-fold enrichment of Rph1-PA at the *ATG7* promoter compared to

Rph1^{ΔZ}-PA (Figure 5.5G). A similar enrichment was found at the *PHR1* promoter, which was used as a positive control [30], but not at the non-coding region located at the tip of chromosome VI (ChrVI-260K), which was used as a negative control. This indicates that Rph1 directly binds the promoter region of *ATG7* and that this binding is significantly reduced upon deletion of the zing-finger domains of the protein. Furthermore, even though Rph1^{ΔZ}-PA was found over-accumulated compared to Rph1-PA (Figure 5.5C), this mutant form of the protein was unable to rescue the *ATG* gene overexpression phenotype or the increased autophagy activity induction of the *rph1Δ* cells (Figure 5.5D, Figure 5.S3C), thus showing that the DNA-binding domain of Rph1 is strictly required for its function in autophagy.

Together these results show that the histone demethylase activity of Rph1 is not required for its function in autophagy and suggest that, instead, Rph1 represses the expression of *ATG* genes by restricting the access of the transcriptional machinery or potential activators at these loci as has been proposed for other Rph1-regulated genes [23, 33].

5.2.5 *Rph1 Phosphorylation upon Nitrogen Starvation Releases its Repression of Autophagy*

As mentioned above, the deletion of *RPH1* induced the expression of *ATG* genes in rich conditions but had no effect on mRNA levels after nitrogen starvation (Figure 5.1). These results suggest a model in which Rph1 represses the transcription of these targets when cells grow in nutrient-replete medium and that upon nitrogen starvation this repression is released thereby allowing the induction of *ATG* genes and autophagy. Previous studies describe Rph1 as a phosphoprotein and show that Rph1 phosphorylation inhibits its activity [23]. Similarly, we observed a shift in the molecular weight of Rph1-PA as well as the appearance of a faint upper band in conditions of nitrogen depletion, suggesting that Rph1 undergoes phosphorylation at multiple sites (Figure 5.6A, left panel, and Figure 5.6C). This shift was accompanied by a

modest decrease in protein level shortly after nitrogen starvation (Figure 5.6A,C). In order to get a better resolution of the phosphorylation status of Rph1 we used Phos-tag, a molecule that binds specifically to phosphorylated ions, thereby increasing the molecular weight of phospho-isoforms. With addition of Phos-tag, Rph1-PA was observed as several higher molecular weight bands in nitrogen starvation conditions compared to rich conditions, strongly supporting the hypothesis that Rph1 is phosphorylated upon starvation (Figure 5.6A, right panel). Note that this analysis also revealed Rph1-PA as a doublet in rich conditions (Figure 5.6A, right panel) indicating that the protein undergoes some phosphorylation even in the presence of nitrogen. Furthermore, phosphatase treatment of the protein samples prevented the changes in Rph1 mobility demonstrating that the change in migration represents genuine phosphorylation of the protein (Figure 5.6B).

To test the importance of Rph1 phosphorylation for autophagy induction, we next aimed to identify the phosphorylated residues upon nitrogen starvation. In order to identify such sites we used previously published data from large-scale phosphoproteomic analyses. In particular Huber et al. [34] identified 5 sites (group II, Figure 5.S4) at which phosphorylation was suggested to be upregulated upon treatment with rapamycin, a drug that induces autophagy; in addition the work by Bodenmiller et al. [35], proposed that phosphorylation at T411 and S412 (group I, Figure 5.S4) is upregulated when the gene encoding Tpk2, a subunit of the autophagy repressor PKA, is deleted. Based on these data we generated Rph1 mutants where the phosphoresidues in group I or group I and II were mutated to alanine. In addition serine 429 which is also predicted to be phosphorylated was mutated to alanine because of its proximity to the residues in group I. The mutants showed only a partial reduction in phosphorylation based on gel migration, and a concomitant accumulation of the non-phosphorylated form of the protein after starvation (Figure

5.S4B). Accordingly, autophagy activity was only reduced to a minor, yet significant, level in these mutants (Figure 5.S4C), suggesting that additional residues that were not identified by mass spectrometry may also be involved in phospho-regulation of Rph1. Together these results show that residues in group I and II participate in the phosphorylation of Rph1 after starvation and suggest that this modification of the protein inhibits its activity upon autophagy induction.

5.2.6 Rim15 Mediates the Phosphorylation of Rph1 upon Nitrogen Starvation thereby inducing Autophagy

Next, we attempted to identify the kinase responsible for Rph1 phosphorylation prior to autophagy activation; Rim15 appeared to be a good candidate as it is phosphorylated and translocated into the nucleus after nitrogen starvation at which time it activates autophagy [36-38]. Analysis of Rph1-PA showed a strong block in Rph1 molecular mass shift when *RIM15* was deleted (Figure 5.6C,D) showing that this kinase is, at least partly, responsible for Rph1 phosphorylation upon nitrogen starvation. Moreover, the inhibition of Rph1 phosphorylation in the *rim15Δ* cells was accompanied by a stabilization of the Rph1 protein compared to wild-type cells where the protein level decreased after nitrogen starvation. In addition, the *RIM15* deletion caused a partial block in the induction of some of the *ATG* genes and Atg proteins that we analyzed, concomitant with the reduction of autophagy activity seen in the same conditions (Figure 5.6E,F and Figure 5.S4D-F). Furthermore, deletion of *RPH1* in the *rim15Δ* cells rescued the defect in Atg7-PA level in response to nitrogen starvation (Figure 5.6G), showing that Rim15 acts upstream of Rph1 to regulate *ATG7* expression during autophagy.

These findings strongly support the idea that the Rim15-dependent phosphorylation of Rph1 is required for proper induction of autophagy upon nitrogen starvation. Our previous work showed that Rim15 also phosphorylates Ume6 leading to an inhibition of Ume6 activity and an

upregulation of *ATG8* after nitrogen starvation [21]. As previously described, the *ume6Δ* cells showed an increase in the expression of *ATG8* in nutrient-rich conditions compared to the wild type ([21], Figure 5.S4G); this was accompanied by an upregulation of *ATG1* and *ATG9*. In contrast the expression of *ATG7*, *ATG14* and *ATG29* was unaffected by the deletion of *UME6*. Because *rph1Δ* cells showed higher expression of *ATG7* and *ATG29* we suggest that the block of, at least, *ATG7* and *ATG29* induction in the *rim15Δ* cells is specifically due to the loss of Rph1 phosphorylation and propose that this contributes to the reduction of autophagy activity in this mutant background.

5.2.7 The Regulation of Autophagy by Rph1/KDM4 Is Conserved from Yeast to Mammals

To test if the mechanism of autophagy regulation that we uncovered here was conserved in higher eukaryotes we studied the role of one mammalian homolog of *RPH1*, *KDM4A*, in the autophagy pathway. A reduction of *KDM4A* level was associated with an increase in the mRNA level of several *ATG* genes including *ATG7*, *WIP1* and *ATG14*, whereas there was essentially no effect on *MAP1LC3B* (Figure 5.7A). HeLa cells transformed with *siKDM4A* showed an accumulation of LC3-II compared to control cells pointing to an increase in basal autophagy in this condition (Figure 5.7B, left panel). To verify that the increase in LC3-II reflected an upregulation of autophagy rather than a block in flux, we treated the cells with the autophagy inhibitor bafilomycin A₁. We detected a further increase in the level of LC3-II upon the addition of bafilomycin A₁, suggesting that the knockdown of *KDM4A* did not interfere with, but instead enhanced, autophagic flux. Conversely, the overexpression of *KDM4A* led to a reduction in the level of LC3-II compared to control cells (Figure 5.7B, right panel) further supporting the conclusion that *KDM4A* is a repressor of autophagy.

To extend this analysis, we monitored the autophagic flux using a tandem reporter construct, mRFP-GFP-LC3, a probe that allows distinction between autophagosomes (AP, GFP⁺ RFP⁺, yellow puncta, Figure 5.7C) and autolysosomes (AL, GFP⁻ RFP⁺, red puncta, Figure 5.7C). Compared to the control, cells knocked down for KDM4A showed an increase in yellow puncta representing autophagosomes, in both basal autophagy (DMSO) conditions or after autophagy induction by Torin1 (Figure 5.7C,D). Following Torin1 treatment there was an increase in autolysosomes in both the control and si*KDM4A* cells, again indicating that autophagic flux was not inhibited by KDM4A depletion.

We found that the level of KDM4A was reduced in response to Torin1 treatment (Figure 5.7E) indicating that KDM4A is degraded in this condition. A previous phosphoproteomic analysis indicated that KDM4A is phosphorylated at residue Y547 [39]; analysis of KDM4A with a phosphospecific antibody directed towards Y547 showed that phosphorylation at this residue is upregulated by treatment with Torin1. Together, these results suggest that, similar to Rph1, the phosphorylation of KDM4A acts as a switch to promote autophagy induction in mammalian cells.

5.3 Discussion

In this study, a screen for transcription factors modulating *ATG* gene expression identified Rph1 as a transcriptional repressor of autophagy. We show that Rph1 is a negative regulator of the expression of, at least, *ATG7*, *ATG8*, *ATG9*, *ATG14* and *ATG29*. Consistent with our results, a recent microarray analysis reported the induction of *ATG7*, and *ATG14*, as well as *ATG16*, *ATG17*, *ATG23* and *ATG24* in *rph1Δ* cells in physiological conditions [23] suggesting that Rph1 might control a large set of *ATG* genes.

Our results show that the deletion of *RPH1* can be partially complemented by Gis1, its paralog, indicating that Gis1 plays a minor role in the regulation of *ATG* genes. Rph1 and Gis1 are JmjC-domain containing proteins; while Rph1 histone demethylase activity is well established [29], controversies exist concerning Gis1 [29, 40]. Whether or not Gis1 is catalytically active, its JmjC domain is not required for its transcriptional activity [24,41]. Similarly we show here that the histone demethylase activity of Rph1 is not required for its control of autophagy, but that its DNA binding domain is critical. Rph1 and Gis1 share a high homology in their C₂H₂ zinc finger DNA-binding domain suggesting that they could bind similar motifs, which might explain the partial redundancy between the two proteins. Yet, the deletion of *RPH1* has a strong effect on the expression of *ATG* genes and affects autophagy activity, whereas deleting *GIS1* alone did not affect autophagy suggesting that Rph1 has higher affinity for the promoters of *ATG* genes and plays a major role in the repression of autophagy in nitrogen-replete conditions.

The deletion of *RPH1* has no effect on the expression of *ATG* genes after nitrogen depletion, and the phenotype of the *RPH1* null strain is attenuated after prolonged starvation suggesting that the activity of the protein is repressed in this condition. Indeed, we found that Rph1 is phosphorylated in a Rim15-dependent manner upon nitrogen starvation and that this phosphorylation is accompanied with a partial degradation of the protein. Inhibition of Rph1 phosphorylation or overexpression of the protein leads to a strong block of *ATG* gene induction as well as autophagy activity, showing that the phosphorylation of Rph1 represses its activity and is a prerequisite for autophagy induction. Altogether, these data propose a model in which, by repressing the expression of *ATG* genes, Rph1 maintains autophagy at a low level in nutrient-replete conditions. Upon nitrogen starvation, Rim15 mediates Rph1 phosphorylation, which

causes a partial autophagy-independent degradation of the protein and an inhibition of its activity (Figure 5.6, Figure 5.S4 and data not shown). This leads to a release of Rph1 repression of *ATG* genes, an induction of their expression and an overall induction of autophagy activity.

Rim15 controls many aspects of the nutrient-regulatory pathways, including autophagy, by integrating signals from TORC1 and PKA [38, 42]; yet little is known about the downstream effectors in these signaling pathway. We show that Rim15 phosphorylates Rph1, thereby releasing its repression of the expression of several *ATG* genes including *ATG7* and *ATG29*, upon nutrient limitation. Conversely, although Rph1 controls the expression of *ATG14*, its expression was not affected by the deletion of *RIM15*. Rim15 is under the control of both positive and negative regulators of autophagy [38], and it is therefore possible that the result of competitive effectors controlling the expression of *ATG14* account for this observation. Uncovering the Rim15-dependent Rph1-mediated transcriptional control of autophagy here brings further comprehension to the overall signaling pathways leading to autophagy induction upon starvation.

How does the level of *ATG* gene transcription regulate autophagy activity? Several *ATG* genes show higher expression after nitrogen starvation ([16]; Figure 5.1), suggesting that this increase is required to support optimal autophagy activity; yet the physiological relevance of the induction of particular *ATG* genes is still largely unknown. Our previous work showed that the amount of Atg9 correlates with the number of autophagosomes [16], whereas the induction of *ATG8* promotes the formation of larger autophagosomes [22] thereby leading to an increase in the amount of cargo delivered to the autophagy pathway. Here we show that Rph1 plays a major role in the control of the expression of *ATG7*. Upon autophagy induction, Atg7 functions in the formation of Atg8–PE conjugates, which is a prerequisite to the membrane recruitment of Atg8

and the elongation of the phagophore [43]. Our results show that negatively modulating the expression of *ATG7* causes defects in autophagy activity (Figure 5.3), suggesting that the amount of Atg7 is rate limiting in the lipidation of the large pool of newly synthesized Atg8 after starvation. It is therefore tempting to speculate that, upon autophagy induction, a concomitant upregulation of both *ATG7* and *ATG8* is strictly required to support efficient autophagosome formation and thereby an increase in the magnitude of autophagy activity.

Besides its role in cell survival upon starvation, autophagy activity is also critical for cellular clearance of protein aggregates and damaged organelles, which, when accumulated, result in severe pathologies, such as neurodegenerative diseases [10]. Interestingly, a recent genomic study of sporadic Parkinson disease patients identified mutations in the *ATG7* promoter causing decreased ATG7 expression [17]. In this context, our finding that the transcriptional control of *ATG7* is critical for autophagy activity points to the physiological importance of the Rph1-mediated control of autophagy that we identified here. In particular, we show that the function of Rph1 is conserved from yeast to mammals. Four isoforms of KDM4, the homolog of Rph1, are present in mammalian cells. Here we show that KDM4A is a negative regulator of autophagy; whether other isoforms are also involved in this process remains to be investigated. Knocking down KDM4A increased autophagy activity, especially at base line, suggesting that modulating this novel regulatory pathway could be a good target for the development of disease therapies.

5.4 Experimental Procedures

5.4.1 Yeast Strains, Media and Culture

Gene disruptions were performed using a standard method [44]. Yeast cells were grown in YPD or SMD [16] and autophagy was induced in SD-N [16]. The yeast strains used in this study are listed in Table 5.1.

HeLa cells were purchased from Sigma and grown in MEM supplemented with penicillin/streptomycin, L-glutamine, non-essential amino acids and sodium pyruvate.

5.4.2 Plasmids

The *pRS416-PA* plasmid was constructed by inserting two copies of the protein A open reading frame (ORF) followed by the *ADHI* terminator in the *pRS416* plasmid between the *XbaI* and *EcoRI* sites. For constructing the plasmid *ATG7p-ATG7-PA*, (where “*ATG7p*” indicates the promoter of the *ATG7* gene), the *ATG7* ORF and promoter region (-800-0) was amplified by PCR, digested by *SacII* and *NotI* and ligated into the *pRS416-PA* plasmid. For constructing the plasmids *GAL3p-ATG7-PA*, *FLO5p-ATG7-PA* and *SEF1p-ATG7-PA*, a region of approximately 800 bp upstream of the corresponding ORF was amplified by PCR and fused to a PCR-amplified *ATG7* ORF by overlapping PCR. The resulting products were digested by *SacII* and *NotI* and ligated into the *pRS416-PA* plasmid. The *RPH1p-RPH1-PA* plasmid was constructed by amplifying the *RPH1* ORF and promoter region (-500-0) by PCR followed by digestion with *NotI* and *XbaI* and ligation into the *pRS416-PA* plasmid. The *RPH1p-RPH1^{H235A}-PA* plasmid was constructed by amplifying (1) the *RPH1* ORF and promoter region up to the sequence corresponding to histidine 235 with a reverse primer containing the histidine-to-alanine mutation and (2) the *RPH1* ORF starting from the sequence corresponding to histidine 235 until the last codon before the stop codon with a forward primer containing the histidine to alanine mutation.

RPH1p-RPH1^{H235A} was amplified by overlapping PCR using the PCR (1) and PCR (2) products resulting from the previous step as template, digested by NotI and XbaI and ligated into *pRS416-PA*. The *RPH1p-RPH1^{AZ}-PA* plasmid was constructed by amplifying (1) the *RPH1* ORF and promoter region up to the sequence corresponding to the first zinc-finger domain with a reverse primer containing the inter zinc-domain sequence and (2) the *RPH1* ORF starting from the sequence following the last zinc-finger domain until the last codon before the stop codon with a forward primer containing the inter zinc-domain sequence. *RPH1p-RPH1^{AZ}* was amplified by overlapping PCR using the PCR (1) and PCR (2) products resulting from the previous step as template, digested by NotI and XbaI and ligated into *pRS416-PA*.

For constructing the strains YAB363, YAB364 and YAB366, *RPH1p-RPH1-PA*, *ZEO1p-RPH1-PA* and *ZEO1p-RPH1^{H235A}-PA* were generated as described above, digested by NotI and SalI and ligated into *pRS406*. The resulting plasmids were digested by NcoI (for integration at the *URA3* locus). For generating the strains YAB374, YAB375 and YAB376, we constructed the following plasmids: *RPH1p-RPH1-PA(406)*, *RPH1p-Rph1-S425A-S426A-S429A-S430A-S557A-S561A-PA(406)* and *RPH1p-Rph1-T411A-S412A-S425A-S426A-S429A-S430A-S557A-S561A-PA(406)*. The *RPH1* ORF and promoter region was amplified as previously described. Mutations were introduced by overlapping PCR as described above. Inserts were digested by NotI and SalI and ligated into *pRS406*. The resulting plasmids were digested by AflIII (for integration at the *RPH1* promoter).

5.4.3 RNA and RT-qPCR

Total RNA was extracted using the RNeasy mini kit (Qiagen). To eliminate genomic DNA contamination an additional DNase treatment was performed according to the RNeasy kit instruction with the RNase-free DNase set (Qiagen). One microgram of total RNA was reverse-

transcribed into cDNA in a 20 μ l reaction mixture using the High-capacity cDNA Reverse Transcription kit (Applied Biosystems). The cDNA levels were then analyzed using the Eppendorf Realplex⁴ with the gene-specific primers listed in Table 5.2. Each sample was tested in a 96-well plate (Applied Biosystems). The reaction mix (15- μ l final volume) consisted of 7.5 μ l of Power SYBR Green master mix (Applied Biosystems), 0.5 μ l of each primer (333.3 nM final concentration), 1.5 μ l of H₂O, and 5 μ l of a 1/5 dilution of the cDNA preparation. The thermocycling program consisted of one hold at 95°C for 10 min, followed by 40 cycles of 15 s at 95°C and 1 min at 60°C. After completion of these cycles, melting-curve data were then collected to verify PCR specificity and the absence of primer dimers, and to examine potential contamination. The transcript abundance in samples was determined using a comparative threshold cycle method. The relative abundance of the reference mRNAs of *TAF10* and *TFC1* [45] in each sample was determined and used to normalize for differences of total RNA amount according to the method described by Vandesompele et al. [46]. Unless specified, the mRNA level of individual *ATG* genes was normalized to the mRNA level of the corresponding gene in wild-type cells grown in rich conditions, which was set to 1.

5.4.4 Chromatin Immunoprecipitation

ChIP was performed as previously described [47] with minor modifications. Rph1-PA and Rph1 ^{Δ Z}-PA were affinity isolated with Dynabeads[®] (Life technologies) coupled to purified human IgG (Invitrogen) according to the Dynabeads[®] Antibody Coupling Kit directions (Life technologies). Primers used for ChIP are listed in Table 5.2.

5.4.5 Transmission electron microscopy

TEM and sample analysis were performed as previously described [16].

5.4.6 Lambda Protein Phosphatase Treatment

The equivalent of 5 OD units of yeast cells were lysed in 50 μ l of λ -phosphatase buffer (New England Biolabs) supplemented with 1% Triton X-100, 0.1% sodium deoxycholate, 1 mM PMSF, protease inhibitor cocktail (ProBlockTM-50, Gold Biotechnology), with or without phosphatase inhibitor cocktail (PhosSTOP, Roche). A 2.5- μ l aliquot of lysate was used as template in a 50- μ l reaction with λ -phosphatase buffer, 1 mM MnCl₂ and with or without 1200 units of λ -phosphatase (New England Biolabs). The samples were incubated at 30°C for 1.5 h. The reaction was stopped and proteins were precipitated by addition of 10% trichloroacetic acid.

5.4.7 Other Methods

Protein extraction, immunoblot, GFP-Atg8 processing, and alkaline phosphatase (Pho8 Δ 60) assays were performed as previously described [48, 49, 28]. Phos-tag was used according to the manufacturer's (Wako) instruction at a final concentration of 50 μ M. Antisera to Atg8 [50], Atg1 [51], Atg9 [52], Pgc1 (a generous gift from Dr. Jeremy Thorner, University of California, Berkeley), monoclonal YFP (JL-8, Clontech) a commercial antibody that reacts with PA (anti-PA, no longer available), and anti-H3K36m3 (Active Motif, 61101) were used as previously described.

5.4.8 Mammalian Cell Transfection

HeLa cells were transfected with siRNA using Lipofectamine 2000 reagent (Invitrogen). Transfection was performed in 6-well dishes using a final siRNA concentration of 50 nM and 7 μ l of transfection reagent. The medium was changed 3 h after transfection. *KDM4A* (L-004292) and non-targeting ON-TARGET (D-001810) SMARTpool siRNAs were purchased from Dharmacon. HeLa cells were transfected with a *KDM4A* plasmid or pcDNA using 6 μ l Xtreme

Gene HP Reagent (Roche)/2 µg of DNA per well in a 6-well dish. The medium was changed 3 h after transfection. The *KDM4A* overexpression plasmid was a generous gift from Dr. Kristian Helin (University of Copenhagen, BRIC).

5.4.9 Tandem Fluorescence Reporter Flux Assay

The green fluorescence of the tandem reporter mRFP-GFP-LC3 is attenuated in the acidic pH lysosomal environment, whereas the mRFP is not. Therefore, the green fluorescent component of the composite yellow fluorescence (green + red = autophagosome) from the mRFP-GFP-LC3 reporter is lost upon autophagosome fusion with a lysosome, whereas the red fluorescence (red = autolysosome) remains detectable. At 24 h after plating, the cells were transfected with the mRFP-GFP-LC3 plasmid using 6 µl Xtreme Gene HP Reagent (Roche)/2 µg of DNA per well in a 6-well dish. The medium was changed 3 h after transfection. On the subsequent day cells were transfected with siRNA as described above. The next day, cells were treated for an extra 24 h with the indicated compounds (DMSO or 250 nM Torin1). Cells were then fixed using 4% paraformaldehyde, nuclei were stained with Hoechst, and autophagy was determined by quantification of the number of cells with LC3-positive puncta; cells with at least 5 detectable LC3 puncta were considered positive. The mRFP-GFP-LC3 plasmid was a kind gift of Dr. Tamotsu Yoshimori (National Institute of Genetics, Mishima, Japan).

5.4.10 Mammalian Cell Western Blot

Cells were seeded in 6-well dishes and on the subsequent day transfected using Xtreme Lipofectamine 2000 (see above). After 3 h of transfection the medium was changed and on the next day the indicated wells were treated with bafilomycin A₁ (40 nM). Total cell lysate was harvested 48 h after transfection using Laemmli buffer and a cell scraper. Extracts were sonicated and subsequently boiled for 6 min at 96°C. SDS-PAGE was run using 15% acrylamide

gels. Proteins were subsequently transferred to nitrocellulose (0.2- μ m pores) using wet transfer (Bio-Rad). Primary antibodies were purchased from Sigma (KDM4A, HPA007610; actin A3853; MAP1LC3B, L7543) or USBiological Life Sciences (JMJD2A phosphorylated at Y547, 037196).

5.4.11 Mammalian RNA qPCR

For analysis of RNA expression, HeLa cells were seeded in a 6-well dish. At 24 h after plating, the cells were transfected with siRNA (see above). The medium on the cells was changed after 3 h transfection and cells were grown for another 45 h (48 h total after transfection). RNA was extracted using the RNeasy Kit (Qiagen) performing on-column DNase digestion. RNA concentration was determined using Nanodrop, and 1 μ g of total RNA was used for first strand synthesis with SuperScript II Reverse Transcriptase (Invitrogen). QPCR was run on an ABI 7500 and *GAPDH* or *ACTB* was used as a housekeeping gene for normalization. All primers were predesigned oligos (used at 4 nM/well) purchased from Sigma (KiCqStart). qPCR analysis and statistical analysis was done using R.

5.4.12 Statistical analyses

Statistical differences were assayed using one-sample *t* test and student *t* test; * $p < 0.05$, ** $p < 0.01$, *** $p < 0.001$.

5.5 Acknowledgments

This work was supported by NIH grant GM053396 to DJK, and by grants from the Swedish Cancer Society, the Swedish Childhood Cancer Foundation and the Swedish Research Council to BJ.

5.6 References

1. Lenstra, T.L., Benschop, J.J., Kim, T., Schulze, J.M., Brabers, N.A., Margaritis, T., van de Pasch, L.A., van Heesch, S.A., Brok, M.O., Groot Koerkamp, M.J., et al. (2011). The specificity and topology of chromatin interaction pathways in yeast. *Mol Cell* *42*, 536-549.
2. Xie, Z., and Klionsky, D.J. (2007). Autophagosome formation: core machinery and adaptations. *Nat Cell Biol* *9*, 1102-1109.
3. Tsukada, M., and Ohsumi, Y. (1993). Isolation and characterization of autophagy-defective mutants of *Saccharomyces cerevisiae*. *FEBS Lett* *333*, 169-174.
4. Levine, B., and Klionsky, D.J. (2004). Development by self-digestion: molecular mechanisms and biological functions of autophagy. *Dev Cell* *6*, 463-477.
5. Deretic, V., and Levine, B. (2009). Autophagy, immunity, and microbial adaptations. *Cell Host Microbe* *5*, 527-549.
6. Shi, C.S., Shenderov, K., Huang, N.N., Kabat, J., Abu-Asab, M., Fitzgerald, K.A., Sher, A., and Kehrl, J.H. (2012). Activation of autophagy by inflammatory signals limits IL-1beta production by targeting ubiquitinated inflammasomes for destruction. *Nat Immunol* *13*, 255-263.
7. Huang, J., and Klionsky, D.J. (2007). Autophagy and human disease. *Cell Cycle* *6*, 1837-1849.
8. Mizushima, N., Levine, B., Cuervo, A.M., and Klionsky, D.J. (2008). Autophagy fights disease through cellular self-digestion. *Nature* *451*, 1069-1075.
9. Lynch-Day, M.A., and Klionsky, D.J. (2010). The Cvt pathway as a model for selective autophagy. *FEBS Lett* *584*, 1359-1366.
10. Nixon, R.A. (2013). The role of autophagy in neurodegenerative disease. *Nat. Med.* *19*, 983-997.
11. Chen, Y., Azad, M.B., and Gibson, S.B. (2009). Superoxide is the major reactive oxygen species regulating autophagy. *Cell Death Differ* *16*, 1040-1052.
12. Levine, B., and Yuan, J. (2005). Autophagy in cell death: an innocent convict? *J Clin Invest* *115*, 2679-2688.
13. Ravikumar, B., Sarkar, S., Davies, J.E., Futter, M., Garcia-Arencibia, M., Green-Thompson, Z.W., Jimenez-Sanchez, M., Korolchuk, V.I., Lichtenberg, M., Luo, S., Massey, D.C., Menzies, F.M., Moreau, K., Narayanan, U., Renna, M., Siddiqi, F.H., Underwood, B.R., Winslow, A.R., and Rubinsztein, D.C. (2010). Regulation of mammalian autophagy in physiology and pathophysiology. *Physiol Rev* *90*, 1383-1435.
14. Jin, M., and Klionsky, D.J. (2014). Regulation of autophagy: Modulation of the size and number of autophagosomes. *FEBS Lett* *588*, 2457-2463.
15. Parzych, K.R., and Klionsky, D.J. (2014). An overview of autophagy: morphology, mechanism, and regulation. *Antioxid Redox Signal* *20*, 460-473.
16. Jin, M., He, D., Backues, S.K., Freeberg, M.A., Liu, X., Kim, J.K., and Klionsky, D.J. (2014). Transcriptional regulation by pho23 modulates the frequency of autophagosome formation. *Curr Biol* *24*, 1314-1322.
17. Chen, D., Pang, S., Feng, X., Huang, W., Hawley, R.G., and Yan, B. (2013). Genetic analysis of the ATG7 gene promoter in sporadic Parkinson's disease. *Neurosci Lett* *534*, 193-198.
18. Liu, H., He, Z., von Rutte, T., Yousefi, S., Hunger, R.E., and Simon, H.U. (2013). Down-regulation of autophagy-related protein 5 (ATG5) contributes to the pathogenesis of early-stage cutaneous melanoma. *Sci Transl Med* *5*, 202ra123.
19. Wang, J., Pan, X.L., Ding, L.J., Liu, D.Y., Da-Peng, L., and Jin, T. (2013). Aberrant expression of Beclin-1 and LC3 correlates with poor prognosis of human hypopharyngeal squamous cell carcinoma. *PLoS ONE* *8*, e69038.

20. Jo, Y.K., Kim, S.C., Park, I.J., Park, S.J., Jin, D.H., Hong, S.W., Cho, D.H., and Kim, J.C. (2012). Increased expression of ATG10 in colorectal cancer is associated with lymphovascular invasion and lymph node metastasis. *PLoS ONE* 7, e52705.
21. Bartholomew, C.R., Suzuki, T., Du, Z., Backues, S.K., Jin, M., Lynch-Day, M.A., Umekawa, M., Kamath, A., Zhao, M., Xie, Z., et al. (2012). Ume6 transcription factor is part of a signaling cascade that regulates autophagy. *Proc Natl Acad Sci U S A* 109, 11206-11210.
22. Xie, Z., Nair, U., and Klionsky, D.J. (2008). Atg8 controls phagophore expansion during autophagosome formation. *Mol Biol Cell* 19, 3290-3298.
23. Liang, C.Y., Wang, L.C., and Lo, W.S. (2013). Dissociation of the H3K36 demethylase Rph1 from chromatin mediates derepression of environmental stress-response genes under genotoxic stress in *Saccharomyces cerevisiae*. *Mol Biol Cell* 24, 3251-62.
24. Jang, Y.K., Wang, L., and Sancar, G.B. (1999). RPH1 and GIS1 are damage-responsive repressors of PHR1. *Mol Cell Biol* 19, 7630-7638.
25. Zhang, N., and Oliver, S.G. (2010). The transcription activity of Gis1 is negatively modulated by proteasome-mediated limited proteolysis. *J Biol Chem* 285, 6465-6476.
26. Orzechowski Westholm, J., Tronnorsjo, S., Nordberg, N., Olsson, I., Komorowski, J., and Ronne, H. (2012). Gis1 and Rph1 regulate glycerol and acetate metabolism in glucose depleted yeast cells. *PLoS One* 7, e31577.
27. Noda, T., and Klionsky, D.J. (2008). The quantitative Pho8Delta60 assay of nonspecific autophagy. *Methods Enzymol* 451, 33-42.
28. Shintani, T., and Klionsky, D.J. (2004). Cargo proteins facilitate the formation of transport vesicles in the cytoplasm to vacuole targeting pathway. *J Biol Chem* 279, 29889-29894.
29. Tu, S., Bulloch, E.M., Yang, L., Ren, C., Huang, W.C., Hsu, P.H., Chen, C.H., Liao, C.L., Yu, H.M., Lo, W.S. et al. (2007). Identification of histone demethylases in *Saccharomyces cerevisiae*. *J Biol Chem* 282, 14262-14271.
30. Liang, C.Y., Hsu, P.H., Chou, D.F., Pan, C.Y., Wang, L.C., Huang, W.C., Tsai, M.D., and Lo, W.S. (2011). The histone H3K36 demethylase Rph1/KDM4 regulates the expression of the photoreactivation gene PHR1. *Nucleic Acids Res* 39, 4151-4165.
31. Strahl, B.D., Grant, P.A., Briggs, S.D., Sun, Z.W., Bone, J.R., Caldwell, J.A., Mollah, S., Cook, R.G., Shabanowitz, J., Hunt, D.F. et al. (2002). Set2 is a nucleosomal histone H3-selective methyltransferase that mediates transcriptional repression. *Mol Cell Biol*, 22, 1298-1306.
32. Venters, B.J., Wachi, S., Mavrich, T.N., Andersen, B.E., Jena, P., Sinnamon, A.J., Jain, P., Roller, N.S., Jiang, C., Hemeryck-Walsh, C., et al. (2011). A comprehensive genomic binding map of gene and chromatin regulatory proteins in *Saccharomyces*. *Mol Cell* 41, 480-492.
33. Nordberg, N., Olsson, I., Carlsson, M., Hu, G.Z., Orzechowski Westholm J., and Ronne, H. (2014). The histone demethylase activity of Rph1 is not essential for its role in the transcriptional response to nutrient signaling. *PLoS one* 9, e95078.
34. Huber, A., Bodenmiller, B., Uotila, A., Stahl, M., Wanka, S., Gerrits, B., Aebersold, R., and Loewith, R. (2009). Characterization of the rapamycin-sensitive phosphoproteome reveals that Sch9 is a central coordinator of protein synthesis. *Genes Dev* 23, 1929-1943.
35. Bodenmiller, B., Wanka, S., Kraft, C., Urban, J., Campbell, D., Pedrioli, P.G., Gerrits, B., Picotti, P., Lam, H., Vitek, O., Brusniak, M.Y., Roschitzki, B., Zhang, C., Shokat, K.M., Schlapbach, R., Colman-Lerner, A., Nolan, G.P., Nesvizhskii, A.I., Peter, M., Loewith, R., von Mering, C., and Aebersold, R. (2010). Phosphoproteomic analysis reveals interconnected system-wide responses to perturbations of kinases and phosphatases in yeast. *Sci Signal* 3, rs4.

36. Pedruzzi, I., Dubouloz, F., Cameroni, E., Wanke, V., Roosen, J., Winderickx, J., and De Virgilio, C. (2003). TOR and PKA signaling pathways converge on the protein kinase Rim15 to control entry into G0. *Mol Cell* 12, 1607–1613.
37. Wanke, V., Pedruzzi, I., Cameroni, E., Dubouloz, F. and De Virgilio, C. (2005). Regulation of G0 entry by the Pho80–Pho85 cyclin–CDK complex. *EMBO J* 24, 4271–4278.
38. Yang, Z., Geng, J., Yen, W.L., Wang, K., and Klionsky, D.J. (2010). Positive or negative roles of different cyclin-dependent kinase Pho85-cyclin complexes orchestrate induction of autophagy in *Saccharomyces cerevisiae*. *Mol Cell* 23, 250-264.
39. Tao, W.A., Wollscheid, B., O'Brien, R., Li, X.J., Bodenmiller, B., Watts, J.D., Hood, L., and Aebersold, R. (2005). Quantitative phosphoproteome analysis using a dendrimer conjugation chemistry and tandem mass spectrometry. *Nat Methods* 2, 591-598.
40. Klose, R.J., Kallin, E.M., and Zhang, Y. (2006). JmjC-domain-containing proteins and histone demethylation. *Nat Rev Genet* 7, 715–727.
41. Yu Y, Neiman AM, Sternglanz R (2010) The JmjC domain of Gis1 is dispensable for transcriptional activation. *FEMS Yeast Res* 10: 793–801.
42. Swinnen, E., Wanke, V., Roosen, J., Smets, B., Dubouloz, F., Pedruzzi, I., Cameroni, E., De Virgilio, C., and Winderickx, J. (2006). Rim15 and the crossroads of nutrient signalling pathways in *Saccharomyces cerevisiae*. *Cell Div* 1, 3.
43. Geng, J., Nair, U., Yasumura-Yorimitsu, K., and Klionsky, D.J. (2010). Post-Golgi Sec proteins are required for autophagy in *Saccharomyces cerevisiae*. *Mol Biol Cell* 21, 2257-2269.
44. Longtine, M.S., McKenzie, A. III, Demarini, D.J., Shah, N.G., Wach, A., Brachat, A., Philippsen, P., and Pringle, J.R. (1998). Additional modules for versatile and economical PCR-based gene deletion and modification in *Saccharomyces cerevisiae*. *Yeast* 14, 953–961.
45. Teste, M.A., Duquenne, M., François, J.M., and Parrou, J.L. (2009). Validation of reference genes for quantitative expression analysis by real-time RT-PCR in *Saccharomyces cerevisiae*. *BMC Mol Biol* 10, 99.
46. Vandesompele, J., De Preter, K., Pattyn, F., Poppe, B., Van Roy, N., De Paepe, A., and Speleman, F. (2002). Accurate normalization of real-time quantitative RT-PCR data by geometric averaging of multiple internal control genes. *Genome Biol* 3, H0034.
47. Govin, J., Dorsey, J., Gaucher, J., Rousseaux, S., Khochbin, S., and Berger, S.L. (2010). Systematic screen reveals new functional dynamics of histones H3 and H4 during gametogenesis. *Genes Dev* 24, 1772-1786
48. Yorimitsu, T., Zaman, S., Broach, J.R., and Klionsky, D.J. (2007). Protein kinase A and Sch9 cooperatively regulate induction of autophagy in *Saccharomyces cerevisiae*. *Mol Biol Cell* 18, 4180–4189.
49. Noda, T., Matsuura, A., Wada, Y., and Ohsumi, Y. (1995). Novel system for monitoring autophagy in the yeast *Saccharomyces cerevisiae*. *Biochem Biophys Res Commun* 210, 126–132.
50. Huang, W.-P., Scott, S.V., Kim, J., and Klionsky, D.J. (2000). The itinerary of a vesicle component, Aut7p/Cvt5p, terminates in the yeast vacuole via the autophagy/Cvt pathways. *J Biol Chem* 275, 5845-5851.
51. Abeliovich, H., Zhang, C., Dunn Jr., W.A., Shokat, K.M., and Klionsky, D.J. (2003). Chemical genetic analysis of Apg1 reveals a non-kinase role in the induction of autophagy. *Mol. Biol. Cell* 14,477–490.

52. Noda, T., Kim, J., Huang, W.-P., Baba, M., Tokunaga, C., Ohsumi, Y., and Klionsky, D.J. (2000). Apg9p/Cvt7p is an integral membrane protein required for transport vesicle formation in the Cvt and autophagy pathways *J Cell Biol* *148*, 465–480.

Table 5.1. Strains used in this study

Name	Genotype	Reference
BY4742	<i>MATα his3Δ1 leu2Δ0 ura3Δ0</i>	ResGen/Invitrogen
FRY143	SEY6210, <i>pep4Δ::LEU2 vps4Δ::TRP1</i>	(1)
SEY6210	<i>MATα his3Δ200 leu2-3,112 lys2-801 suc2-Δ9 trp1Δ901 ura3-52</i>	(2)
<i>ume6Δ</i>	<i>BY4742 ume6Δ::KanMX6</i>	Invitrogen
WLY176	SEY6210 <i>pho13Δ pho8::pho8Δ60</i>	(3)
WLY192	WLY176, <i>atg1Δ::HIS5</i>	(4)
YAB288	WLY176, <i>rph1Δ::LEU2</i>	This study
YAB292	YTS158, <i>atg7Δ::HIS5</i>	This study
YAB300	YTS158, <i>rph1Δ</i>	This study
YAB301	YTS158, <i>gis1Δ</i>	This study
YAB302	YTS158, <i>rph1Δ gis1Δ</i>	This study
YAB312	YTS158, <i>Atg7-PA::HIS5</i>	This study
YAB313	YAB300, <i>Atg7-PA::HIS5</i>	This study
YAB314	YAB301, <i>Atg7-PA::HIS5</i>	This study
YAB315	YAB302, <i>Atg7-PA::HIS5</i>	This study
YAB318	YTS158, <i>set2Δ::HIS5</i>	This study
YAB308	YTS158, <i>Rph1-PA::HIS5</i>	This study
YAB323	WLY176, <i>Rph1-PA::HIS5</i>	This study
YAB329	YAB323, <i>ZEO1p-Rph1::KanMX6</i>	This study
YAB341	YAB308, <i>rim15Δ::URA3</i>	This study
YAB342	YAB312, <i>rim15Δ::URA3</i>	This study
YAB346	FRY143, <i>ZEO1p-Rph1::KanMX6</i>	This study
YAB347	YAB313, <i>rim15Δ::URA3</i>	This study
YAB348	YTS158, <i>Atg14-PA::His5</i>	This study
YAB349	YAB300, <i>Atg14-PA::His5</i>	This study
YAB350	YTS158, <i>Atg10-PA::HIS5</i>	This study
YAB351	YAB300, <i>Atg10-PA::HIS5</i>	This study
YAB352	YAB301, <i>Atg10-PA::HIS5</i>	This study
YAB353	YAB302, <i>Atg10-PA::HIS5</i>	This study
YAB354	YTS158, <i>Atg29-PA::His5</i>	This study
YAB355	YAB300, <i>Atg29-PA::His5</i>	This study
YAB363	YAB288, <i>ZEO1p-Rph1-PA::URA3</i>	This study
YAB364	YAB288, <i>ZEO1p-Rph1H235A-PA::URA3</i>	This study
YAB366	YAB288, <i>RPH1p-Rph1-PA::URA3</i>	This study
YAB374	YAB300, <i>RPH1p-Rph1-PA::URA3</i>	This study
YAB375	YAB300, <i>RPH1p-Rph1-S425A-S426A-S429A-S430A-S557A-S561A-PA::URA3</i>	This study
YAB376	YAB300, <i>RPH1p-Rph1-T411A-S412A-S425A-S426A-S429A-S430A-S557A-S561A-PA::URA3</i>	This study
YTS158	BY4742, <i>pho13Δ::KanMX6 pho8::pho8Δ60</i>	(5)

Table References:

- (1) Cheong, H., Yorimitsu, T., Reggiori, F., Legakis, J.E., Wang, C.-W., and Klionsky, D.J. (2005). Atg17 regulates the magnitude of the autophagic response. *Mol Biol Cell* *16*, 3438-3453.
- (2) Robinson, J. S., Klionsky, D. J., Banta, L. M., and Emr, S. D. (1988). Protein sorting in *Saccharomyces cerevisiae*: isolation of mutants defective in the delivery and processing of multiple vacuolar hydrolases. *Mol Cell Biol* *8*, 4936-4948.
- (3) Mao, K., Chew, L.H., Inoue-Aono, Y., Cheong, H., Nair, U., Popelka, H., Yip, C.K., and Klionsky, D.J. (2013). Atg29 phosphorylation regulates coordination of the Atg17-Atg31-Atg29 complex with the Atg11 scaffold during autophagy initiation. *Proc Natl Acad Sci U S A* *110*, E2875-2884.
- (4) Kanki, T., Wang, K., Baba, M., Bartholomew, C.R., Lynch-Day, M.A., Du, Z., Geng, J., Mao, K., Yang, Z., Yen, W.-L., and Klionsky, D.J. (2009). A genomic screen for yeast mutants defective in selective mitochondria autophagy. *Mol Biol Cell* *20*, 4730-4738.
- (5) He, C., Song, H., Yorimitsu, T., Monastyrska, I., Yen, W.-L., Legakis, J. E., and Klionsky, D. J. (2006). Recruitment of Atg9 to the preautophagosomal structure by Atg11 is essential for selective autophagy in budding yeast. *J Cell Biol* *175*, 925-935.

Table 5.2. RT-qPCR primers used in this study

Gene name	Sequence (5' 3')
<i>ATG1 F</i>	ATCTAAGATGGCCGCACATATG
<i>ATG1 R</i>	AGGGTAGTCACCATAGGCATTC
<i>ATG7 F</i>	ATGAGCATTGTCCAGCATGTAG
<i>ATG7 R</i>	GACCTCCTGCTTTATGACTGAC
<i>ATG8 F</i>	GAAGGCCATCTTCATTTTTGTC
<i>ATG8 R</i>	TTCTCCTGAGTAAGTGACATAC
<i>ATG9 F</i>	CGTACTAACAGAGTCTTTCCTTG
<i>ATG9 R</i>	CTAAGACACCACCCTTATTGAG
<i>ATG14 F</i>	TACTGGACCAGTACGATGTG
<i>ATG14 R</i>	TGCAGGATGTCCTCTTTGTG
<i>ATG29 F</i>	ATGAGGCGTTACAACATTTGC
<i>ATG29 R</i>	TCGTCATCTGAACTACCGCAC
<i>TAF10 F</i>	ATATTCCAGGATCAGGTCTTCCGTAGC
<i>TAR10 R</i>	GTAGTCTTCTCATTCTGTTGATGTTGTTGTTG
<i>TFC1 F</i>	GCTGGCACTCATATCTTATCGTTTTACAATGG
<i>TFC1 R</i>	GAACCTGCTGTCAATACCGCCTGGAG
<i>WIPI1 F</i>	TCCAGTGGACACCTTTATATG
<i>WIPI1 R</i>	AGCTGTGGGTTTTGATTAAG
<i>mATG7 F</i>	GATTGTCCTAAAGCAGTTGG
<i>mATG7 R</i>	CTTTTAGGGTCCATACATTCAC
<i>mATG14 F</i>	AATTTACTCGAGCAGTGAAG
<i>mATG14 R</i>	TTAGATTCCTGAGGGTATGC
<i>MAP1LC3B F</i>	ATAGAACGATACAAGGGTGAG
<i>MAP1LC3B R</i>	CTGTAAGCGCCTTCTAATTATC
<i>GAPDH F</i>	ACAGTTGCCATGTAGACC
<i>GAPDH R</i>	TTTTTGGTTGAGCACAGG
<i>ACTB F</i>	GATCAAGATCATTGCTCCTC
<i>ACTB R</i>	TTGTCAAGAAAGGGTGTAAC
<i>ATG7 ChIP F</i>	TGGAAGAACAAGCCACCACATG
<i>ATG7 ChIP R</i>	GGGTGTCCAAAGGAATCTCATG
<i>PHR1 ChIP F</i>	GGGTGAAAGTATGCTTACTTTGAC
<i>PHR1 ChIP R</i>	ACAATCTCCATTGGTTTAGCCC
<i>ChrVI ChIP F</i>	ATTCCAAACGGTGTTTCCTTTAC
<i>ChrVI ChIP R</i>	AAAGTAAACGGTGGTCTCTGTG

Table 5.3. WT vs. OE Rph1 TEM data

	Autophagic body size					Vacuole size				Autophagic body number	
	Measured cross-sectional		Estimated original			Measured cross-sectional		Estimated original		Measured cross-sections/cell	Estimated bodies/cell
	Mean rad (nm)	SD rad (nm)	Mean rad (nm)	SD rad (nm)	Volume (nm ³)	Mean rad (nm)	SD rad (nm)	Mean rad (nm)	SD rad (nm)		
WT	157.5	55.3	175.5	48.5	2.82E+07	840.5	232.7	923.3	212.1	5.53	23.13
OE Rph1	145.9	46.5	164.3	38.5	2.18E+07	835.6	236	912.2	216.8	1.72	1.72

Table 5.4. Analysis of Rph1 binding motifs in *ATG* promoters

Gene name	Rph1 DNA binding motifs								
	2162	279	547	1087	2228	1088	1699	1252	TWAGGG
<i>ATG1</i>									
<i>ATG2</i>				1				1	
<i>ATG3</i>									
<i>ATG4</i>									
<i>ATG5</i>						2			
<i>ATG6</i>									
<i>ATG7</i>	1			2					1
<i>ATG8</i>	1	2							
<i>ATG9</i>	1	1	1	1		1			1
<i>ATG10</i>								1	
<i>ATG11</i>									
<i>ATG12</i>					1	1			
<i>ATG13</i>						1			
<i>ATG14</i>	1								1
<i>ATG15</i>						1			
<i>ATG16</i>				1		1			
<i>ATG17</i>	1								1
<i>ATG18</i>									
<i>ATG19</i>	1	1				1		1	
<i>ATG20</i>	1	1		1		2			1
<i>ATG21</i>				1		1			
<i>ATG22</i>				1	1				
<i>ATG23</i>									
<i>ATG24</i>		1		1					
<i>ATG26</i>								1	
<i>ATG27</i>									
<i>ATG29</i>	1	1				1			
<i>ATG31</i>									
<i>ATG32</i>				1					
<i>ATG33</i>	1								1
<i>ATG34</i>	1	1	1			1		1	1
<i>ATG36</i>						1			
Total occurrence in <i>ATG</i> promoters	10	8	2	10	2	14	0	5	7
	5	4	1	4	0	2	0	0	3

Promoter regions of *ATG* genes were analyzed using the online software YetFasCo (available at <http://yetfasco.cabr.utoronto.ca>). The number of occurrence of each motif is indicated. Genes upregulated in the *RPH1* deletion strain (Figure 5.1A) are highlighted. See Table 5.5 for motif identities.

Table 5.5. Rph1 DNA binding motifs



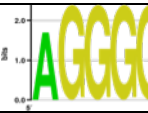
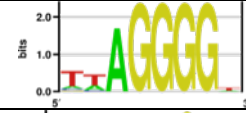











	Rph1 DNA binding motifs #	References
2162		(1)
823		(2)
279		(3)
547		(4)
1085		(5)
1087		(5)
2228		(6)
675		(6)
1862		(7)
1698		(7)
1697		(7)
1088		(5)
1086		(5)
1699		(7)
1252		(8)

Table references:

- (1) Zhao, Y., Granas, D., and Stormo, G.D. (2009). Inferring binding energies from selected binding sites. *PLoS Comput Biol* 5, e1000590.
- (2) Zhu, C., Byers, K.J., McCord, R.P., Shi, Z., Berger, M.F., Newburger, D.E., Saulrieta, K., Smith, Z., Shah, M.V., Radhakrishnan, M., Philippakis, A.A., Hu, Y., De Masi, F., Pacek, M., Rolfs, A., Murthy, T., Labaer, J., and Bulyk, M.L. (2009). High-resolution DNA-binding specificity analysis of yeast transcription factors. *Genome Res* 19, 556-566.
- (3) Jang, Y.K., Wang, L., and Sancar, G.B. (1999). *RPH1* and *GIS1* are damage-responsive repressors of *PHR1*. *Mol Cell Biol* 19, 7630-7638.
- (4) Badis, G., Chan, E.T., van Bakel, H., Pena-Castillo, L., Tillo, D., Tsui, K., Carlson, C.D., Gossett, A.J., Hasinoff, M.J., Warren, C.L., Gebbia, M., Talukder, S., Yang, A., Mnaimneh, S., Terterov, D., Coburn, D., Li Yeo, A., Yeo, Z.X., Clarke, N.D., Lieb, J.D., Ansari, A.Z., Nislow, C., and Hughes, T.R. (2008). A library of yeast transcription factor motifs reveals a widespread function for Rsc3 in targeting nucleosome exclusion at promoters. *Mol Cell* 32, 878-887.
- (5) Reddy, T.E., DeLisi, C., and Shakhnovich, B.E. (2007). Binding site graphs: a new graph theoretical framework for prediction of transcription factor binding sites. *PLoS Comput Biol* 3, e90.
- (6) MacIsaac, K.D., Wang, T., Gordon, D.B., Gifford, D.K., Stormo, G.D., and Fraenkel, E. (2006). An improved map of conserved regulatory sites for *Saccharomyces cerevisiae*. *BMC Bioinformatics* 7, 7:113.
- (7) Foat, B.C., Tepper, R.G., and Bussemaker, H.J. (2008). TransfactomeDB: a resource for exploring the nucleotide sequence specificity and condition-specific regulatory activity of trans-acting factors. *Nucl Acids Res* 36, D125-31.
- (8) Lee, T.I., Rinaldi, N.J., Robert, F., Odom, D.T., Bar-Joseph, Z., Gerber, G.K., Hannett, N.M., Harbison, C.T., Thompson, C.M., Simon, I., Zeitlinger, J., Jennings, E.G., Murray, H.L., Gordon, D.B., Ren, B., Wyrick, J.J., Tagne, J.-B., Volkert, T.L., Fraenkel, E., Gifford, D.K. and Young, R.A. (2002). Transcriptional regulatory networks in *Saccharomyces cerevisiae*. *Science* 298, 799-804.

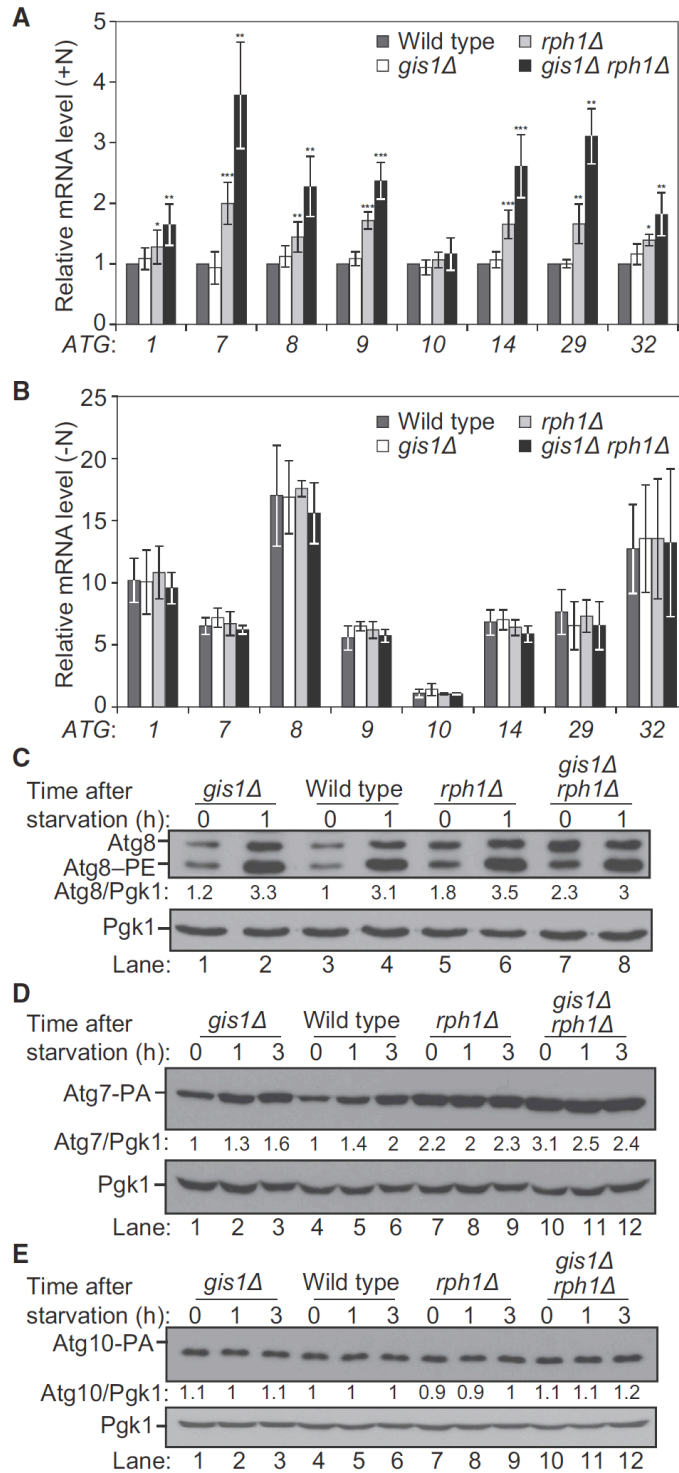


Figure 5.1. Rph1 represses the expression of nitrogen-sensitive *ATG* genes in nutrient-replete conditions

(A-B) Rph1 represses the expression of *ATG1*, *ATG7*, *ATG8*, *ATG9*, *ATG14* and *ATG29* in nutrient-replete conditions. Wild-type (YTS158), *rph1Δ* (YAB300), *gis1Δ* (YAB301) and *gis1Δ rph1Δ* (YAB302) cells were grown in YPD (+N) until mid-log phase (A) and then starved for

nitrogen (-N) for 1 h (B). mRNA levels were quantified by RT-qPCR. Error bars indicate the standard deviation of the average of at least 3 independent experiments. (C-E) Rph1 represses the expression of the Atg7 and Atg8 proteins. (C) For the analysis of Atg8, wild-type (YTS158, BY4742), *rph1* Δ (YAB300), *gis1* Δ (YAB301) and *gis1* Δ *rph1* Δ (YAB302) cells were grown in YPD until mid-log phase and then starved for nitrogen for the indicated times. Protein extracts were analyzed by western blot with anti-Atg8 and anti-Pgk1 (loading control) antisera. (D) To analyze Atg7 abundance, a protein A tag was integrated in the chromosome. Wild-type (YAB312, BY4742), *rph1* Δ (YAB313), *gis1* Δ (YAB314) and *gis1* Δ *rph1* Δ (YAB315) cells were grown in the same conditions as in (C). Protein extracts were analyzed as in (C) with an antibody that detects PA or anti-Pgk1 antiserum. (E) To analyze Atg10 abundance, a protein A tag was integrated in the chromosome. Wild-type (YAB350, BY4742), *rph1* Δ (YAB351), *gis1* Δ (YAB352) and *gis1* Δ *rph1* Δ (YAB353) cells were grown in the same conditions as in (C). Protein extracts were analyzed as in (D).

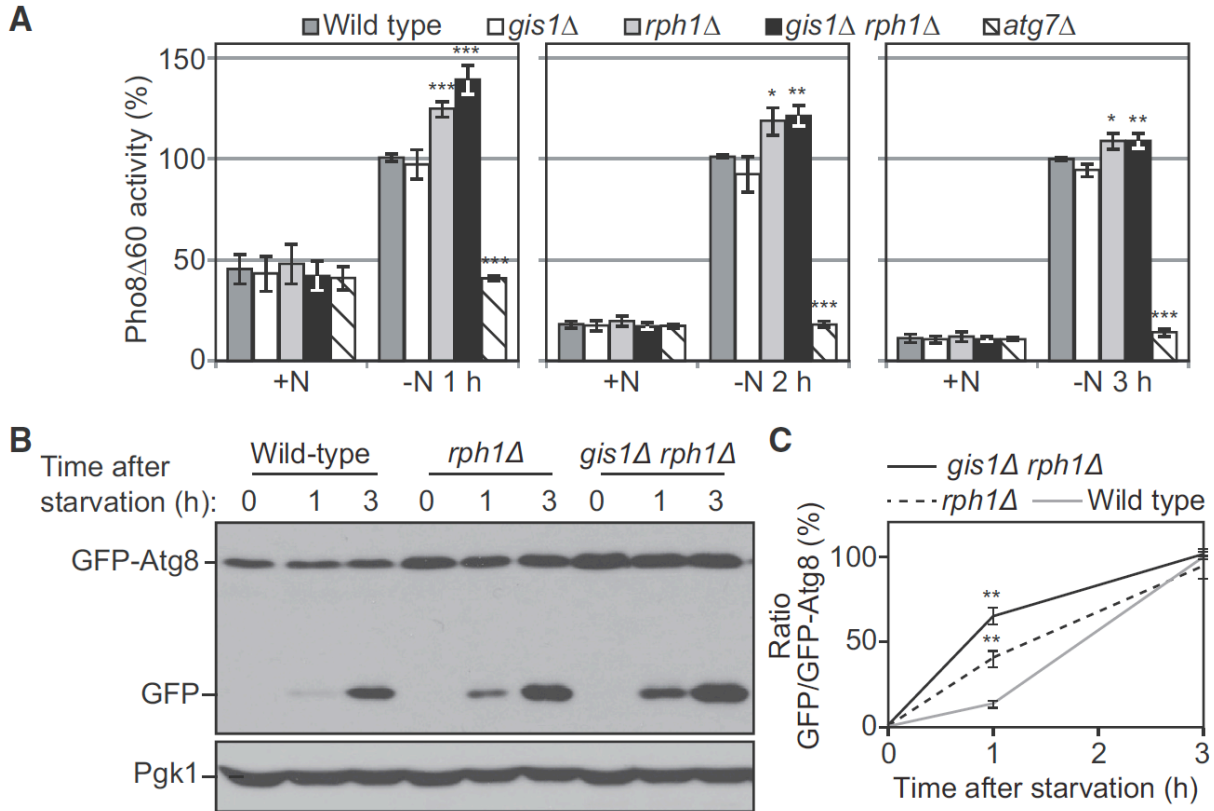


Figure 5.2. Rph1 negatively regulates autophagy

(A) Autophagy as measured by the Pho8Δ60 assay is increased in *rph1Δ* and *gis1Δ rph1Δ* cells. Wild-type (YTS158, BY4742), *rph1Δ* (YAB300), *gis1Δ* (YAB301), *gis1Δ rph1Δ* (YAB302) and *atg7Δ* (YAB292) cells were grown in YPD (+N) and then starved for nitrogen (-N) for the indicated times. The Pho8Δ60 activity was measured and normalized to the activity of wild-type cells after starvation, which was set to 100% at each time point. The data represent the average of 3 independent experiments; error bars indicate standard deviation. (B) Autophagy as measured by the GFP-Atg8 processing is increased in *rph1Δ* and *gis1Δ rph1Δ* cells. Wild-type (YTS158, BY4742), *rph1Δ* (YAB300) and *gis1Δ rph1Δ* (YAB302) cells transformed with a CEN plasmid carrying a GFP-Atg8 construct were grown in rich selective medium and then starved for 1 and 3 h. Cells were collected and protein extracts were analyzed by western blot with anti-YFP antibody and anti-Pgk1 (loading control) antiserum. (C) Quantification of (B). The ratio free GFP:GFP-Atg8 was measured and normalized to that of wild-type cells after 3 h starvation, which was set to 100%. Average values ± standard deviations of 2 independent experiments are indicated.

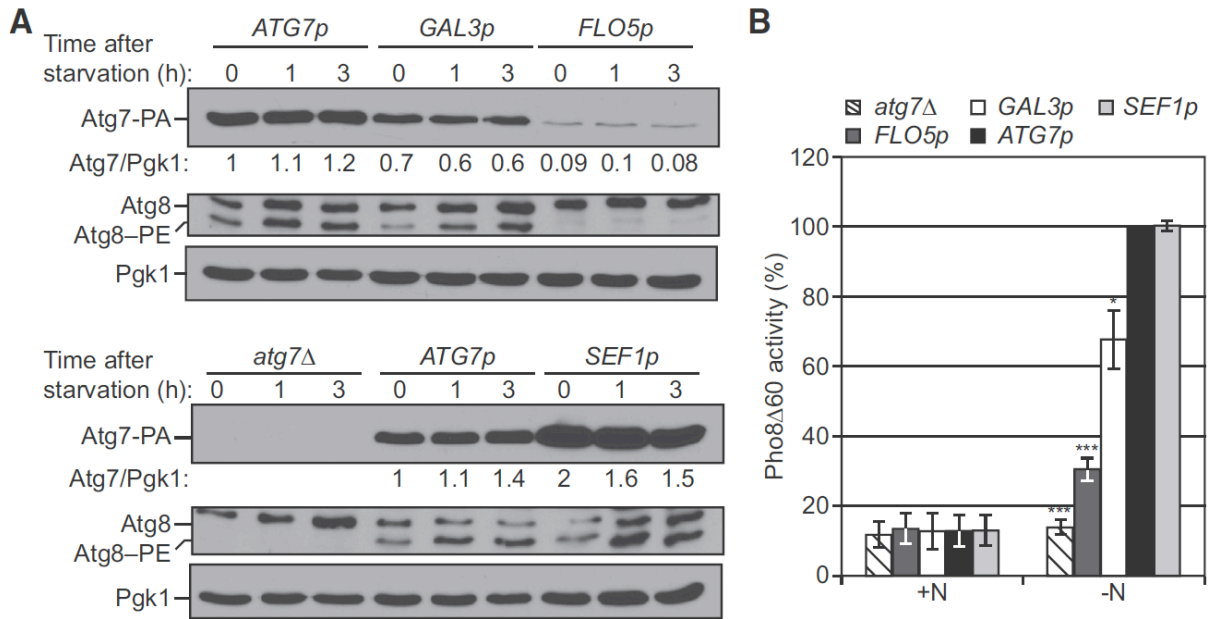


Figure 5.3. The level of Atg7 regulates autophagy

(A-B) Lowering the level of Atg7 results in a decrease in Atg8-PE conjugation and a decrease in autophagy activity. *atg7Δ* cells (YAB292) were transformed with the *ATG7p-ATG7-PA*, *GAL3p-ATG7-PA*, *FLO5p-ATG7-PA*, or *SEF1p-ATG7-PA* plasmid or the corresponding empty plasmid (*pRS416-PA*). Cells were grown in rich selective medium (SMD-Ura) until mid log phase and then starved for nitrogen for the indicated times. (A) Cells were collected and protein extracts were analyzed by western blot with either an antibody that recognizes PA, or anti-Atg8 and anti-Pgk1 (loading control) antisera. (B) Cells were starved for 3 h. The Pho8Δ60 activity was measured and normalized to the activity of *ATG7p-ATG7-PA* cells, which was set to 100%. Data represent the average of 3 independent experiments.

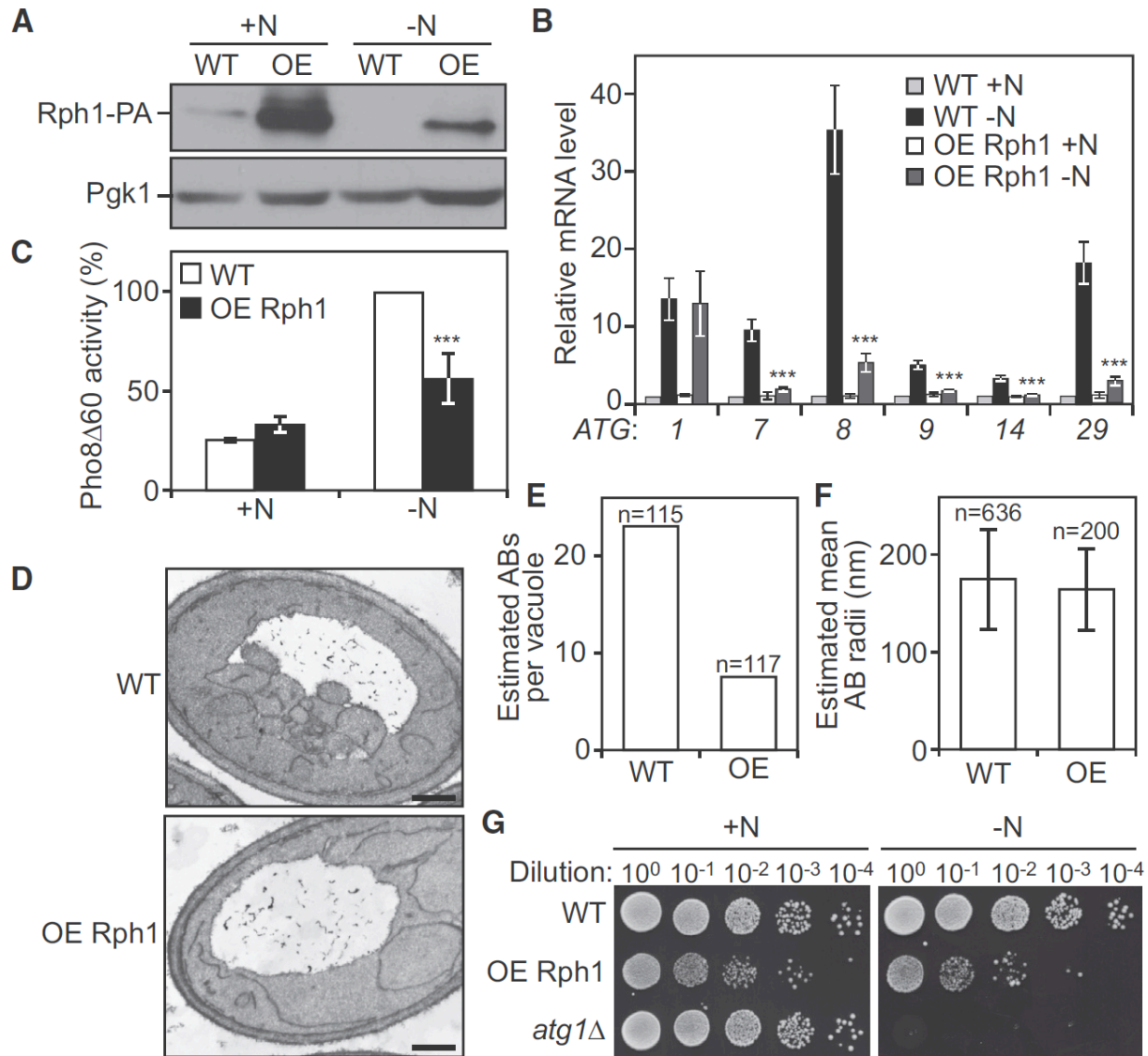


Figure 5.4. The overexpression of Rph1 inhibits autophagy and decreases cell survival in nitrogen starvation conditions

(A-C) Overexpressed Rph1 (*ZEO1p-RPH1-PA*) results in a block in *ATG* genes expression and autophagy flux. Rph1-PA cells (WT, YAB323, SEY6210) and cells overexpressing Rph1-PA (OE Rph1, YAB329) were grown in YPD (+N) until mid-log phase and then starved for nitrogen (-N). (A) Cells were starved for 2 h, and protein extracts were analyzed by western blot with either an antibody that recognizes PA or anti-Pgk1 (loading control) antiserum. (B) Total RNA of cells in mid-log phase (+N) as well as after 1 h of nitrogen starvation (-N) was extracted and the mRNA levels were quantified by RT-qPCR. The mRNA level of individual *ATG* genes was normalized to the mRNA level of the corresponding gene in Rph1-PA cells (WT), which was set to 1. Data represent the average of 3 independent experiments \pm standard deviation. (C) The Pho8 Δ 60 activity was measured and normalized to the activity of Rph1-PA cells (WT) after 2 h of nitrogen starvation (-N), which was set to 100%. Error bars indicate standard deviation of 3 independent experiments. (D-E) Rph1 overexpression blocks the biogenesis of autophagic bodies. Wild-type cells (WT, FRY143) and cells overexpressing Rph1 (OE Rph1, YAB346)

were imaged using transmission electron microscopy after 2 h of nitrogen starvation. (D) Representative TEM images showing a reduced accumulation of autophagic bodies in the vacuole of cells overexpressing Rph1 compared to wild type. Scale bar, 500 nm. (E) Estimated average number of autophagic bodies (AB) per vacuole. Estimation was based on the number of autophagic body cross-sections observed by TEM [50]. Over 100 unique cells per strain were captured and analyzed. (F) The estimated mean radii (in nm) of the original autophagic bodies (AB) observed by TEM in wild-type and OE Rph1 cells was analyzed as in (E). (G) Rph1 overexpression reduces cell survival after prolonged nitrogen starvation. Rph1-PA cells (WT, YAB323, SEY6210), cells overexpressing Rph1-PA (OE-Rph1, YAB329) and *atg1* Δ cells (WLY192) were grown in YPD (+N) until mid-log phase and then starved for nitrogen for 15 days (-N). Dilutions as indicated were grown on YPD plates for 2 days, then imaged.

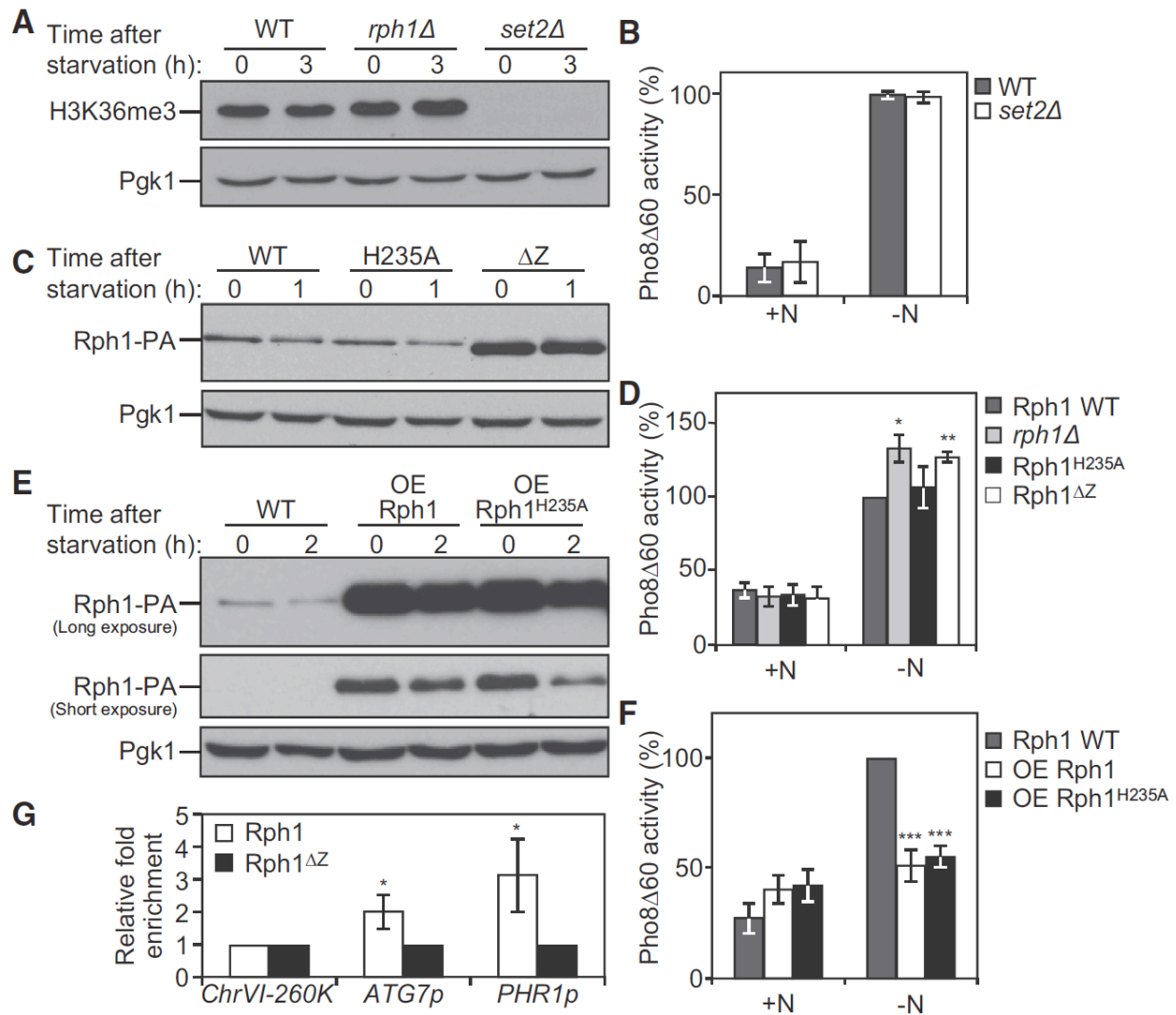


Figure 5.5. Rph1 DNA binding ability but not histone demethylase activity is required for its function in autophagy

(A) Wild-type (YTS158), *rph1Δ* (YAB300) and *set2Δ* (YAB318) cells were grown in YPD (+N) and then starved for nitrogen (-N) for 3 h. Protein extracts were analyzed by western blot with anti-H3K36me3 antibody and anti-Pgk1 (loading control) antiserum. (B) Wild-type (YTS158, BY4742) and *set2Δ* (YAB318) cells were grown in YPD (+N) and then starved for nitrogen (-N) for 3 h. The Pho8Δ60 activity was measured and normalized to the activity of wild-type cells, which was set to 100%. For panels B, D, F and G, the data represent the average of 3 independent experiments ± standard deviation. (C-D) *rph1Δ* cells were transformed with the *RPH1p-RPH1-PA* (Rph1, Wild-type), *RPH1p-RPH1^{H235A}-PA* (H235A), or *RPH1p-RPH1^{ΔZ}-PA* (ΔZ) plasmids or the corresponding empty plasmid (*pRS461-PA*, *rph1Δ*). Cells were grown in rich selective medium (SMD-Ura) until mid-log phase and then starved for nitrogen for 1 h. (C) The stability of Rph1 mutants was analyzed by western blot with either an antibody that recognizes PA or anti-Pgk1 (loading control) antiserum. (D) The Pho8Δ60 activity was measured and normalized to the activity of wild-type Rph1 cells after 1 h of nitrogen starvation (-N), which was set to 100%. (E-F) Rph1-PA cells (WT, YAB366) and cells overexpressing Rph1-PA (OE Rph1, YAB363) or Rph1^{H235A}-PA (OE Rph1^{H235A}, YAB364) were grown in YPD (+N) until

mid-log phase and then starved for nitrogen for 2 h (-N). (E) Protein extracts were analyzed by western blot with either an antibody that recognizes PA or anti-Pgk1 (loading control) antiserum. (F) The Pho8 Δ 60 activity was measured and normalized to the activity of wild-type cells after 2 h of nitrogen starvation (-N), which was set to 100%. (G) Rph1-PA binds the *ATG7* promoter. *rph1* Δ cells transformed with the *RPH1p-RPH1-PA* (Rph1) or *RPH1p-RPH1 ^{Δ Z}-PA* (Rph1 ^{Δ Z}) plasmids were analyzed by ChIP. ChIP was conducted on the *ATG7* promoter (*ATG7p*), a large non-coding region located at 260 kb on chromosome VI (*ChrVI-260K*) which was used as a negative control, and on the *PHR1* promoter (*PHR1p*) which was used as a positive control. Results were normalized to the input DNA and calibrated to the ChrVI-260K PCR product; results are presented as fold-enrichment of Rph1 binding compared to Rph1 ^{Δ Z}, which was set to 1.

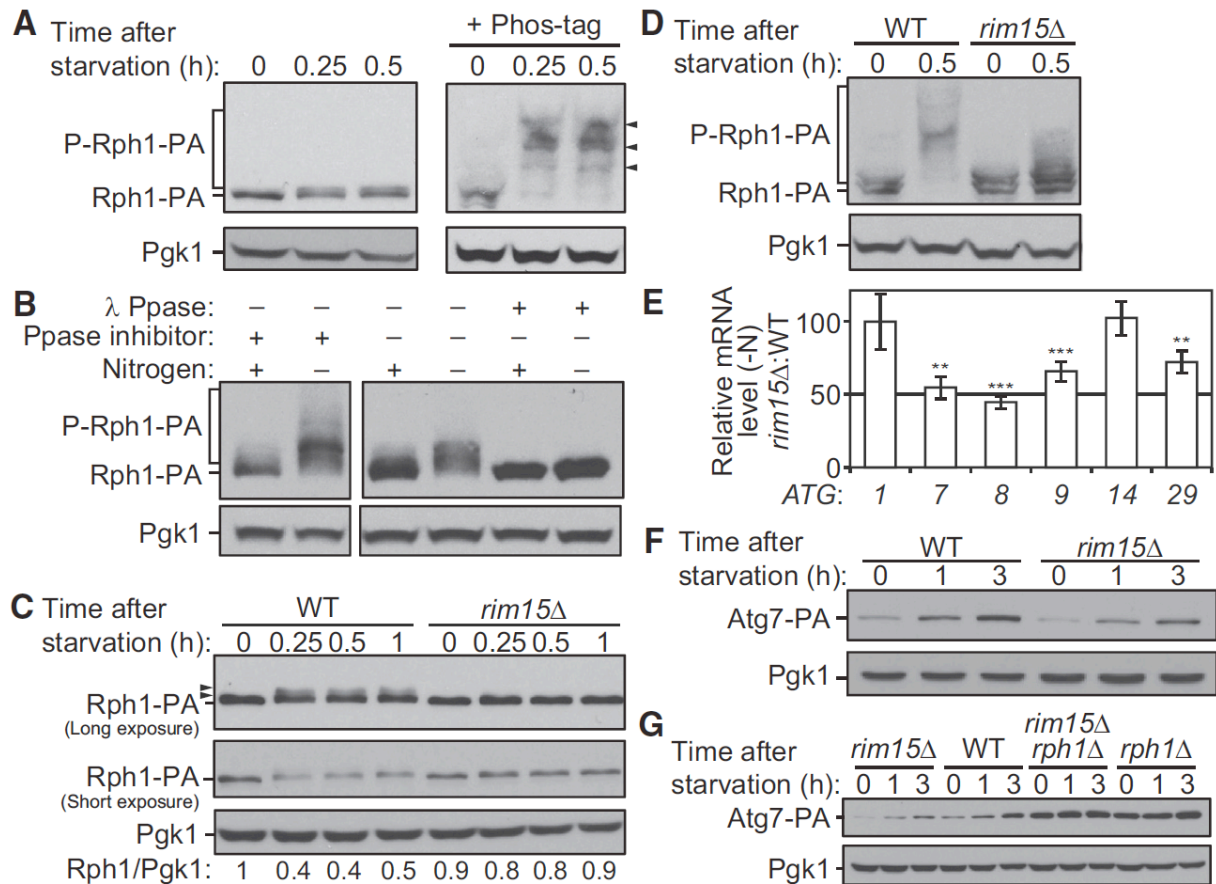


Figure 5.6. Rim15-dependent phosphorylation of Rph1 upon nitrogen starvation releases its repression on *ATG* gene expression and autophagy.

(A-B) Rph1 is phosphorylated upon nitrogen starvation. Rph1 was chromosomally tagged with PA tag and Rph1-PA cells (YAB308) were grown in YPD until mid-log phase and then starved for nitrogen for the indicated times. (A) Protein extracts were analyzed by western blot with or without 50 μ M Phos-tag as indicated and with either an antibody that recognizes PA or anti-Pgk1 (loading control) antiserum. Arrowheads indicate shifts in molecular weight of Rph1-PA suggesting phosphorylation. (B) Rph1-PA band shifts represent phospho-isoforms of the protein. Cells were lysed with or without phosphatase (Ppase) inhibitors. An aliquot of cell lysates was incubated at 30°C for 90 minutes in λ -phosphatase buffer with or without λ -phosphatase (λ Ppase). The reaction was stopped and proteins were precipitated by addition of 10% trichloroacetic acid. Protein extracts were analyzed by western blot as in (A) from gels containing Phos-tag. (C-D) Rph1 phosphorylation upon nitrogen starvation is blocked in *rim15* Δ cells. *RPH1* was chromosomally tagged with PA in wild-type (WT) and *rim15* Δ cells. Cells were grown in YPD until mid-log phase and then starved for nitrogen for the indicated times. WT (YAB308) and *rim15* Δ cells (YAB341) were collected and protein extracts were analyzed by western blot with either an antibody that recognizes PA or anti-Pgk1 (loading control) antiserum. (E) The deletion of *RIM15* reduces the induction of *ATG* gene expression after nitrogen starvation. WT (YAB308) and *rim15* Δ (YAB341) cells were grown in YPD until mid-log phase and then starved for 1 h (-N). mRNA levels were quantified by RT-qPCR. The mRNA levels of individual *ATG* genes were normalized to the mRNA level of the corresponding gene in WT cells in nitrogen starvation condition (-N), which was set to 100. Data represent the average of at

least 3 independent experiments \pm standard deviation. (F) *ATG7* was chromosomally tagged with PA in WT (YAB312) and *rim15* Δ (YAB342) cells. Cells were grown in YPD until mid-log phase and then starved for nitrogen for the indicated times. Protein extracts were analyzed by western blot with either an antibody that recognizes PA or anti-Pgk1 (loading control) antiserum. (G) *ATG7* was chromosomally tagged with PA in WT (YAB312), *rim15* Δ (YAB342), *rph1* Δ (YAB313) and *rim15* Δ *rph1* Δ (YAB347) cells. Proteins extracts were analyzed as in (F).

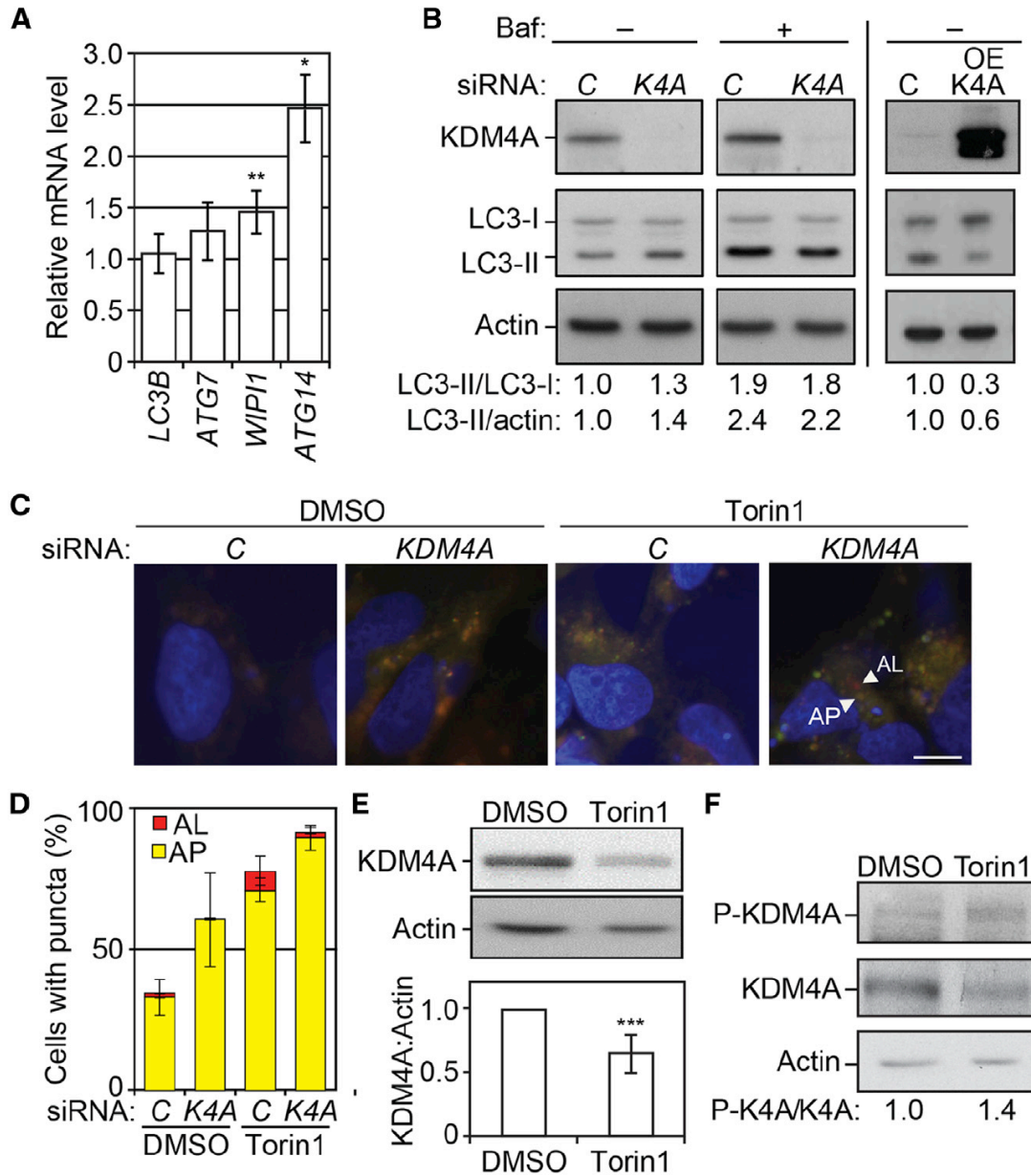


Figure 5.7. *KDM4* regulates autophagy in mammalian cells

(A) Transfected cells were grown for 48 h post transfection. Total RNA was extracted and the mRNA levels were quantified by RT-qPCR. The mRNA level of individual *ATG* genes was normalized to the mRNA level of the corresponding gene in the control cells (transfected with non-targeting siRNAs), which was set to 1. Error bars indicate the standard deviation of at least 3 independent experiments. (B) Left panel: HeLa cells transfected with siRNA against *KDM4A* (*K4A*) show a reduction in the expression of *KDM4A* and a concomitant increase in the LC3-II/LC3-I and LC3-II/actin ratio compared to the cells transfected with non-targeting siRNAs (control, C). In the presence of bafilomycin A₁ (Baf), control and si*KDM4A* cells show a similar accumulation of LC3-II. Right panel: HeLa cells transfected with a plasmid overexpressing *KDM4A* (OE-*KDM4A*) show a decrease in the LC3-II/LC3-I and LC3-II/actin ratio compared to control cells (C). Total cell lysates were harvested 48 h after transfection and protein extracts

were analyzed by western blot using antibodies to the indicated proteins. (C-D) Cells were transfected with the mRFP-GFP-LC3 plasmid. On the subsequent day, cells were transfected with si*KDM4A* (*KDM4*) or non-targeting siRNAs (control, C). Cells were treated for 24 h with DMSO or 250 nM Torin1 as indicated. (C) Cells were analyzed by fluorescence microscopy. Scale bar, 5 μ m. (D) Autophagy was determined by quantification of the number of cells with LC3-positive organelles. The histogram represents the mean of 3 independent experiments with SEM. AL, autolysosomes; AP, autophagosomes; *K4A*, *KDM4A*. (E) *KDM4A* is degraded upon autophagy induction by Torin1. Cells were treated with 250 nM Torin1 for 24 h. Protein extracts were analyzed by western blot using antibodies to the indicated proteins. The average and standard deviation of 7 independent experiments are provided. (F) Phosphorylation of *KDM4A* at Tyr547 is upregulated by treatment with Torin1. Cells were treated with Torin1 and protein extracts analyzed by western blot as in (E). K4A, *KDM4A*; P-*KDM4A*/P-K4A, phosphorylated *KDM4A*.

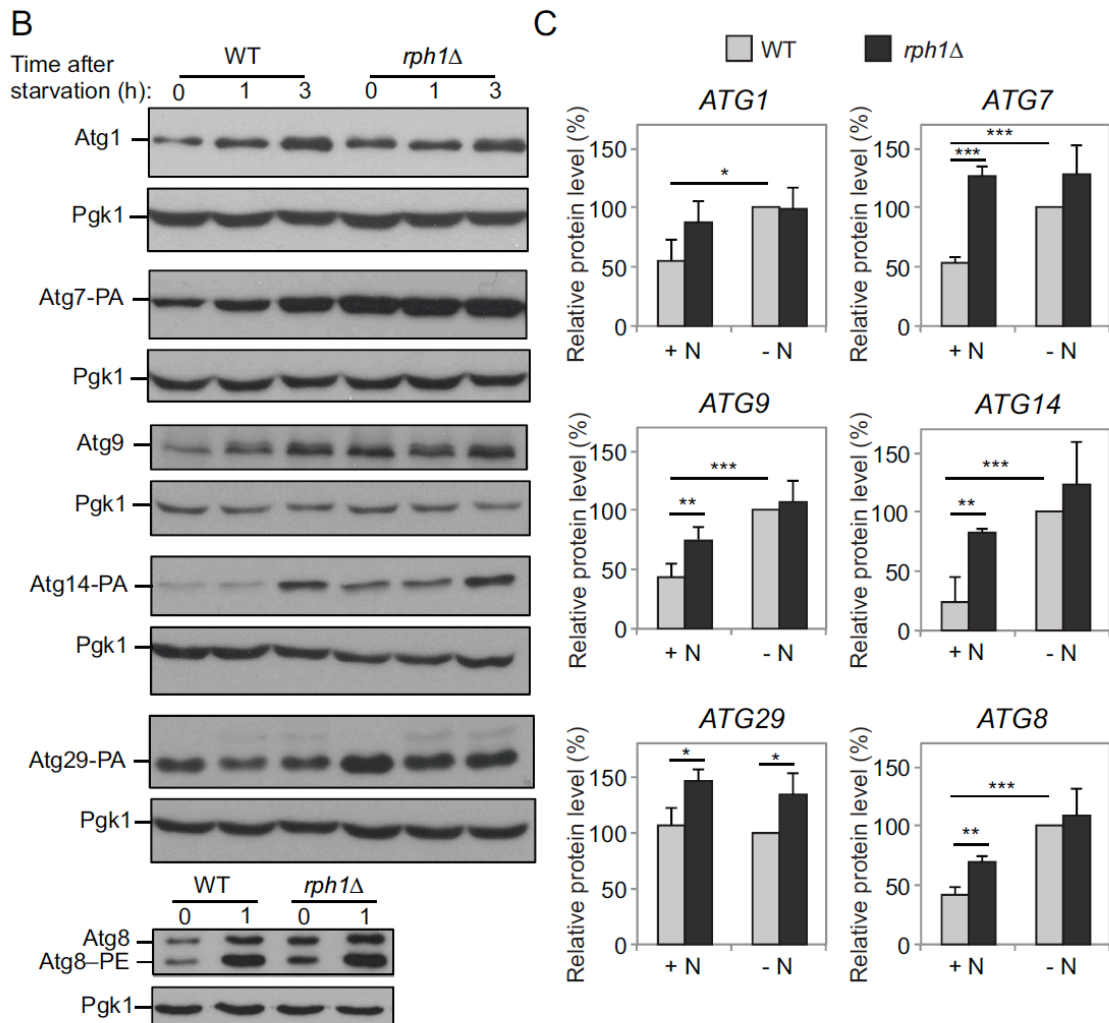
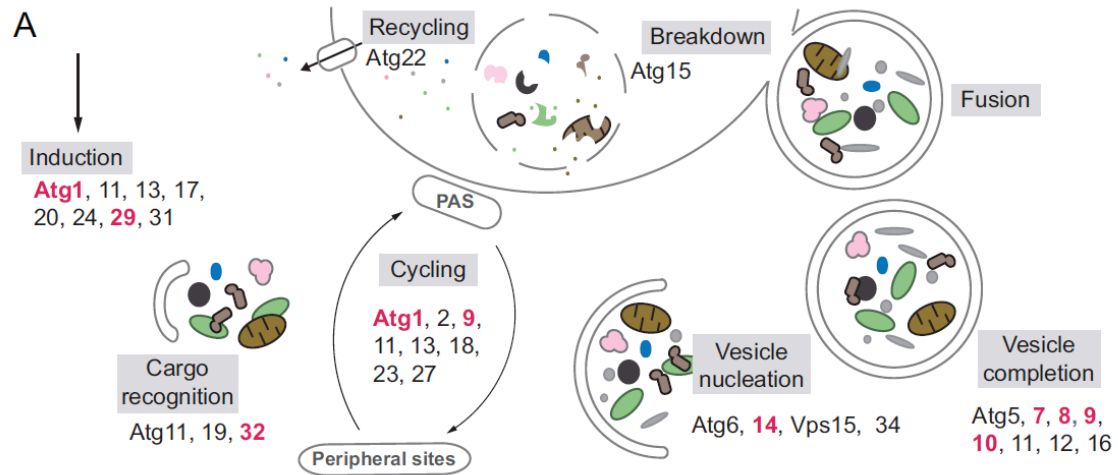


Figure 5.S1. Rph1 represses the expression of nitrogen-sensitive *ATG* genes in nutrient-replete conditions

(A) Schematic of the autophagy pathway; *ATG* genes analyzed in this study are highlighted in pink. PAS, phagophore assembly site. (B) Rph1 represses the expression of the Atg1, Atg7, Atg8, Atg9, Atg14 and Atg29 proteins. Cells were grown in YPD until mid-log phase and then starved for nitrogen for the indicated times. For the analysis of Atg1, Atg8 and Atg9, wild-type (YTS158, BY4742) and *rph1* Δ (YAB300) cells were used; protein extracts were analyzed by western blot with antibodies to the indicated proteins. Pgk1 was used as a loading control. For the analysis of Atg7, Atg14 and Atg29 the corresponding genes were fused to the protein A coding sequence on the chromosome in either wild-type (YTS158, BY4742) or *rph1* Δ (YAB300) cells. Cells were collected and protein extracts were analyzed by western blot with either an antibody that detects PA or anti-Pgk1 (loading control) antiserum. (C) Quantification of (B). The protein level of individual Atg proteins in rich conditions (+N) and after 3 h of starvation (-N) was normalized to the Pgk1 signal. Results present protein levels as percentage of the corresponding protein in wild-type cells after starvation, which was set to 100%. Error bars indicate the standard deviation of the average of at least 3 independent experiments.

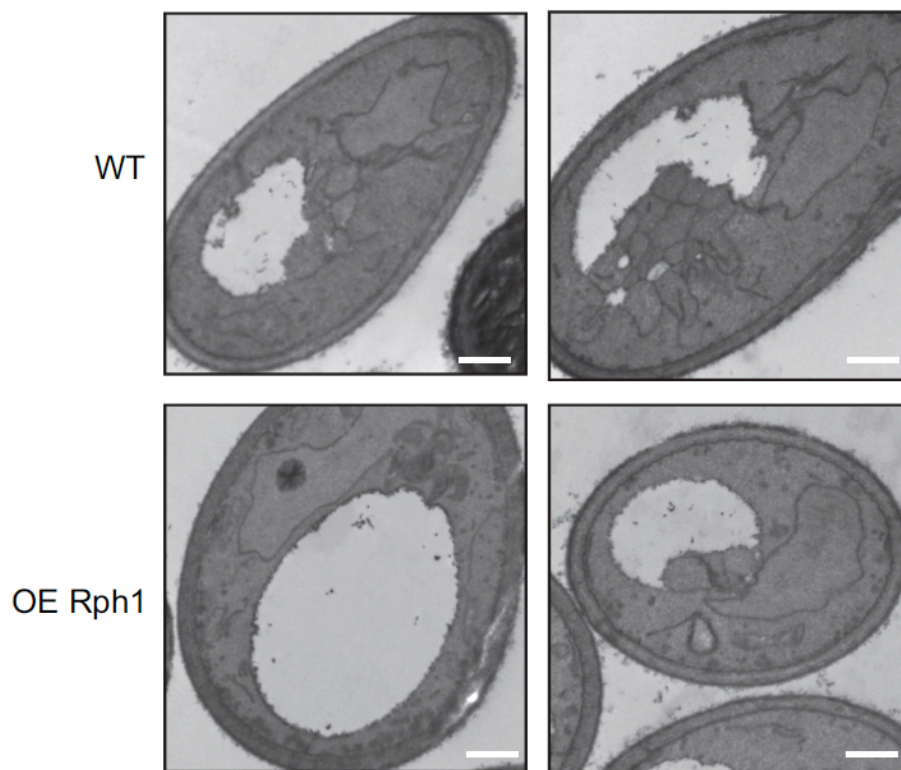


Figure 5.S2. The overexpression of Rph1 blocks the biogenesis of autophagic bodies
Wild-type cells (WT, FRY143) and cells overexpressing Rph1 (OE Rph1, YAB346) were imaged using transmission electron microscopy after 2h of nitrogen starvation. Representative TEM images showing a reduced accumulation of autophagic bodies in the vacuole of cells overexpressing Rph1 compared to wild type. Scale bar, 500 nm.

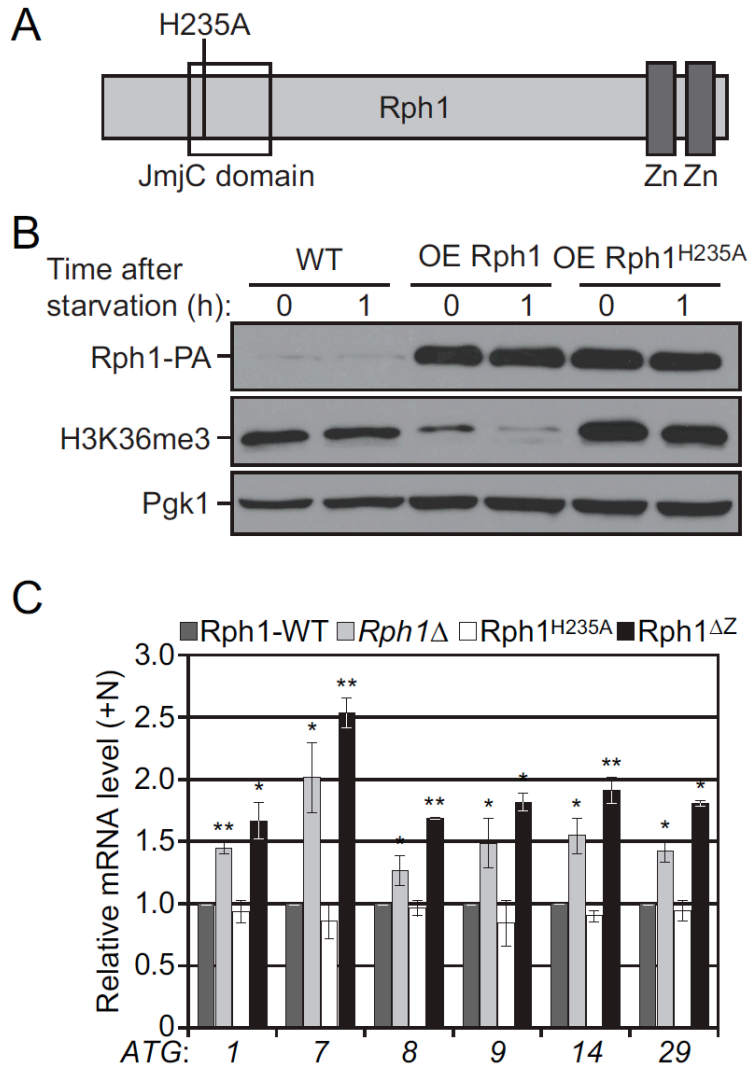


Figure 5.S3. Rph1 DNA binding ability but not histone demethylase activity is required for its function in autophagy

(A) Schematic of the Rph1 protein indicating the relative position of histidine H235 in the Jumonji C (JmjC) domain as well as the zinc-finger (Zn) DNA-binding domains. (B) The mutation of H235 to an alanine inhibits Rph1 demethylase activity. In contrast to the overexpression of Rph1, which leads to a drastic reduction in tri-methylation at H3K36, overexpressing Rph1^{H235A} had no effect on H3K36me3. Rph1-PA cells (WT, YAB366) and cells overexpressing Rph1-PA (OE Rph1, YAB363) or Rph1^{H235A}-PA (OE Rph1^{H235A}, YAB364) were grown in YPD until mid-log phase and then starved for nitrogen for 1 h. Cells were collected and protein extracts were analyzed by western blot with either an antibody that detects PA, H3K36me3 or anti-Pgk1 (loading control) antiserum. (C) *rph1* Δ cells were transformed with the *RPH1p-RPH1-PA* (Rph1-WT), *RPH1p-RPH1^{H235A}-PA*, or *RPH1p-RPH1 ^{Δ Z}-PA* plasmids or the corresponding empty plasmid (*pRS461-PA*, *rph1* Δ). Cells were grown in rich selective medium (SMD-ura) until mid-log phase and then starved for nitrogen for 1 h. Total RNA of cells in mid-log phase was extracted and the mRNA levels were quantified by RT-qPCR. Data represent the average of 3 independent experiments. Error bars indicate the standard deviation.

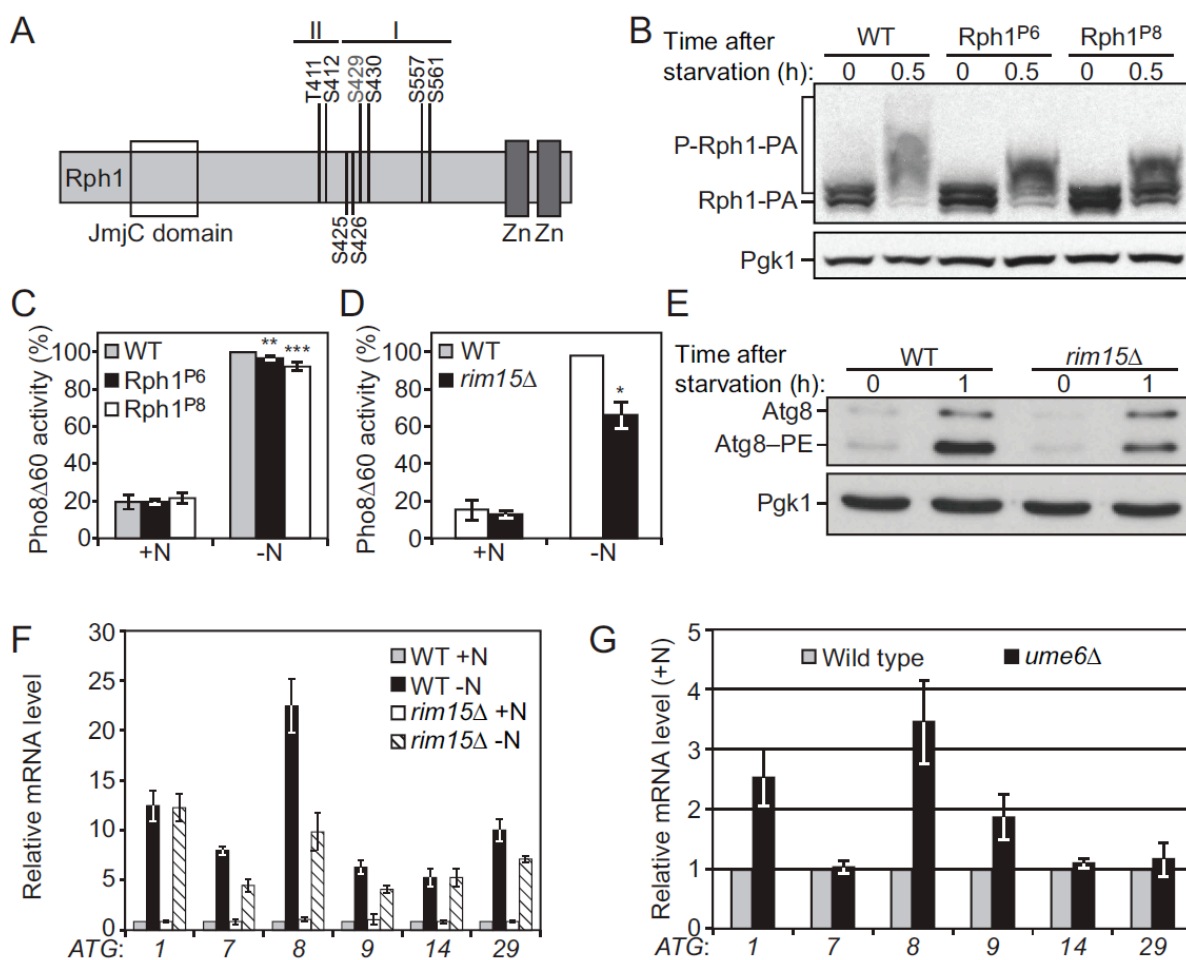


Figure 5.S4. Rim15-dependent phosphorylation of Rph1 upon nitrogen starvation releases its repression on *ATG* gene expression and autophagy

(A) Schematic of the Rph1 protein indicating the relative position of putative autophagy-dependent phosphorylated residues in Rph1. The Jumonji C (JmjC) domain as well as the zinc-finger (Zn) DNA-binding domains are indicated. (B-C) The mutation of Rph1 putative phosphorylation sites partially inhibits Rph1 phosphorylation and autophagy upon nitrogen starvation. Wild-type (WT, YAB374, BY4742), Rph1^{P6} (YAB375, S425A-S426S-S429A-S430A-S557S-S561A) and Rph1^{P8} (YAB376, T411A-S412A-S425A-S426S-S429A-S430A-S557S-S561A) cells were grown until mid-log phase and then starved for the indicated time. (B) Cells were collected and protein extracts were analyzed by western blot from gels containing 50 μ M Phos-tag, with an antibody that detects PA or anti-Pgk1 (loading control) antiserum. (C) Autophagy as measured by the Pho8 Δ 60 assay shows a minor decrease in Rph1 phosphomutants. Cells were starved for nitrogen (-N) for 2 h. The Pho8 Δ 60 activity was measured and normalized to the activity of wild-type cells after starvation, which was set to 100%. Error bars indicate the standard deviation of at least 3 independent experiments. (D) Autophagy as measured by the Pho8 Δ 60 assay is decreased in *rim15* Δ cells. Wild-type (YAB308, BY4742) and *rim15* Δ (YAB341) cells were grown in YPD (+N) and then starved for nitrogen (-N) for 3 h. The Pho8 Δ 60 activity was measured and normalized to the activity of wild-type cells after starvation,

which was set to 100%. Error bars indicate the standard deviation of 3 independent experiments. (E) The deletion of *RIM15* causes a decrease in Atg8 protein level. WT (YAB308, BY4742) and *rim15* Δ cells (YAB341) were grown in YPD until mid-log phase and then starved for nitrogen for the indicated times. Cells were collected and protein extracts were analyzed by western blot with anti-Atg8 and anti-Pgk1 (loading control) antisera. (F) The deletion of *RIM15* reduces the induction of *ATG* gene expression after nitrogen starvation. Wild type (WT; YAB308, BY4742) and *rim15* Δ (YAB341) cells were grown in YPD until mid-log phase (+N) and then starved for 1 h (-N). Total RNA was extracted and the mRNA levels were quantified by RT-qPCR. The mRNA level of individual *ATG* genes was normalized to the mRNA level of the corresponding gene in WT cells in rich conditions (+N), which was set to 1. Data represent the average of at least 3 independent experiments \pm standard deviation. (G) Ume6 represses the expression of *ATG1*, *ATG8* and *ATG9* but not *ATG7* and *ATG29* in growing-conditions. WT (BY4742) and *ume6* Δ cells were grown in YPD until mid-log phase (+N). Total RNA was extracted and the mRNA levels were quantified by RT-qPCR. The mRNA level of individual *ATG* genes was normalized to the mRNA level of the corresponding gene in WT cells, which was set to 1. Data represent the average of 3 independent experiments. Error bars indicate the standard deviation.

CHAPTER 6. Summary⁶

How autophagy activity is regulated: Size and number of autophagosomes

Autophagy activity, which corresponds to the amount of cytoplasmic material, whether random portions of the cytoplasm or selective cargos, sequestered by autophagosomes per unit time, followed by degradation within the vacuole and permease efflux, is modulated primarily by two features of autophagosomes: Size and number.

6.1 Regulation of the size of autophagosomes

A Cvt vesicle, which is the predominant type of sequestering compartment formed in growing conditions, is approximately 140-160 nm in diameter. Upon autophagy induction, much larger autophagosomes are formed; nitrogen-starvation induced autophagosomes range from 300-900 nm in diameter [1]. Therefore, the mechanism involved in determining the size of the autophagosome, that is, which Atg (or other) proteins play a central role in the formation of the larger autophagosome is an interesting question. The flexibility in the size of autophagosomes allows the sequestration of different sizes and amounts of cargo by autophagy. During nonselective autophagy, premature closure of the phagophore would result in smaller autophagosomes, which would in turn attenuate the efficiency of autophagic sequestration and

⁶ Chapter 1 and this chapter is reprinted from Meiyang Jin and Daniel J. Klionsky, Regulation of autophagy: Modulation of the size and number of autophagosomes, FEBS Letters, 2014;588(15): 2457-63, doi: 10.1016/j.febslet.2014.06.015, with minor modifications, with permission from John Wiley and Sons.

degradation. During selective autophagy, the size of the cargo may determine the size of the sequestering compartment directly through protein-protein interactions between the cargo/ligand-receptor and Atg8 family proteins that are located on the concave face of the phagophore. However, there is a limit to the size of the autophagosomes that form during selective autophagy, indicating that this simple model is not the complete explanation, and there likely exists other machinery (which may be the same as that used in nonselective autophagy) to control the expansion of the phagophore. Under physiological conditions the diameter of the Cvt vesicle is essentially the size of the cargo, the Cvt complex composed primarily of prApe1 and its receptor Atg19. When the prApe1 cargo protein is overexpressed, a larger Cvt complex is formed that cannot be efficiently sequestered by a Cvt vesicle [1]. However, after starvation, when autophagy is induced and larger autophagosomes are generated, the larger Cvt complex can be sequestered and delivered to the vacuole. For both mitophagy and pexophagy, a fission complex is needed for the efficient sequestration of the targeted organelles [2,3], suggesting that matching the size of the cargo with the phagophore may be important. Therefore, for selective autophagy, the size of the autophagosome not only regulates efficiency, but may also be critical for the cargo selectivity.

A series of studies in our lab on *ATG8* and its regulation provides some clues for the regulation of autophagosome size. The amounts of both *ATG8* mRNA and its protein product are elevated dramatically within a short time following nitrogen starvation or rapamycin (an inhibitor of TOR) treatment. To reveal the roles of the increased level of Atg8 during autophagy induction, several strains with various, but reduced, expression levels of *ATG8* were generated through the use of heterologous promoters. Based on transmission electron microscopy, in conjunction with other autophagy assays, the correlation between Atg8 protein amount and

autophagosome size/autophagy activity was determined [4]. It is still unclear how Atg8 regulates the size of the autophagosome. The observation that the Atg12–Atg5-Atg16 complex together with Atg8 can form highly oligomerized network structures on giant unilamellar vesicles in vitro, indicates the possibility that Atg8 along with the Atg12–Atg5-Atg16 complex forms a protein coat on the outer membrane of the phagophore to regulate its curvature [5]. As PE, a cone-shaped lipid that is the target of Atg8 conjugation, can modulate membrane curvature [6], Atg8 may also regulate the size of the autophagosome through its binding to PE, possibly due to differential distribution on the two faces of the phagophore.

Considering that the amount of Atg8 plays an important role in determining the size of the autophagosome, we became interested in understanding how the transcription of *ATG8* is regulated. We identified a transcriptional repressor, Ume6, which can directly bind at the promoter of *ATG8* and suppress its transcription in nutrient-rich conditions. In agreement with our previous study, *ume6*Δ cells, which express an elevated amount of Atg8 even in nutrient-rich conditions, generate larger autophagosomes than the wild-type cells. Phosphorylation of Ume6 by Rim15 after starvation releases its suppression, and these findings suggest a model for a regulatory signaling axis of autophagy: In nutrient-rich conditions upstream sensors such as PKA inhibit the effector kinase Rim15, resulting in active Ume6 that suppresses *ATG8* transcription; the resulting low level of Atg8 is sufficient to generate the small Cvt vesicles. During starvation, inhibition of PKA allows the now active Rim15 to inhibit Ume6; the resulting increase in Atg8 allows the formation of larger autophagosomes (Figure 6.1) [7, Chapter 2]. Therefore, the Ume6-dependent control of *ATG8* transcription is an example of size regulation during autophagosome formation.

6.2 Regulation of the number of autophagosomes

The second feature, which is as important as the size of autophagosomes, is their number, which can be viewed as the frequency of autophagosome formation. In budding yeast cells, usually only one PAS is observed, but the frequency of autophagosome formation can be increased by autophagy induction to approach a condition of continuous and accelerated autophagy. Data suggest that the half-life of prApe1 processing through the Cvt pathway is approximately 45 min [8], whereas after starvation-induction the half-life of an autophagosome is approximately 10 min [9]. There are multiple PAS sites in fission yeast, and in mammalian cells phagophore nucleation is not limited to a single location. In these systems, as a consequence of increased autophagosome formation frequency, the number of PAS is increased by autophagy induction. It had been not clear, however, which Atg proteins play a role in determining the number of autophagosomes. From my thesis studies of transcriptional regulators of autophagy, we found that cells deleted for the *PHO23* gene, encoding a transcription repressor, formed more (but not larger) autophagosomes relative to the wild-type cells. Pho23 regulates transcription of more than one *ATG* gene, but *ATG9* expression is changed the most among these genes in the *pho23Δ* mutant (Figure 6.1) [10, Chapter 3]. To determine the contribution of Atg9 to the *pho23Δ* phenotype we used yeast strains with different *ATG9* gene expression levels. We found that the amount of Atg9 protein correlated with the numbers of autophagic bodies, supporting our hypothesis that Atg9 levels determine the number of autophagosomes [10, Chapter 3]. Considering the role of Atg9 in autophagy as a potential membrane carrier or in directing the delivery of membrane to the PAS, we conclude that Atg9 may regulate the rate of phagophore expansion, and consequently the time required for generating each autophagosome through its cycling between the PAS and the peripheral sites/TVCs.

Mathematical modeling of the energy status of double-membrane structures suggests that a minimal change of the rim curvature on the edge of the double-membrane sheet may drive its bending and closure to form a vesicle [11]. Interestingly, Atg9 appears to localize only at the edge of the phagophore [12], suggesting another possibility that Atg9 regulates closure of the phagophore by affecting the rim curvature on the edge of this structure. If this is the case, the Atg17-Atg31-Atg29 scaffold, which forms a crescent structure with a similar curvature as that of the phagophore rim and also only localizes on the edge of the phagophore, may cooperate with Atg9 in this aspect of autophagy regulation [12-14]. Our studies with Atg8 and Atg9 indicate that the size and number of autophagosomes may be separately regulated by different autophagy components. This makes sense considering that modulating size may affect primarily cargo selectivity, while regulating the number of autophagosomes could be carried out to regulate mostly autophagy flux. Interestingly, Pho23 and Ume6 both play roles in the Rpd3 large complex, but Pho23 regulates *ATG9* transcription in a Ume6-independent manner, suggesting a dual function of the Rpd3 complex in regulating autophagy activity.

6.3 Future directions

How the size and number of autophagosomes are regulated by different subgroups of Atg proteins is an interesting question to pursue, as it will reveal the different modulations of autophagy activity and selectivity by different autophagy proteins. Furthermore, identifying new transcriptional regulators of autophagy and the corresponding gene targets will help to dissect their functions in modulating autophagy activity. Our study involving the large-scale analysis of *ATG* gene transcription and the subsequent study of the candidate autophagy regulators (Chapters 4 and 5) open the way for future genomic research on transcriptional regulation of autophagy.

Increasing evidence suggests that histone modification complexes, such as HDACs, histone acetyltransferases, and histone methyltransferases play important roles in autophagy by both regulating expression and direct post-translational modifications of Atg proteins [15-19]. In yeast, the Rpd3 large (Rpd3L) complex, the homolog of mammalian HDAC complex 1, is involved in autophagy regulation through different mechanisms. Yi and colleagues reported that Rpd3 inhibits autophagy activity through its direct modification of Atg3 [20]. My previous studies reveal that two different subunits of Rpd3L, Ume6 and Pho23, negatively regulate the size and number of autophagosomes through transcriptional regulation of *ATG8* and *ATG9*, respectively (Chapters 1 and 2). Small molecule HDAC inhibitors have been examined with regard to their effects in heart disease through the regulation of autophagy, and the results are paradoxical. The HDAC inhibitor suberoylanilide hydroxamic acid (SAHA) blunts ischemia/reperfusion injury by inducing cardiomyocyte autophagy [21]. However, another HDAC inhibitor, trichostatin A (TSA), attenuates both load- and agonist-induced hypertrophic myocardial growth by suppressing autophagy [22]. Therefore, it is critical to gain an understanding of how the finely tuned regulation of autophagy is coordinated by different histone modification enzymes for the therapeutic modulation of autophagy activity in order to maintain this process within its beneficial range in various autophagy-related human diseases. Considering that most regulatory pathways of autophagy are conserved among different organisms, a future genomic study in yeast to reveal the complexities of autophagy transcriptional and epigenetic regulation on a large-scale would provide valuable information that can be used for the therapeutic treatment of a wide range of diseases that are affected by autophagic dysfunction.

6.4 References

- [1] Baba, M., Osumi, M., Scott, S.V., Klionsky, D.J. and Ohsumi, Y. (1997) Two distinct pathways for targeting proteins from the cytoplasm to the vacuole/lysosome. *J Cell Biol.* 139, 1687-95.
- [2] Mao, K., Wang, K., Liu, X. and Klionsky, D.J. (2013) The scaffold protein Atg11 recruits fission machinery to drive selective mitochondria degradation by autophagy. *Dev Cell.* 26, 9-18.
- [3] Mao, K., Liu, X., Feng, Y. and Klionsky, D.J. (2014) The progression of peroxisomal degradation through autophagy requires peroxisomal division. *Autophagy.* 10, 652-61.
- [4] Xie, Z., Nair, U. and Klionsky, D.J. (2008) Atg8 controls phagophore expansion during autophagosome formation. *Mol Biol Cell.* 19, 3290-8.
- [5] Kaufmann, A., Beier, V., Franquelim, H.G. and Wollert, T. (2014) Molecular mechanism of autophagic membrane-scaffold assembly and disassembly. *Cell.* 156, 469-81.
- [6] Vance, J.E. and Tasseva, G. (2013) Formation and function of phosphatidylserine and phosphatidylethanolamine in mammalian cells. *Biochim Biophys Acta.* 1831, 543-54.
- [7] Bartholomew, C.R., Suzuki, T., Du, Z., Backues, S.K., Jin, M., Lynch-Day, M.A., Umekawa, M., Kamath, A., Zhao, M., Xie, Z., Inoki, K. and Klionsky, D.J. (2012) Ume6 transcription factor is part of a signaling cascade that regulates autophagy. *Proc Natl Acad Sci U S A.* 109, 11206-10.
- [8] Klionsky, D.J., Cueva, R. and Yaver, D.S. (1992) Aminopeptidase I of *Saccharomyces cerevisiae* is localized to the vacuole independent of the secretory pathway. *J Cell Biol.* 119, 287-99.
- [9] Geng, J., Baba, M., Nair, U. and Klionsky, D.J. (2008) Quantitative analysis of autophagy-related protein stoichiometry by fluorescence microscopy. *J Cell Biol.* 182, 129-40.
- [10] Jin, M., He, D., Backues, S.K., Freeberg, M.A., Liu, X., Kim, J.K. and Klionsky, D.J. (2014) Transcriptional regulation by Pho23 modulates the frequency of autophagosome formation. *Curr Biol.* in press.
- [11] Knorr, R.L., Dimova, R. and Lipowsky, R. (2012) Curvature of double-membrane organelles generated by changes in membrane size and composition. *PLoS One.* 7, e32753.
- [12] Suzuki, K., Akioka, M., Kondo-Kakuta, C., Yamamoto, H. and Ohsumi, Y. (2013) Fine mapping of autophagy-related proteins during autophagosome formation in *Saccharomyces cerevisiae*. *J Cell Sci.* 126, 2534-44.
- [13] Mao, K., Chew, L.H., Inoue-Aono, Y., Cheong, H., Nair, U., Popelka, H., Yip, C.K. and Klionsky, D.J. (2013) Atg29 phosphorylation regulates coordination of the Atg17-Atg31-Atg29 complex with the Atg11 scaffold during autophagy initiation. *Proc Natl Acad Sci U S A.* 110, E2875-84.
- [14] Ragusa, M.J., Stanley, R.E. and Hurley, J.H. (2012) Architecture of the Atg17 complex as a scaffold for autophagosome biogenesis. *Cell.* 151, 1501-12.
- [15] Fullgrave, J., D.J. Klionsky, and B. Joseph. (2014) The return of the nucleus: transcriptional and epigenetic control of autophagy. *Nature reviews. Molecular cell biology.* 15(1), 65-74.
- [16] Artal-Martinez de Narvajás, A., et al. (2013) Epigenetic regulation of autophagy by the methyltransferase G9a. *Molecular and cellular biology.* 33(20), 3983-93.
- [17] Cao, D.J., et al. (2011) Histone deacetylase (HDAC) inhibitors attenuate cardiac hypertrophy by suppressing autophagy. *Proceedings of the National Academy of Sciences of the United States of America.* 108(10), 4123-8.

- [18] Park, J.H., et al. (2012) A new synthetic HDAC inhibitor, MHY218, induces apoptosis or autophagy-related cell death in tamoxifen-resistant MCF-7 breast cancer cells. *Investigational new drugs*. 30(5), 1887-98.
- [19] Xie, M., et al. (2014) Histone deacetylase inhibition blunts ischemia/reperfusion injury by inducing cardiomyocyte autophagy. *Circulation*. 129(10), 1139-51.
- [20] Yi, C., Ma, M., Ran, L., Zheng, J., Tong, J., Zhu, J., Ma, C., Sun, Y., Zhang, S., Feng, W., et al. (2012). Function and molecular mechanism of acetylation in autophagy regulation. *Science* 336, 474-477.
- [21] Xie, M., Kong, Y., Tan, W., May, H., Battiprolu, P.K., Pedrozo, Z., Wang, Z.V., Morales, C., Luo, X., Cho, G., et al. (2014). Histone deacetylase inhibition blunts ischemia/reperfusion injury by inducing cardiomyocyte autophagy. *Circulation* 129, 1139-1151.
- [22] Cao, D.J., Wang, Z.V., Battiprolu, P.K., Jiang, N., Morales, C.R., Kong, Y., Rothermel, B.A., Gillette, T.G., and Hill, J.A. (2011). Histone deacetylase (HDAC) inhibitors attenuate cardiac hypertrophy by suppressing autophagy. *Proc Natl Acad Sci U S A* 108, 4123-4128.

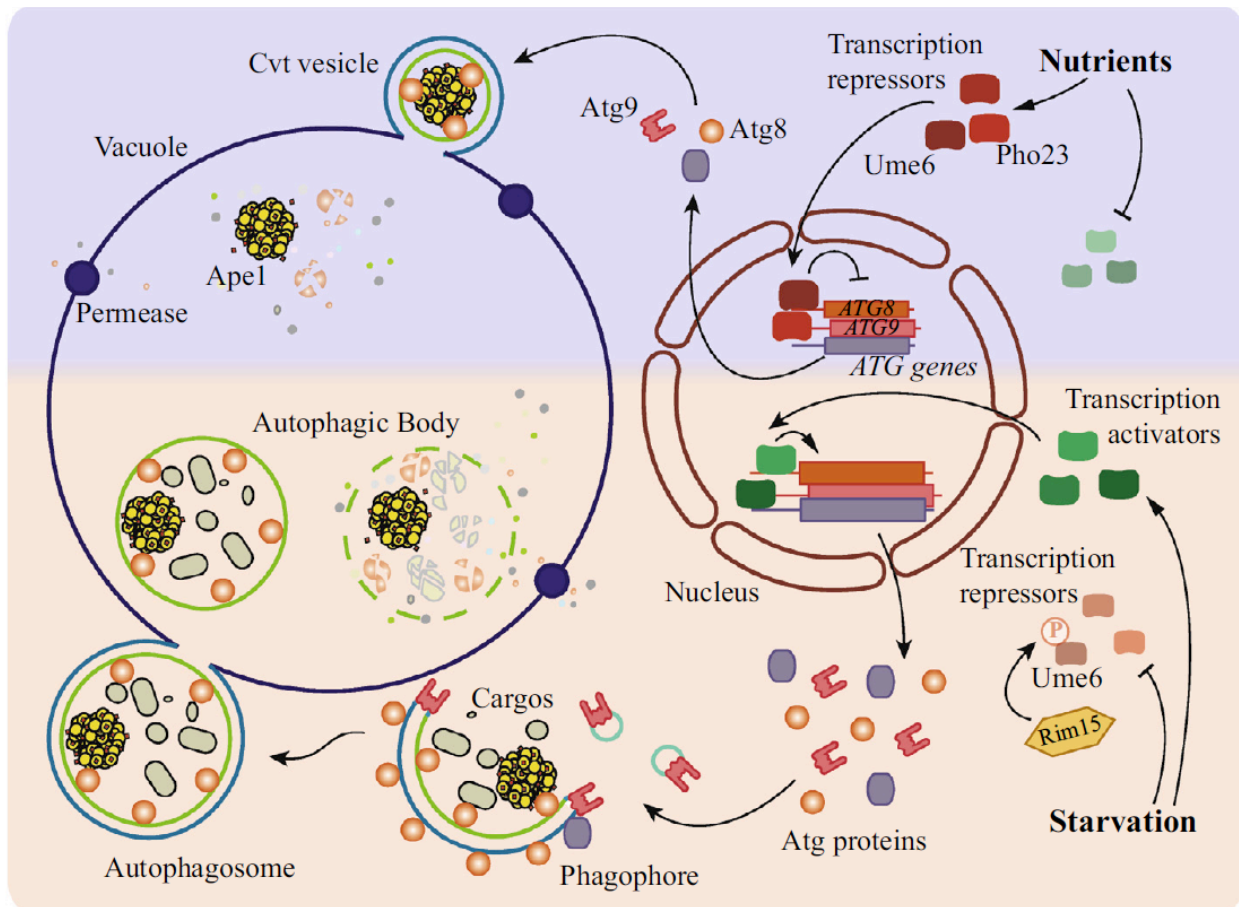


Figure 6.1. A model of transcriptional regulation of autophagy in yeast.

When nutrients are present, the transcription of most *ATG* genes is repressed due to the inhibition of autophagy transcription activators, and/ or activation of transcription repressors. For example, Ume6 represses the transcription of *ATG8*, and Pho23 represses the expression of *ATG9*. Repression of transcription in growing conditions leads to a relatively low amount of Atg proteins that are sufficient for basal autophagy, and consequently the autophagosomes that are formed under these conditions are predicted to be smaller in size (due to limited Atg8) and generated at a slower rate (due to limited Atg9). The Cvt pathway, which is the main type of autophagy-like process in growing conditions, generates Cvt vesicles to sequester prApel dodecamers and deliver them to the vacuole to allow maturation of the zymogen. After starvation, transcription activators of autophagy become functional, and the repressors are inhibited. For example, Ume6 is phosphorylated by Rim15 kinase, releasing its repression of *ATG8* transcription. Upregulation of *ATG* gene expression allows larger amounts of Atg components, such as Atg8 and Atg9, to participate in the formation of the autophagosome. As a result, more and larger autophagosomes are generated. During starvation-induced autophagy, Atg proteins are initially recruited to a peri-vacuolar site to generate the double-membrane structure named the phagophore. The phagophore randomly sequesters cytoplasmic material, and after the expansion phase is complete it seals to generate the double-membrane autophagosome. The outer membrane of the autophagosome fuses with vacuole, releasing the inner vesicle, now termed an autophagic body. This single-membrane vesicle along with its cargo is degraded in the vacuole lumen, and the resulting macromolecules are released back into the cytosol.